

Erosion in Geomechanics Applied to Dams and Levees

Erosion in Geomechanics Applied to Dams and Levees

Edited by
Stéphane Bonelli

Series Editor
François Nicot

ISTE

WILEY

First published 2013 in Great Britain and the United States by ISTE Ltd and John Wiley & Sons, Inc.

Apart from any fair dealing for the purposes of research or private study, or criticism or review, as permitted under the Copyright, Designs and Patents Act 1988, this publication may only be reproduced, stored or transmitted, in any form or by any means, with the prior permission in writing of the publishers, or in the case of reprographic reproduction in accordance with the terms and licenses issued by the CLA. Enquiries concerning reproduction outside these terms should be sent to the publishers at the undermentioned address:

ISTE Ltd
27-37 St George's Road
London SW19 4EU
UK

www.iste.co.uk

John Wiley & Sons, Inc.
111 River Street
Hoboken, NJ 07030
USA

www.wiley.com

© ISTE Ltd 2013

The rights of Stéphane Bonelli to be identified as the author of this work have been asserted by him in accordance with the Copyright, Designs and Patents Act 1988.

Library of Congress Control Number: 2012955966

British Library Cataloguing-in-Publication Data
A CIP record for this book is available from the British Library
ISBN: 978-1-84821-409-5



Printed and bound in Great Britain by CPI Group (UK) Ltd., Croydon, Surrey CR0 4YY

Table of Contents

Foreword	xiii
Jean-Louis BRIAUD	
Introduction	xv
Stéphane BONELLI	
Chapter 1. State of The Art on the Likelihood of Internal Erosion of Dams and Levees by Means of Testing.	1
Robin FELL and Jean-Jacques FRY	
1.1. An overview of the internal erosion process as it affects dams and levees.	1
1.1.1. A description of the overall process.	1
1.1.2. The four mechanisms of initiation and progression of internal erosion	2
1.1.3. Concentrated leak erosion	6
1.1.4. Backward erosion	7
1.1.5. Contact erosion	8
1.1.6. Suffusion	9
1.2. Concentrated leak erosion	11
1.2.1. Situations where concentrated leaks may occur.	11
1.2.2. Estimation of crack width and depth of cracking	23

1.2.3. The mechanics of erosion in concentrated leaks	23
1.2.4. Commentary on the state of the art and the role of laboratory testing in assessing concentrated leak erosion	35
1.3. Backward erosion piping	37
1.3.1. The mechanics of backward erosion piping	37
1.3.2. Soils that are subject to backward erosion piping.	40
1.3.3. Methods available for assessing whether backward erosion piping will initiate and progress.	43
1.3.4. Some field observations	51
1.3.5. Global backward erosion.	52
1.3.6. Commentary on the state of the art and the role of laboratory testing in assessing backward erosion piping and global backward erosion	53
1.4. Suffusion	57
1.4.1. The mechanics of suffusion	57
1.4.2. Methods of identifying soils that are internally unstable and potentially subject to suffusion (geometric criterion)	58
1.4.3. Hydraulic conditions where soils are internally unstable and potentially subject to suffusion	69
1.4.4. Commentary on the state of the art and the role of laboratory testing in assessing suffusion	71
1.5. Contact erosion.	74
1.5.1. The mechanics of contact erosion.	74
1.5.2. Methods available to assess the likelihood of contact erosion	76
1.5.3. Contact erosion or “scour” at the interface between open joints in rock foundations and the core of dams	82

1.5.4. Commentary on the state of the art and the role of laboratory testing in assessing contact erosion	83
1.6. Bibliography	85
Chapter 2. Contact Erosion	101
Pierre PHILIPPE, Rémi BEGUIN and Yves-Henri FAURE	
2.1. Introduction	101
2.2. General presentation	103
2.2.1. Typical conditions of occurrence	103
2.2.2. Specific nature of CE	107
2.3. At sample scale: quantification of the CE threshold and kinetics	110
2.3.1. Influence of geometry on the occurrence of CE	111
2.3.2. Direct configuration	112
2.3.3. Inverse configuration	129
2.3.4. Summary	133
2.4. At pore scale: local hydrodynamics of CE and statistical modeling	134
2.4.1. Experimental characterization of local hydrodynamics	135
2.4.2. Integration at macroscopic scale	143
2.4.3. Contribution made by the local scale study	158
2.5. At hydraulic structure scale: identification of failure scenarios by CE and scale effects.	162
2.5.1. Reasons for a study at this scale	162
2.5.2. Description of the experimental rig and instrumentation	163
2.5.3. Test protocol and the results obtained	167
2.5.4. Proposed interpretation and description of the erosion process.	172
2.5.5. Scale effect	176
2.5.6. Summary	179
2.6. Conclusion and outlook	179
2.6.1. Description of CE mechanisms.	180

2.6.2. Impact on the safety of hydraulic structures	182
2.7. Bibliography.	186
Chapter 3. Backward Erosion Piping	193
Vera VAN BEEK, Adam BEZUIJEN and Hans SELLMER	
3.1. Introduction	193
3.2. Phases leading to failure due to backward erosion	197
3.2.1. Seepage	198
3.2.2. Backward erosion – initiation and progression	199
3.2.3. Widening	204
3.2.4. Failure	205
3.3. Backward erosion in the laboratory – overview and setup	206
3.3.1. Overview of experimental research	207
3.3.2. Setup	208
3.4. Backward erosion piping in the laboratory – erosion mechanism	214
3.4.1. Single grain transport	215
3.4.2. Sand boiling phase.	216
3.4.3. Regressive or equilibrium phase	217
3.4.4. Progressive phase	220
3.4.5. Which process will occur when?	221
3.5. Backward erosion in the laboratory – critical gradient	226
3.5.1. Initiation of backward erosion piping.	226
3.5.2. Progression of backward erosion piping	234
3.5.3. Progression of pipes for vertical seepage paths.	240
3.6. Analysis tools	245
3.6.1. Initiation of the pipe.	246
3.6.2. Progression of the pipe	250
3.6.3. Progression for structures.	256
3.6.4. Summary	258
3.7. From laboratory to field – challenges for the future	259

3.7.1. Scale effects	259
3.7.2. Heterogeneity	262
3.7.3. Uncertainties	263
3.8. Conclusion	264
3.9. Bibliography	264
Chapter 4. Concentrated Leak Erosion	271
Stéphane BONELLI, Robin FELL and Nadia BENAHMED	
4.1. Introduction	271
4.2. Theoretical background	275
4.2.1. Assumptions	275
4.2.2. The model for pipe flow with erosion	276
4.2.3. The singular head loss factor	278
4.2.4. The momentum loss factor	279
4.2.5. Characteristic values	280
4.2.6. Closed-form solution in the case of a constant pressure drop	281
4.2.7. Closed-form solution in the case of a constant flow rate	282
4.3. The HET: testing procedure	283
4.3.1. The HET apparatus	283
4.3.2. Preparation of the specimen	285
4.3.3. Determination of the final hole diameter	288
4.4. The HET: method of interpretation	289
4.4.1. Determination of the pipe radius and the wall shear stress	289
4.4.2. Determination of the friction coefficient	291
4.4.3. Determination of the head loss coefficient	292
4.4.4. Determination of the parameters of erosion	294
4.4.5. Examples of results	294
4.4.6. Slaking at upstream or downstream faces of sample of HET	296
4.5. Mechanically based relations for time to failure and peak flow	299
4.5.1. A simplified approach	299
4.5.2. Onset of erosion in the pipe	301

4.5.3. Visual detection of the leak	302
4.5.4. Enlargement of the pipe	303
4.6. Dam and levee break modeling.	307
4.6.1. Order of magnitude on case studies	307
4.6.2. A model for dam- and levee-break due to concentrated leak erosion	311
4.6.3. Application to the failure of a homogeneous moraine dam by piping	313
4.6.4. Model analysis.	317
4.7. Modeling concentrated leak erosion statistically	319
4.7.1. The probabilistic approach	319
4.7.2. The probability density function of the stress ratio.	321
4.7.3. Probabilistic description of erosion.	323
4.7.4. Order of magnitude of the relative intensity of the shear stress fluctuations.	325
4.7.5. Order of magnitude of the coefficient of variation of the soil critical stress.	326
4.7.6. A stochastic erosion law for cohesive soils.	327
4.8. Comments	329
4.8.1. Comment on the friction coefficient	329
4.8.2. Comment on the linearity of the erosion law.	333
4.9. Bibliography.	335
Chapter 5. Relationship between the Erosion Properties of Soils and Other Parameters	343
Robin FELL, Gregory HANSON, Gontran HERRIER, Didier MAROT and Tony WAHL	
5.1. Introduction	343
5.2. Definitions of soil erosion properties and the relationships between them	344
5.3. Effects of test methods on soil erosion properties.	346
5.3.1. Effect of testing methods on erosion rate	346

5.3.2. Effect of testing methods on critical shear stress (τ_c)	350
5.3.3. Correlation between critical shear stress and erosion rate index	353
5.4. Relationship to field performance	355
5.4.1. JET tests done in the laboratory and in the field	355
5.4.2. Assessment of rates of erosion from JET and large-scale laboratory tests	355
5.5. Effects of the type of soil	358
5.5.1. General trends	358
5.5.2. Relationship to soil classification	359
5.5.3. Effects of soil structure	360
5.6. Effects of compaction parameters	360
5.6.1. Relationship to compaction parameters	360
5.6.2. Relationship to degree of saturation after compaction	364
5.7. Effects of dispersivity and slaking	366
5.7.1. Effects of dispersivity on erosion rate and critical shear stress	366
5.7.2. Effects of slaking on erosion rate and critical shear stress	369
5.8. Modifications of soil erosion properties	371
5.8.1. Modification by lime	371
5.8.2. Modification by cement	376
5.9. Bibliography	376
List of Authors	383
Index	387

Foreword

In recent years, hydraulic and geotechnical engineers have displayed an increased interest in understanding soil erosion. The Technical Committee TC 213 on “Scour and Erosion” was initiated by the International Society for Soil Mechanics and Geotechnical Engineering (ISSMGE) to discuss scour processes and countermeasures in the geotechnical community, a topic that was primarily covered by hydraulic engineers.

TC 213 was instigated in 1997 as TC 33 “Scour of Foundations” under ISSMGE President Ishihara by Jean-Louis Briaud from Texas A&M University (College Station, USA) who held the chair from 1997 to 2009. In 2009, Jean-Louis Briaud was elected President of ISSMGE and the committee members chose Michael Heibaum of BAW in Germany as the next chair of TC 213.

The wide range of topics considered by TC 213 is covered and discussed during international biannual conferences, focused on the original goal of finding a combined geotechnical and hydraulic understanding of scour processes, while considering, as well, other consequences of the interaction between water, soil and rock.

The European Working Group on Internal Erosion (EWGIE) of the European Club of the International Committee on Large Dams (ICOLD) has dedicated considerable effort to better understand the physical processes and mechanics of internal erosion.

In 2008, it was decided during the meeting in Tokyo with Jean-Jacques Fry with EDF in France, who held the chair of the EWGIE from 2004 to 2012, to include the discussion of surface erosion and internal erosion in dams and levees within TC 213 activities. As a result, the ISSMGE biannual conferences on scour and erosion have included this special field since the 2010 conference in San Francisco.

Erosion is the cause of failure of the majority of dams and levees whether through internal erosion or external erosion. Consequently, understanding the erosion process is critical to understanding the performance of dams and levees. This is the wide scope of this book, which focuses on internal erosion and piping.

A handwritten signature in black ink, reading "Jean-Louis Briaud". The signature is written in a cursive style with a vertical line to its right.

Jean-Louis Briaud
President
International Society for Soil Mechanics
and Geotechnical Engineering
February 2013

Introduction

Erosion is the most common cause of failures in earth-dams, dikes and levees, whether through overtopping and overflowing, or internal erosion and piping. The failure of a river dike or levee, sea dike or levee, or embankment dam by internal erosion and piping may occur under high water levels due to high riverine discharges in the river; waves, storm surges and high tides in the sea; or due to high reservoir levels in the reservoir stored by a dam during a flood event. Internal erosion and piping may also occur as a result of cracking of the embankment or levee during an earthquake, or during normal operating conditions without an apparent triggering event.

The prediction of the initiation of erosion is very important. This involves the determination of the hydraulic head difference for the onset of erosion, given the mode of internal erosion; that is a concentrated leak, backward erosion piping, suffusion or contact erosion. Unique structure designs and site-specific conditions are always encountered, so this cannot be done reliably using empirical rules, and a fundamental knowledge of the internal erosion processes is necessary.

The warning time prior to breach is also very important for both evacuation plans and the assessment of the consequences of embankment failures. This is directly related to the rate of the progression of erosion. At present this time is often not taken into account when considering the safety of embankments because those involved are not aware of the methods which are available to assess the time from when an erosion may be detected and the dam or levee first breaches. This situation may lead to over-conservative designs on the one hand, or to unknowingly having high risks at the other hand. Over-conservatism is, in fact, a very important economical issue when geotechnical structures are applied at a large scale (e.g. in river and coastal defences), because of the the limited resources available to construct them.

An immediate conclusion that may be drawn is the need for fundamental understanding of the erosion processes and failure mechanisms. Although an old issue, this question remains open to date, and an intensive research effort has been made during recent decades to understand the problem.

Erosion is the removal of material caused by the eroding power of the flow. External erosion (overtopping and overflowing) is most often approached from the hydraulic viewpoint, whereas internal erosion and piping is considered in the geomechanics community.

This book deals with the phenomenon of internal erosion and piping within the framework of earth dams and flood defense structures (dikes and levees). It is not intended to be exhaustive on the subject, but it brings together some of the latest international research and advances. The emphasis is on physical processes, how well they can be studied in the laboratory, and how findings obtained can be applied to real levees and dams.

Internal erosion can lead to failure of levees and dams in different ways. There are four dominant mechanisms for a water-retaining structure or its foundation: suffusion, backward erosion, contact erosion and concentrated leak erosion. In Chapter 1, Robin Fell and Jean-Jacques Fry present the state of the art on the likelihood of the internal erosion of dams and levees by means of testing. They present an overview of the laboratory tests available, and discuss their usefulness and limitations.

In Chapter 2, Rémi Beguin, Yves-Henri Faure and Pierre Philippe describe the contact erosion process, where particles of a fine soil are pulled by a water flow through a coarse zone in contact with the fine zone. Such interfaces between two soils of different grain sizes are frequently encountered in real earth embankments where the occurrence of contact erosion is consequently suspected. At the sample scale, the threshold and the kinetics of contact erosion can be quantified due to specific devices in two configurations and with either cohesive or non-cohesive fine soils. At the large scale, scenarios can be identified to describe the consequences of contact erosion on overall behavior and integrity of an embankment structure based on several full-scale tests.

Vera van Beek, Adam Bezuijen and Hans Sellmeijer are the authors of Chapter 3. They deal with the backward erosion piping process, which can occur in the foundation of a water-retaining structure, where an impermeable cohesive layer overlies a sandy aquifer. Seepage through the aquifer can result in the erosion of sand grains, thereby forming shallow pipes, for which the cohesive cover layer forms a roof. This chapter contains a detailed description of the conditions that result in pipe development, based on experimental research, and a review of the design of experimental setups and test methods. A model for the analysis of the progression of backward erosion is explained

and the practical difficulties in applying results to real levees and dams are discussed.

Chapter 4, written by Nadia Benahmed, Stéphane Bonelli and Robin Fell, discusses the concentrated leak erosion process. Concentrated leak erosion involves the formation of a crack or concentrated leak directly from the source for water to an exit point. Erosion initiates along the walls of the concentrated leak. This chapter provides the salient features of the hole erosion test, and the latest breakthroughs in modeling the failure of an earth dam or a levee by concentrated leak erosion and piping.

In Chapter 5, Robin Fell, Gregory Hanson, Gontran Herrier, Didier Marot and Tony Wahl have discussed the relationship between the erosion properties of soils and other soil parameters. Recent advances and current controversies allow for a better understanding of the relationship between soil classification, compaction conditions, degree of saturation, and soil–water chemistry on the erosion properties of soils, that is erosion sensibility. This includes the erosion properties of treated soils (dispersive or non-dispersive) by adding lime.

This book integrates the results from several research projects in Australia, France, the Netherlands and the United States. Throughout the years, the Working Group of the European Club of the International Commission on Large Dams (ICOLD) devoted to *internal erosion in embankment dams* has brought the authors together.

The fact that there is no chapter on suffusion deserves a comment. Suffusion is the most controversial of the four processes of internal erosion and piping. This is a highly debated subject, and more research is needed before putting forward relevant methods and efficient tools for the analysis of earth dams and levees, well grounded in experiments and modeling.

In this book, our aim is to share the most recent findings in our field with students, researchers and practitioners. Understanding the failure of an earth dam or a levee by erosion in a unified framework, be it internal erosion or surface erosion, requires continuous research in this field. We hope that the reader finds in this book a key for further progress in the challenging field of the safety of levees and dams.

To conclude, I wish to warmly thank the authors of these chapters, who have generously offered their time and shared their expertise in the writing of this book.

Chapter 1

State of The Art on the Likelihood of Internal Erosion of Dams and Levees by Means of Testing

1.1. An overview of the internal erosion process as it affects dams and levees

1.1.1. A *description of the overall process*

Failures and incidents by internal erosion of embankment dams and their foundations are categorized into the following four general failure modes:

- 1) Internal erosion associated with through-penetrating structures, such as conduits associated with outlet works, spillway walls or others adjoining a concrete gravity structure supporting the embankment;
- 2) Internal erosion through the embankment;
- 3) Internal erosion through the foundation;

4) Internal erosion of the embankment into or at the foundation; including seepage through the embankment eroding material into the foundation or seepage in the foundation at the embankment contact eroding the embankment material.

The process of internal erosion and piping may be broadly classified into four phases:

- 1) initiation of erosion;
- 2) continuation of erosion;
- 3) progression to form a pipe;
- 4) initiation of a breach.

This is shown in Figure 1.1(a) for internal erosion through the embankment initiated by a concentrated leak. Similar processes apply for piping through the foundation, and from the embankment to the foundation, are shown in Figure 1.1(b) and 1.1(c).

When assessing the safety of a dam and its foundation for internal erosion using engineering judgment or risk assessment methods, it is useful to consider it through eight stages as detailed in Table 1.1.

This chapter focuses on the initiation and progression phases of the internal erosion process of affected dams and levees. For a discussion of other phases see ICOLD [ICO 12] and Fell *et al.* [FEL 05].

1.1.2. The four mechanisms of initiation and progression of internal erosion

The first condition for internal erosion to occur is particle detachment. Water seeping through the soil in the dam or flowing in cracks or concentrated leaks must be doing so

with sufficient velocity to provide sufficient energy to detach particles from the soil structure. The nature of the soil in the dam determines its vulnerability to erosion. Three classes have to be distinguished:

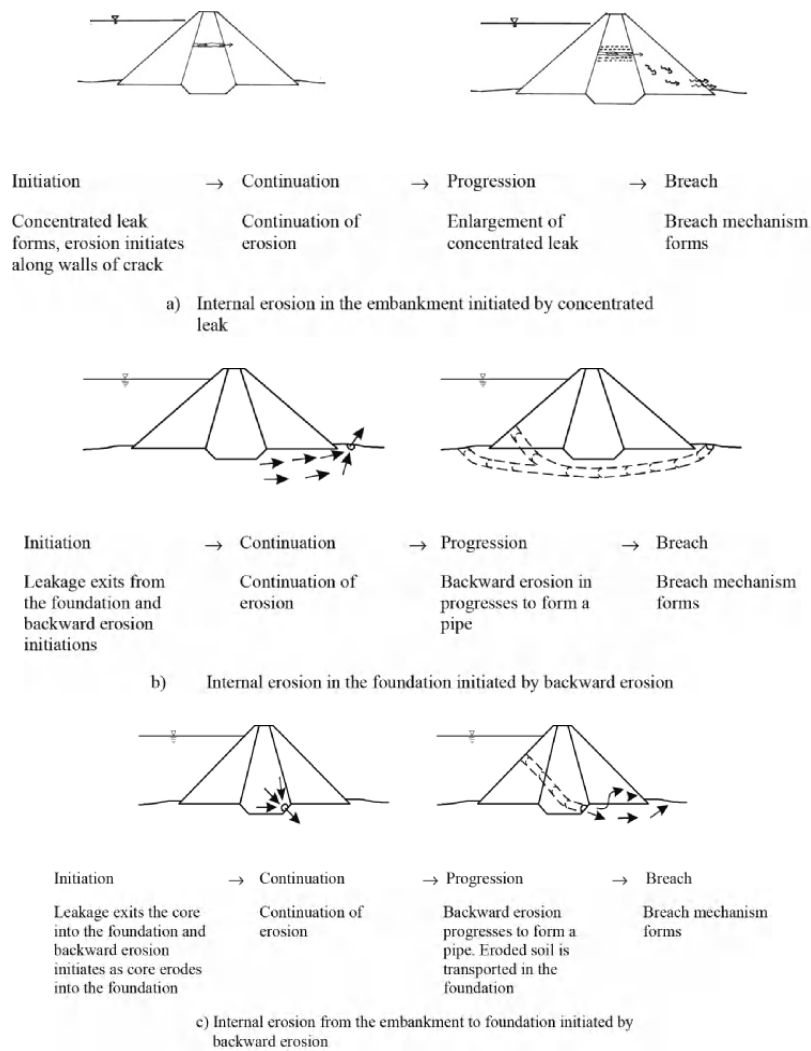


Figure 1.1. Models for the development of failure by internal erosion [FOS 99b]

4 Erosion in Geomechanics Applied to Dams and Levees

1) Non-plastic soils such as silts, sands, silty sands, and silt, sand, gravel soils. These collapse when saturated under flooding; will not sustain a crack when saturated, and are relatively easily eroded. As non-plastic soils become coarser through silts, sands, gravels and cobbles they progressively require more energy to initiate erosion. Erosion resistance is related to particle weight. It may be related to the stress state, and involves the detachment of individual particles. These soils are subject to backward erosion, contact erosion or suffusion depending on their particle size distribution.

Steps	Matters to be considered
1. Loading	<i>Hydrostatic or reservoir loads:</i> frequent water level, rare flood and dam safety flood
	<i>Seismic:</i> a range of loading including operating basis earthquake (OBE) and maximum design earthquake (MDE)
2. Location of initiation of erosion	<i>Embankment:</i> upper portion, lower portion, along conduit and adjacent wall
	Over changes in slope in the cross-valley foundation profile and at construction features such as haul roads and river closure sections
	<i>Foundation:</i> valley and abutment
	<i>Embankment to foundation:</i> valley and abutment
3. Initiation	<i>Erosion mechanism:</i> concentrated leak, backward erosion, contact erosion and suffusion
	Whether erosion will initiate under the seepage gradients
4. Continuation (Filtration)	Assess whether filters, transition zones or downstream zones will prevent erosion continuing
	<i>Particle size methods:</i> this can provide no erosion, excessive erosion and continuing erosion limits. If there is no filter, erosion will continue
	Equivalent opening size methods
	Permeability-based methods

Table 1.1. *The eight steps of the framework for assessment of internal erosion for a dam adapted from Fell and Fry [FEL 07]*

5. Progression	For concentrated leak and contact erosion:
	Will a developing pipe stay open?
	Upstream and downstream flow limitation taking into account erosion properties
	For backward erosion and suffusion:
	Is the critical gradient or velocity reached for erosion to progress?
6. Detection	Piping process
	Monitoring type and frequency
	Surveillance frequency
7. Intervention	Piping process
	Personnel availability and training
	Equipment and materials availability
	Weather and the impacts of flooding on access
	The erosion rate and its impact on the time to available intervene
	Whether the reservoir can be drawn down in time to prevent breach
8. Breach	Gross enlargement of the pipe
	Overtopping
	Slope instability of the downstream slope
	Unraveling of the downstream face
	Static liquefaction

Table 1.1. (Continued) *The eight steps of the framework for assessment of internal erosion for a dam adapted from Fell and Fry [FEL 07]*

2) Plastic soils, such as clays, clayey sands and clayey sandy gravels are generally more resistant to erosion than cohesionless soils. These soils are subject to concentrated leak erosion and contact erosion. Clay soils will hold a crack even when saturated. Higher energy is generally required to detach particles from cracks or concentrated leaks within a cohesive fill, but the particles thus removed are small and easily carried through the crack. Erosion resistance is related to contact forces between the water flowing in the crack or concentrated leak, and the soil on the sides of the crack.

- Backward erosion and suffusion cannot occur in these soils under the gradients normally experienced in dams and levees and their foundations. It may occur if local gradients are very high, however.

3) Dispersive plastic soils are soils in which, because of their clay mineralogy and the water chemistry, erosion will initiate in cracks or concentrated leaks under very low hydraulic stresses and gradients.

Initiation of erosion occurs in four mechanisms, which are described in the following sections.

1.1.3. Concentrated leak erosion

Concentrated leak erosion in a dam, levee or its foundation may occur through a crack or hydraulic fracture caused by differential settlement during construction of the dam or levee or in operation, hydraulic fracture due to low stresses around conduits or in the upper parts of the dam due to differential settlement, or through desiccation at high levels in the fill.

Cracks or other continuous open paths for water may occur because of the collapse of settlement of poorly compacted fill in the embankment, around conduits and adjacent walls. They may also occur due to the action of animals burrowing into levees and small dams and tree roots rotting in the dam and forming a hole.

Given there is a crack, the geometrical and hydraulic conditions within the crack and the resulting hydraulic forces imposed on the sides of the crack determine whether the water flowing through the crack will initiate erosion.

The erosion will progress to form a pipe unless:

1) the soil will not hold open the pipe (“it will not hold a roof”);

2) there are upstream or in some cases downstream zones that will limit the hydraulic gradient and the erosion process is limited;

3) there are filters that are effective in stopping the erosion process;

4) the water flowing through the crack causes the soil on the sides of the crack to swell, closing the crack or reducing the width so the forces imposed on the sides of the crack by the water flowing through the crack are insufficient for erosion to progress.

1.1.4. Backward erosion

There are two types of backward erosion [ICO 12]:

– *Backward erosion piping*: This mainly occurs in foundations as in Figure 1.2 but may occur within embankments. The erosion process begins at a free surface on the downstream side of a dam or levee. This free surface may be in a ditch or other excavation penetrating into the eroding cohesionless soil or may form by first heaving of the cohesive strata overlying the cohesionless soil. The process progresses beneath the levee or dam. For this to occur, the levee or dam, or the cohesive strata, must form a roof for the eroding “pipe”. The presence of backward erosion piping is often exhibited by the presence of sand boils at the downstream side of the dam or dike. Backward erosion piping occurs where critically high hydraulic gradients at the toe of a dam erodes particles upward and backward below the dam through small erosion channels and flow velocity can transport the eroded particles downstream.

– *Global backward erosion*: This leads to the development of a near vertical pipe in the core of an embankment as shown in Figure 1.3.

8 Erosion in Geomechanics Applied to Dams and Levees

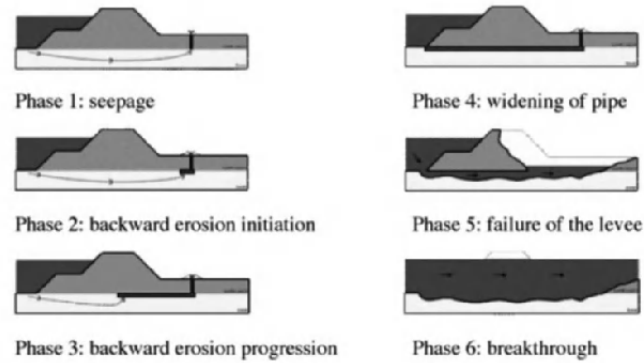


Figure 1.2. *Backward erosion piping model [SEL 11]*

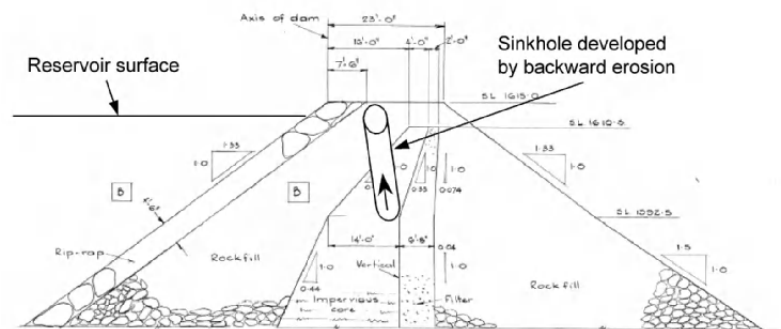


Figure 1.3. *Global backward erosion potentially leading to formation of a sinkhole*

1.1.5. Contact erosion

Contact erosion occurs where a coarse soil such as a gravel is in contact with a fine soil, and flow parallel to the contact in the coarse soil erodes the fine soil. For example, flow through gravel alluvium in the foundations of a dam or a dike may erode the base of an overlying silt layer, or erosion of the finer layers of soil in a core may occur into a coarse gravelly layer formed by segregation during construction as shown in Figure 1.4.

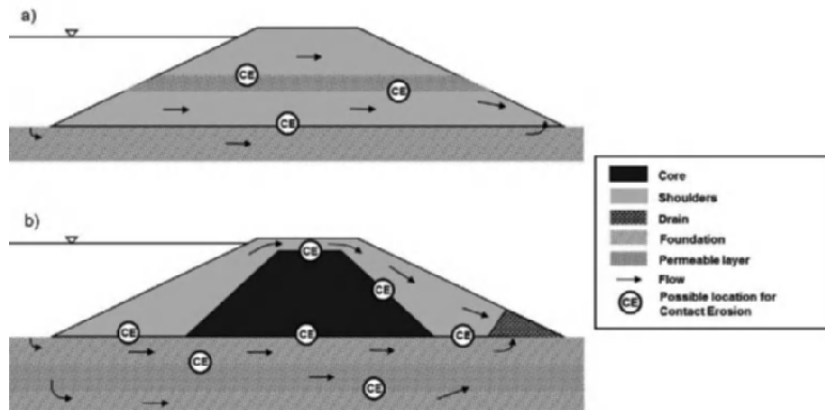


Figure 1.4. Possible location of contact erosion initiation: a) homogeneous dam with layered fill due to segregation during construction and a coarse foundation soil; b) zoned dam with potential for contact erosion at high reservoir levels above the core and for erosion into coarse layers in the foundation [BEG 09]

1.1.6. Suffusion

Suffusion occurs when water flows through widely graded or gap-graded cohesionless soils such as alluvium of a large river, colluvium in the bed of rivers in mountainous areas, embankment cores constructed of glacial origin soils and in filters which have very broad or gap gradings or excessive fines content.

The small particles of soil are transported by the seepage flow through the pores of the coarser particles. The coarser particles are not transported and the effective stresses are largely transferred through the matrix of the coarser particles. Movement of particles occurs throughout the soil, not just from the downstream surface as in backward erosion.

For suffusion to occur, the following three criteria: geometric criterion, stress criterion and hydraulic criterion, have to be satisfied:

1) *Criterion 1*: the size of the finer soil particles must be smaller than the size of the constrictions between the coarser particles, which form the basic skeleton of the soil.

2) *Criterion 2*: the amount of finer soil particles must be less than enough to fill the voids of the basic skeleton formed by the coarser particles. In such a matter, the effective stresses are transferred by the coarser particles only. In consequence, some fines particles are not confined and are free to move.

3) *Criterion 3*: the velocity of flow through the soil matrix must impose a high enough stress to overcome the particle weight of the finer soil particles and to move them through the constrictions between the larger soil particles.

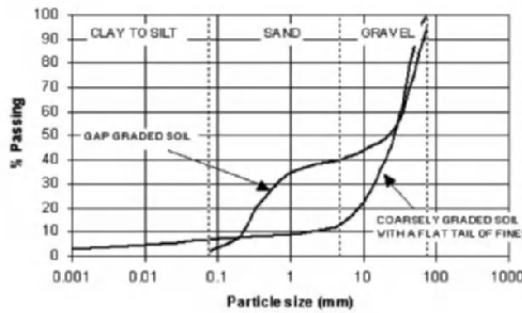


Figure 1.5. Soil gradation types which are potentially internally unstable and susceptible to suffusion

Figure 1.5 shows how the “finer soil” fraction is defined, in this case, as the point of inflection of the particle size distribution plot. Experiments may also determined the percentage of finer fraction which gives the maximum density, that is which just fills the voids in the coarser fraction. Soils with more finer fraction are over-filled, those with less are under-filled and subject to suffusion: they are termed internally unstable.

1.2. Concentrated leak erosion

1.2.1. *Situations where concentrated leaks may occur*

1.2.1.1. *Internal erosion associated with conduits embedded in the embankment*

Many internal erosion and piping failures and incidents occur where conduits are embedded in the embankment. The conduit facilitates the initiation of internal erosion by following ways:

1) By causing stress distributions due to the stiff conduit and its less stiff surrounding soil, which lead to low principal stresses and hydraulic fracture. This is discussed by Sherard *et al.* [SHE 72] and Charles [CHA 97]. This can occur on the sides of culverts that are constructed in a trench. Sherard *et al.* [SHE 72] point out that it can also occur where the concrete culvert, or concrete surround around a pipe, has a sharp corner. In this case, piping can be expected above the culvert.

2) Drying of the soil in sides of the trench in which the culvert is placed during construction can also cause cracks which allow initiation of piping.

3) By making the compaction of soil difficult, particularly if collars are provided at close intervals or the concrete is formed with a corrugated steel sheet or other non-smooth formwork, preventing compaction of the soil adjacent to the conduit. It can also be difficult to compact the soil surrounding the conduit if the space between the conduit and the sides of the trench in which it is placed is small and compaction by rollers is not possible.

4) Poor compaction is likely to lead to collapse settlement of the soil on saturation forming a gap adjacent to the conduit. Note that it is the continuity of the potential defect caused by a conduit and the excavation through the dam which is so critical to the initiation of internal erosion;

5) Leaks or deterioration by aging of the conduit.

Internal erosion may also occur in open joints or other defects in conduits or into conduits which have deteriorated due to corrosion or have cracked after differential settlements.

FEMA [FEM 06] “Conduits through embankment dams: best practices for design, construction, problem identification and evaluation, inspection, maintenance, renovation and repair” provides a comprehensive coverage of the issues relating to conduits in embankment dams. Fell *et al.* [FEL 08] provide some guidance on how to assess the likelihood of these features leading to initiation of erosion.

1.2.1.2. *Cracking and hydraulic fracture due to cross-valley differential settlement of the core*

As an embankment dam is constructed the partially saturated compacted soil in the embankment consolidates and settlement occurs. Where the valley sides are steep and/or have steps in the profile, such as shown in Figure 1.6, differential settlements occur due to the variations in the height of the embankment, and these can lead to tensile or low-stress zones in which cracks may form. This has been recognized for some time by Sherard [SHE 73, SHE 85, SHE 86], Høeg *et al.* [HOE 98], Kjaernsli *et al.* [KJA 92] and others. Hydraulic fracture through these low-stressed zones as the dam is filled or under flood conditions is an associated phenomenon as discussed by Sherard *et al.* [SHE 72] and Sherard ([SHE 85], [SHE 86]). For most dams, approximately 80 – 90% of the total settlement occurs during construction [HUN 03a, HUN 03b], so the stresses set up in the construction phase largely control the likelihood of low-stress zones and cracking. It should be recognized that these stresses are inevitable even in well-designed and constructed dams and are not caused by poor design or construction practice.

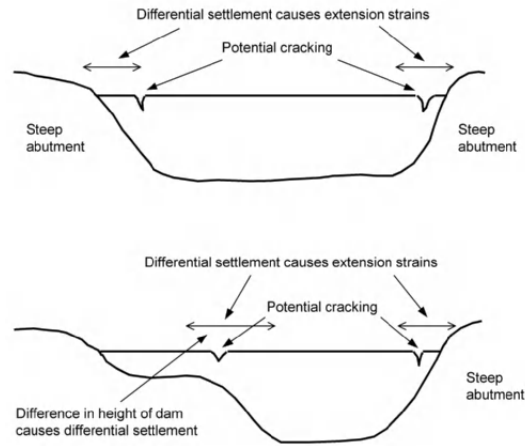


Figure 1.6. Situations in which cross-valley differential settlement may lead to cracking or extension strains and low-stress zones subject to hydraulic fracture

Embankments with abutments steeper than approximately 45° and particularly steeper than 60° are likely to be susceptible to cracking. Embankments with a step in the foundation profile where the height of the embankment above the step is less than half the maximum embankment height and the width of the step is greater than the lower embankment are also susceptible to cracking.

1.2.1.3. Cracking and hydraulic fracture due to cross-valley arching

If the valley in which the dam is constructed is narrow and steep, cross-valley arching can occur and the vertical stresses are shed onto the sides of the valley. This can lead to a situation where hydraulic fracture can occur. Fell *et al.* [FEL 08] suggest that cross-valley arching is most likely to occur if the width of the valley base is less than a quarter of the dam height, and the valley sides are steeper than approximately 60° . It is unlikely to be an issue if the width of the valley base is greater than three quarters the dam height and the valley sides are flatter than 45° .

1.2.1.4. Cracking and hydraulic fracture due to differential settlement in the foundation under the core

Figure 1.7, adapted from Sherard *et al.* [SHE 63], shows the foundation conditions that are likely to lead to differential settlement and cracking or low-stress zones conducive to hydraulic fracture. Zones which may lead to differential settlement greater than 0.5% of the dam height, with steep changes in the foundation profile, are most likely to suffer cracking and hydraulic fracture. Differential settlements of less than 0.2% of the dam height spread over some distance are unlikely to lead to cracking and low-stress zones.

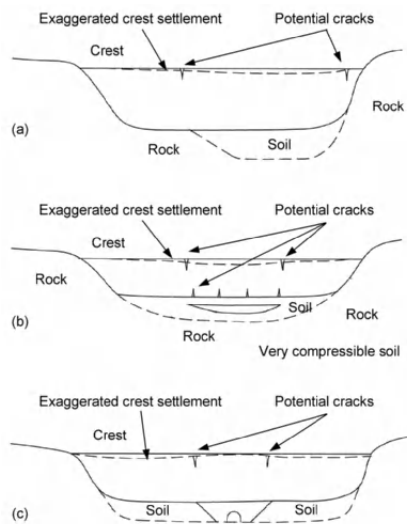


Figure 1.7. Situations which may cause differential settlement in the foundation of dams leading to cracking, lateral strains and low-stress zones subject to hydraulic fracture ([FEL 08] based on [SHE 63])

1.2.1.5. Cracking and hydraulic fracture due to small-scale irregularities in the foundation profile under the core

Small-scale irregularities in the foundation of the core can lead to cracking or low stresses conducive to hydraulic

fracture, e.g. NGI [NGI 84]. For cracking or low stresses to occur the small-scale irregularities need to be persistent over all or most of the distance across the core, and have steps greater than approximately 3 – 5% of the embankment height. There are examples of these irregularities being formed by constructing haul roads across the core [NEW 06], and steps in slope correction concrete [GIL 07].

1.2.1.6. *Cracking and hydraulic fracture due to arching of the core onto the shoulders of the embankment*

As detailed in Bui *et al.* [BUI 04, BUI 05] and Fell *et al.* [FEL 08], this is most likely to be a problem for cores with a very narrow width of less than 0.25 the embankment height, and for soils subject to collapse compression on saturation (poorly compacted soil, placed dry, of optimum moisture content). It is unlikely to be a problem for cores that are wider than 0.5 – 1.0 the embankment height and the core is well compacted at around the optimum moisture content. It is not sufficient to cause hydraulic fracture to just have stiff shoulders and a less stiff core. There needs to be differential movement of the core after construction.

1.2.1.7. *Crack or gap adjacent to a spillway or abutment walls and where concrete dams abut embankment dams*

Cracking or a gap may form adjacent to walls due to the earthfill settling away from the wall during and after construction. Figure 1.8 shows some situations where this is likely to occur. Well-designed walls with uniform contact slopes flatter than approximately 0.25H:1V are unlikely to have gaps form. Vertical or over-hanging walls are likely to have gaps. Cracking and gaps may form due to deformations of flexible and/or under-designed retaining walls (e.g. designed for active rather than at-rest earth pressures). Where there is a wrap-around junction between a concrete gravity dam and an embankment dam, differential settlements similar to those described above may occur. For more details, see Fell *et al.* [FEL 08].

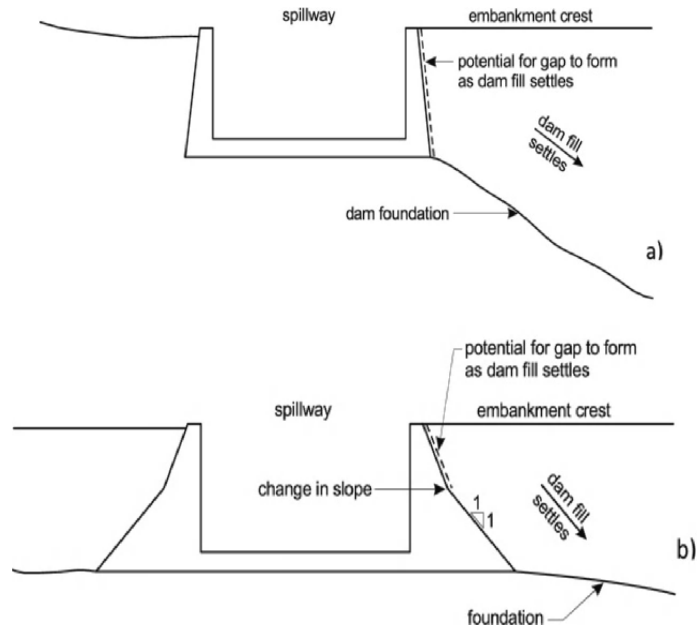


Figure 1.8. Situations where a gap may form between the dam fill and spillway wall: a) steep foundation adjacent spillway wall; b) change in slope of the retaining wall [FEL 05]

1.2.1.8. Crack, hydraulic fracture or openings in poorly compacted and/or segregated layers in the embankment

It is well documented (e.g. Sherard [SHE 73], Foster *et al.* [FOS 00]) that internal erosion and piping occurs in poorly compacted cohesive soils (often also more than 2% dry of the optimum). This is particularly so for dispersive soils. The mechanism is potentially of two types:

- 1) The soil behaves as a series of clods with openings between the clods in which water passes.
- 2) The soil collapses on saturation forming a flaw (open pathway) in which the water flows.

This is most likely where there is poorly compacted soil against a conduit but is possible within layers of soil.

Sherard [SHE 73] gives examples of this. The authors are aware of cases where a gap has been seen in test pits and/or zero Cone Penetration Test cone resistance value occurs just below the phreatic surface. This has been caused by the settlement of the soil in the saturated zone and the arching of the unsaturated soil over this. In these cases, the gap may be a pathway for water at reservoir levels greater than the historic high.

There are examples where it appears, a crack may form adjacent to a conduit due to freezing and differential movements even if the soil is well compacted.

The large number of sinkhole incidents experienced in Swedish central core earth and rockfill dams [NIL 07a, NIL 07b] constructed with broadly graded glacial till cores may be initiated mainly by the formation of openings due to collapse settlement on wetting of the core and possibly the segregation of the 800 mm thick layers.

Broadly graded glacial soils have been widely used as impervious cores of dams, and this type of material is relatively similar throughout the world with typical gradings (Figure 1.9).

The fines are mostly non-plastic except for some of the tills from west and central Canada. Ravaska [RAV 97] tested soil samples (taken from existing Finnish earth dams, for example, Uljua dam) by performing erodibility pinhole tests and showed that a more rapid erosion rate occurred for moraines than clays. Wan and Fell [WAN 04c] also showed that glacial till had a very rapid erosion rate and low critical shear stress. Ravaska [RAV 97] found that the eroded material in the tested soils was predominately of coarse-silt and fine-sand fractions, which should be taken into account when designing filters to prevent erosion as is recommended in the Sharrsd and Dunnigan [SHR 89] method.

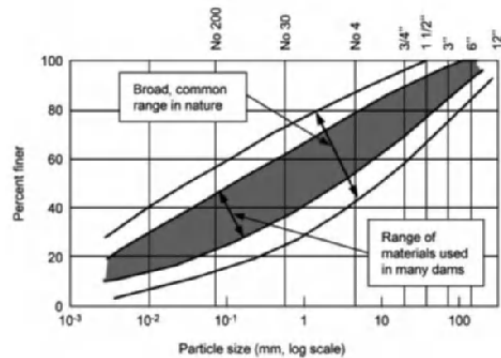


Figure 1.9. Typical widely and broadly graded glacial soils used as impervious cores in dams [SHE 89]

No-erosion tests (NEF-test) on the coarser parts of glacial moraine showed that, under relatively low gradients, large erosion tunnels developed with gravel particles that formed roofs over the tunnels [SHE 89, RON 10].

1.2.1.9. Cracking due to desiccation

Desiccation cracking is most likely to be an issue in climates with less than 250 mm annual rainfall, in high plasticity cores and where there is no surface layer over the core. Experience in excavating into the crest of embankments is that if there is a road pavement of granular road base or a rockfill or other non-plastic layer of at least 300 mm thick, then cracking is not generally observed even in seasonal climates with extended dry periods. The likelihood of cracking is further reduced if the road pavement is sealed with asphalt, concrete or bitumen seal.

Desiccation cracking does not commonly persist to a great depth so only becomes an issue for reservoir levels nearing the crest level.

Desiccation cracking may also occur on seasonal shut down surfaces during construction, or on the surface of the

first stage of dams which are built in two stages. Good construction practice would be to remove the desiccated soil but this was not always done. Desiccation cracking may also occur in soil exposed to drying during construction particularly if it is compacted very wet.

1.2.1.10. *Transverse cracking caused by settlement during earthquakes*

When embankment dams experience a large earthquake they often settle and spread in the upstream–downstream direction. Many exhibit longitudinal cracking and some transverse cracking. Some examples are the Austrian Dam [HAR 91, FOR 98], the Guadalupe dam [HAR 91] and James J. Lenihan dam [FON 95]. Pells and Fell [PEL 02, PEL 03] analyzed case data for dams not subject to liquefaction which showed that dams which settled more than approximately 1.5% of their height were almost certain to exhibit transverse cracks; those which settled between 0.5% and 1.5% had approximately a 20% chance of exhibiting transverse cracks; and dams which settled between 0.2% and 0.5% had approximately a 5% chance of transverse cracking.

These cracks are in the upper part of the embankment and whether they are a potential initiator of internal erosion depends on the reservoir level and depth of cracking.

If liquefaction occurs the deformations are likely to be large and the likelihood of cracking greater. These may be estimated by numerical analyzes methods.

1.2.1.11. *Cracking or high-permeability layers due to freezing*

The effects of frost on embankment dams are described in Vuola *et al.* [VUO 07]. The effects of frost are to cause extra water to be drawn into the soil by capillary action. This causes water pumping and ice lenses to form with associated heave and potentially cracking and/or loosening of the soil. The cracking is most likely to be longitudinal but may also

be transverse at the crest of the dam. Figures 1.10, 1.11 and 1.12 show the potential effects.

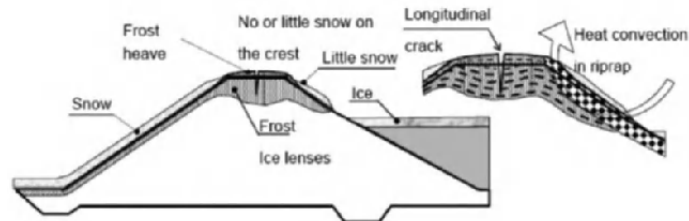


Figure 1.10. *Effects of frost on an embankment dam [VUO 07]*

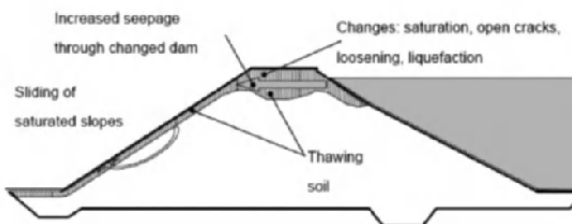


Figure 1.11. *Damage phenomena occurring in embankment dams from frost thaw [VUO 07]*

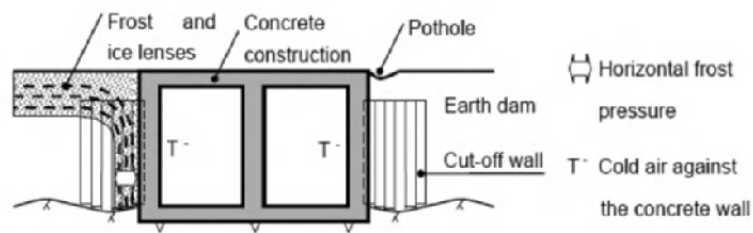


Figure 1.12. *Effect of frost against a spillway structure [VUO 07]*

Vuola *et al.* [VUO 07] provide an equation for estimating the depth of frost penetration. There are a number of references which provide information on the susceptibility of

soils to frost penetration. These include Wallace [WAL 87], Holtz and Kovacs [HOL 81], Vuola *et al.* [VUO 07] and USACE [USA 56] giving the most specific data. Core materials that are most susceptible to freezing and ice lens formation include silts, clayey silts, silty sands, silty gravels and clayey sands and gravels with a plasticity index < 12 .

1.2.1.12. *Internal erosion initiated by the effects of animal burrows and vegetation*

Animal burrows in the embankment or levee can lead to a situation where there are nearly continuous holes through the embankment, or situations where high gradients between holes may result in the initiation of erosion.

The FEMA report [FEM 05a], Impacts of animals on earthen dams, FEMA Report 473, provides a comprehensive coverage of the issues.

Vegetation growing on dams and levees can lead to situations which may lead to a potential concentrated leak and initiation of erosion. The effects include:

- 1) decaying roots that create seepage paths;
- 2) roots penetrating into open joint and cracks in foundation rock, potentially creating seepage paths;
- 3) root penetration of conduit joints and joints in concrete structures and opening the joints to allow erosion into or out of the conduit or wall.

The FEMA report [FEM 05b], Technical manual for dam owners, impacts of plants on earthen dams, FEMA Report 534, provides information and guidance on how to manage this problem.

1.2.1.13. *Internal erosion initiated by “canalicules” or other holes in residual soils*

The macrostructure of residual soils generally controls the permeability. In saprolites, relic structures (joints, bedding

planes and quartz veins), root holes and holes formed by insects and other creatures are often predominant paths of flow for water seepage.

Another factor affecting the permeability of some tropical residual soils is their cemented structure that creates big particles, big voids and numerous micro-tunnels, called “canalicules”. These features generate greater permeability than those typical of soils with similar grain size distribution [ICO 10].

Insects, mainly termites, have generated in some deposits large diameter holes, which can act as preferential flow paths. Besides leading to high seepage flow, this condition can lead to piping in the first few meters of the dam foundation. This feature has been in evidence in the Amazon region of Brazil, where this specific type of features have been called “Canaliculi”. The tubes or galleries have been found to range from a few millimeters to 20 cm. De Mello *et al.* [VER 88] described problems with termite channels in the foundations of a 30 m high earth dam. “Canaliculi” or biologically worked soils have been encountered at the following dam sites: Tucuruí, Vereda Grande, Balbina, Samuel and Kararao [DEM 85]. Both phenomena lead to numerous failures of small dams in dry, tropical, Africa (see Figure 1.13).

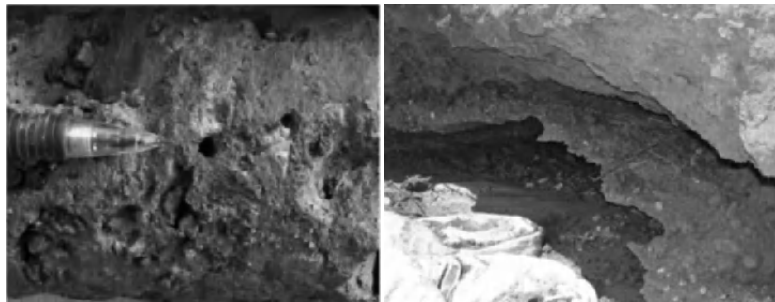


Figure 1.13. *Canalicules and Failure of a small dam caused by canalicules in Burkina-Fasso (Courtesy of Photo J-J Fry)*

1.2.2. Estimation of crack width and depth of cracking

The width and depth of cracks or hydraulic fractures, which can be present in the embankment, may be estimated using methods detailed in Fell *et al.* [FEL 08]. These are based on a review of the literature on observed cracking, including Sherard [SHE 73], Talbot [TAL 94] and Lawrence [LAW 02], and the results of numerical modeling by Bui *et al.* [BUI 04, BUI 05] which assists in assessing the likely depth of cracking. The values estimated by these methods are very approximate.

To model collapse settlement of poorly compacted layers it is most practical to assume a crack or continuous pathway is formed, as well as estimate the width of the crack from the knowledge of the thickness of the poorly compacted layer and the estimated amount of collapse settlement of the layer. This procedure is described by Fell *et al.* [FEL 08] who include tables relating the likely amount of collapse settlement related to the degree of compaction and compaction moisture content relative to optimum moisture content.

Lawton *et al.* [LAW 92] describe some laboratory tests to assess the amount of collapse settlement as related to the degree of compaction and applied stress.

1.2.3. The mechanics of erosion in concentrated leaks

1.2.3.1. The procedure

The procedure for assessing whether erosion will initiate in a crack or hydraulic fracture is carried out by:

- 1) estimating the hydraulic shear stresses in the crack for the reservoir level under consideration, taking account of the geometry of the core of the embankment and the assumed crack dimensions and location relative to the reservoir surface so the flow gradient can be determined;

2) comparing this hydraulic shear stress to the critical shear stress which will initiate erosion for the soil in the core of the embankment (τ_c) at the degree of saturation of the soil on the sides of the crack. In doing this, take account of the dispersion properties of the soil and the chemistry of the seepage water.

There is always some uncertainty regarding the input parameters so the analysis should check the sensitivity to the assumptions made.

1.2.3.2. *The estimation of hydraulic shear stresses in cracks and pipes*

Wan [WAN 06], Wan and Fell [WAN 02, WAN 04a, WAN 04b] and Fell *et al.* [FEL 08] give details on how to estimate the hydraulic shear stresses in cracks and cylinders. These may be used to determine the hydraulic shear stress in a crack or erosion pipe for the reservoir level under consideration, taking account of the geometry of the core of the embankment and the assumed crack dimensions and location relative to the reservoir surface so the flow gradient can be determined.

They give the following equations for estimating the hydraulic shear stress on the surface of a cylindrical pipe, or parallel-sided transverse crack in an embankment. The assumptions are as follows:

- 1) Linear head loss from upstream to downstream;
- 2) Steady uniform flow along the crack;
- 3) Uniform frictional resistance along the surface of the crack or cylindrical pipe;
- 4) Driving force = frictional resistance.

$$1) \quad \text{Cylindrical pipe:} \quad \tau = \rho_w \frac{gH_f d}{4L}$$

$$2) \quad \text{Vertical transverse crack} \quad \tau = \frac{\rho_w gH_f^2 W}{2(H_f + W)L}$$

where τ = hydraulic shear stress in N/m²;
 ρ_w = density of water in kg/m³;
 g = acceleration due to gravity = 9.8 m/s²;
 H_f = head loss in pipe or crack due to friction in meters;
 L = length of pipe or crack in meters;
 d = diameter of the pipe in meters;
 W = width of crack in meters.

1.2.3.3. Erosion properties of soils in the core of embankment dams: basic principles

It is important to reiterate that the resistance to initiation of erosion of the core to concentrated leak erosion is characterized by the critical shear stress, and the rate of enlargement of the pipe in the progression phase is characterized by the erosion coefficient. The erosion law (see Table 1.2) is expressed in terms of volume erosion by Hanson [HAN 90] or of mass erosion by Wan and Fell [WAN 02].

Erosion law	Volume	Mass
	$\epsilon_r = k_d(\tau - \tau_c)$ [1.1]	$\epsilon_i^* = C_e(\tau - \tau_c)$ [1.2]
Erosion rate per unit area	ϵ_r (m ³ /s/m ²)	ϵ_i^* (kg/s/m ²)
Shear stress	τ (N/m ² or Pa)	
Critical shear stress for initiation of erosion	τ_c	
Erosion or erodibility coefficient	k_d (m ³ /N/s)	C_e (s/m)

Table 1.2. Erosion laws in terms of volume and mass

The erosion properties of soils for concentrated leak erosion can be determined by rotating cylinder tests

[ARU 83, CHA 86a, CHA 86b, LIM 06, LIM 10]; Slot Erosion Tests (SET) and the Hole Erosion Tests (HET) [WAN 06, WAN 02, WAN 04a, WAN 04b, BON 07]; and Jet Erosion Tests (JET) [HAN 90, HAN 91, HAN 04]. These tests allow determination of the critical shear stress for the initiation of erosion and the erosion rate. At the time of writing the most widely used tests are the HET and JET.

Wan and Fell [WAN 02, WAN 04a, WAN 04b] and Wan [WAN 06] expressed the erosion rate in the form of an erosion rate index, I_{HET} , defined by:

$$I_{\text{HET}} = -\log_{10}(C_e)$$

The representative erosion rate index \check{I}_{HET} is the hole erosion index I_{HET} for soil compacted to a density ratio of 95% of standard maximum dry density at the optimum moisture content.

Soils can be classified into six groups according to their representative erosion rate index, \check{I}_{HET} . The six groups are shown in Table 1.4. Note that this is a logarithmic scale and the rate of erosion of soils varies by up to five orders of magnitude. In the absence of laboratory test values, the representative erosion rate index (\check{I}_{HET}) can be related approximately to soil properties. Table 1.4 has been developed from test data to give a first approximation to the likely range of \check{I}_{HET} for different classifications of non-dispersive soils.

Group No.	Erosion rate index	Description
1	< 2	Extremely rapid
2	2–3	Very rapid
3	3–4	Moderately rapid
4	4–5	Moderately slow
5	5–6	Very slow
6	> 6	Extremely slow

Table 1.3. *Descriptors for erosion rates of soils [WAN 06]*

Unified soil classification	Erosion rate index (I_{HET})		
	Likely minimum	Best estimate	Likely maximum
SM with < 30% fines	1	< 2	2.5
SM with > 30% fines	< 2	2–3	3.5
SC with < 30% fines	< 2	2–3	3.5
SC with > 30% fines	2	3	4
ML	2	2–3	3
CL-ML	2	3	4
CL	3	3–4	4.5
CL-CH	3	4	5
MH	3	3–4	4.5
CH with liquid limit < 65%	3	4	5
CH with liquid limit > 65%	4	5	6

Notes: (1) Use best estimate value for best estimate probabilities. Check the sensitivity if the outcome is strongly dependent on the results; (2) For important decisions carry out HET, rather than relying on this table which is approximate.

Table 1.4. *Representative erosion rate index (I_{HET}) versus soil classification for non-dispersive soils based on Wan and Fell [WAN 02]*

For non-dispersive soils the critical shear stress is related to the erosion rate index. Figure 1.14 shows the data from a number of tests. Wan and Fell [WAN 02] use the term “initial shear stress” to define the critical shear stress determined by varying the head in the HET. It will be noted that there is a wide scatter in the data and it is emphasized that it is better to carry out a series of HET at varying heads or to use the method of Bonelli *et al.* [BON 07], and Bonelli and Brivois [BON 08] to determine the critical shear stress (τ_c) from laboratory tests than to rely on these relationships.

Hole erosion index (I_{HET})	Initial shear stress (τ_c) Pa			
	Non-dispersive soil behavior		Dispersive soil behavior	
	Best estimate	Likely range	Best estimate	Likely range
< 2	2	1–5	1	0.5–2
2–3	2	1–5	1	0.5–2
3.5	5	2–20	2	1–5
4	25	10–50	5	2–10
5	60	25–100	5	2–10
6	100	60–140	5	2–10

Note: To be used with caution. For important decisions carry out HET to determine the critical shear stress (τ_c).

Table 1.5. Approximate estimates and likely range of initial shear stress (τ_c) versus hole erosion index (I_{HET}) [FEL 08]

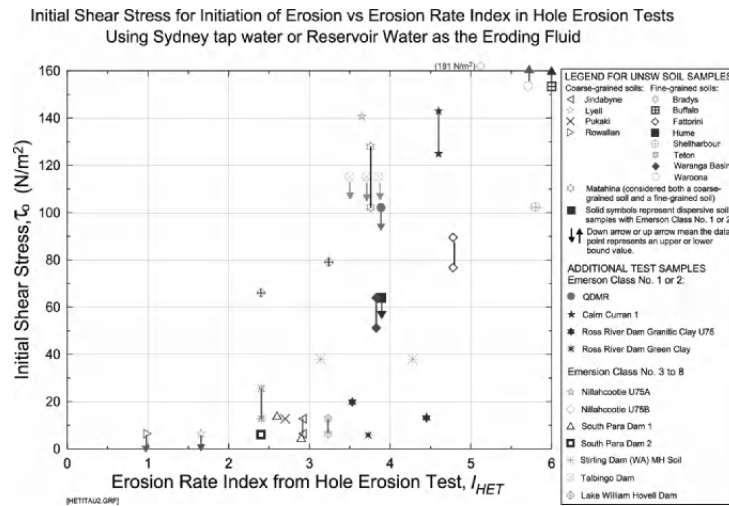


Figure 1.14. Critical shear stress (τ_c) versus representative erosion rate index (I_{HET}) for soils which are non-dispersive, and for dispersive soils with eroding water suppressing dispersion (source: Courtesy of C.F. Wan [WAN 06])

The parameters that affect the erosion properties of soil are discussed in the following sections.

1.2.3.3.1. Degree of saturation

Wan and Fell [WAN 02, WAN 04a, WAN 04b], Lim [LIM 06] and Lim and Khalili [LIM 10] found that most clay soils tested have significantly higher erosion rate indices (slower erosion) and higher critical shear stresses when saturated than at the partially saturated compaction condition. There was, however, less dependence on the degree of saturation for silty soils. This is an important finding because it means that once the core of a dam constructed of clay soil is saturated and consolidated, it may have a slower rate of erosion, and a higher critical shear stress.

Just as important is that this does not apply to silty sand cores, such as decomposed and residual granites.

From a practical point of view, it is therefore better to compact cohesive soils to the normal requirements for dam cores, for example to 98% standard maximum dry density, on the wet side of optimum, because the erosion resistance increases with the degree of saturation of the soil.

1.2.3.3.2. Dispersion and slaking properties of the soil

Soils which show dispersive behavior soils classifying as Emerson Crumb Class 1 or 2, and Pinhole Dispersion D1 and D2, will have a very low critical shear stress if the eroding fluid is sufficiently free of salts (high salt content water inhibits dispersion). It should be noted that under flood conditions the salts content of the water in the reservoir is likely to drop, so tests done in reservoir water may be unconservative. If in doubt with dispersive soils it is best to assume that the reservoir water will not inhibit dispersion and rely on the results of tests using distilled water.

Lim [LIM 06] and Khalili [KHA] showed that for rotating cylinder tests the erosion rate index is not greatly affected by whether the soil is dispersive after the initially rapid part of the erosion process. So the major effect of dispersion is on the critical shear stress at which erosion initiates, not the rate of erosion. They showed that there is a strong correlation between the rates of slaking from a sample held statically in water to the erosion rate index from the rotating cylinder test. They also showed that the slaking process was correlated strongly to the degree of saturation of the soil, with the slaking rate being up to 30 – 50 times lower between soils at 70% degree of saturation and those at 100% degree of saturation. This corresponds with the behavior of the erosion rate index for clay soils.

1.2.3.3.3. Soil structure

Lim [LIM 06] and Wahl *et al.* [WAH 08] have all noted that soil structure has an important effect on the erosion properties. They find that erosion rates are significantly higher for the same soil if the soil is compacted dry of optimum moisture content and the soil forms aggregated particle, and/or microcracks. These allow erosion of blocks of the soil rather than of individual particles. This is one of the reasons why higher erosion rates are measured in JET than HET, as the HET is stopped with a relatively small hole diameter not allowing the “blocks” of soil to dislodge from the sides of the hole. This behavior was also noted in rotating cylinder tests by Lim [LIM 06].

1.2.3.3.4. Effect of undrained shear strength or “cohesion” of the soil

The erosion rate and critical shear stress are poorly related to the undrained shear strength or “cohesion” of the soil. Soils with similar undrained strengths can have an erosion rate 100 or 1,000 times different; and critical shear stresses ranging over 1 – 100 Pa depending on dispersion properties, clay mineralogy and degree of saturation.

1.2.3.4. *Comparison of the hydraulic shear stress in the crack (τ) to the critical shear stress which will initiate erosion for the soil in the core of the embankment (τ_c)*

To assess the likelihood that erosion will initiate in a crack the estimated hydraulic shear stress is compared to the initial shear stress for the soil taking account of the moisture content of the soil in the core, and the chemistry of the water in the reservoir. When doing this assessment, allowance should be made for the uncertainty in the calculations and properties.

For an average gradient of 0.5 in a 2 mm wide crack the hydraulic shear stress is 5 Pa for a 5 mm wide crack, 12 Pa, and for a 20 mm wide crack 50 Pa. Hence from Table 1.4, for dispersive and other highly erodible soils even narrow cracks will be sufficient for erosion to initiate.

It is important to recognize that erosion in cracks or flaws is not a result of establishment of a flow net in a continuous media, but is due to flow in open cracks or erosion pipes. This occurs quickly as the reservoir rises into the cracked zone. Transient flow net analyzes are irrelevant to this process.

1.2.3.5. *Assessing the rate of development of the pipe*

From the hole erosion index of the eroding soil and average hydraulic gradient along the pipe it is possible to estimate the rate at which a piping hole will enlarge, assuming that the filters are absent or ineffective. This is important to know because it is a significant factor in assessing the likelihood of successful intervention to stop the piping process. The results are summarized in Figure 1.15 assuming (1) unrestricted potential for erosion (i.e. no flow limitation and continuing erosion condition); (2) initial pipe diameter of 25 mm; (3) zero critical shear stress which is conservative, particular for $I_{HET} > 3.5$; and (4) reservoir level remains constant. It will be seen from Figure 1.13 that the

time for erosion to progress is very dependent on the soil erosion properties.

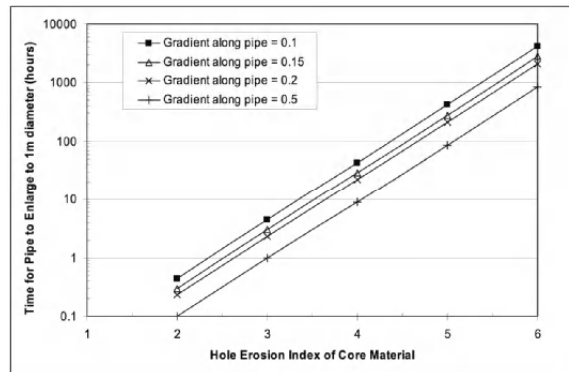


Figure 1.15. Approximate times for pipe to enlarge from 25 mm to 1 m diameter. The time to erode to 2 m diameter is about 20% greater (source: Courtesy of M. Foster)

The rates of the development of the pipe are consistent with case studies and the method for assessing the time to progress from the first signs of a concentrated leak to a breach as described in Fell *et al.* [FEL 01, FEL 003].

Bonelli and Benahmed [BON 11] develop this concept further by incorporating the maximum diameter of a pipe which can breach the dam or levee, in order to propose new expressions for the peak flow and the time remaining to breaching Δt_u , which is also the time from the detection (e.g. eyewitness's observations) to the peak discharge. The evolution of pipe radius during erosion with constant pressure gradient obeys an exponential scaling law as a function of time—Bonelli and Brivois [BON 08].

$$R(t) = R_0 \left[\frac{\tau_c}{P_0} + \left(1 - \frac{\tau_c}{P_0} \right) \exp\left(-\frac{t}{t_{er}} \right) \right]$$

with $P_0 = R_0 \Delta i / 2A$, where R_0 is the initial radius, P_0 is the driving pressure (Pa), t_{er} is the characteristic piping erosion

time (s), $t_{er}=2\rho_d/(C_e\Delta p/L)$, where ρ_d is the dry soil density, $\Delta p/L$ is the pressure gradient in the pipe and C_e is the coefficient of soil erosion. The time remaining to breaching is found to be proportional to the characteristic time t_{er} .

$$\Delta t_u \approx t_{er} \ln\left(\frac{R_u}{R_d}\right)$$

with R_d , the radius at the time of the detection and R_u , the radius at the time of the roof collapse. On 14 documented failure cases, with dam height ranged from 6 m to 93 m and failure time, Δt_u , ranged from 0.5 h to 5.25 h and peak flow ranged from 79 m³/s to 65,120 m³/s, they calculated by back-analysis shear stress at failure (*prior to* roof collapse) ranged from 262 Pa to 8,051 Pa, water velocity at failure ranged from 7 m/s to 40 m/s and erosion index rate I_e from 1.6 to 3.0. The range of the erosion index, shorter on site than in laboratory, means that other phenomena occur on site under very high flow velocity (instability, scale effect and turbulence)

1.2.3.6. *Assessing whether the soil will hold a roof to a developing pipe*

For internal erosion and piping through the dam or piping from the embankment into a rock foundation, the core must be capable of holding the roof of a pipe.

Based on the case studies [FOS 99a, FOS 99b], the most important factors are:

1) The fines content of the soil (% passing 0.075 mm) $\geq 15\%$ fines likely to be able to hold a roof regardless of whether the fines were non-plastic or plastic.

2) Whether the soil was partially saturated or saturated.

Other factors that were considered to be likely to have an influence were degree of compaction (loose soil would be less likely to support a roof to a pipe than dense soil), and reservoir operation (cyclic reservoir levels were more likely to cause collapse than steady levels).

Fell *et al.* [FEL 08] developed Table 1.6 based on these case data and taking into account of results of testing by Park [PAR 03], which showed sandy gravels with 5–15% non-plastic fines collapsed quickly when saturated. Sandy gravels with 5% cohesive fines collapsed after some time, but very slowly with 15% cohesive fines.

Soil classification	Percentage of fines (%)	Plasticity of fines	Moisture condition	Likelihood of supporting a roof
Clays, sandy clays (CL, CH, CL-CH)	> 50	Plastic	Moist or saturated	1.0
ML or MH	> 50	Plastic or non-plastic	Moist or saturated	1.0
Sandy clays, Gravely clays, (SC, GC)	15–50	Plastic	Moist or Saturated	1.0
Silty sands, Silty gravels, Silty sandy gravel (SM, GM)	> 15	Non-plastic	Moist Saturated	0.7–1.0 0.5–1.0
Granular soils with some cohesive fines (SC-SP, SC-SW, GC-GP, GC-GW)	5–15	Plastic	Moist Saturated	0.5–1.0 0.2–0.5
Granular soils with some non-plastic fines (SM-SP, SM-SW, GM-GP, GM-GW)	5–15	Non-plastic	Moist Saturated	0.05–0.1 0.02–0.05
Granular soils (SP, SW, GP, GW)	< 5	Non-plastic Plastic	Moist and saturated Moist and saturated	0.0001 0.001–0.01

Notes:

1) Lower range of probabilities is for poorly compacted materials (i.e. not rolled), and upper bound for well-compacted materials.

2) Cemented materials give higher probabilities than indicated in the table. If soils are cemented, use the category that best describes the particular situation.

Table 1.6. *Likelihood of a soil being able to support a roof of an erosion pipe [FEL 08]*

1.2.4. Commentary on the state of the art and the role of laboratory testing in assessing concentrated leak erosion

1) Cracking and hydraulic fracture:

i) The state of the art is poor with regard to the prediction of the likelihood of cracking or low-stress zones subject to hydraulic fracture.

ii) The state of the art is even poorer in predicting the depth and width of cracking, and the width of hydraulic fractures.

iii) Laboratory tests are not able to predict these by themselves, but can be useful in determining the tensile strength, soil water characteristics and stress-strain properties for use in numerical modeling.

iv) Research is needed to refine numerical methods for these predictions including modeling partially saturated soil behavior. These need to be calibrated against field case data, which are not readily available. Research is about to begin into this at UNSW.

2) Collapse settlement forming concentrated leak:

i) The state of the art is poor. There is little research available.

ii) Laboratory tests will be useful in modeling this but the test setup will need to model the actual mechanics involved. UNSW is developing research into this.

3) Erosion properties:

There is a relatively mature science for the HET, and recent improvements by Bonelli and Brivois [BON 08] and Bonelli *et al.* [BON 07] to the method make the determination of critical shear stress more reliable. However, many test data are non-classical plots and are

difficult to interpret. This part of the equation is far less uncertain than the prediction of crack width and depth:

i) Refinements are required and are in progress for interpretation of the JET.

ii) For new embankments, enough care is often not taken to replicate actual field conditions with regard to the degree of saturation, because in many cases the persons involved do not recognize how important this is for the erosion properties. For an existing embankment, it is best to take undisturbed samples and test with holes drilled into the sample so that any natural cementing is retained.

iii) Very few are doing critical shear stress tests, instead relying on correlation with IHET or soil classification. These are quite approximate and should not be relied upon for important decisions.

iv) It is critical that dispersive soils are recognized and tested with water, with chemistry replicating what may happen in the field. Allowance must be made for the fact that in flood conditions, water salinity may drop compared to the dry periods and so dispersion may occur.

v) A rotating cylinder test shows quite different erosion rates than HET for some dry-of-optimum soils. This appears to be related to soil structure.

4) Hydraulics of the flow in cracks:

i) A simplified crack geometry is assumed by most of the practitioners including the first author. It may be that these result in very conservative assessments.

ii) It is important to consider potential head losses in the zones upstream and downstream in zoned dams when estimating the gradients in the crack.

1.3. Backward erosion piping

1.3.1. *The mechanics of backward erosion piping*

1.3.1.1. *The overall process*

The backward erosion piping process initiates at a free surface on the downstream side of a dam or levee as shown in Figures 1.2 and 1.16.

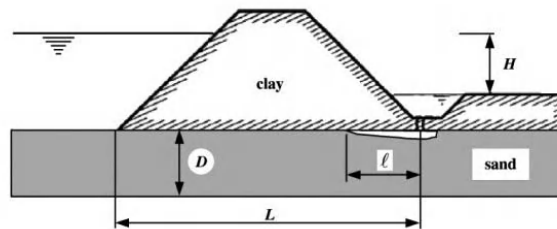


Figure 1.16. *Geometry of the Delft backward erosion piping model [KOE 92]*

This free surface may be in a ditch as shown in Figure 1.16 or may form by cracking due to heaving of the cohesive strata overlying the cohesionless soil, or in some cases may be the seeping surface on the downstream face of the dam, or in other cases the stream bed downstream of the levee or dike.

The backward erosion process progresses beneath the dike or dam. For its occurrence, the levee or dam, or cohesive strata in the foundation above the strata subject to backward erosion must form a roof for the eroding “pipe”. The presence of backward erosion piping is often exhibited by the presence of sand boils at the downstream side of the dam or dike.

Sellmeijer and co-workers from Delft Hydraulics and Delft Geotechnics Laboratories in the Netherlands carried out more than 70 backward erosion piping tests. The first tests were in flumes and are reported in [WIT 81, SIL 91, WEI 93]

and [TEC 99]. The tests were mostly on fine-to-medium sands, with a few tests on medium-to-coarse sands. The sands were uniform with uniformity coefficients $C_u = 1.58\text{--}3.53$. Early tests were on small-scale models (base length 0.8 m), but latter tests were on very large models as shown in Figure 1.17. These experiments showed that:

1) Backward erosion initiates in the slot through the strata overlying the eroding soil representing a crack or drainage ditch excavated through the strata, and progresses in multiple small “channels” rather than a single “pipe”. Figure 1.18 shows an example of the development of the channels.

2) The channels are quite small. The height of the channels is typically $4\text{--}10 (d_{15})$; that is, often less than 2 mm.

3) For any head less than a critical head, the development of the channels stops. If the head is increased, erosion begins again. Figure 1.15 shows some examples. The critical head occurs when the length of the channel (l) is about 0.3–0.5 of the flow path length L. For heads less than this, the progression of the pipe reaches a stable condition. For heads greater than the critical head, the piping channel extends upstream and breaks through to the reservoir.

4) The erosion then progresses rapidly as the erosion in an open pipe. For these experiments, the rate of progression of the pipe was relatively uniform until the length approaches about 40% of the total seepage path. It then accelerates. The piping progressed about 6 m in an hour in the largest of the experiments.

In 2009 and 2010, further experiments were carried out at Deltares. These are reported in Van Beek *et al.* [BEE 10a, BEE 10b], Sellmeijer *et al.* [SEL 11] and Van Beek *et al.* [BEE 11]. These were conducted at three scales as discussed

later in Chapter 4. The largest of these was virtually full scale. From these experiments, Van Beek *et al.* [BEE 11] refined the understanding of the backward erosion process as follows:

1) *Phase 1: Seepage occurs in the permeable strata:* in the experiments, there were no confining strata.

2) *Phase 2: Backward erosion.* At the beginning of the process, there is the rearrangement of grains, individual grain movements and the formation of small channels. The process reaches equilibrium for the hydraulic head applied. Very small amounts of sand are transported, in the order of cubic centimeters in this phase of the process. With an increase in the hydraulic head to the critical head, sand is transported continuously. A variety of erosion patterns is observed in the small- and medium-scale experiments. In the large-scale experiment, sand boils are formed, and in the small- and medium-scale experiments craters are formed. These characterize the reaching of the critical head. The flow barely increases in this phase of the process. At a head greater than the critical head, the erosion does not cease and the erosion rate is in the order of cubic decimeters per hour. The rate of erosion increases with increasing head.

3) *Phase 3: Widening of the channel:* as soon as the pipe reaches the upstream side, a pressure surge occurs in the pipe. In the small-scale experiments, this in turn causes a large amount of sand to be eroded rapidly. In the medium- and large-scale experiments, blockages caused by local collapse of the roof of the pipe take place and the widening process takes a longer time. The widening pipe develops from the upstream to the downstream. The flow and sand transport to the exit point and do not increase significantly. The widening process took up to a few days in the large-scale experiments. When the widening pipe has almost reached the downstream side, the sand transport and flow increases

suddenly. The situation can change from sand boils to this condition without warning.

4) *Phase 4: Failure and breakthrough*: failure occurs soon after the widening phase is complete, but can be delayed due to the collapse of the levee causing the first pipes to close.

1.3.2. Soils that are subject to backward erosion piping

The experience in the USA and Europe is that backward erosion piping mostly occurs in the foundations of levees, dikes and dams where the eroding soil is fine to medium grain size sand, with a uniformity coefficient $C_u < 3$.

The participants at the Aussois Workshop [FEL 07] considered that at gradients likely to occur within a dam or its foundation backward erosion is probably restricted to non-plastic soils or soils with only limited plasticity. For practical purposes, Fell *et al.* [FEL 08] have concluded that based on the available data, the results of Wan and Fell [WAN 04c, WAN 07, WAN 08] tests on internal instability and their experience and judgment, soils with plasticity index > 7 should be considered not subject to backward erosion piping.

Laboratory tests by [SUN 89], [MAR 07] and [BEN 08] showed that backward erosion could occur in more cohesive soils, but initiate at very high gradients that were not likely to occur in dams or their foundations. Bendahmane *et al.* [BEN 08] carried out tests, which showed that soils consisting of 10% kaolin / 90% fine sand initiated backward erosion at gradients between 90 and 140 depending on confining pressure. For kaolin contents 20% and 30%, no backward erosion occurred at gradients as high as 100. They observed suffusion with gradients as low as 5, but noted that this value should not be taken as generally applicable.

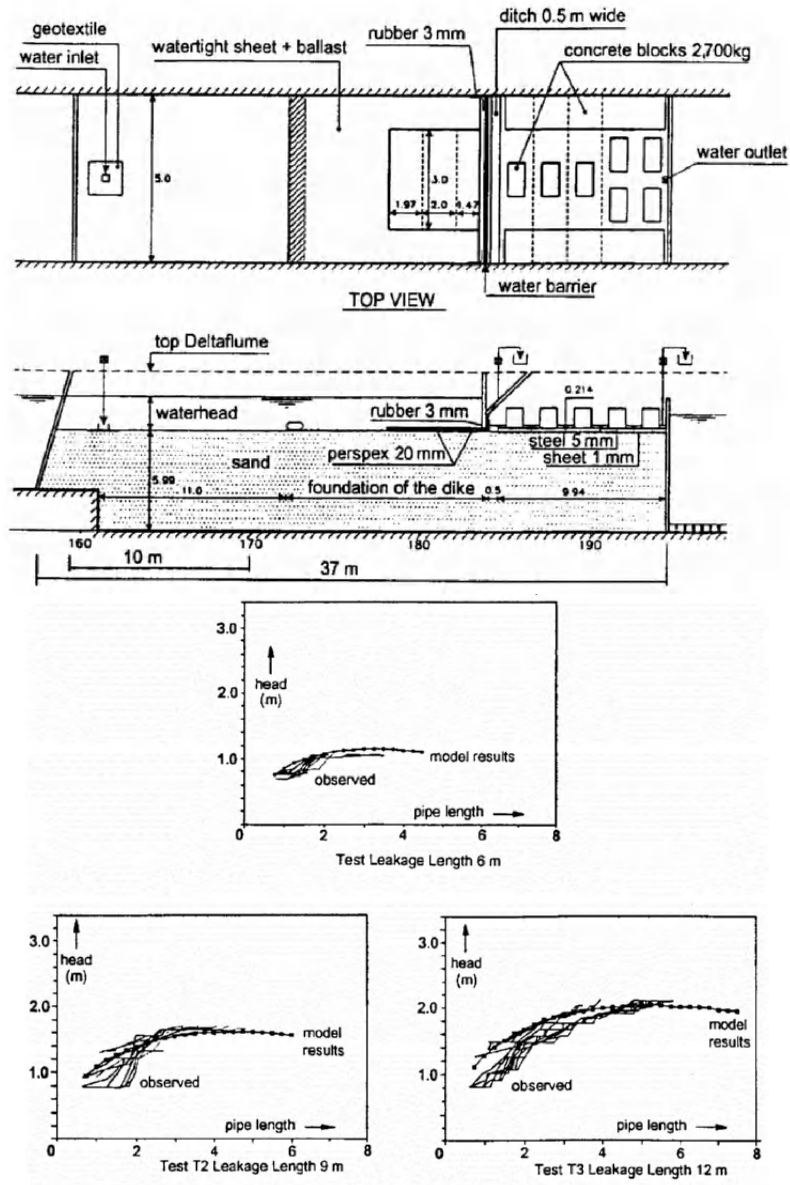


Figure 1.17. Delft Hydraulics laboratory piping flume test model (a) test equipment, (b) typical test results showing the development of the length of the tunnel as the head increases [WEI 93]

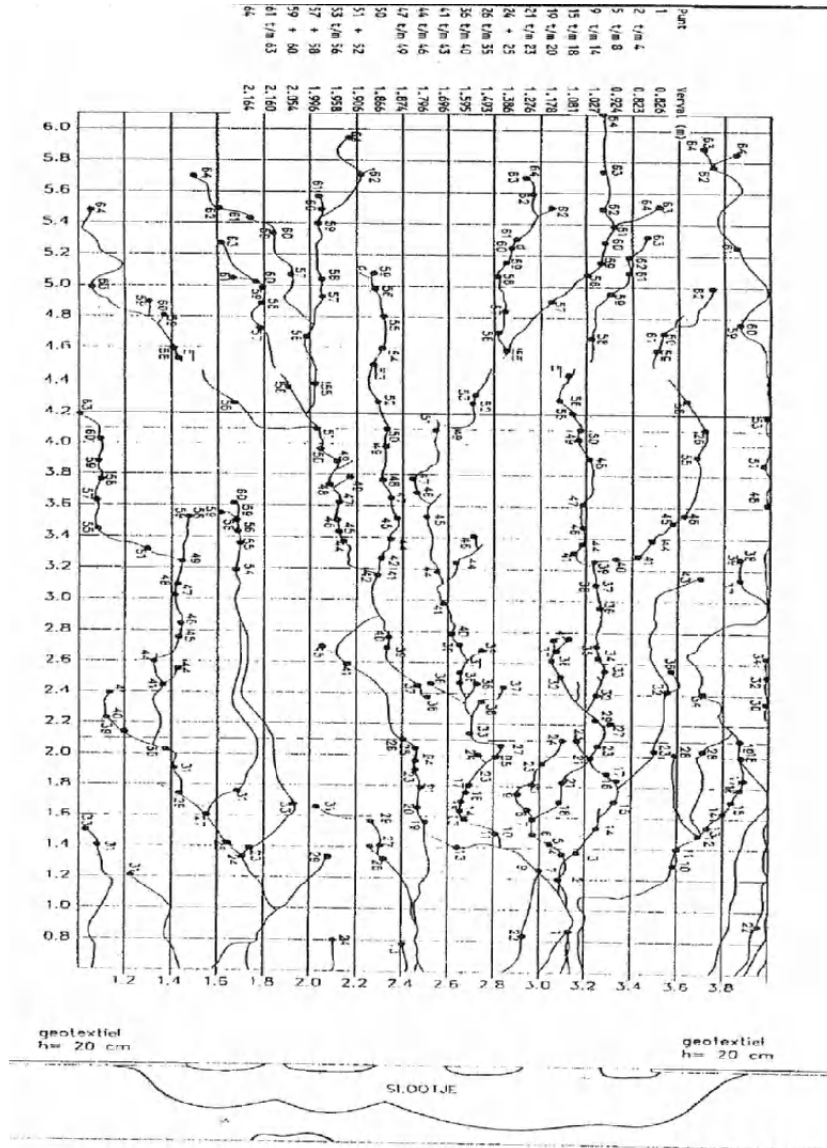


Figure 1.18. Plan view and section of an example of the development of piping channels in the Delft experiments. The numbers are the time in minutes from when erosion initiated [SIL 91]

1.3.3. Methods available for assessing whether backward erosion piping will initiate and progress

1.3.3.1. Terzaghi and Peck [TER 48]

Terzaghi and Peck [TER 48] show that backward erosion piping will occur when a heave or zero effective stress condition occurs within seepage flow in cohesionless soils. They also point out that:

- 1) Most piping failures occur at average heads from upstream to downstream, much less than required for a factor of safety of 1.0 for zero effective stress at the exit point.
- 2) Piping requires that there should be a soil overlying the erodible strata, which is cohesive or cemented and will form a roof to the developing pipe.
- 3) The failures usually occur from a few weeks to many years after the reservoir is filled.
- 4) The ratio of the actual to critical average gradient decreases with grain size.
- 5) The erosion process starts at the sand boil (spring in their terminology), and proceeds along erosion paths leading to the reservoir. They indicate that the erosion will almost certainly “get more serious” (progress) as time goes by, because the flow from the sand boil increases as the seepage- and erosion-affected area extends.

The Terzaghi and Peck [TER 48] philosophy has been the dominating influence in design of levees and dams, particularly in the USA (e.g. USACE). It has however commonly been assumed, at least implicitly, that if backward erosion initiates, it will progress to form a pipe, at least under repeated loading from successive floods. This does not seem to be supported by the fact that many (hundreds, even thousands) of the sand boils occur in the foundation of levees on the Mississippi in any flood but there

are few failures. Either the extensive intervention by those during the flood prevents failure or the process self-limits as suggested by the Delft laboratory tests as described earlier. However, the Deltares experiments show that several days are required in the development of the erosion pathways, so the performance of the levee is probably related to the severity and duration of the past floods. Another important fact that Deltares observed to inhibit backward erosion is the settlement of the embankment and the collapse of the widening pipes.

1.3.3.2. USACE simplified method

The simplified model of USACE [USA 93] may be used to localize area where backward erosion could initiate downstream the levee without drainage trench. The zero effective stress condition is calculated with the assumption that the horizontal seepage flow discharge in the aquifer layer under the impervious blanket is equal to the vertical flow through the silty or clayey soils that form the impervious blanket of the alluvial valley.

When the upstream impervious blanket is very long and not cut by a drainage trench, the upstream effective length L_1 (m) and the effective length of the downstream blanket L_3 (m) are:

$$L_1 = \sqrt{\frac{k_f}{k_{bu}} Z_{bu} d} \quad \text{and} \quad L_3 = \sqrt{\frac{k_f}{k_{bd}} Z_{bd} d}$$

where k_f is the horizontal permeability of the pervious foundation (m/s), d is the thickness of the pervious aquifer (m), k_{bu} and k_{bd} are the vertical permeabilities of the upstream and downstream blanket, respectively, (m/s) and Z_{bu} and Z_{bd} are the thickness of the upstream and downstream blanket, respectively, (m) (Figure 1.19).

$$h_0 = \frac{hL_3}{L_1 + L_2 + L_3}$$

Heave occurs where the factor of safety against uplift, F , reaches one at the downstream toe of the levee. F is the ratio between the critical pressure head $h_c = Z_{bd} \gamma' / \gamma_w$, and the hydraulic head h_0 :

$$F = \frac{Z_{bd} \gamma' L_1 + L_2 + L_3}{h \gamma_w L_3}$$

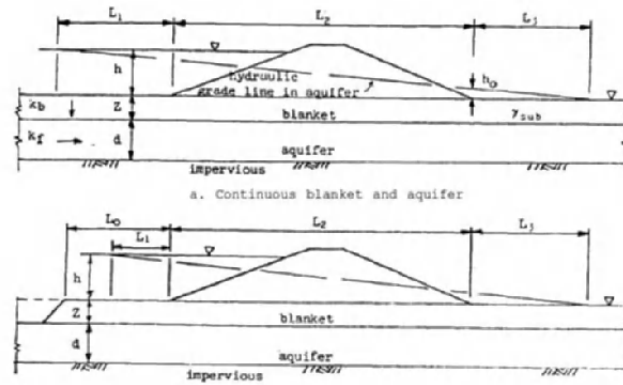


Figure 1.19. Notations for underseepage analysis [USA 93]

1.3.3.3. *The Netherlands experiments and design methods 1980 to 1999*

Sellmeijer [SEL 88], Sellmeijer and Koenders [SEL 91] and Koenders and Sellmeijer [KOE 92] developed a mathematical model for backward erosion based on these experiments. There are various forms of the equation for the critical head, but the latest is given in Weijers and Sellmeijer [WEI 93] and Technical Advisory Committee [TEC 99]. The most important variables are d_{70} , the sieve size for which 70% by weight of the soil (m) is finer and the permeability. They indicate that the theory gave good correlation with their small- and large-scale tests.

1.3.3.4. Recent research at Deltares, Delft

During 2008–2009, an extensive series of experiments was carried out at Deltares, Delft, to further investigate the effects of scale, relative density of the eroding soil and grain size. This research is reported in Van Beek *et al.* [BEE 10a, BEE 10b, BEE 12] and Bezuijen and Steedman [BEZ 10]. Three scales were used with seepage path lengths of 0.34, 1.45 and 15 m.

The earlier Sellmeijer model was refined using the results of the Deltares testing and is presented in Van Beek *et al.* [BEE 11] and Sellmeijer *et al.* [SEL 11].

The critical gradient is determined as a product of three contributions: resistance factor, scale factor and geometrical shape factor. The refined equations for the critical gradient at which backward erosion will progress are:

$$\frac{H}{L} = \frac{1}{c} = F_R F_S F_G$$

$$F_R = \eta \frac{\gamma'_p}{\gamma_w} \tan \vartheta \left(\frac{RD}{RD_m} \right)^{0.35} \left(\frac{U}{U_m} \right)^{0.13} \left(\frac{KAS}{KAS_m} \right)^{-0.02}$$

$$F_S = \frac{d_{70}}{\sqrt[3]{\kappa L}} \left(\frac{d_{70m}}{d_{70}} \right)^{0.6}$$

$$F_G = 0.91 \left(\frac{D}{L} \right)^{\frac{0.28}{\left(\frac{D}{L} \right)^{2.8} - 1} + 0.04}$$

where

- H [m]: hydraulic head across structure
 L [m]: seepage length (= base length of the embankment)
 D [m]: thickness of sand layer under the embankment
 C [-]: erosion coefficient

F_R [-]:	resistance factor
F_S [-]:	scale factor
F_G [-]:	geometrical shape factor
RD [%]:	relative density
U [-]:	uniformity coefficient $C_u = d_{60}/d_{10}$
KAS [%]:	roundness
d_{70} [m]:	soil particle diameter for which 70% by weight of the soil is finer
γ'_p [kN/m ³]:	submerged unit weight of soil particles 9.8(G-1)
G [t/m ³]:	soil particle density
γ_w [kN/m ³]:	unit weight of water
η [-]:	Whites drag coefficient
ϑ [DEG]:	bedding angle (angle of repose) of sand
K [m ²]:	intrinsic permeability
KAS [%]	is the roundness of particles
RD [%]	is the relative sand density
d_{70} [m]	is the sand diameter at 70% passing
Where $K = \frac{\nu}{g} k$	
ν [m ² /s]:	kinematic viscosity
G [m/s ²]:	gravity
k [m/s]:	hydraulic permeability

H, D and L are defined in Figure 1.16. In these equations, the variables are normalized by the mean values in the data set. For the data set used by those authors, the mean values are as detailed in Table 1.1.

Sellmeijer *et al.* [SEL 11] indicate that their data set assumes a bedding angle of 37° , and a Whites coefficient of 0.25. For water at 20°C , $K = 1.02 \times 10^{-7}$ (k) where K is in m^2 and k is in m/s . They indicate that they ignore the roundness and uniformity coefficient terms as they do not contribute significantly.

They indicate that the refinements have been determined from the small-scale tests and it is not altogether clear if there may be a scale effect, so that the outcome for large structures may not be properly modeled. They also indicate that the equations should only apply within the limits of the parameters during testing. These limits are given in Table 1.7.

Parameter	Minimum	Maximum	Mean
RD	34%	100%	72.5%
U	1.3	2.6	1.81
KAS	35%	70%	49.8%
d_{70}	150 μm or 1.5E-04m	430 μm or 4.3E-04m	207 μm or 2.07E-04m

Table 1.7. Limits of the Sellmeijer *et al.* [SEL 11] method

They found that the equations predicted the large-scale experimental behavior quite well for the fine grained soil, but that it was not so accurate for the soil with a $d_{70} = 260 \mu\text{m}$.

There are very significant scale effects; the smaller the structure, the higher the critical gradient. In the tests, the value of the scale factor F_s ranged from 0.134 for the large-scale IJkdijk tests to 0.192 for the medium-scale tests and 0.421 for the small-scale tests.

It should be noted that Sellmeijer *et al.* [SEL 11] emphasize that the above equations do not include any margin of safety and that for design rules they are likely to apply factors of safety.

1.3.3.5. Hoffmans [HOF 12b]

Dr. Gijs Hoffmans, from Deltares, Delft, the Netherlands, reanalyzed the results of the Delft experiments [HOF 12]. He, like Sellmeijer, recognizes that for backward erosion to progress, the particles being released from the initiating zone at the upstream end of the piping channel must be transported down the channel. Hence, it is the interaction of the gradients at the backward eroding head of the piping channel, and the flow gradient in the piping channels, which controls the process. The latter is controlled not only by the gradients of flow into the pipes but also by the permeability of the soil as this affects the flow quantity in the pipes.

The most important variables in Hoffmans [HOF 12] approach are hydraulic conductivity (K), particle sizes d_{50} , d_{15} and the critical pipe height (ℓ_c) and a coefficient α_f . The latter two are determined from experiments.

$$\frac{(H_1 - H_2)_c}{L} = \frac{\sqrt{g} (\Psi_{lam,c} \Delta d_{15})^{\frac{1}{2}}}{v \sqrt{\alpha_{Re,\ell}}} + \left(1 - \frac{\ell_c}{L}\right) \frac{d_{50} v}{\ell_{Re} K D}$$

with

$$\frac{\ell_c}{L} = \exp\left(-\left(\frac{\alpha_f D}{L}\right)^2 \frac{\sqrt{g} (\Psi_{lam,c} \Delta d_{15})^{\frac{1}{2}}}{v \sqrt{\alpha_{Re,\ell}}}\right)$$

Table 2.5 Piping parameters

symbol	indicative range	comment
d_{15}	$0.08 \text{ mm} < d_{15} < 0.32 \text{ mm}$	d_{15} for which 15% of the particles is finer than d_{15}
d_{50}	$0.13 \text{ mm} < d_{50} < 0.75 \text{ mm}$	mean particle diameter
$D = d_{50} (\Delta g / v^2)^{\frac{1}{2}}$	$4 < D, < 16$	dimensionless particle diameter
g	$g = 9.81 \text{ m/s}^2$	acceleration of gravity
$(H_1 - H_2)/L$	$0 < (H_1 - H_2)/L < 1$	critical hydraulic gradient
K	$10^{-6} \text{ m/s} < K < 10^{-3} \text{ m/s}$	hydraulic conductivity (see also Eq. 6.36)
ℓ_c	$0 < \ell_c/L < 1$	ratio of critical pipe length and seepage length
ℓ_{Re}	$\ell_{Re} = 18.2 \cdot 10^{-6} \text{ m}$	calibrated length scale
α_f	$\alpha_f = 5$	calibration coefficient
$\alpha_{Re,\ell}$	$\alpha_{Re,\ell} = 6.8$	calibration coefficient
$\Delta = \rho_s/\rho - 1$	$\Delta = 1.65$ (sand)	relative density
ν	$10^{-6} \text{ m}^2/\text{s} < \nu < 1.4 \cdot 10^{-6} \text{ m}^2/\text{s}$	kinematic viscosity
$\Psi_{lam,c} = 0.2(D)^{-0.3}$	$0.08 < \Psi_{lam,c} < 0.16$	critical Shields parameter (for laminar flow)
if $\ell = 0$ then the equilibrium is stable (or no erosion occurs);		
if $0 < \ell \leq \ell_c$ then the equilibrium is unstable (or occasional erosion occurs);		
if $\ell > \ell_c$ then there is no equilibrium anymore (or erosion occurs until the dike fails).		

1.3.3.6. *Schmertmann [SCH 00] method for modeling initiation and progression of backward erosion*

Schmertmann [SCH 00] carried out backward erosion piping tests in flumes at the University of Florida. The tests were carried out in a number of sets, including those by Townsend *et al.* [TOW 88] who carried out 15 tests. Those tests were carried out on a range of soils from fine to medium sands, up to coarse sand/fine gravel mixes. The tests were carried out with a “starter pipe” as described in Townsend *et al.* [TEL 88]. The soils were mostly fairly uniform ($C_u = 1.5-3$) but with C_u up to 6.1.

The test geometries used at the University of Florida and Delft were not the same, so Schmertmann [SCH 00] applied correction factors for geometry and was then able to plot all the results together. He found that there is a sharp increase of the critical average gradient related to the uniformly coefficient C_u (d_{60}/d_{10}) of the soils tested.

$$i_c = 0.05 + 0.183 (C_u - 1)$$

He also analyzed the Delft tests and found a similar correlation.

The proposed relationship is based on little data in the larger uniformity coefficient range and was not confirmed by other authors. On close inspection of the Townsend *et al.* [TOW 88] data, which include the larger C_u values, it is apparent that some of these may be affected by internal instability. It is therefore questionable whether the correlation with C_u is reliable and caution should be exercised in using the method for soils with $C_u > 3$. Sellmeijer *et al.* [SEL 11] found only a weak correlation with C_u for their soils.

1.3.4. *Some field observations*

The USACE have responsibility for managing the levee systems along major US rivers including the Mississippi. They have carried out extensive studies of backward erosion piping over many years. Some observations from these include:

1) In any one flood, the levee system in one USACE district, for example St. Louis, may experience many hundreds of sand boils in the foundations. However, there are few cases of breaching of the levees from piping. This is influenced by the “flood fighting” efforts of the Corps and the Levee district authorities. They build sand bags and in some cases sublevees around the sand boils to stop the flow of sand (but not the flow of water) but it seems to support the laboratory tests that show erosion initiates at lower average gradients than is required to progress the erosion to form a continuous pipe from the river side to the land side.

2) Sills and Vroman [SIL 07], Wolff [WOL 02] and Glynn and Kusmaul [GLY 04] report that there are cases of levees that have sand boil activity occurring at successively lower average gradients (lower river stages). This phenomenon does not appear to have been investigated by the laboratory flume tests described earlier.

3) Glynn and Kusmaul [GLY 04] show that greater sand boil activity occurred in the 1995 flood than the 1993 flood, even though the river stage was lower in 1995. It is not clear why this is so, but it may relate to the duration of the flood and the time it takes to set up a seepage flow net.

4) USACE [USA 56] and Wolff [WOL 02] show that local geology has an important influence on the occurrence of sand boils. Sand boils are more likely to occur where swales from the point bar deposits cross the levee at an angle and concentrate seepage at the toe.

1.3.5. *Global backward erosion*

There is a potential backward erosion piping mode that may occur in narrow or even reasonably wide central core dams not properly protected by filters or a transition zone such as that shown in Figure 1.3. Particles are detached at the downstream surface of the core, which is inadequately protected by the filter or transition zone. The progression of the erosion process is assisted by gravity, and there is no need for a cohesive soil layer to form the roof for the pipe. It may be one of the causes of sinkholes in dams constructed of glacial tills.

The available evidence is that unless the core is cohesionless internally unstable soil subject to suffusion, this internal erosion mode will only occur at relatively high gradients. This evidence includes:

1) Laboratory tests by Sun [SUN 89], Marot *et al.* [MAR 07] and Bendahmane *et al.* [BEN 08] showed that backward erosion could occur in more cohesive soils, but initiated at very high gradients that were not likely to occur in dams or their foundations. The Bendahmane *et al.* [BEN 08] tests showed that soils consisting of 10% kaolin / 90% fine sand initiated backward erosion at gradients between 90 and 140 depending on confining pressure. For kaolin contents 20% and 30%, no backward erosion occurred at gradients as high as 100. They observed what they called suffusion with gradients as low as five, but noted that this value should not be taken as generally applicable. Sail *et al.* [SAI 11] used non-plastic gap-graded soils with 40% finer fraction. They observed some particle movement at a gradient of about five and major movement at much higher gradients.

2) Tests done at the VNII Vodgeo Laboratory and reported by Istomina [IST 57] showed that the critical hydraulic gradient of a soil with a very low plasticity and liquid limit

equal to 14 is higher than 10 at moisture content close the optimum proctor. They showed that the critical hydraulic gradient not only depends on the plasticity but also on the soil consistency as well.

3) Moffat and Fannin [MOF 11b] and Moffat *et al.* [MOF 11a] indicate that there is an initial movement of finer particles at gradients of about four for the non-plastic soils that they tested and more extensive movement of finer and some coarser fraction soils at higher gradients, from about 10 to 30 in the soils tested. These movements of particles are accompanied by a reduction in volume as particles are eroded from the soil through inadequate filters.

4) Some recent tests on glacial till soils from an Australian dam showed that for vertical downward flow to model the condition in Figure 1.3, backward erosion occurred in broadly graded non-plastic soils at a gradient of nine. Erosion had progressed for about 40 days at a gradient of five and may have reached the failure condition without the increased gradient if the test had gone longer. What is not clear is whether a form of suffusion also contributed to the erosion process as the soil was marginally likely to be subject to suffusion using the Wan and Fell [WAN 08] method. A second sample that was definitely not internally unstable did not experience significant erosion under a gradient of nine.

1.3.6. Commentary on the state of the art and the role of laboratory testing in assessing backward erosion piping and global backward erosion

1.3.6.1. Backward erosion piping

1) Understanding the mechanics of the backward erosion piping process:

The experiments carried out at Delft/Deltares/University of Florida have contributed very significantly to the understanding of the mechanics.

i) These show that progression of backward erosion involves the development of the many small delta-like “pipes” that are only a few millimeters in vertical dimension. The development of the pipes may stop before progressing all the way beneath the dam or levee, so it is conservative to assume that just because erosion has initiated (as evidenced by sand boils), it will progress all the way under the dam or levee.

ii) The critical factor on whether the erosion will progress is not whether particles will detach at the upstream end of the pipes, but whether the detached particles will be transported downstream in the pipes. This is related to the particle size distribution of the eroding soil, and the flow into and along the pipes. This is controlled by the geometry of the foundation strata and its permeability.

iii) There is a scale effect. It is not correct to do laboratory-scale experiments and apply these directly to the field scale without correction.

2) Applicability and limitations of the available methods for predicting critical gradient:

i) The methods developed by Sellmeijer and his colleagues at Delft, and refined by Sellmeijer, Van Beek and colleagues at Deltares, are based on extensive laboratory trial embankments up to the field scale. They are applicable to the soils that were tested, that is fine- to medium-grained uniform grain size soils.

ii) The methods have not been shown to apply to more broadly graded soils. Schmertmann’s method is designed to be applicable to more broadly graded soils up to uniformity coefficient of six, but is calibrated on too few data to be relied upon.

iii) The authors are not aware of design methods that apply to broadly graded soils and silty sands.

iv) The analytical model developed by Hoffmans [HOF 12] apparently fits experimental data without scale effect.

3) Some detailed comments:

i) A limited amount of testing has been done to assess the effects of the effective stress conditions in the eroding strata. These show that it is not a critical factor that what is to be expected as progression is controlled by transport of the eroding particles in the open pipes, but more needs to be done to confirm this.

ii) The Deltares testing of low relative density soils gave “forward” not “backward” erosion. This may be due to collapse settlement or compressibility of the loose strata under hydraulic gradient for a concentrated leak.

iii) Methods in hydraulics use the d_{50} , or others use d_{60} and d_{70} particle sizes to characterize the gradation of the eroding strata. It may be that using a single size is not sufficient. More research on widely graded soils is needed.

iv) There appears to have been limited testing to check if the exit conditions affect the critical gradients. That is, whether erosion into a slot, requiring vertical transport of the particles, is different to the eroding to a free sloping face as used in most of the experiments. The testing that has been done appears to show that this is not significant.

v) The testing carried out does not seem to have cycled the reservoir/river level. Given that USACE have observed sand boil activity re-initiating at lower river levels, this may not be conservative. More research is needed to validate the hypothesis that reverse flows are more destructive of arching effects between grains than single direction flows.

vi) It is apparent that the permeability of the eroding strata, and the other strata contributing to flow into the pipes, is a critical factor. However, it must be recognized that this is a difficult property to measure reliably. Laboratory

tests on reconstituted samples are not likely to properly model the soil stratification and structure within strata and may overestimate or underestimate vertical and horizontal permeabilities.

1.3.6.2. *Global backward erosion*

1) Broadly graded silt–sand–gravel soils are subject to segregation during placement in the dam or levee. The degree to which this has occurred must be carefully investigated and the soil particle size distribution used in the laboratory tests should be as actual as that in the dam because the likelihood of global backward erosion is significantly greater for the segregated soil than for non-segregated soil. Segregation in placing the samples into laboratory test equipment is also a potential problem requiring careful laboratory test procedures. Segregation is also a problem of broadly graded transitions or filters and causes excessive and continuing erosions.

2) The authors are not aware of methods for predicting backward erosion in broadly graded non-plastic soils such as glacial tills in the cores of dams. For these situations, specifically designed laboratory tests should be carried out.

3) This is a phenomenon that has not been extensively researched to date. The research, which has been carried out, has sometimes referred to the phenomena as suffusion or suffosion, at least in the later stages of the tests where at very high gradients erosion occurs within the body of the soil, not only as backward erosion.

4) The limited tests on the Australian dam core material raise questions as to time effects for this type of backward erosion as it seems the process may be very slow.

5) Great care must be taken in carrying out laboratory-scale tests for this phenomena. The common practice of using a “scalped” grading with the coarser particles replaced by particles of a size that can fit into the laboratory test

cylinders potentially makes the samples internally unstable and the tests will not be representative of the actual soil behavior.

1.4. Suffusion

1.4.1. *The mechanics of suffusion*

Suffusion is caused by mobile particles being detached, transported and sometimes plugged by flow velocity through the largest voids of the soil. Under constant total stress and by increasing the hydraulic gradient, four stages are observed: no fines movement, some fines movements, massive fines movement and, finally, clogging and hydraulic fracture may occur (see section 1.2).

The second stage results in an increase in permeability, greater seepage velocities and potentially higher hydraulic gradients, possibly accelerating the rate of suffusion.

Stable situations may be reached after the washout of the mobile particles, the other fraction of the fines remaining in equilibrium with the seepage stresses.

Suffusion may recommence during cycling periods of water loads or during higher reservoir or river water levels.

Suffusion occurring within an embankment core or the foundation of a dam may also lead to some settlement of the embankment. Kumano *et al.* [KUW 12] indicate that cavities were discovered during the snow thawing season in a backfill built with a suffusive silty volcanic ash (IP = 6 and 8) (Figure 1.20).

A filter constructed of internally unstable materials will have a potential for erosion of the finer particles in the filter, rendering the filter coarser and less effective in protecting the core materials from erosion.

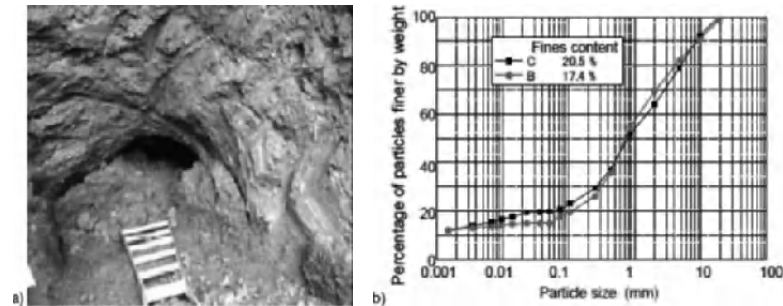


Figure 1.20. Observed cavities a) in soil subject to suffusion b) from Kuwano et al. [KUW 12]

Suffusion may result in an increase or decrease in the permeability depending on the value of the hydraulic gradient, the soils tested and stress conditions.

1.4.2. Methods of identifying soils that are internally unstable and potentially subject to suffusion (geometric criterion)

1.4.2.1. General requirements

Figures 1.21 and 1.22 show particle size distributions of some soils that have been found to be internally unstable in laboratory tests. It will be noted that there are gap-graded and broadly graded soils. The soils used by Kenney and co-authors are sandy gravels, whereas the soils used by Wan and Fell are silty sandy gravels. Soils 14A and 15 had 11% and 21% kaolin in them, so were slightly plastic.

As pointed out by Kenney and Lau [KEN 85b, KEN 86], for a soil to be internally unstable and subject to suffusion, the percentage of finer fraction (finer than the point of inflection of the particle size plot) must be smaller than the available void space. They suggested this lay between 20% of the total soil for well-graded soils and 30% for narrow-graded soils. Wan and Fell [WAN 04c, WAN 07] showed that this could theoretically be as high as 40% but in their samples it

was between 22 and 33% for broadly graded soils and 29 and 38% for the gap-graded soils.

Homberg *et al.* [HOM 12] found that the percentage of finer fraction free to move under hydraulic gradient is slightly lower than the porosity of the coarser fraction.

These soils are described as having underfilled voids (between the coarse particles).

For a greater proportion of finer soil, the coarse particles are surrounded by the finer particles. Such soils are not subject to suffusion but may be subject to global backward erosion. Such soils are described as having overfilled voids.

For practical purposes, Fell *et al.* [FEL 08] have concluded that based on the data described, available soils with plasticity index > 7 should be considered not subject to suffusion at the gradients usually experienced in dams and their foundations. If for some particular reason the gradient is higher than about 4, then soils with a plasticity index ≤ 12 should be considered for suffusion. This was considered to be a somewhat conservative approach.

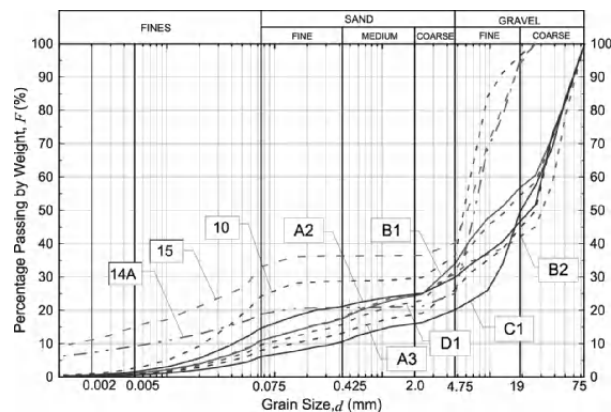


Figure 1.21. Samples of silty-sandy-gravel tested as being internally unstable (suffusive) by Wan and Fell [WAN 04c, WAN 07]

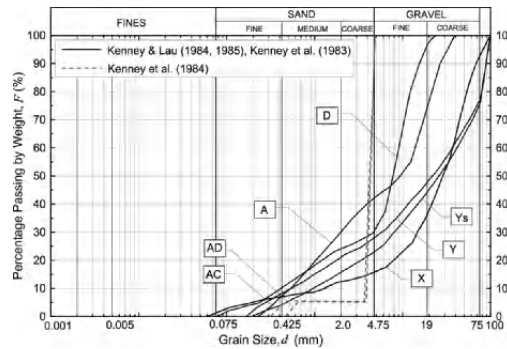


Figure 1.22. Samples of sandy-gravel tested as being internally unstable (suffusive) by Kenney and Lau [KEN 85a] and Kenney et al. [KEN 85a]

1.4.2.2. Some methods for assessing whether a soil is subject to suffusion

There are a number of methods available to determine whether a soil is subject to suffusion.

The following are some of the more widely used and/or later methods. It is suggested that the method or methods that were developed for soils most closely matching the soil being assessed, be used. For important decisions, it may be necessary to carry out tests on the soils under consideration given the uncertainty in the methods currently available.

Whenever assessing soils, allowances must be made for the effects of segregation as the dam or levee was constructed. Segregation can transform an internally stable soil into an internally unstable one. In view of this, it will generally be necessary to test several gradations to model the potential range of gradations that may occur after segregation.

1.4.2.2.1. Russian approaches

The Russian researchers who concentrated on suffusive soils were motivated by using well-graded gravelly filters in

embankment dams instead of several layered filters. The objectives were a minimum void ratio, a uniform distribution of constriction sizes with a small mean value and a granular structure where all the grains are fixed by a large number of contact forces.

In Eastern Europe, the graphical approach by Lubockov [LUB 65] was used by comparing the normalized grain size distribution with empirical upper and lower bound thresholds (Figure 1.23). This approach is valid for convex, concave and linear grain size distributions in semi-logarithmic scale. Gap-graded grain size distributions cannot be analyzed.

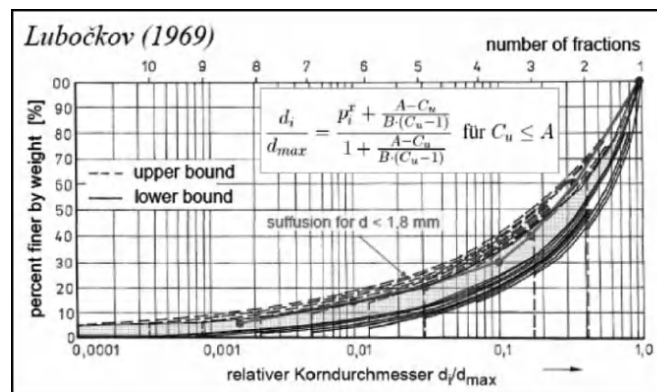


Figure 1.23. Upper and lower bound of non-suffusive soils by Lubockov [LUB 65] (Courtesy of J. Witt)

The current Russian guidelines are based on both the following criteria, where d_s is the largest suffusive grain size diameter, d_{p0} is the effective opening size of the material and d_{17} is the grain size diameter with 17% finer by weight and $d_{3-5\%}$ loss from 3% to 5% finer by weight.

Condition of particle mobility:

$$d_s \geq 0.77d_{p0}$$

for $Cu < 25$:

$$d_{po} = 0.455(1 + 0.05Cu)^{\frac{6}{5}}\sqrt[6]{Cu \cdot e \cdot d_{17}}$$

For $Cu > 25$:

$$d_{po} = 0.16(3 + \sqrt[3]{Cu \cdot \lg(Cu)})^{\frac{6}{5}}\sqrt[6]{Cu \cdot e \cdot d_{17}}$$

Condition of erosion in excess:

$$\frac{d_{3-5\%}}{d_{17}} \geq 0.32(1 + 0.05Cu)^{\frac{6}{5}}\sqrt[6]{Cu \cdot e}$$

1.4.2.2.2. Cambefort approach

Cambefort [CAM 64] pointed out that gap-graded soil in alluvial foundations is the deposits of high flow velocity (gravel) and low flow velocity (clayey and sandy silts) sediments. Their gradations appear in a log-log diagram of the grain size distribution. A Terzaghi criteria may be applied between both the gradations to check the stability (Figure 1.24)

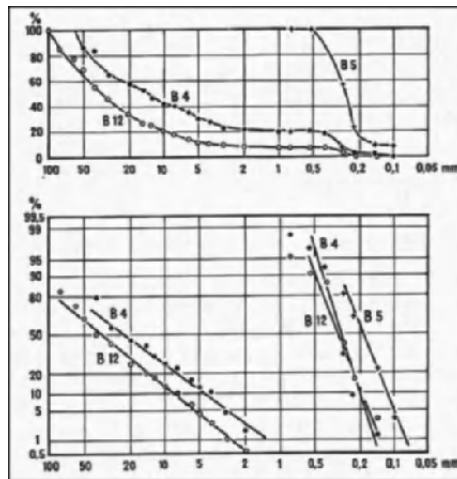


Figure 1.24. Gradation of silt and gravel from the particle size distribution of alluvium

1.4.2.2.3. Kenney and Lau method

The Kenney and Lau [KEN 85b, KEN 86] method plots F , the mass fraction smaller than grain size D (as in a conventional particle size distribution plot), for the soil and from this a plot of F versus H , the mass fraction between D and $4D$. For particles to move, there must be a deficiency in the mass of particles in the range D – $4D$. Figures 1.25 and 1.26 show the method.

If the soil plots to the right of the boundary of Figure 1.20 ($H < F$), it is likely to be internally unstable provided that it satisfies the rules on limiting finer fraction; that is, $F = 0.2$ for widely graded soils and $F = 0.3$ for narrow-graded soils. This is an important part of the method, which is to ensure that the voids between the coarse particles are underfilled, a prerequisite for soils being internally unstable.

The method was developed for a sandy gravel filter and transition zones with less than 5% fines passing 0.075 mm.

Rönqvist [RON 07, RON 08, RON 09, RON 10] applied Kenney and Lau's method [KEN 85b, KEN 86] to assess the internal stability of the filters and core grading of a number of existing moraine (glacial till) core dams, a number of which had exhibited signs of internal erosion and many had not. He found a correlation between dams with historic performance of internal erosion and internal instability of the filter and the core. However, this was related to the fact that the filters of the dams showing internal erosion were coarser than the no-erosion filters. Most were in the "some erosion" or "excessive erosion" range as defined by Foster and Fell [FOS 01].

Li and Fannin [LI 08a] proposed a unified approach combining the methods of Kezdi and Kenney and Lau. A plot of the Kezdi and Kenney and Lau boundaries in (F, H) space

is shown in Figure 1.27. The Kenney and Lau criterion is the more conservative of the two methods at $F > 15\%$, while the Kezdi criterion is more conservative at $F < 15\%$.

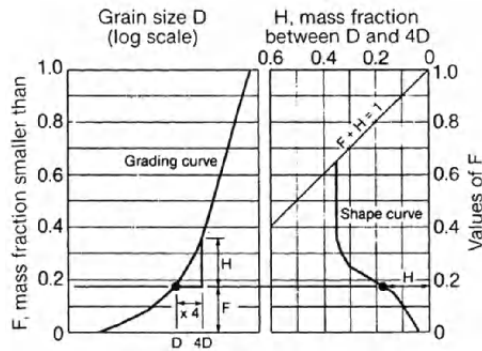


Figure 1.25. Method of characterizing the shape of a grading curve [KEN 85a]

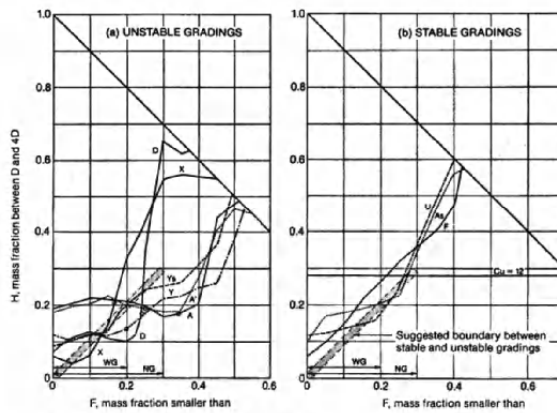


Figure 1.26. Method of assessing internal instability by Kenney and Lau [KEN 85a], with the revised criteria from Kenney and Lau [KEN 86].
 Legend: WG, soils widely graded ($C_u > 3$) in the range $F = 0.2-1.0$;
 NG, soils narrowly graded ($C_u < 3$) in the range $F = 0.3-1.0$

Semar *et al.* [SEM 10] determined from the above criteria the soils that are not vulnerable to suffusion:

- 1) Soils with a factor of uniformity C_u around 1.
- 2) Soils with a rather linear grain size distribution in semi-logarithmic scale and $C_u < 10$ irrespective of the relative density.
- 3) Steady curved grain size distribution with $C_u < 8$.
- 4) Well-graded soils that are very close to the Fuller, Talbot or Lubockov grain size distribution.

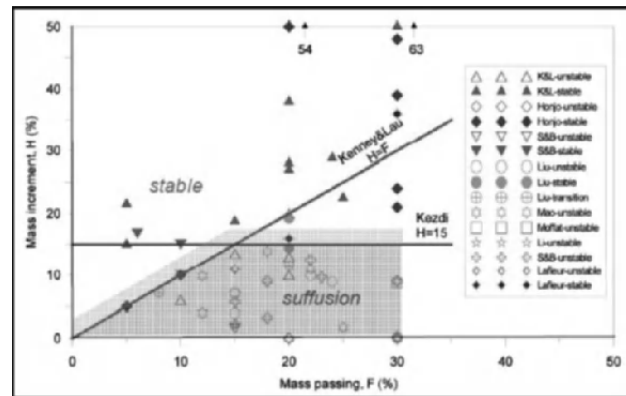


Figure 1.27. A unified approach for geometric criterion of suffusion [LI 08]

1.4.2.2.4. Wan and Fell adaptation of the Burenkova method

Wan and Fell [WAN 04c, WAN 07] found that the Burenkova [BUR 93] method gave reasonable assessments of whether a soil was internally unstable when used for the soils they had tested. However, the method does not give a clear-cut boundary between internally stable and unstable soils in the data set. To model this, logistic regression was used by Wan and Fell [WAN 04c, WAN 07] to define contours of equal probability of internal instability. Figures 1.28 and 1.29 show the contours and the logistic equations.

Figure 1.28 needs to be applied to silt–sand–gravel and clay–silt–sand–gravel mixtures with a plasticity index less than 13% and less than 10% clay size fraction (% passing

0.002 mm) and Figure 1.29 to sand–gravel soils with less than 10% non-plastic silt fines passing 0.075 mm.

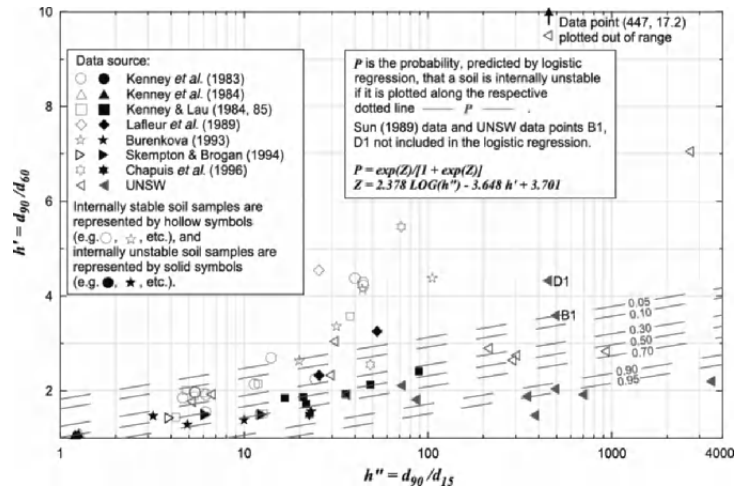


Figure 1.28. Contours of the probability of internal instability (potentially suffusive) for silt–sand–gravel soils and clay–silt–sand–gravel soils of limited clay content and plasticity [WAN 04c, WAN 07]

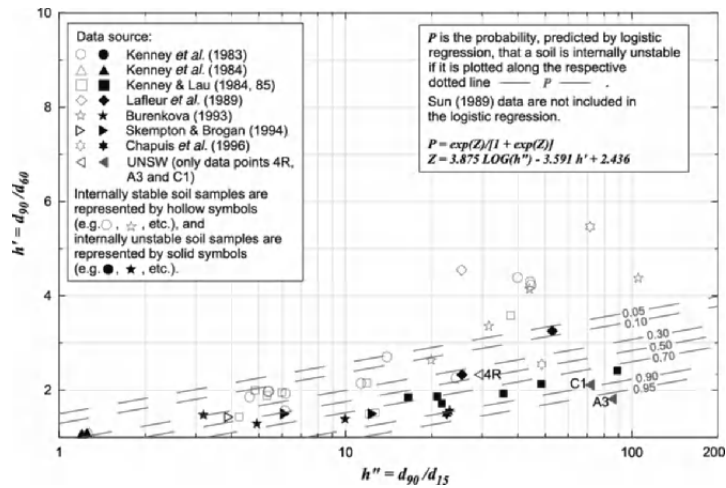


Figure 1.29. Contours of the probability of internal instability potentially suffusive for sand–gravel soils with less than 10% non-plastic fines passing 0.075 mm [WAN 04c, WAN 07]

Wan and Fell [WAN 04c, WAN 07] found that for the silty–sandy–gravel soils they tested, the Kenney and Lau [KEN 85b, KEN 86] method was too conservative, identifying the silt–sand–gravel soils they tested as internally unstable when they tested as stable. Wan and Fell [WAN 04c, WAN 07] also found that the Istomina [IST 57], Sherard [SHE 79] and Sun [SUN 89] methods were conservative for these silt–sand–gravel soils.

1.4.2.2.5. Testing of some internally stable cohesionless soils and cohesive

Some authors have used the terms suffusion and suffosion to describe internal erosion in global backward erosion laboratory experiments on internally stable cohesionless soils and cohesive soils under very high gradients. This includes the tests by Moffat and Fannin [MOF 11b] and Moffat *et al.* [MOF 11a] on some internally stable cohesionless soils and Marot *et al.* [MAR 07], Bendahmane *et al.* [BEN 08] and Sail *et al.* [SAI 11] mainly on cohesive soils.

Many of these soils tested have overfilled voids between the coarser particles, so the finer fraction is not free to move under the gradients normally experienced in dams. Therefore, they are by basic definition accepted by many authors, including Kenney and Lau, Burenkova, Wan and Fell, not internally unstable and subject to suffusion.

These authors have observed some particle movement at relatively low gradients but the major movement occurs at high gradients such as 20 or 30.

The question is whether the phenomena they observed is or is not suffusion as commonly used and as defined in this chapter. It is unlikely. It may be a concentrated leak erosion due to hydraulic fracture or a form of global backward erosion, or in some cases it may be somewhere between backward erosion and suffusion.

1.4.2.3. *Assessment of the largest erodible particles in suffusion*

Wan [WAN 06] and Wan and Fell [WAN 04c] give details of a method to determine what fraction of the soil will be eroded. Fell *et al.* [FEL 08] have found that in the practical terms for the soils they tested, it can be assumed that 50% of the finer fraction as defined by the point of inflection of broadly graded soils and the fine limit of the gap in gap-graded soils is eroded, and the particle size distribution is replotted.

They suggest that if this becomes critical, laboratory tests should be carried out on the internally unstable soil. The tests should cycle the loading and be allowed to run for long durations.

The second author has experienced changes of permeability from year-to-year, in alluvial foundations where the cyclic rise of water occurred during floods. After more than 40 years, the local permeability has increased to as high as 10^{-1} m/s indicating that all of the finer fraction was eroded.

Witt and Salehi Sadaghiani [WIT 12a] proposed two methods to define the largest erodible particle. In the first method, the largest mobile particle as the largest grain size D (as in a conventional particle size distribution plot) splits the soil into the fine part (characterized by d_{85}) and the coarse part (characterized by D_{15}), where the limit state $D_{15}/d_{85} > 9$ is observed. In the example in Figure 1.30, the largest erodible particle is between 1.2 and 2 mm. The second method proposed by Witt and Salehi Sadaghiani [WIT 12b] used the sequential fill test designed to measure relative height and porosity of the soil by filling the soil fractions from the coarsest to the finest. The size of the largest mobile particles is estimated when relative height is one and the porosity is no more constant and begins to

decrease. The clustering results of soil particles distribution function using two normal distributions is another method agreeing fairly well with the conducted test results.

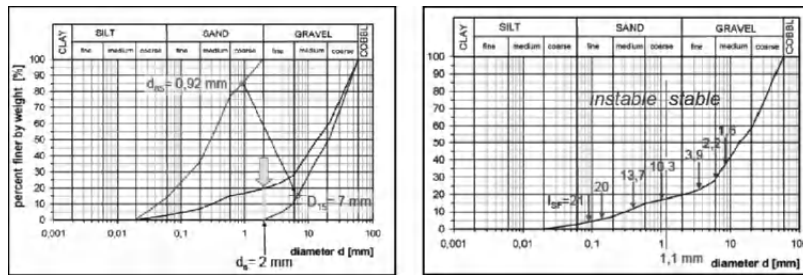


Figure 1.30. Assessment of the largest erodible particle in suffusion [WIT 12a, WIT 12b]

1.4.3. Hydraulic conditions where soils are internally unstable and potentially subject to suffusion

1.4.3.1. The role of numerical modeling of particle transport

- There have been some promising developments in modeling particle transport (e.g. Shire and O’Sullivan [SHI 11]).

- These appear to have potential to model individual particles in internally unstable soils.

1.4.3.2. Assessment of the flow velocity that will cause suffusion

Golz *et al.* [GOL 10] developed hydraulic criteria based on the constriction of opening size and Shields transport relationship between diameter, flow velocity and a Reynold’s number. This hydraulic criteria, based on the Darcy flow velocity, corresponds to that proposed for contact erosion. This has so far been trialed on limited test data.

1.4.3.3. *Assessment of the seepage gradient that will cause suffusion*

Skempton and Brogan [SKE 94] show that erosion will begin in internally unstable cohesionless soils at seepage gradients lower than the Terzaghi critical or zero effective stress gradient. Wan and Fell [WAN 04c, WAN 07] found that all internally unstable soils they tested eroded with upward gradients of 0.8 or less, with several eroding with gradients less than 0.3. They found that soils with a higher porosity begin to erode at lower hydraulic gradients and the loose, higher porosity soils tested began to erode at gradients less than 0.3. They found that soils with plastic fines required higher gradients to begin to erode at lower gradients than non gap-graded soils with the same fines content.

Monnet [MON 98] correlated the hydraulic gradient initiating failure measured by Skempton and Brogan [SKE 94] to the measured permeability, showing that the hydraulic criterion governs the value of hydraulic gradient moving finer particles.

Li and Fannin [LI 08b] proposed a hydromechanical criterion deduced from tests on internally stable and unstable materials. Starting from the fact that seepage failure occurs in stable soils under the Terzaghi critical hydraulic gradient, i_{CT} , Li and Fannin [LI 08b] deduced the critical gradient, i_c , for any unstable soil, from the proportion of the effective stress α sustained by the fines.

$$i_c = \alpha \cdot i_{CT} = \alpha \frac{\gamma'}{\gamma_w}$$

where γ_w and γ' are the water and buoyant soil-specific weight and α is the reduction factor of the vertical effective stress σ'_v carried by the finer particles in internally unstable soil and was first proposed by Skempton and

Brogan [SKE 94]. The finer grains carry a reduced portion of the effective stress, σ'_f :

$$\sigma'_f = \alpha \cdot \sigma'_v$$

The reduction stress factor α is related to the mobility of the finer particles and is dependent on the geometric criterion d'_{85}/O_{50} , where d'_{85} is the d_{85} of the finer fraction of soil and O_{50} is the effective constriction size of the coarse fraction, as follows:

$$\alpha = 3.85(d'_{85}/O_{50}) - 0.616$$

This method needs more test data on internally unstable soils that are subject to suffusion so the variables can be calibrated for those soils.

1.4.4. *Commentary on the state of the art and the role of laboratory testing in assessing suffusion*

There are very few data on the coupling of suffusion and deformation. Recent data from Chang *et al.* [CHA 12] show a rather important coupling. During the suffusion process of a soil, they define two critical hydraulic gradients: the initiation of erosion and skeleton-deformation hydraulic gradients. The initiation hydraulic gradient is defined as the gradient that initiates internal erosion. When the applied hydraulic gradient is further increased to another critical value, referred to as skeleton-deformation hydraulic gradient, sudden increases in eroded soil mass, soil permeability, and deformation are observed. The skeleton-deformation hydraulic gradient is mainly controlled by the stress state, followed by soil porosity. The skeleton-deformation hydraulic gradient under an isotropic stress condition is much larger than those under shearing conditions. The skeleton-deformation critical gradient is a suitable parameter for geotechnical design because the

structural behavior will be adversely affected after the applied gradient exceeds this critical value. The critical hydraulic gradients determined using conventional one-dimensional (1D) seepage tests fail to capture the shear stress effects and tend to be unsafe. More research is needed to confirm that results.

1) There is an unfortunate development in recent years of authors describing as suffusion internal erosion in soils that have over filled voids between the coarse particles and are therefore not internally unstable as defined in most literature including Kenney and Lau [KEN 85a, KEN 86]. This is potentially confusing.

2) The available methods for identifying internally unstable soils rely on simple combinations of particle sizes from the particle size distribution of the soil. As shown by Wan and Fell [WAN 08], these are not sufficient to give a clear demarcation between internally unstable and stable soils. This is related to the inability of such simple relationships to define such soils, but probably also to the fact there is a transitional behavior between suffusion of truly internally unstable soils, and backward erosion and or hydraulic fracture that occurs at higher gradients. In many of the internally stable soils tested, the gradients to initiate internal erosion are so high that they are unlikely to occur in dams, levees or their foundations.

3) As there are no generalized methods for accurately predicting the critical seepage gradient and the amount and gradation of the eroded particles, laboratory tests should be carried out that carefully simulate the field conditions. It may be necessary to construct specific test equipment because of the large particles involved and potential for segregation.

4) Great care must be taken in carrying out laboratory scale tests for this phenomena. The common practice of using

a “scalped” grading with the coarser particles replaced by particles of a size that can fit into the laboratory test cylinders potentially makes the samples internally unstable and the tests will not be representative of the actual soil behavior.

5) The experience in tests of internal instability by Wan and Fell [WAN 08] showed that small variations in the shape of the particle size distribution resulted in soils from being stable to unstable. It is therefore essential to test the actual gradations in the dam, rather than using mean or average gradations. For the same reason, researchers should refrain from suggesting that their methods based on only a small number of sample particle size distributions may be globally applicable.

6) Broadly graded silt-sand-gravel soils are subject to segregation during placement in the dam or levee. The degree to which this has occurred must be investigated and the soil particle size distribution used in the laboratory tests should be as actually in the dam because the likelihood of global backward erosion may be significantly greater for the segregated soil than for non-segregated soil. Segregation in placing the samples into laboratory test equipment is also a potential problem requiring careful laboratory test procedures.

7) The way in which samples are compacted in the laboratory should simulate so far as practicable the field compaction technique. They should be compacted partially saturated, as they are in a dam or levee.

8) There has been little research to assess the effects of flow direction on the critical gradient. Ideally the test equipment should replicate the field condition because the mechanics of particle transport will be somewhat different for vertical and horizontal flow.

1.5. Contact erosion

1.5.1. *The mechanics of contact erosion*

Contact erosion occurs where a coarse soil such as a gravel is in contact with a fine soil, and flow parallel to the contact in the coarse soil erodes the fine soil as shown in Figure 1.31.

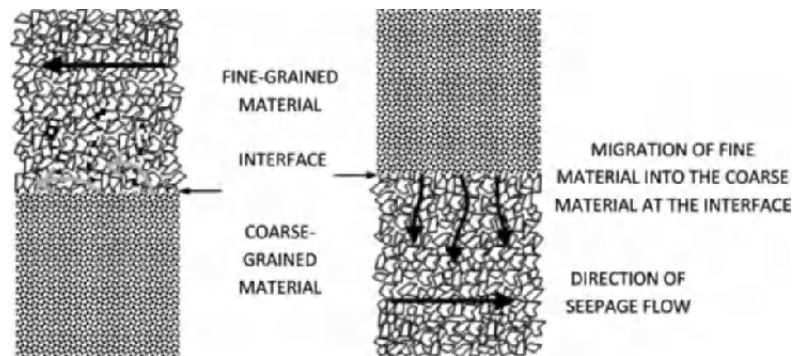


Figure 1.31. *Diagram of soil contact erosion*

Particles of the finer layer may be destabilized by the water flow and transported through the pores of the coarser layer parallel to the interface.

Interfaces between different soils that exist in the dam or in the foundation (Figure 1.4) with possible high velocities in the coarser layer and high particle size grading contrast between layers are the most likely to experience contact erosion. These characteristics usually correspond to the interface between the core and a gravelly foundation. For example, at the zoned dikes on the river Rhône, with clayey silt core and gravel shoulders, some 20 cases of leakage associated with development of a sinkhole or subsidence have been reported [CFG 97]. The process starts with contact erosion at the interface between the silt and the gravel, often at the contact between the fill and the foundation or in the foundation. This causes a cavity within the unsaturated fill, and then the stresses drop around that cavity, causing the

roof to collapse. Those materials fill in the lower part of the cavity and enlarge it at the top; then the roof of the new cavity is decompressed and, step-by-step, the cavity progresses along a practically vertical chimney toward the crest or the upstream face (Figure 1.32(a)). Leakage flow decreases after the materials fall, and then progressively builds up again, carrying away the fallen material until the next collapse.

Other consequences of contact erosion are possible as shown in Figure 1.32. First, depending of the mechanical properties of the core, the cavity created by contact erosion may not collapse and may progress downstream and form an erosion pipe, until the pressure fractures the downstream face and begins backward erosion piping (consequence b). This process has been identified in hydraulic flume tests at a scale of 1/1, where the downstream gravel shoulder was too thin to prevent hydraulic fracture [BEG 12]. Second, a weaker zone, less dense because of the development of contact erosion, can cause a loss of stability (consequence c). Finally, the fines particles eroded may clog the permeable layer and increase pore water pressure that may result in instability or sloughing of the downstream slope (consequence d).

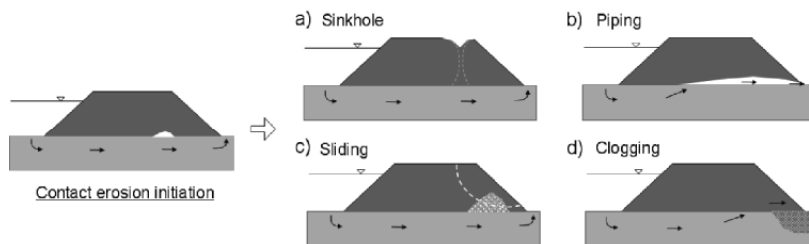


Figure 1.32. Consequences of contact erosion. Black arrows indicate a groundwater flow through a more permeable layer (light gray) under a less permeable dam (dark gray). a) Sinkhole daylight, b) beginning of backward erosion piping, c) creation of a weaker zone initiating instability and d) clogging of the permeable layer and increase of pore water pressure [BEG 09]

1.5.2. Methods available to assess the likelihood of contact erosion

Two conditions are needed for initiation of contact erosion:

1) *Geometrical condition*: Pores of the coarse layer have to be sufficiently large to allow particles to pass through.

2) *Hydraulic condition*: Flow velocity has to be sufficient to detach the particles and also to transport them.

If both conditions are fulfilled, contact erosion is likely to occur. The following summarizes the available methods.

1.5.2.1. Brauns, Wörman, and Den Adel methods for assessing the geometrical condition

Brauns [BRA 85], Wörman [WOR 92] and Den Adel [DEN 94] studied contact erosion in non-plastic soils and proposed expressions for the hydraulic conditions for the detachment and transport of particles on the basis of experimental results. They stated that close to the geometrical limit, the hydraulic loading for erosion initiation is increasing and a transition zone of combined influence where the hydraulic loading needed to initiate contact erosion is higher than in the domain of pure hydraulic influence as shown in Table 1.8.

	Grading ratio D_{15}/d_{85} →				
Brauns (1985) soil with $n = 0.4$	Geometrical condition	7.5	Geometrical and Hydraulic condition	25	Hydraulic condition
Wörman (1992) soil with $D_{15} = 0.88D_H$				14.6	
Den Adel (1994) soil with $d_{85} = d_{90}/0.9$		8.1		11.7	

Note. D_{15} is the particle size of the coarser soil for which 15% is finer, d_{85} is the particle size of the finer soil for which 85% is finer and n is porosity.

Table 1.8. Domain of geometrical and hydraulic influence for non-plastic soils (Courtesy of R. Beguin, from [BRA 85], [WOR 92] and [DEN 94])

Brauns [BRA 85], Wörman [WOR 92] and Den Adel [DEN 94] found that for D_{15}/d_{85} ratios less than in the third column in Table 1.8, there is geometrical filtration whatever the hydraulic loading, so contact erosion could not occur. They found that if the D_{15}/d_{85} ratio in the fifth column is more than 25 hydraulic loading controls erosion and there is no filtration effect. In between these two limits, both geometric and hydraulic factors control erosion.

The second boundary between “Geometrical and Hydraulic condition” and “Hydraulic condition”, defines if the coarse layer grading has, or has not, an influence on the hydraulic criteria for erosion initiation. For example, Brauns [BRA 85] obtained that in the “Hydraulic condition” domain, the critical velocity for a fine soil can be calculated without taking into account the coarse soil grading (this is valid in its experimental range $25 < D_{15}/d_{85} < 57$). In the “Geometrical and Hydraulic condition” domain, for $7.5 < D_{15}/d_{85} < 25$, the critical velocity will also be the function of the coarse soil grading. In a same manner, erosion laws proposed by Den Adel [DEN 94] and Wörman [WOR 92] are valid in their “Hydraulic condition” domain, where the influence of the coarse layer on the initiation of erosion can be neglected.

For any particular fine soil, the “critical” gradient, which corresponds to the gradient in the coarse layer parallel to the contact at which the erosion initiates, can vary by one order of magnitude, depending of the permeability of the coarse layer. However, in the same tests, the “critical” Darcy velocity for erosion initiation does not significantly depend on the coarse layer permeability, and is only related to the fine soil resistance to erosion. Therefore, the Darcy velocity has been chosen by the majority of authors as a good indicator of the hydraulic loading. The hydraulic conditions for contact erosion depend of the configuration considered.

1.5.2.2. Methods for assessing the critical hydraulic conditions

– *For fine cohesionless soil below a coarse soil layer:* This configuration has been widely studied ([IST 57], [BRA 85], [BEZ 87], [GUI 10], [BEG 11], [HOF 12b]).

In the case of sand erosion, particles are mainly transported as bedload and authors have concluded that classical river erosion criteria can be empirically adapted to the case of contact erosion. They have proposed methods on the basis of the Shields [SHI 36] criterion. One conclusion of these works is that the diameter of the coarse layer particles has a weak influence on the critical velocity. Experimental results are shown in Figure 1.33.

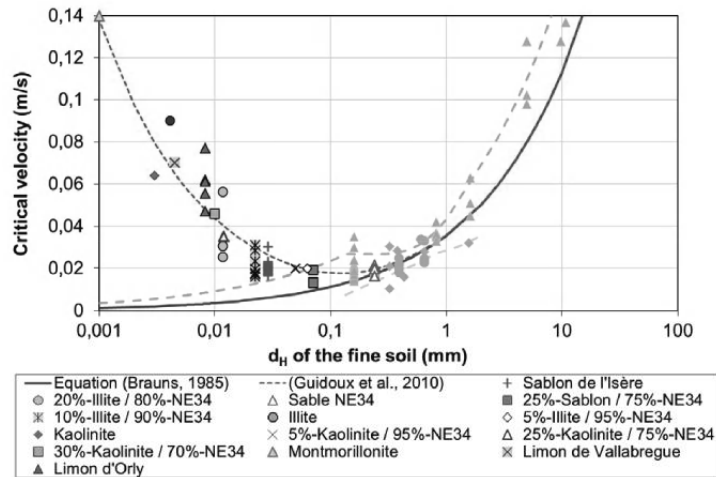


Figure 1.33. Critical Darcy velocities for contact erosion of sand below a gravel layer [BEG 11]

Experimental results range between 0.01 and 1 m/s for the critical Darcy velocity, and a minimum value seems to appear for particles of diameter 1.0×10^{-4} m (100 μ m). Braun's [BRA 85] law is the simplest formula to use and gives a good approximation for sand:

$$U_{crit} = 0.65.n_D \sqrt{\frac{(\rho_s - \rho_w)}{\rho_w} g d_{50}}$$

where n_D is the porosity of the gravel layer, ρ_s (kg/m³) is the density of the sand particles, ρ_w (kg/m³) is the water density and d_{50} (m) is the median diameter of sand grading curve.

Hoffmans [HOF 12] generalizes the shear stress approach of Shields for loose-packed granular materials (say $d > 10^{-4}$ m) with an equation, based on Darcy's law, the Poiseuille flow, the Shields number $\Psi_{lam,c}$ of sediment transport in laminar flow, $\Delta = (\rho_s - \rho_w)/\rho_w$ and some geometrical assumptions regarding the pipes, giving the critical Darcy velocity U_{crit} :

$$U_{crit} = \sqrt{\frac{1}{2} \text{Re}_{m,c} \Psi_{lam,c} \Delta g d_{15}}$$

Thus, U_{crit} depends on the maximum critical Reynolds number and the critical bed shear velocity. Considering the laminar flow conditions, where the Reynolds filter number (Re_f) is smaller than 10, it is noted that Hoffman's equation is comparable with the method as proposed by Guidoux *et al.* [GUI 10] and generalizes it at all the open filter.

Three models of sand erosion have been developed that allow estimation of the amount of transported sand as a function of the hydraulic loading ([WOR 92], [DEN 94], [SCH 02]). However, these models have been validated only for the soils tested by their author, and they have to be used with caution.

– *Erosion of silt and clay (particles < 75 μm):*

Guidoux *et al.* [GUI 10] carried out some experimental tests of contact erosion with silt and clay. They adapted the critical Darcy velocity U_{crit} from Braun's [BRA 85] method

with an added empirical parameter β to take into account the adhesive forces.

$$U_{crit} = 0.65.n_D \sqrt{\left(\frac{\rho_s - \rho_w}{\rho_w}\right) g d_H \left(1 + \frac{\beta}{d_H^2}\right)}$$

The effective diameter d_H of the fine soil, instead of the d_{50} , conserves the specific surface of the initial grain size distribution. It is defined by:

$$d_H = \left(\sum_{j=1}^m \frac{F_j}{d_j}\right)^{-1},$$

where F_j is the percentage of the fraction of diameter d_j in the grading curve of the soil, the parameter β has been selected as $5.3 \times 10^{-9} \text{ m}^2$ and other variables are as for Braun [BRA 85] above.

This formula gives a reasonable fit to the experimental data for these finer soils but cannot fit all the cohesive soils that exhibit different erosion behavior linked to other more relevant properties than particle diameter such as the clay mineralogy and degree of saturation.

– *Erosion of a fine soil above a coarse soil layer:*

Schmitz [SCH 07] carried out experimental tests of erosion of silt layers above coarse layers (Figure 1.34). In contrast to the previous configuration (fine soil below coarse soil), he noticed an influence of the confining stress on the critical velocity. For higher vertical stresses on the sample, he measured higher critical velocities. Except for one value, the critical velocities measured are of the same order of magnitude than in the other configuration, between 1 and 10 cm/s but lower than the critical velocities proposed by Guidoux *et al.* [GUI 10].

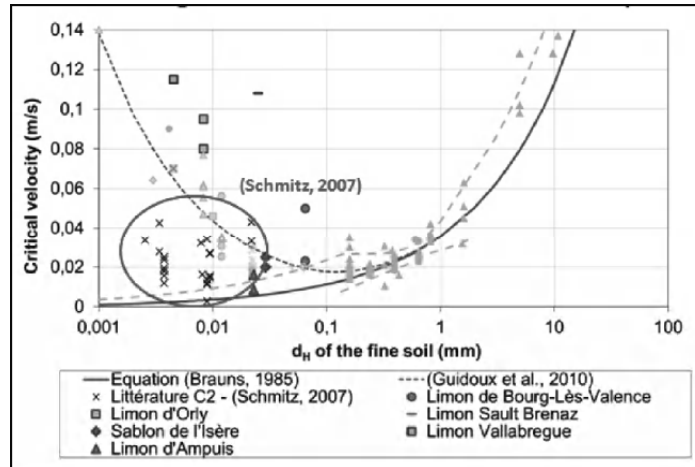


Figure 1.34. Tests data of Schmitz [SCH 07]

For clay soils, he proposed a method for estimating the critical velocity depending on results of a vane shear stress test on the soil, but comparison of its model with results are not very convincing. This is to be expected as the critical shear stress for clay soils is not related to the shear strength as discussed in section 2.3.3.

– *Influence of uniformity:* When contact erosion occurs in a widely graded fine soil, segregation processes usually influence the process. Fines particles are eroded preferentially because they are more sensitive to hydraulic loading. Coarser particles are also likely to clog the pores of the coarse layer and generates a filter layer at the surface of the fine layer. This can occur for a fine layer above or below the coarse soil and tends to result in a decrease of the erosion rate with the development of this filter layer. As a result, the geometrical and the hydraulic condition for erosion may be fulfilled for contact erosion but after a certain amount of eroded soil that can be excessive for dam safety or not, erosion stops under constant flow velocity.

1.5.3. Contact erosion or “scour” at the interface between open joints in rock foundations and the core of dams

This considers the likelihood that seepage flows within a continuous pathway in a rock or soil foundation may initiate erosion of the core material at the core-foundation contact. This is really a form of concentrated leak erosion but is included in the section on contact erosion because some think of it as contact erosion or scour. The steps in the assessment are as follows:

1.5.3.1. Hydraulic criteria

1) Estimate the probability of a continuous pathway for erosion at the core-foundation contact (P_{path}) from geological information and construction records.

2) Estimate the likelihood of erosion of the core material at the core-foundation contact using the method for erosion in a crack in the core as described in section 1.2.3. The hydraulic gradient used in the assessment should be based on the estimated seepage gradient on the core-foundation contact. This assumes that the hydraulic shear stresses imposed on the core by the water flowing in the open joints is equivalent to those for an equivalent crack width.

There may be foundations where the information available from construction and site investigations indicates that there will be continuous open defects in the foundation but they are of varying width. Figure 1.35 shows some examples of this.

For these situations, it is necessary to consider both parts of the defect because the largest gradient will be in the narrower crack width area, but the hydraulic shear stresses will be smaller in these areas.

1.5.3.2. *Geometric criteria*

For erosion to continue through an open defect, the defect needs to be sufficiently open to allow the soil surrounding the defect to pass through it. According to Hoffmans [HOF 12b], based on the principles of continuing erosion criteria given in [FOS 01], erosion into an open joint will continue if the joint opening is greater than d_{95} of the soil. The d_{95} should be based on the average soil grading after re-grading on 4.75 mm particle size.

1.5.4. *Commentary on the state of the art and the role of laboratory testing in assessing contact erosion*

1) The geometric criteria (filtration) have been extensively researched and are well developed for non-plastic soils.

2) It should be possible to apply the Foster and Fell [FOS 01] criteria for filters that do not satisfy modern filter design criteria to contact erosion of plastic and non-plastic soils.

3) The hydraulic criteria are reasonably well developed for non-plastic soils but with a significant uncertainty as shown in the data in Figure 1.34.

4) The hydraulic criteria for plastic soils requires further research, which should take account of the mechanics and methods for concentrated leak erosion because the erosion process is similar, but the hydraulics of the flow are more complex.

5) Care should be taken in reaching conclusions based on short-term laboratory tests. Relation of laboratory tests to field performance is important.

6) It would be worthwhile to carry out experiments modeling the scour into an open joint in rock foundations, and to refine the hydraulics of flow in the crack more precisely than assumed in [FEL 08].

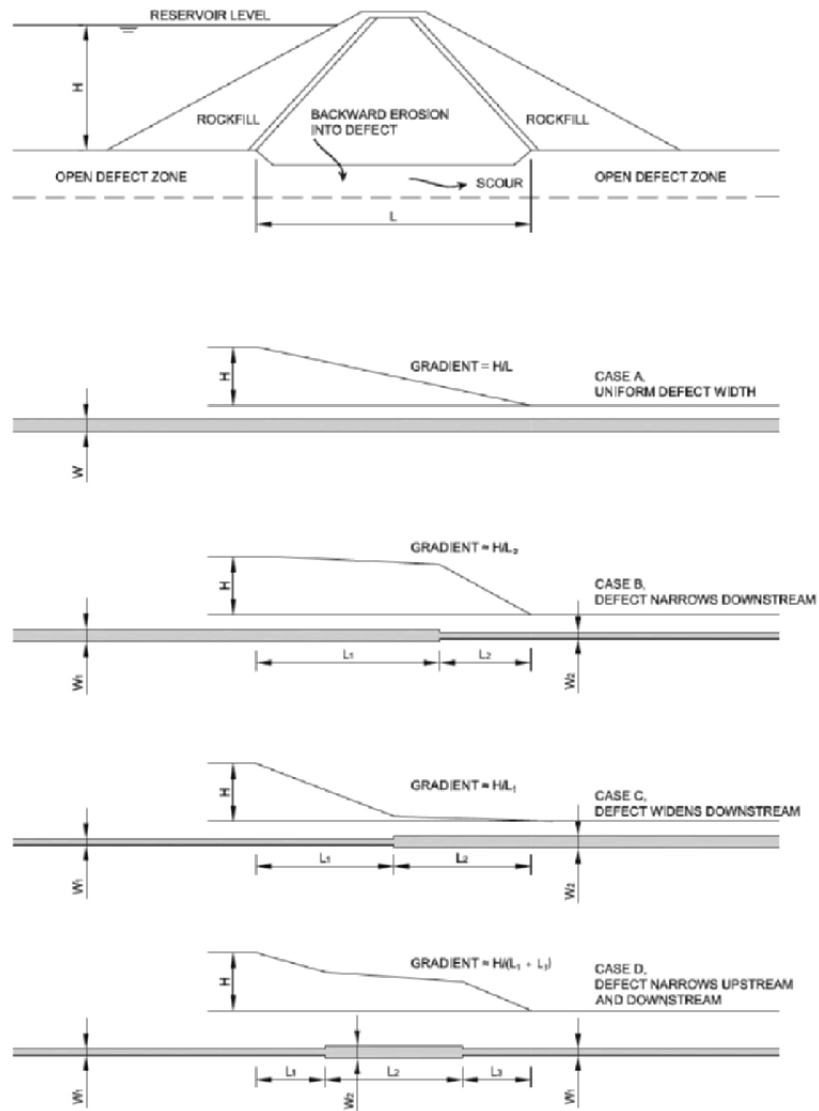


Figure 1.35. Examples of foundations with continuous open defects of varying width

1.6. Bibliography

- [ARU 83] ARULANANDAN K. and PERRY E.B., “Erosion in relation to filter design criteria in earth dams”, *Journal of the Geotechnical Engineering Division, ASCE*, 109 (GT5), pp. 682–698, 1983.
- [BEE 10a] VAN BEEK V.M., BEZUIJEN A., ZWANENBURG C., “Piping: centrifuge experiments on scaling effects and levee stability”, *7th int. conf. on Physical Modeling in Geotechnics*, Zurich, 28 June-1 July 2010.
- [BEE 10b] VAN BEEK V.M., KNOEFF J.G., RIETDIJK J., *et al.*, “Influence of sand characteristics and scale on the piping process – experiments and multivariate analysis”, *7th Int. Conf. on Physical Modeling in Geotechnics*, Zurich, 28 June - 1 July 2010.
- [BEE 11] VAN BEEK V.M., KNOEFF J.G., SELMEIJER J.B., “Observations on the process of backward piping by underseepage in cohesionless soils in small-, medium- and full-scale experiments”, *European Journal of Environmental and Civil Engineering*, vol. 15/8, 2011, pp 1115–1137.
- [BEG 09] BEGUIN R., GUIDOUX C., FAURE Y.H., *et al.*, “Stability conditions and erosion rates at the contact between two soils, subjected to a water flow parallel to the interface”, *Presentation at ICOLD European Working Group on Internal Erosion St. Petersburg*, April 2009.
- [BEG 10] BEGUIN R., FAURE Y.-H., GUIDOUX C., *et al.*, “Hydraulic erosion along the interface of different soil layers scour and erosion”, *Proceedings of the 5th International Conference on Scour and Erosion*, ASCE Geotechnical Special Publication No. 210, pp. 387–396, 2010.
- [BEG 11] BEGUIN R., Etude multi-échelle de l'érosion de contact dans les ouvrages hydrauliques, Thesis, University Joseph Fourier Grenoble, 2011.
- [BEG 12] BEGUIN R., FRY J.-J., PICAULT C., *et al.*, Control of the risk of dike failure caused by contact erosion, Paper 270, ICSE6 Paris, pp. 1551–1558, 27–31 August 2012.

- [BEN 08] BENDAHMANE F., MAROT D., ROSQUOËT F., *et al.*, “Experimental parametric study of suffusion and backward erosion”, *International Journal of Geotechnical and Geoenvironmental Engineering*, vol. 134, no. 1, pp. 57–67, 2008.
- [BEZ 87] BEZUIJEN A., KLEIN-BRETELLER M., BAKKER K.J., “Design criteria for placed block revetments and granular filters”, *Proceedings of the 2nd International Conference on Coastal & Port Engineering in Developing Countries*, Beijing, China, 1987.
- [BEZ 10] BEZUIJEN A., STEEDMAN R.S., *Scaling of Hydraulic Processes, Physical Modelling in Geotechnics*, Taylor and Francis Group, Zürich, 2010.
- [BON 07] BONELLI S., OLIVIER B., DAMIEN L., “The scaling law of piping erosion”, *18 ième Congrès Français Mécanique*, Grenoble, 2007.
- [BON 08] BONELLI S., BRIVOIS O., “The scaling law in the hole erosion test with a constant pressure drop”, *International Journal for Numerical Methods in Engineering*, vol. 32, pp. 1573–1595, 2008.
- [BON 11] BONELLI S., BENAHMED N., “Piping flow erosion in water retaining structures”, *International Journal of Hydropower and Dams*, vol. 18, no. 3, pp. 94–98, 2011.
- [BRA 85] BRAUNS J., “Erosionsverhalten geschichteten Bodens bei horizontaler Durchströmung”, *Wasserwirtschaft*, vol. 75, pp. 448–453, 1985.
- [BUI 04] BUI H., FELL R., SONG C., Two and three dimensional numerical modelling of the potential for cracking of embankment dams during construction, UNICIV report no. 426, The School of Civil and Environmental Engineering, The University of New South Wales, Sydney, 2004.
- [BUI 05] BUI H., TANDRIJANA V., FELL R., *et al.*, Two and three dimensional numerical modeling of the potential for cracking of embankment dams-supplementary report, UNICIV report no. 438, The School of Civil and Environmental Engineering, University of New South Wales, Sydney, 2005.

- [BUR 93] BURENKOVA V.V., “Assessment of suffusion in non-cohesive and graded soils. Proceedings, the First International Conference “Geo-Filters”, Karlsruhe, Germany, 20–22 October 1992”, in BRAUNS J., HEIBAUM M., SCHULER U. (eds), *Filters in Geotechnical and Hydraulic Engineering*, Balkema, Rotterdam, pp. 357–360, 1993.
- [CAM 64] CAMBEFORT H., *Injection des sols. Tomes 1. Principes et methods*, in BRAUNS J., HEIBAUM M., SCHULER U. (eds), Editions Eyrolles, 1964.
- [CFG 97] CFGB, Internal erosion: typology, detection, repair, Bulletin du Comité Français des Grands Barrages FRCOLD NEWS, Barrages & Reservoirs. No. 6 – Special Congress CIGB Florence – May, 1997.
- [CHA 12] CHANG D.S., ZHANG L., XU T.H., “Laboratory investigation of initiation and development of internal erosion in soils under complex stress states”, in: *Proc. 6th Int. Conference on Scour and Erosion (ICSE-6)*, 27–31 August 2012, Paris, pp. 895–902, 2012.
- [CHA 86a] CHAPIUS R.P., Use of Rotational Device on Cohesive Soils, Transportation Research Record, p. 1089, 1986.
- [CHA 86b] CHAPIUS R.P., “Quantitative measurement of the scour resistance of natural soil clays”, *Canadian Geotechnical Journal*, vol. 23, pp. 132–141, 1986.
- [CHA 97] CHARLES J.A., “General report, special problems associated with earthfill dams”, *19th International Congress on Large Dams, Florence, GR Q73*, vol. II, International Commission on Large Dams, Paris, pp. 1083–1198, 1997.
- [DEM 85] DE MELLO V.F.B., “Peculiarities of ‘in situ’ behavior of tropical lateritic and saprolitic soils in their natural conditions: dam foundations”, *Proceedings TropicaLS’85, First International Conference on Geomechanics in Tropical Lateritic and Saprolitic Soils*, Brasília, Feb 11–14, pp. 73–104, 1985.
- [DEN 94] DEN ADEL H., KOENDER M.A., BAKKER K.J., “The analysis of relaxed criteria for erosion-control filters”, *Canadian Geotechnical Journal*, vol. 31, no. 6, pp. 829–840, 1994.

- [FEL 01] FELL R., WAN C.F., CYGANIEWICZ J., *et al.*, The Time for Development and Detectability of Internal Erosion and Piping on Embankment Dams and Their Foundations. UNICIV Report No.R-399, School of Civil and Environmental Engineering, University of New South Wales, 2001.
- [FEL 03] FELL R., WAN C.F., CYGANIEWICZ J., *et al.*, “Time for development of internal erosion and piping in embankment dams”, *ASCE Journal of Geotechnical and GeoEnvironmental Engineering*, vol. 129, no.4, pp. 307–314, 2003.
- [FEL 05] FELL R., MACGREGOR P., STAPLEDON D., *et al.*, *Geotechnical Engineering of Dams*, Balkema, Leiden, 2005.
- [FEL 07] FELL R., FRY J.J., “The state of the art of assessing the likelihood of internal erosion of embankment dams, water retaining structures and their foundations”, in FELL R., FRY J.J. (eds), *Internal Erosion of Dams and their Foundations*, Taylor and Francis, London, pp. 1–24, 2007.
- [FEL 08] FELL R., FOSTER M., DAVIDSON R., *et al.*, A Unified Method for Estimating Probabilities of Failure of Embankment Dams by Internal Erosion and Piping, UNICIV report no. 446, The School of Civil and Environmental Engineering, University of New South Wales, Sydney, Australia, 2008.
- [FEM 05a] FEMA, Impacts of animals on earthen dams, US Federal Emergency Agency, Report 473, 2005.
- [FEM 05b] FEMA, Technical manual for dam owners, impacts of plants on earthen dams, US Federal Emergency Agency, Report 534, 2005.
- [FEM 06] FEMA, Conduits Through Embankment Dams. Best Practices for Design, Construction, Problem Identification and Evaluation, Inspection, Maintenance, Renovation and Repair, US Federal Emergency Agency, 2006.
- [FON 95] FONG F.C., BENNETT W.J., “Transverse cracking on embankment dams due to earthquakes”, paper presented at the *1995 ASDSO Western Regional Conference*, Red Lodge, Montana, 1995.

- [FOR 98] FORSTER I.R., MAC DONALD R.B., Post-earthquake response procedures for embankment dams – lessons from the Loma Prieta earthquake”, *ANCOLD Bulletin*, no. 109, pp. 46–64, 1998.
- [FOS 99a] FOSTER M.A., The probability of failure of embankment dams by internal erosion and piping, PhD Thesis, School of Civil and Environmental Engineering, The University of New South Wales, 1999.
- [FOS 99b] FOSTER M.A., FELL R., A framework for estimating the probability of failure of embankment dams by piping using event tree methods, UNICIV report no. R377, School of Civil and Environmental Engineering, University of New South Wales, 1999.
- [FOS 00] FOSTER M., FELL R., SPANNAGLE M., “The statistics of embankment dam failures and accidents”, *Canadian Geotechnical Journal*, vol. 37, no. 5, pp. 1000–1024, 2000.
- [FOS 01] FOSTER M., FELL R., “Assessing embankment dams filters which do not satisfy design criteria”, *Journal of Geotechnical and Geoenvironmental Engineering*, vol. 127, no. 4, pp. 398–407, 2001.
- [GIL 07] GILLON M.D., “Re-evaluation of internal erosion incidents at Matahina Dam, New Zealand”, in FELL R., FRY J.-J. (eds), *Internal Erosion of Dams and their Foundations*, Taylor and Francis, pp. 115–132, 2007.
- [GIR 09] GIROUX J.-P., “The Terzaghi lecture: criteria for geotextile and granular filters”, *9th IGS-UK Chapter Invitational Lecture, 9 September 2009*, Joint meeting IGS/British Geotechnical Association Terzaghi lecture, 2009.
- [GLY 04] GLYNN M.E., KUSMAUL J., Prediction of piping erosion along middle Mississippi River levees - an empirical model, ERDC/GSL TR-04-12, US Army Corps of Engineers, Engineering Research Center, Geotechnical and Structural Laboratory, 2004.

- [GOL 09] GOLTZ M., ETZER T., AUFLEGER S., *et al.*, “Assessing the critical seepage velocity causing transport of fine particles in embankment dams and their foundations”, *Long Term Behaviour of Dams Proceeding of the 2nd International Conference*, Graz, Austria, pp. 479–484, 12–13 October 2009.
- [GOL 10] GOLTZ M., AUFLEGER M., PERZLMAIER S., *et al.*, “Assessing the critical seepage velocity causing transport of fine particles – the approach of Muckenthaler”, *8th ICOLD European Club Symposium*, 22–23 Sept, Innsbruck, Austria, 2010.
- [GUI 10] GUIDOUX C., FAURE Y.-H., BÉGUIN R., *et al.*, “Contact erosion at the interface between granular filter and various base-soils with tangential flow”, *Journal of Geotechnical and Geoenvironmental Engineering*, vol. 136, no. 5, pp. 755–775, 2010.
- [HAN 90] HANSON G.J., “Surface erodibility of earthen channels at high stresses. Part II, developing an in-situ device”, *Transactions American Society of Agricultural Engineers*, vol. 33, no. 1, pp. 132–137, 1990.
- [HAN 91] HANSON G.J., “Development of a jet index to characterize erosion resistance of soils in earthen spillways”, *Transactions American Society of Agricultural Engineers*, vol. 36, no. 5, pp. 2015–2352, 1991.
- [HAN 04] HANSON G.J., COOK K.R., “Apparatus test procedure and analytical methods to measure soil erodibility in-situ”, *Applied Engineering in Agriculture*, vol. 20, no.4, pp. 455–462, 2004.
- [HAR 91] HARDER L.F. Jr., BRAY J.D., VOLPE R.L., *et al.*, “Performance of earth dams during the Loma Prieta earthquake proceedings”, *Second International Conference on Recent Advances in Geotechnical Earthquake Engineering and Soil Dynamics*, Paper No. LP05, March 11–15, 1991, St-Louis, MO.
- [HOE 98] HØEG K., JOHANSEN P.M., KJÆRNSLI B., *et al.*, *Internal Erosion in Embankment Dams*, Research project sponsored by Norwegian Electricity Federation (EnFO), 1998.
- [HOF 12a] HOFFMANS G.J.C.M., Personal Communication, 2012.

- [HOF 12b] HOFFMANS C.J.C.M., *The Influence of Turbulence on Soil Erosion*, Eburon Academic Publishers, Netherlands, 2012.
- [HOL 81] HOLTZ R.D., KOVACS W.D., *Introduction to Geotechnical Engineering*, Prentice Hall, 1981.
- [HOM 12] HOMBERG U., BAUM D., PROHASKA S., *et al.*, “Automatic extraction and analysis of realistic pore structures from mCT data for pore space characterization of graded soil”, in: *Proc. 6th Int. Conference on Scour and Erosion (ICSE-6)*, 27–31 August 2012, Paris, pp. 66–73, 2012.
- [HUN 03a] HUNTER G., The deformation behaviour of embankment dams and landslides in natural and constructed soil slopes, PhD Thesis, School of Civil and Environmental Engineering, The University of New South Wales, 2003.
- [HUN 03b] HUNTER G., FELL R., The deformation behaviour of embankment dams, School of Civil and Environmental Engineering, University of New South Wales, 2003. UNICIV report no. R-416.
- [ICO 10] ICOLD, Tropical residual soils as dam foundation and fill material, Technical Bulletin, 2010.
- [ICO 12] ICOLD, Internal Erosion of Existing Dams, Levees and Dikes, and their Foundations, International Commission on Large Dams, Paris, 2012.
- [IST 57] ISTOMINA V.S., *Filtration Stability of Soils*, Gostroizdat, Moscow, 1957.
- [KEN 85a] KENNEY T.C., CHANAL R., CHIN E., *et al.*, “Controlling construction size of granular filters”, *Canadian Geotechnical Journal*, vol. 22, pp. 32–43, 1985.
- [KEN 85b] KENNEY T.C., LAU D., “Internal stability of granular filters”, *Canadian Geotechnical Journal*, vol. 22, pp. 215–225, 1985.
- [KEN 86] KENNEY T.C., LAU D., “Closure to: internal stability of granular filters”, *Canadian Geotechnical Journal*, vol. 23, pp. 420–423, 1986.

- [KJA 92] KJAERNSLI B., VALSTAD T., HOEG K., *Rockfill Dams, Design and Construction*, Norwegian Institute of Technology, Oslo, 1992.
- [KOE 92] KOENDERS M.A., SELLMELJER J.B., “Mathematical model for piping”, *Journal of Geotechnical Engineering*, vol. 118, no. 6, pp. 943–946, 1992.
- [KUW 12] KUWANO R., KOHATA Y., SATO M., *et al.*, A case study of ground cave-in due to large scale subsurface erosion in old land fill, Paper 228, ICSE6 Paris, pp. 265–271, 27–31 August 2012.
- [LAW 02] LAWRENCE, Summary of outcomes of “workshop on cracking of homogeneous earth dams in semi-arid environments”, Maricopa County, 2002.
- [LAW 92] LAWTON E.C., FRAGASZY R.J. and HETHERINGTON M.D., “Review of wetting-induced collapse in compacted soil”, *Journal of Geotechnical Engineering, ASCE*, vol. 118, no. 9, pp. 1376–1394, 1992.
- [LI 08b] LI M., Seepage induced instability in widely graded soils, PhD Thesis, University of British Columbia, 2008.
- [LI 08a] LI M., FANNIN R.J., “A comparison of two criteria for internal instability of granular soils”, *Canadian Geotechnical Journal*, vol. 45, pp. 1303–1309, 2008.
- [LI] LI M., FANNIN R.J., “A theoretical envelope for internal instability of cohesionless soil”, *Geotechnique*, forthcoming.
- [LIM 06] LIM S.S., Experimental investigation of erosion in variably saturated clay soils, PhD Thesis, School of Civil and Environmental Engineering, University of New South Wales, Sydney, Australia, 2006.
- [LIM 10] LIM S.S., KHALILI N.K., “Laboratory measurement of erosion of clay soils using rotating cylinder test”, *Geotechnical Testing Journal*, vol. 32, no. 3, pp. 1–7, 2010.
- [LUB 65] LUBOCKOV E.A., “The calculation of suffusion properties of non-cohesive soils when using the non-suffusion analogue”, in: *International Conference on Hydraulic Research*, Brno, Czech Republic, pp. 135–148, 1965.

- [MAR 07] MAROT D., ALEXIS A., BENDAHDANE F., “A specific triaxial device for the study of internal erosion in cohesive soils”, *Proceedings of Workshop on Internal Erosion and Piping of Dams*, Balkema, Aussois France, May 2005, pp. 159–166, 2007.
- [MEL 85] DE MELLO V.F.B., MORI R.T., “Dam foundations on tropical laterites and saprolites. General report”, *International Conference on Tropical Residual Soils, Saprolites and Laterites*, Brasilia, Brazil, 1985.
- [MOF 11a] MOFFAT R.M., FANNIN R.J., GARNER S.J., “Spatial and temporal progression of internal erosion in cohesionless soil”, *Canadian Geotechnical Journal*, vol. 48, no. 3, pp. 399–412, 2011.
- [MOF 11b] MOFFAT R.M., FANNIN R.J., “A hydromechanical relation governing the internal stability of cohesionless soil”, *Canadian Geotechnical Journal*, vol. 48, no. 3, pp. 413–424, 2011.
- [MON 98] MONNET A., “Boulance, érosion interne, renard: les instabilités sous écoulement”, *Revue française de Géotechnique*, vol. 82, pp. 3–10, 1998.
- [NEW 06] NEWMAN S., FOSTER M., Lake buffalo dam risk reduction upgrade. ANCOLD bulletin, no. 132, Australian National Committee on Large Dams, Brisbane, pp. 45–56, 2006.
- [NGI 84] NGI, Jukla Sekundærdam Lkkaasjer, Reparasjoner, Påvisning av erosjonskanaler Gjennom Tetningskjernen, Internal Report 53600-1, Norges Geotekniske Institutt, Oslo, 1984.
- [NIL 07a] NILSSON A., “The susceptibility of internal erosion in the Suova dam”, in FELL R., FRY J.J. (eds), *Internal Erosion of Dams and their Foundations*, Taylor and Francis, pp. 167–172, 2007.
- [NIL 07b] NILSSON A., “Filters and internal erosion in Swedish dams”, in FELL R., FRY J.J. (eds), *Internal Erosion of Dams and their Foundations*, Taylor and Francis, pp. 173–178, 2007.
- [PAR 03] PARK Y., Investigation of the ability of filters to stop erosion through cracks in dams, PhD dissertation, Virginia Polytechnic Institute, Blacksburg, VA, 2003.

- [PEL 02] PELLIS S., FELL R., Damage and cracking of embankment dams by earthquakes, and the implications for internal erosion and piping, UNICIV report no. R-406, School of Civil and Environmental Engineering, University of New South Wales, 2002.
- [PEL 03] PELLIS S., FELL R., “Damage and cracking of embankment dams by earthquake and the implications for internal erosion and piping”, *Proceedings of the 21st Internal Congress on Large Dams, Montreal*, ICOLD, Paris Q83-R17, International Commission on Large Dams, Paris, 2003.
- [RAV 97] RAVASKA O., Piping susceptibility of glacial till, *Proceedings 21st International Congress on Large Dams, Montreal*, ICOLD, Paris Q83-R17, International Commission on Large Dams, Paris, pp. 455–471, 1997.
- [RON 07] RÖNNQVIST H., “Assessing potential for internal erosion in glacial moraine core embankment dams”, *Dam Engineering*, vol. XVIII, no. 2, pp. 101–117, 2007.
- [RON 08] RÖNNQVIST H., “Review of moraine core dams and internal erosion”, *Dam Engineering*, vol. XIX, no. 2, pp. 99–121, 2008.
- [RON 09] RÖNNQVIST H., “Long-term behaviour of internal erosion afflicted dams comprising broadly graded soils”, *Dam Engineering*, vol. XX, no. 2, pp. 149–197, 2009.
- [RON 10] RÖNNQVIST H., Predicting surfacing internal erosion in moraine core dams, Licentiate Thesis, KTH Land and Water Resource Engineering, Stockholm, 2010.
- [SAI 11] SAIL Y., MAROT D., SIBILLE L., ALEXIS A., “Suffusion tests on cohesionless granular matter”, *European J. of Environmental and Civil Eng.*, vol. 15, pp. 799–817, 2011.
- [SCH 02] SCHEUERMANN A., VARDOULAKIS I., PAPANASTASIOU P., STAVROPOULOU M., “A sand erosion problem in axial flow conditions on the example of contact erosion due to horizontal groundwater flow”, in WOLFGANG E. (ed.), *IUTAM Symposium on Theoretical and Numerical Methods in Continuum Mechanics of Porous Materials*, Springer, Netherlands, pp. 169–175, 2002.

- [SCH 00] SCHMERTMANN J.H., “The non-filter factor of safety against piping through sands”, in SILVA F., KAVAZANJIAN E. (eds), *ASCE Geotechnical Special Publication No. 111, Judgment and Innovation*, ASCE, Reston, 2000.
- [SCH 07] SCHMITZ, Zur hydraulischen Kontakterosion bei bindigen Basiserdstoffen, Doctoral Thesis, University of the Bundeswehr, 2007.
- [SEL 88] SELLMELJER J.B., On the mechanism of piping under impervious structures, Doctorate dissertation, Delft University of Technology, 1988.
- [SEL 91] SELLMELJER J.B., KOENDERS M.A., “A mathematical model for piping”, *Applied Mathematical Modelling*, vol. 115, pp. 646–661, 1991.
- [SEL 11] SELLMELJER J.B., LOPEZ DE LA CRUZ J., BEEK V.M. van, *et al.*, “Fine-tuning of the piping model through small-scale, medium-scale and IJkdijk experiments”, *European Journal of Environmental and Civil Engineering*, vol 15, no. 8, pp.1139–1154, 2011.
- [SEM 08] SEMAR O., WITT K.J., “Modelling of suffusion processes with simulation in an uncorrelated bond-percolation model”, *Proceeding of the Annual Workshop of the European Working Group on Internal Erosion in Embankment Dams*, Obergurgl, Austria, 2008.
- [SEM 10] SEMAR O., WITT K.J., FANNIN R.J., “Suffusion evaluation – comparison of current approaches”, *Proceedings of the Fifth International Conference on Scour and Erosion*, ASCE Geotechnical Special Publication No. 210, pp. 251–262, 2010.
- [SHE 72a] SHERARD J.L., DECKER R.S., RYKER N.L., “Piping in earth dams of dispersive clay”, in HIRSCHFIELD R.C. and POULOS S.J. (eds), *Proceedings, Specialty Conference on Performance of Earth and Earth-Supported Structures*, ASCE, vol. 1, Part 1, John Wiley & Sons, pp. 589–626, 1972.
- [SHE 72b] SHERARD J.L., DECKER J.L., RYKER N.L., “Hydraulic fracturing in low dams of dispersive clay”, *Proceeding of the Specialty Conference on Performance of Earth and Earth Supported Structures*, ASCE, vol. 1, no. 1, pp. 653–689, 1972.

- [SHE 63] SHERARD J.L., WOODWARD R.J., GZIENSKI S.F., *et al.*, *Earth and Earth Rock Dams*, Chapter 2, Part 5, John Wiley & Sons, New York, 1963.
- [SHE 73] SHERARD J.L., “Embankment dam cracking”, in HIRSCHFIELD R.C., POULOS S.J. (eds), *Embankment Dam Engineering*, John Wiley and Sons, 1973.
- [SHE 79] SHERARD J.L., “Sinkholes in dams of coarse, broadly graded soils”, *13th International Congress on Large Dams, New Delhi*, Q47, R2, International Commission on Large Dams, Paris, pp. 325–334, 1979.
- [SHE 85] SHERARD J.L., “Hydraulic fracturing in embankment dams”, *Seepage and Leakage from Dams and Impoundments*, ASCE Geotechnical Engineering Division Conference, 1985.
- [SHE 86] SHERARD J.L., “Hydraulic fracturing in embankment dams”, *Journal of Geotechnical Engineering*, vol. 112, no. GT10, pp. 905–927, 1986.
- [SHI 11] SHIRE T., O’SULLIVAN, C., “Particle scale numerical modelling to develop insight into suffusion in granular filters”, in FRY J.J., JULINEK T., RIHA J. (eds), *Internal Erosion of Dams and their Foundations, Proceedings of the Institute of Water Structures, FCE*, Brno, Czech Republic, 2011.
- [SHI 36] SHIELDS A., *Anwendung der Ähnlichkeitsmechanik und der Turbulenzforschung auf die Geschiebebewegung*, Preussische Versuchsanstalt für Wasserbau und Schiffbau, Berlin, Heft 26, 1936.
- [SHR 89] SHERARD J.L., DUNNIGAN L.P., “Critical filters for impervious soils”, *J. Geotech. Eng. ASCE*, vol. 115, no. 7, pp. 927–947, 1989.
- [SIL 07] SILLS G.L., VROMAN N., “A review of corps of engineers levee seepage practices in the United States”, in FELL R., FRY J.J. (eds), *Internal Erosion of Dams and their Foundations*, Taylor and Francis, pp. 209–218, 2007.
- [SIL 91] SILVIS F., Verificatie piping model; Proeven in de Deltagoot. Evaluatierapport. Rapport Grondmechanica Delft, CO 317710/7, 1991.

- [SKE 94] SKEMPTON A.W., BROGAN J.M., “Experiments on piping in sandy gravels”, *Geotechnique*, vol. 44, no. 3, pp. 449–460, 1994.
- [SUN 89] SUN B.C.B., Internal stability of clayey to silty sands, PhD Thesis, Department of Civil Engineering, University of Michigan, 1989.
- [TAL 94] TALBOT J.R., “The mechanics of cracking in embankment dams”, *Proceeding of the Fracture Mechanics applied to Geotechnical Engineering*, ASCE, Georgia, pp. 118–130, Oct. 9–13, 1994.
- [TEC 99] TECHNICAL ADVISORY COMMITTEE, Technical Report on Sand Boils (Piping). Technical Advisory Committee on Flood Defences, The Netherlands, Road and Hydraulic Engineering Institute, Delft, Netherlands, 1999.
- [TER 48] TERZAGHI K., PECK R.B., *Soil Mechanics in Engineering Practice*, Wiley International, New York, 1948.
- [TOW 88] TOWNSEND F.C., BLOOMQUIST D., SHIAU J.-M., *et al.*, Evaluation of Filter Criteria and Thickness for Migrating Piping in Sands, Report for U.S. Bureau of Reclamation, Department of Civil Engineering, University of Florida, 1988.
- [USA 56] USACE, Investigation of under-seepage and its control, lower Mississippi river levees, Technical Memorandum No. 3-424, USACE Waterways Experimental Station, Vicksburg, 1956.
- [USA 93] USACE, Seepage analysis and control for dams, Engineer manual No. EEM 1110-2-1901, Engineering and Design, Department of the Army, U.S. Army Corps of Engineers, Washington D.C., 392 p., 1993.
- [VAR 88] VARDÉ I.O., “Lessons of adjustments to tropical saprolites and laterites”, contribution in Special Lecture Embankment Dams and Dams Foundations, *Proceedings XII International Conference on Soil Mechanics and Foundation Engineering*, Rio de Janeiro, vol. 4, pp. 2180–2198, 1989.

- [VUO 07] VUOLA P., KONRAD J.M., BARTSCH M., “Effects of frost and thaw on dams”, in AUFLEGER M., FRY J.J, GOLTZ M., PERZLMAIER S. (eds), *Assessment of the Risk of Internal Erosion of Water Retaining Structures: Dams, Dykes and Levees*, Intermediate Report of the European Working Group of ICOLD, 2007.
- [WAH 08] WAHL T.L., REGAZZONI P., ERDOGAN Z., Determining Erosion indices of cohesive soils with the hole erosion test and jet erosion test, Bureau of Reclamation Report DSO-08-05, US Department of Interior, 2008.
- [WAL 87] WALLACE M., “How to prevent frost heave”, *Concrete Construction*, vol. 32, no. 4, pp. 369–372, 1987.
- [WAN 06] WAN C.F., Experimental investigation of piping erosion and suffusion of soils in embankment dams and their foundations, PhD Thesis, School of Civil and Environmental Engineering, University of New South Wales, Sydney, Australia, 2006.
- [WAN 02] WAN C.F., FELL R., Investigation of internal erosion and piping of soils in embankment dams by the slot erosion test and the hole erosion test, UNICIV report no. R-412, School of Civil and Environmental Engineering, University of New South Wales, 2002.
- [WAN 04a] WAN C.F., FELL R., “Investigation of rate of erosion of soils in embankment dams”, *Journal of Geotechnical and Geoenvironmental Engineering*, vol. 130, no. 4, pp. 373–380, 2004.
- [WAN 04b] WAN C.F., FELL R., “Laboratory tests on the rate of piping erosion of soils in embankment dams”, *Geotechnical Testing Journal*, vol. 27, no. 3, pp. 295–303, 2004.
- [WAN 04c] WAN C.F., FELL R., Experimental investigation of internal instability of soils in embankment dams and their foundations, UNICIV report no. 429, School of Civil and Environmental Engineering, The University of New South Wales, Sydney, 2004.

- [WAN 07] WAN C.F., FELL R., “Investigation of internal erosion by the process of suffusion in embankment dams and their foundations”, in FELL R., FRY J.J. (eds), *Internal Erosion of Dams and their Foundations*, Taylor and Francis, London, pp. 219–234, 2007.
- [WAN 08] WAN C.F., FELL R., “Assessing the potential of internal erosion and suffusion in embankment dams and their foundations”, *Journal of Geotechnical and Geoenvironmental Engineering*, vol. 134, no. 3, pp. 410–407, 2008.
- [WEI 93] WEIJERS J.B.A., SELLMELJER J.B., “A new model to deal with the piping mechanism”, in BRAUNS, HERBAUM, SCHULER (eds), *Filters in Geotechnical and Hydraulic Engineering*, Balkema, Rotterdam, 1993.
- [WIT 81] DE WIT G.N., SELLMELJER J.B., PENNING A., “Laboratory tests on piping”, *Proceeding of the 10th International Conference Soil Mechanics and Foundation Engineering, Stockholm*, Balkema, Rotterdam, pp. 517–520, June 1981.
- [WIT 12a] WITT K.J., SALEHI SADAGHIANI M.R., Identifying of mobile particles in internally unstable soils, Paper 49, ICSE6 Paris, pp. 845–849, 27–31 August 2012.
- [WIT 12b] WITT K.J., SALEHI SADAGHIANI M.R., Analysis of internal stability of widely graded soils based on identification of mobile particles, Paper 50, ICSE6 Paris, pp. 258–264, 27–31 August 2012.
- [WOL 02] WOLFF T.F., Performance of Levee Under-Seepage Controls: A Critical Review, US Army Corps of Engineers, Engineering Research Center, Geotechnical and Structural Laboratory, ERDC/GSL TR-02-19, 2002.
- [WÖR 92] WÖRMAN A., OLAFSDOTTIR R., “Erosion in a granular medium interface”, *Journal of Hydraulic Research*, vol. 30, no. 5, pp. 639–655, 1992.
- [ZIE 69] ZIEMS J., Beitrag zur Kontakterosion nichtbindiger Erdstoffe, PhD Thesis, Faculty of Civil Water and Forestry, Dresden, Germany, 1969.

Chapter 2

Contact Erosion

2.1. Introduction

Specific hydraulic erosion is liable to develop inside dikes in the presence of an interface between two layers of soil with different grain sizes and permeabilities. Located in the contact zone and thus called “contact erosion” (CE), this mode of internal erosion occurs when two criteria are satisfied simultaneously. The first condition is purely hydraulic because the stress exerted by the water flowing at a tangent to the surface of the layer of fine material is sufficient to erode it. From the geometric point of view, a second condition must be satisfied by ensuring the passage of the eroded particles through the pores of the coarser material thus crossing the inter-granular constrictions, that is the zones with smaller sections that connect the pores together.

The safety of a structure can thus be ensured by simply conforming to the geometric criterion, but if the latter is defective, it is then necessary to use an adapted hydraulic criterion to estimate the CE initiation threshold and assign a

safety factor to it. River dikes can often fail to conform to the geometric criterion. On the one hand, because alluvial plains are naturally composed of a succession of sedimentary strata whose characteristics vary from one layer to another, and on the other hand due to the structure of the dike body that is composed of different zones that fulfill different functions (sealing, stability and drainage) and thus made up of different materials in terms of grain size and permeability.

After providing a brief presentation of the conditions leading to the occurrence of the CE phenomenon in a structure, in this chapter we have decided to focus on the problem of CE according to three different scales in order to deal with the subject as exhaustively as possible.

– First, the phenomenon of erosion can be studied simply in the laboratory on the basis of soil samples. At this level of observation, in the region of 1 m, it is possible to study the material as a continuous entity whose behavior can be considered as representative. Thus it is possible to estimate the threshold of initiation and the average kinetics of the CE process precisely and compare it with different models of the phenomenon. Nonetheless, experimental observations performed at this scale remain difficult to interpret.

– Second, to achieve the latter we will demonstrate that it is necessary to take a much closer look at the contact zone between layers and situate analysis at the scale of the pores of the coarse material. This is the scale, typically centimetric, at which the elementary mechanisms of erosion can be analyzed in detail, essentially on a qualitative basis, by systematically referring to the state of the art relating to sedimentary erosion in rivers and by underlining the differences contributed by the specific situation of CE. This step at the smaller scale permits qualifying the spatial variability of the hydraulic stress involved and can be used as the basis for statistical modeling when returning to the scale of the sample.

– Third, once the behavior at the smaller scale has been elucidated, the scale of the structure can be investigated. Here, CE is only a piece of the puzzle in which an account must also be taken of the internal structure of the dike and its level of saturation, as well as the limit conditions at the borders of the zone subjected to CE as their role is fundamental regarding the potential filtration of eroded particles and maintaining the global stability of the structure.

2.2. General presentation

2.2.1. Typical conditions of occurrence

The occurrence of a CE phenomenon in a hydraulic structure is linked to the existence of a contact zone between a coarse material and a fine material. Highly pervious coarse material is the locus of a hydraulic flow which, if intense enough, can pull out and transport particles away from the surface of the finer soil. Typically, the fine soil is composed of a mixture of sands, clays and silts, whereas the coarse material is mostly composed of gravels possibly mixed with sand and silt. In addition, it should be noted that the coarse soil is pulverulent, meaning that it presents no cohesion, whereas the fine material may in certain cases be more or less cohesive. This is the case for a silt or a clay, for example, whereas sand remains pulverulent.

The same typical structures are used at the time of building dikes and it is easy to distinguish in different configurations the presence of layers with very varied grain sizes. Two main classes of structures must be distinguished:

– Flood protection dikes, subjected to hydraulic loads only punctually, are generally built using the materials available on the site. For the most part they do not present the characteristics best adapted for safety requirements. Indeed,

the layers of alluvial deposits along rivers are composed of silts, sands and pebbles. Several studies on the rivers Rhine, Rhône and Danube have noted the existence of a gap in the size distribution of these alluvial deposits with a lack of material of grain sizes ranging from 1 to 5 mm. A similar gap also appears to be observed, quite generally, for moraines, in the range from 0.1 and 20 mm [GAR 02]. It is thus clear that highly pervious zones can be in contact with fine materials in this type of structure, not only in the foundations but also in the body of the dike which is composed of materials taken from the foundation soils. These sensitive zones can be localized in the typical diagram of a flood protection dike shown in Figure 2.1(a). Nonetheless, the two criteria, hydraulic and geometric, that condition the occurrence of internal erosion in the structure are quite restrictive and it is unlikely that CE can be observed in a structure immediately following its construction. Whatever the case, the hydraulic load may be sufficient to erode the fine material locally, preferentially by suffusion¹ and, in the long term (i.e. several years), the permeability of certain zones will increase in proportions liable to draw close to CE occurrence criteria.

– As shown in Figure 2.1(b), the most sensitive structures in which a permanent hydraulic load is imposed have a zoned structure with a central impervious core made up of clay or silt material, covered up and downstream by coarse material to ensure the mechanical stability of the whole structure. At the foot of the dike, a layer of washed and calibrated gravel-sand mixture is added to ensure drainage. Here the highest risk of observing the development of a CE process is located at the contact between the foundation and

1 Another elementary internal erosion mechanism is the selective erosion, via an internal hydraulic flow, of the finer fraction of soil whereas the coarser fraction remains in place, ensuring the mechanical balance of the whole structure.

the fine soil core. As mentioned previously, certain interfaces may reach the CE initiation threshold after a long period of removal of fine particles by suffusion. Other potentially zones sensitive to CE are possible stratified layers in the foundations, in the drainage system if geometric filtration rules are not conformed to and, in the case of dike overflow, in the coarse layers of the downstream shoulder in contact with the core.

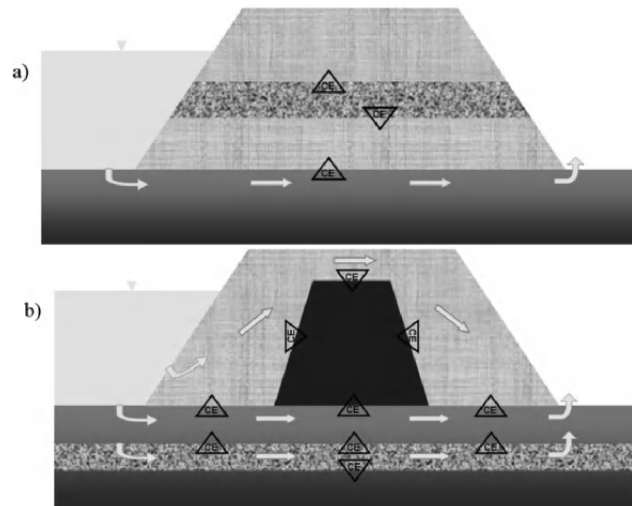


Figure 2.1. a) Typical diagram of a flood protection dike built from materials available in-situ; b) Typical diagram of a zoned river dike. The zones where CE is liable to develop have been identified in direct configuration (down triangle) and in inverse configuration (up triangle)

The contact zones where CE can occur in these different structures have different configurations that depend on the various orientations of the interface, the flow and gravity. These different configurations are presented in Figure 2.2 for an interface that can be either horizontal or vertical, and with a hydraulic flow perpendicular or parallel to this interface. A combination of these specific configurations

makes it possible to establish a general case where the slopes between the interface and gravity, and between the flow and the interface, can be in any arrangement. However, as shown, in particular, in Figure 2.1 for the cross-sections of the structures concerned, the configuration encountered most frequently is a horizontal interface with a parallel flow. This is the case for the sedimentary layers in the foundations and, in the core of the structure, for most of the interfaces between types of materials. It is also the case for the main direction of the natural hydraulic flow that seeps through the structure. Zones of lesser hydraulic resistance can, however, incline the flow so that it penetrates the layers of soil perpendicularly. From the practical point of view, we will restrict ourselves to the most common configuration: a flow circulating tangentially along a horizontal interface between a layer of fine soil and a layer of coarser soil. Two different cases remain that depend on the relative position of these two layers which, under the action of gravity, has a stabilizing effect when the coarse material lies above the fine soil, or a destabilizing effect if the configuration is reversed. The two configurations chosen will be labeled arbitrarily *direct configuration* when the fine soil is located below the coarse soil and *inverse configuration* when a layer of coarse soil lies over the layer of fine soil. The effect of gravity is important in the coarse layer and can possibly induce rearrangement of grains during the process of CE. For fine soil, the effect of gravity is more limited and can become negligible in a coherent material for which particle weight is greatly reduced compared to internal adhesion interactions. According to the identification of zones potentially sensitive to CE shown in Figure 2.1, the direct configuration appears more marginal vis-à-vis the inverse configuration, notably due to the presence of more pervious foundation soils. It should also be noted that the coarse soil is not subject to erosion and remains mainly static except during possible brief sequences of settlement.

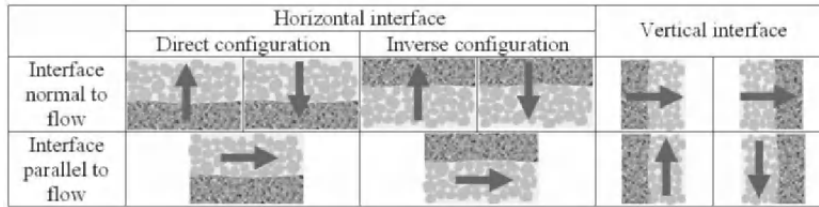


Figure 2.2. Diagram of different base CE configurations according to orientations relative to the flow, the interface and gravity

2.2.2. Specific nature of CE

Surface erosion in the classical meaning corresponds to the flow of a homogeneous fluid over a layer of sediments on the surface of which the hydraulic force exerted is sufficient to set the sediment in motion. Many theoretical, experimental and laboratory studies have been performed and resulted in major advances since the pioneering work of Shields in 1936 [SHI 36], which introduced a dimensionless number Θ formulated as the ratio between the force applied by the flow over the surface of a sediment bed, expressed as shear stress τ_b , and the stabilizing force of gravity via the submerged weight of a grain:

$$\Theta = \frac{\tau_b}{(\rho_s - \rho_w)gd} = \frac{\tau_b}{(s-1)\rho_wgd} \quad [2.1]$$

where ρ_s and ρ_w are respectively the density of the soil and the water, s is the ratio between the two, g is gravity and d is the characteristic size of the sediment.

It has been demonstrated that an empirical curve links critical Shields number Θ_c , measured at the erosion initiation threshold, with the specific Reynolds number defined by $Re^* = U^*d/\nu_w$, where ν_w is the viscosity of the water and U^* is the friction velocity given by $U^* = \sqrt{\tau_0/\rho_w}$. However, the marked disparity between experimental data

[BUF 97] can be explained by a large number of differences between studies (such as choice of criteria, calculation methods, grain shapes and hydraulic regimes). Many analytical expressions have been proposed to represent this curve, in certain zones or over the entire domain. In what follows, we use those expressions developed by Cao *et al.* [CAO 06].

Regarding this reference situation, the specificity of CE is remarkable as this type of erosion does not develop at the frontier between a homogeneous fluid and a soil but at the interface between two porous media presenting substantial separation between spatial scales. As mentioned at the beginning of this chapter, to initiate erosion and transport at the scale of a structure it is necessary to have a sufficiently high grain size ratio (from five to 10 according to the literature) between the two media, to drive the finer particles through the constrictions between the coarser grains. In what follows, we will term the constitutive elements of fine soil “particles” and those of coarse soil “grains”, in order to clearly distinguish the scales of grain sizes in the two layers in contact. Their diameters will be denoted d and D , respectively, or, more precisely, d_x and D_x the x -centile² of their respective grain size distributions. The two porous media therefore have very different permeabilities, with far higher flow velocities in the coarse material than in the fine material. The interface between the two media is therefore a transition zone between two distinct grain sizes and consequently a transition zone for the hydraulic flow.

Furthermore, due to the succession of pores and constrictions through which the water passes, the porous flow is intrinsically heterogeneous from the spatial viewpoint, with fluctuations induced by pore geometry.

² Diameter for which there are $x\%$ (in mass) particles whose size is smaller or the same.

These fluctuations are also probably different between the core of the porous matrix and the zone of contact with the layer of fine soil. It is necessary to provide a more detailed description of the characteristics of a hydraulic flow occurring within the layer of coarse material. The reference size of the pores is a fraction of D , the median size of the grains composing the porous medium, so this is the scale at which the associated Reynolds number, $Re_D = UD / \nu_w$, is formulated, with a characteristic velocity U deduced directly from the flow rate. Because the typical Re_D values of the porous flows liable to trigger CE remain low, from 10 to 100, they tend to fall outside a Darcy type linear regime, for which proportionality between flow rate and pressure gradient exists, and corresponds to a Forchheimer type regime [BEA 72]. Empirical relations have been proposed for the latter to describe the dependence between velocity and pressure drop, particularly by adding a quadratic term in velocity that takes into account the inertial effects induced by irregular head losses in the narrowest constrictions [BEA 72, HLU 06]. Here, we use the empirical formula given by Fand [FAN 87] following an improvement to an earlier law formulated by Ergun [BEA 72]:

$$i \approx 182 \frac{(1-n)^2 \nu_w}{n^3 g D^2} U + 1.92 \frac{(1-n)}{n^3 g D} U^2 \quad [2.2]$$

where hydraulic gradient i corresponds to the ratio between the pressure gradient at the source of the flow and the specific gravity of the water and n is the porosity of the porous medium.

Note that higher Reynolds numbers correspond to non-stationary flows, where the turbulence progressively begins to take effect. However, they are no longer representative of the flows encountered under real conditions in the framework of CE.

Finally, another incidence linked to the presence of the layer of grains concerns, in direct configuration, the fraction of particles located under the grains in contact with the fine layer which are out of reach of the hydraulic stresses caused by the flow. On the contrary, these contact zones undergo efforts transmitted by the granular skeleton.

To sum up, the specificity of the CE is the following: the CE does not involve a single erosion mechanism, but a complex combination of concomitant phenomena linked to the interaction between the flow and fine particles and the pore geometry of the flow zone (surface erosion, hydraulic flow in a porous medium, granular and cohesive soil mechanics, and sediment transport and deposit in a granular filter).

2.3. At sample scale: quantification of the CE threshold and kinetics

Here, the term sample designates a sufficient quantity of material to observe representative behavior. This means that, statistically, the local heterogeneities intrinsic to any system compensate each other and that the global response of the sample weights the diversity of local situations. Analyzing a single sample is therefore sufficient for characterizing the general behavior of the material, considered as a continuous medium, and for developing basic engineering tools.

In the framework of CE, the scale of the sample will mainly depend on the average size of the grains comprising the coarse material, that is about a meter for gravels. When studying the literature, it can be seen that almost all the works have used this scale to analyze CE, by favoring an experimental approach. In the great majority of cases, the direct configuration was studied with a layer of coarse material, usually gravel, laid over a fine soil generally

composed of sand and thus non-cohesive. More recent works have enriched these results with data relative to cohesive soils while others have focused on the inverse configuration. The common objective of each of these studies was to determine a hydraulic threshold from which CE occurs when geometric conditions do not impede the transport of eroded particles. A few studies have also included detailed analyzes of the geometric conditions involved. We present a review of these works in the following sections.

2.3.1. Influence of geometry on the occurrence of CE

For very restrictive geometric conditions in terms of the mobility of fine particles through the pores of a material of larger grain size, it is clear that however intense the hydraulic flow, despite being capable of placing fine grains in suspension locally, it will not succeed in transporting them inside the contact layer. Therefore, we consider that there is no CE at the scale of the sample, although erosion does occur at the scale of the grains. This condition defines an initial geometric threshold expressed as the grain size ratio between D_{15} of the coarser soil and d_{85} of the finer soil. In practice, in the experiments performed, this threshold corresponds to a maximum grain size ratio for which filtration is complete and no erosion is observed at the maximum hydraulic capacity of the experimental device. The values proposed range from 4 to 9: 7.5 according to Brauns [BRA 85], 8.1 according to Den Adel [DEN 94] and 4 or 9 according to Sherard [SHE 84]. It should be noted that these values are of the same magnitude as the ratio of the limit size $D/d = (2/\sqrt{3} - 1)^{-1} \approx 6.5$ permitting the passage of a sphere of diameter d through a construction of spheres of diameter D in a tetrahedral stack.

Conversely, for grain size ratios such that the constrictions no longer impede the passage of fine particles,

the latter can be transported by the flow after erosion. Beyond a limit value, expressed here by the grain size ratio between the two layers of soil, the condition of occurrence of CE becomes insensitive to geometric aspects and is therefore purely hydraulic. This second threshold is identified by a grain size ratio of 25 according to Brauns [BRA 85], 14.6 according to Wörman [WÖR 92] and, finally, 11.7 according to Den Adel [DEN 94]. This limit is rather consistent with the values ranging from 11 to 16 given in sedimentology for the threshold of free percolation from which a sediment particle is not trapped inside a coarser material [GIB 09].

In the intermediate regime between these two values, and *a priori* poorly defined given the dispersion of the values proposed, the CE mechanism is governed by a mixed regime that probably combines geometry and the hydraulic stress exerted in a quite complex way.

From the angle of safety, it is reasonable to situate oneself under the worst geometric conditions, that is beyond the second geometric threshold, to determine the hydraulic load that must not be exceeded to avoid any initiation of CE. This permits anticipating any possible change of contact geometry, for example, by suffusion, as mentioned previously in the section 2.2.2.

2.3.2. Direct configuration

2.3.2.1. Test conditions of CE

Over the past 50 years, several studies have been performed under these geometric conditions which do not allow filtration for a direct configuration in order to measure the hydraulic threshold of CE initiation. The experimental devices used have been very similar: a large rectangular cell in which two layers of soil are installed successively is

connected to a hydraulic circuit that permits subjecting the coarse layer to a flow under an imposed pressure after initial saturation of the sample. In general, an additional static load is applied to the upper layer. The instrumentation used permits at least measuring either the pressure drop or the flow rate imposed in order to deduce the hydraulic gradient i directly or by Darcy's law, provided the permeability of the coarse layer is known beforehand. A measurement of the rate of transport flowing at the outlet of the chamber can be obtained periodically by weighing, or continuously with a turbidity meter. The experimental procedure then consists of imposing a constant hydraulic load for a variable period, from a few minutes to 24 hours depending on the study, then determining whether a CE process has begun. To do this, each author uses different criteria: simple visual observation of the presence of particles in suspension [BRA 85], overshooting of a minimum rate of transport chosen arbitrarily [BEZ 87] or the existence of non-zero turbidity at the end of a time step of about 30 min [GUI 10, BEG 11]. It is also possible to measure several transport values for hydraulic loads higher than the threshold in order to deduce it by extrapolation at zero [DEG 83]. The wide range of methods used highlights the hazy and ambiguous nature of the general notion of a threshold for erosion or transport initiation. Its very existence fails to stir general consensus [LAV 87] and, as seen later on, some of the transport laws proposed in the literature do not include a stress threshold.

By way of illustration, Figure 2.3 represents the experimental device developed in the laboratory LTHE (University of Grenoble, France), during successive works by Guidoux *et al.* [GUI 10] and Béguin [BÉG 11], and is highly representative of the different devices described in the literature [DEG 83, BRA 85].

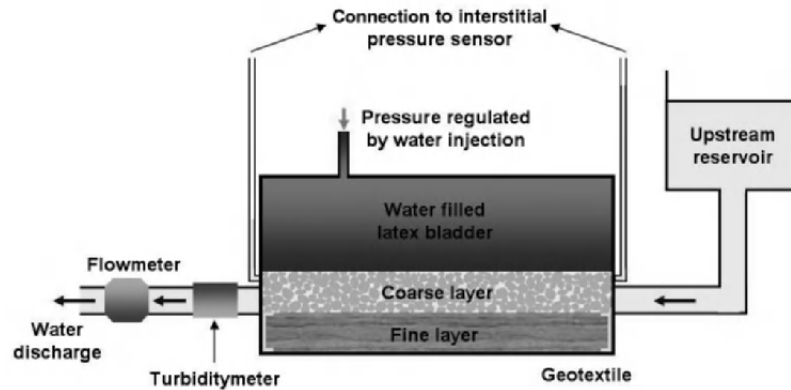


Figure 2.3. Diagram of the experimental device developed in the laboratory LTHE (University of Grenoble, France) and used successively by Guidoux et al. [GUI 10] and Béguin [BÉG 11]

The cell, having internal dimensions of $70 \times 30 \times 12 \text{ cm}^3$, receives two layers of soils. The fine layer is constituted by fine soil (sand, silt, clay, etc.) moisturized at the optimum water content of the Standard Proctor Test, homogenized by a 24 hour rest in a closed bag and compacted manually in successive layers to reach the objective of density. The coarse layer (gravel) is set up dry and without compaction. A diverging system upstream and a converging system downstream make it possible to concentrate the flow in the layer of coarse material with a hydraulic gradient ranging up to 2 and a flow rate capable of reaching 1.5 l/s. A latex bladder filled with water permits maintaining a given additional load on the upper layer of the soil. It has been shown, however, that the influence of this additional load on the CE threshold is negligible. Besides a flowmeter, the measurement channel also includes a differential pressure sensor, which gives the dynamic pressure, and a turbidity meter³. After calibration, the latter is used to estimate the

³ A device that uses photometry to measure the greater or lesser clarity of a liquid and whose unit of measurement for water is the Nephelometric Turbidity Unit (NTU).

concentration of suspended matter. A typical example of a test to determine the CE threshold is reproduced in Figure 2.4 with successive 30 min stages of flow velocity at increasing intensity. During the three first steps, only a small peak of turbidity is observed that corresponds to the transient cleaning of the fine particles most exposed to the flow. From the fourth stage, the amplitude and duration of the turbidity peak are much greater. At the sixth step, non-zero turbidity persists beyond the period of 30 min. This is the criterion that the authors chose to determine that the contact zone is the locus of a CE process. In this specific example, the corresponding threshold velocity is therefore 2 cm/s. As mentioned previously, a large number of alternative definitions of this criterion have been used in the literature.

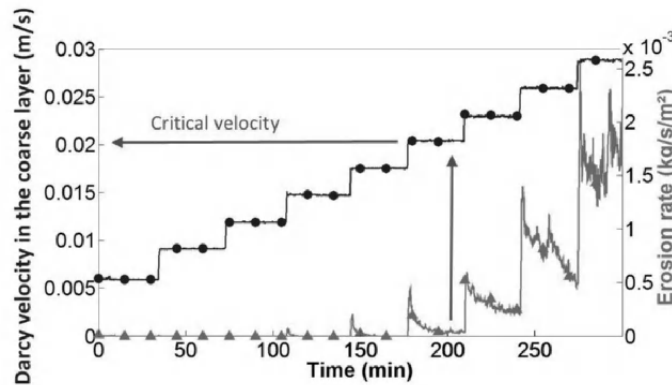


Figure 2.4. A typical example of a CE test with the experimental device described in Figure 2.3. The goal of the test is to determine the CE threshold using successive 30 min stages of flow velocity at increasing intensity

2.3.2.2. Threshold for the occurrence of CE

The different results obtained appear to indicate, concordantly, that the erosion threshold measured is evaluated better in terms of average flow velocity, in the

Darcy meaning, than in terms of global hydraulic gradient. Indeed, for the same layer of fine material, it appears that the critical gradient depends on the grain size of the coarse layer, where the Darcy velocity at the erosion initiation threshold remains almost constant. Chronologically, Istomina [IST 57] was the first to use experimental tests to formulate an abacus capable of predicting a critical value for this erosion initiation velocity. Three decades later, Brauns [BRA 85] proposed a threshold expressed simply in the form of a practically constant Froude⁴ densitometric number, in the region of 0.65–0.7:

$$Fr_c = \frac{U/n}{\sqrt{\left(\frac{\rho_s - \rho_w}{\rho_w}\right) g d_{50}}} = 0.65 - 0.7 \quad [2.3]$$

At the same time, works were dedicated to studying CE in Dutch dikes⁵ [DEG 83, BEZ 87]. Quite naturally these authors sought to model this erosion initiation threshold by adapting the Shields criterion Θ_c presented in the previous section to the specific characteristics of CE. The difficulty resides in the capacity to express the average shear stress exerted by the flow at the interface between a porous medium and an almost impervious layer correctly. The porous layer causes the flow to differ very significantly from what is observed on the bed of a river: as described previously, the flow is slowed down but presents strong spatial variability in terms of amplitude and local flow direction, as will be seen, in particular, in section 2.4 dedicated to pore scale phenomena. Initially, Bezuijen *et al.* [BEZ 87] simply considered that, by analogy with free surface flows, the friction velocity here is simply proportional

⁴ A dimensionless number that characterizes in a fluid the relative magnitude of forces linked to velocity vis-à-vis gravity.

⁵ Coastal dikes, generally in the form of a slope, built of sand and protected by a granular shoulder.

to the pore velocity (the real velocity of the water in the pores of the coarse layer), with a coefficient of proportionality e . In comparison to Brauns' approach, it simply amounts to a different way of expressing the critical Froude number, which in this case is equal to:

$$Fr_c = \frac{\sqrt{\Theta_c}}{e} \quad [2.4]$$

Although not specified by the author, the expression given by Brauns is therefore reasonably equivalent to the Shield criterion type approach. On the basis of experimental results, Bezuijen *et al.* [BEZ 87] obtained empirical results for coefficient e , by introducing a slight residual dependence regarding the grain size of a coarse soil. These authors also studied the influence of the slope of the interface, the presence of a perpendicular hydraulic gradient and the case of a cyclic component in the average flow to simulate breaking waves. A synthetic abacus is finally proposed to determine the CE occurrence threshold as a function of all these parameters. This work was completed recently by Hoffmans [HOF 08] in the case of scouring in a river by pushing the analogy further with free surface flows by using Chézy's friction law and by also introducing dependence empirically via the grain sizes of fine and coarse soils, which differs from that suggested by Bezuijen *et al.* [BEZ 87].

In even more recent works [GUI 10, BEG 11], it was proposed going further in using the Shields criterion by freeing themselves from strong hypotheses made on the basis of direct analogy with free surface flows. To do this, it is necessary to link shear stress to average velocity in two steps rather directly or empirically. First, an attempt is made to express shear stress as a function of the pressure gradient which is assumed to be constant throughout the flow. In practice, the shear stress cannot be measured simply in a porous medium and, for want of empirical laws, it

appears that the only approach possible is analytical. Therefore, by using the calculations in the literature [BEA 72, WÖR 92], a balance of the upstream and downstream pressure forces in the layer of grains permits expressing this average shear stress in the direction of the flow as a function of the hydraulic gradient imposed, assumed to be constant:

$$\tau_0 A_s = n \rho_w g i \quad [2.5]$$

with A_s being the specific surface, that is the surface by unit of volume exposed to the flow inside the porous medium of porosity n . It is therefore necessary to give an expression for this specific surface. The latter can be deduced from k , the intrinsic permeability of the porous medium, by the formula

$A_s = \sqrt{c_0 n^3 / k}$ with Kozeny's parameter c_0 which is generally taken as equal to 0.2 [BEA 72]. A formula has also been proposed to link the specific surface to the grain size distribution of the medium [KOZ 53, BEA 72]: $A_s = \alpha(1-n)/D_{eff}$, where the shape of the grains is expressed

via the value of coefficient α , between 6 and 8, and where D_{eff} is an effective diameter built as follows: $D_{eff}^{-1} = \sum_j f_j D_j^{-1}$ with

f_j being the fraction of the grains in diameter class D_j . Once this relation between the shear stress and the pressure gradient has been established, it is then possible to use the flow law giving the average velocity as a function of the pressure drop. This is Darcy's law in a slow regime or more usually an empirical law such as that of Fand, presented in section 2.2.2 and given in formula [2.2]. Figure 2.5 groups all the experimental results and empirical laws mentioned in this section by imposing the value obtained from the Shields diagram for shear stress τ_0 . Nonetheless, as can be seen, although the dependence between the critical velocity of occurrence of CE and the representative diameter of the fine eroded material is obtained qualitatively, from the

quantitative point of view, there is a systematic error corresponding approximately to a multiplication factor of around two. This leads to two remarks. On the one hand, the physics of the process appears to be identified correctly since the trend is generally well reproduced. On the other hand, several paths can be proposed to explain the quantitative difference observed: the uncertainty associated with the analytical law [2.5] (which cannot be validated experimentally and for which competing formulations exist with non-negligible quantitative differences), the specific nature of the flow zone where there is a grain size transition between the two layers of soil, and, undoubtedly the most serious path, the difficulty of representing the erosion process by an average magnitude since erosion is only generated by the extreme values of the distribution of the local shear stress. It is therefore vital to obtain this type of distribution experimentally to take into account at the scale of the sample the spatial variability existing at the scale of the pores. Section 2.4 is devoted specifically to this task.

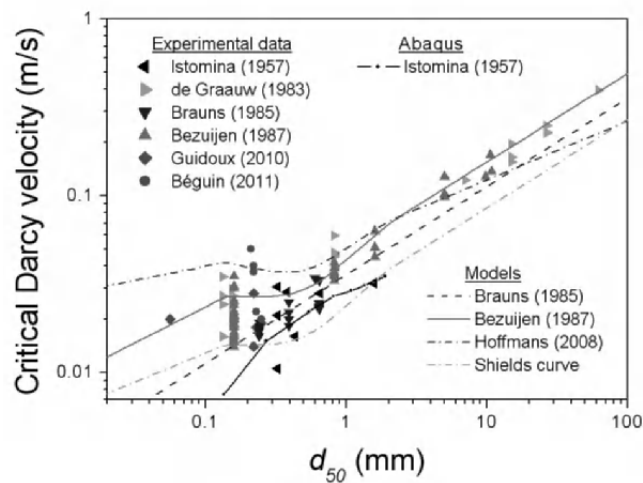


Figure 2.5. Synthesis of experimental data and models proposed relating to the CE initiation threshold in direct configuration for fine, non-cohesive soils

To sum up, a very good consistency between the results obtained can be seen in Figure 2.5 with, for non-cohesive soils whose characteristic diameter varies from 100 μm to 1 mm, initiation velocities in the range from 1 to 10 cm/s, in spite of the large variations observed in terms of the protocol and the criterion chosen to define the occurrence of the CE process.

2.3.2.3. Influence of cohesion

As already mentioned in the introduction of the chapter, almost all the works on CE in direct configuration have concerned fine, non-cohesive materials of sand and very fine sand type. The recent works of Guidoux *et al.* [GUI 10] and Béguin [BÉG 11] are alone in providing an analysis of the CE occurrence threshold for cohesive soils. Figure 2.6 illustrates these data by adding them to those presented previously in Figure 2.5 for non-cohesive soils. A very marked rise of the critical velocity of CE can be observed for increasingly finer soils. These cohesive soils fall completely outside the scope of the application of Shield's diagram.

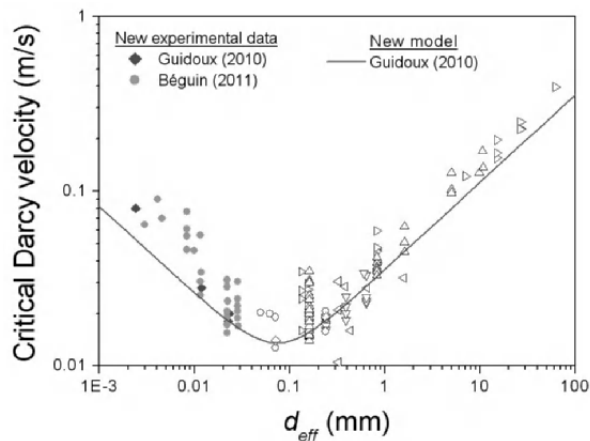


Figure 2.6. Synthesis of Figure 2.5 completed with data obtained in direct configuration for fine cohesive soils [GUI 10, BÉG 11] and with a new model adapted to cohesion [GUI 10]

Certain authors have proposed introducing a corrective term in Shield's expression to model this cohesion effect [CLA 06, RIG 07, TER 08, GUI 10]. This approach consists of adding to gravity force an attractive interaction between particles. This is only possible for little cohesive soil since a greater cohesion makes, by comparison, the weight of the particles completely negligible. The shear stress required to tear away a particle therefore increases proportionally and the critical Shields number with adhesion is written simply as a function of the usual critical Shields number:

$$\Theta_c^{cohesion} = \Theta_c \left(1 + F_{cohesion} / F_g \right) \quad [2.6]$$

The corrective term $\sqrt{1 + F_{cohesion} / F_g}$ is therefore used as a factor in the expression of critical erosion velocity. The different sources of these cohesion forces between the grains make it difficult to evaluate this term with precision. Guidoux *et al.* [GUI 10] proposed choosing it as proportional to the size of the particles, but by using the same effective diameter d_{eff} as that introduced by Kozeny in the expression of the specific surface (see section 2.3.2.2), the idea in this case is to have a representative size that retains the specific surface of the soil in order to better account for the surface nature of the adhesion forces. Other expressions exist such as that assuming an adhesion force inversely proportional to the characteristic diameter of the particles [TER 08] or the one making the distinction between cohesive force and adhesive force with respective linear and quadratic dependence with the average particle diameter [LIC 04, RIG 07]. Guidoux's hypothesis provides a corrective term to the threshold velocity in $\sqrt{1 + \beta_{adh} / d_{eff}^2}$, which satisfactorily reproduces the measurements reported in Figure 2.6 for which a sharp increase of the threshold for the smallest diameters can be observed.

It should be noted however that there is no theory at present capable of correctly describing the influence of these effects of adhesion and attraction between fine particles that are given the generic term “cohesion of material”. Particle size distribution is not the only important factor, as mineralogy and physicochemical aspects also play a fundamental role here. Furthermore, for these strongly cohesive soils, erosion no longer concerns an individual particle that will be transported by the flow but an aggregate, torn from the surface of the fine soil and which will then likely rapidly dislocate in the flow.

2.3.2.4. *CE kinetics*

Here, erosion kinetics means the quantification of the mass of soil eroded or, more precisely, transported, since measured at the outlet of the sample, when the threshold of CE occurrence has been exceeded. In a safety concern, most works in the literature are limited to evaluating this initiation threshold without dealing with the question of kinetics once the process has been triggered. A small number of studies have nonetheless dealt with this aspect of kinetics which is vital for the possible modeling modes of a dike breach by CE and estimating the characteristic times associated with such failures.

In chronological order, we can first mention the model proposed by Wörman [WÖR 92] who aimed at quantifying the CE for the fine non-cohesive soil of an earth dam covered by a granular protective shoulder in a situation of overflow. It resulted in a semi-empirical transport law linking the non-dimensional sediment discharge⁶ $q^* = q/(nUd_{85})$, the particle Reynolds number $Re_{d_{85}}$ and the Shields number $\Theta_{d_{85}}$, all formulated on the basis of the reference diameter chosen as equal to d_{85} . The law proposed takes the form

⁶ The unit of the solid discharge q is m^2/s and corresponds to a volume of particles transported by unit of length crossed and by unit of time.

$q^* \propto (\text{Re}_{d_{85}})^a (\Theta_{d_{85}})^b$ and, contrary to the previous observations, it does not present a minimum threshold that has to be exceeded to initiate erosion and transport. This law remains limited to the initial kinetics of the CE process without the possibility of taking into account possible later evolutions caused by changes to the geometry of the contact zone.

A very different approach was proposed shortly afterwards by Den Adel [DEN 94] via a probabilistic model of CE. The conditional probability of detachment can be obtained analytically by giving lognormal distributions for the probability of velocities in the flow and the probability of detaching a particle with a given flow velocity. The erosion kinetics is then evaluated on the scale of the characteristic advection time of the flow, in this case posed as equal to nD_{15}/U . A correction term proportional to the solid transport allows modeling the transport saturation by bedload which will be described in more detail in what follows. This model can be adjusted to fit previous experimental measurements as long as the grain size does not become too large, that is $D_{15}/d_{50} < 200$.

Returning to a deterministic approach and rather than linking solid transport empirically to the dimensionless numbers of Reynolds and Shields as proposed previously by Wörman [WÖR 92], Scheuermann [SCH 01] adapted a phenomenological model initially proposed by Vardoulakis [VAR 96] to describe the extraction of fuel in a sandy and slightly consolidated environment. The hydraulic flow was modeled differently according to the zones considered: Navier–Stokes equations in the pores of the coarse soil, the Darcy-Brinkman equation in the superficial part of the layer of fine soil and a Darcy equation at greater depth. Two populations of particles of fine materials are introduced: particles at rest and transported particles, with a transfer

term between the two corresponding to the rate of detachment assumed to be proportional to $\phi n C_{tr} U$, where ϕ is the volume fraction of the fine soil and C_{tr} the concentration in transported particles. This very rich formulation makes it possible to model the density profiles of the particles transported, the porosity and the solid discharge transported as well as their temporal evolutions.

These three models share the characteristic of describing only transport by bedload without taking into account the other modes of transport that include the transport of suspended matter which predominates for fine materials such as clay and silt. Consequently, cohesive soils cannot be modeled by the transport laws proposed that are limited to only granular materials such as sand and fine sand type. Finally, it is noteworthy that these laws do not possess a stress threshold⁷, contrary to what has been highlighted experimentally.

If we focus specifically on the case of cohesive soils, semi-empirical laws for describing the surface erosion of these materials have existed for a long time [PAR 65, ARI 78]. These laws are threshold laws that take into account the resistance to erosion τ_c observed experimentally for these soils and, which, is clearly above the value deduced from the Shields criterion as has already been mentioned. The hypothesis then used is that the erosion rate is directly proportional to the difference with the threshold calculated by a power law whose exponent is often equal to 1, in the same way as illustrated in the following example:

$$\varepsilon = \begin{cases} k_{er} (\tau - \tau_c)^\gamma & \text{if } \tau > \tau_c \\ \varepsilon = 0 & \text{else} \end{cases} \quad [2.7]$$

⁷ Nonetheless, Scheuermann's law requires that transport exists beforehand in order for erosion to start.

The erosion rate, ε , is the eroded mass per unit of surface and time, the two parameters k_{er} and τ_c are the erosion coefficient and the critical shear stress, respectively.

In the framework of the hypothesis of a linear law (i.e. $\gamma=1$), the sensitivity of the soil to erosion is characterized by the two parameters k_{er} and τ_c . Specific tests have been developed to evaluate these so-called “soil erodability” parameters on intact or disturbed soils [BRI 01, HAN 01, WAN 04, KNA 07, BON 08].

A similar approach was taken by Béguin [BÉG 11] to analyze CE results obtained with cohesive soils. Indeed, by making the hypothesis that the entire quantity of eroded soil is transported outside the experimental cell, the erosion rate ε , that is the mass eroded by the unit of surface and time, can be deduced from the turbidity measurement. An example, which will be explained in more detail later on, is presented in Figure 2.7. It should be noted that this curve confirms the oldest observations mentioned previously regarding the very slight dependence of the initiation threshold, and also the erosion kinetics, on the grain size of the coarse layer. This possibility of tracking back to the erosion rate on the basis of measurement of the sediment discharge rate at the outlet of the cell is nonetheless founded on the assumption of transport in suspension, without trapping in the coarse layer and by neglecting any deposit by sedimentation. Although this is justifiable for small particles, typically less than 80 μm and, therefore, corresponding for the most part to cohesive soils, this assumption no longer holds for larger particles. The preferential mode of transport is therefore the bedload leading to a sheet of particles in movement on the surface of

the fine soil that gradually attenuates the erosion process⁸. The quantity of particles increases progressively as a function of the length of the soil subject to erosion up to a certain length known as saturation length [CLA 06], after which the transported sediment discharge stabilizes. This also means that the erosion ceases. As the size of the cell is generally larger than this length, typically equal to about 10 grains' diameters [DEN 94, CLA 06], the turbidity measurement is, this time, linked to the saturated sediment discharge rate q_{sat} and not to the erosion rate. However, it should be noted that the literature sometimes refers to erosion rate as being the mass of soil transported by the flow, though this use of the term "erosion rate" is misleading and "sediment discharge rate" is preferred.

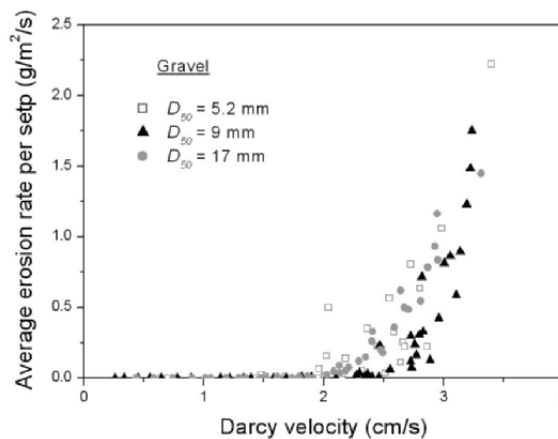


Figure 2.7. Average erosion rate per step of 30 min versus Darcy velocity imposed during each step for three different types of gravel (coarse layer) with respective median sizes $D_{50} = 5.2, 9,$ and 17 mm [BÉG 11]

⁸ A mass balance simply shows that the relationship between the erosion rate ε (in $\text{kg}/\text{m}^2/\text{s}^1$) and the solid flow q (in m^2/s^1) is given by $\varepsilon = \rho_s dq/dx$, where x designates the direction of the flow and ρ_s is the density of the soil.

Regarding the experimental results such as those presented in Figure 2.4, it can be seen that the saturated flow does not remain constant even if the stress exerted by the flow remains unchanged. This simple observation contradicts the different models presented previously, which assume a stationary rate of transport as a function only of the hydraulic stress imposed. More specifically, and as shown in Figure 2.4, what is classically observed in many studies dedicated to erosion and sediment transport during a rapid change of hydraulic stress is peak erosion corresponding to a sudden rise of sediment discharge followed by slower relaxation that brings the rate of transport to a much lower or even zero value. This situation is considered by Guidoux *et al.* [GUI 10] and Béguin [BEG 11] as being below the erosion threshold and they interpret this peak as indicating the cleaning by the flow of particles that are more fragile than the rest of the material, following, for example, the initial laying of the two superposed layers of soil. Once these particles have been carried away by the flow, the transport rate falls to zero. A specific test permitted confirming this hypothesis: by passing successively from a low stage to a slightly higher stage, it can be seen that the peak occurring during the first rise almost disappears as soon as the second stage begins [BÉG 11]. For higher hydraulic stresses, sediment discharge once again reaches a peak very quickly but then falls very slowly, with increasingly marked fluctuations, and, although the decrease is very significant, the flux does not fall back to zero. The maximum value of the peak, that is reached after sufficient relaxation time, or the average value across the entire stress stage (as shown in the example of Figure 2.7), can then be used to test the kinetics laws presented in this section. However, this approach is not wholly satisfactory since the choice of transport rate is far from being univocal and the origin of the decrease is not explained or, for that matter, modeled. To do this, it is necessary to observe the phenomena involved at a smaller scale, as described in the

following section. The reason is that it is necessary to perceive things at the grain scale to understand this progressive reduction of the quantity of particles transported. Indeed, in certain systems equipped with observation windows, progressive paving of the surface of the fine material by grain size sorting can be seen clearly [BÉG 11]. Once again, this sediment transport phenomenon is well-known and we propose two complementary origins: on the one hand, only those particles that resist erosion best, that is the largest, remain at the surface of the soil whereas the finer particles are drawn along by the flow; on the other hand, for higher rates of transport, the agitation in the layer of the sediment load forming at the interface allows the smaller particles to fall deeper through the spaces between the coarser layers. It is clear that this paving process can explain the decrease in the transport rate and even lead to stopping transport altogether. Another complementary phenomenon can also be observed and is specific to CE. This is the progressive clogging of constrictions in the coarse layer by the largest particles of the fine material. As this effect is strongly correlated with the range of size distribution of the fine material, Wörman [WÖR 96] performed CE experiments for sands with large grain size distributions. The results showed a considerable reduction of the sediment discharge transported, by about two orders of magnitude after 15 hours, which can be modeled by taking into account clogging kinetics [WÖR 96].

Following these different developments relating to this reduction of CE through time under constant hydraulic stress, two concluding remarks can be made about the global safety of a structure confronted by CE risks. First, even though the kinetic laws of erosion and transport cannot predict the reduction of sediment discharge linked to grain size sorting, they nonetheless give reference values for the rate of transport from which it is possible to build predictive models with respect to the evolution of a structure when a

CE process is in progress in order to assess the possible urgency for intervention. As they do not take into account the moderating effect of surface reinforcement by progressive paving, these predictions considerably overestimate the risk, especially for long periods, thus they are in line with high security concerns. The second remark concerns the geometric criteria mentioned at the beginning of this section and which also tend toward a conservative assessment of CE risk. Indeed, as has been seen, these criteria are based on the grain size ratio D_{15}/d_{85} , whereas the paving and clogging mechanisms that slow down the global kinetics of the phenomenon build up even in the case of a small portion of large particles. The choice of d_{85} as the reference parameter therefore appears quite restrictive and the use of a higher value, such as d_{95} , is advisable if we are no longer focusing on the initial threshold of CE but on its kinetics in the medium and long terms, or on a new, higher threshold after paving of the fine soil surface has occurred.

2.3.3. Inverse configuration

Since the focus is put exclusively on CE initiation, the geometric criterion of the CE being considered as satisfied, only cohesive soils can be used when studying the process in inverse configuration. Otherwise, without cohesion and with high grain size contrast, the grains of the upper layer could not withstand the force of gravity: they would fall and percolate through the coarse layer. These studies of the inverse configuration with cohesive soils have been performed quite recently by Schmitz [SCH 07], and then by Béguin [BÉG 11].

The works conducted by Schmitz [SCH 07] concerned silty soils with varying degrees of cohesion and showed that, as in direct configuration, the mass of soil eroded increases very significantly, starting from a certain velocity threshold whose value varies between 1 and 5 cm/s according to the

case. Beyond this critical velocity, erosion develops rapidly in the sample by forming cavities that can reach the top of the dam and create a sinkhole⁹. Schmitz [SCH 07] demonstrated a non-negligible influence when an additional load is applied to the layer of fine soil: the critical erosion velocity increases, contrary to what was observed for the direct configuration. The possible influence of grain size within the layer of coarse material could not be demonstrated clearly in the tests performed. Schmitz proposed a theoretical approach that combined a solid type behavior with a fluid type behavior for a fine soil, with a critical velocity linked to the two modes of destabilization for each behavior: erosion for the solid and interface waves for the fluid. However, the physical realism of this model remains to be demonstrated given that confrontation with experimental data has been inconclusive.

The tests performed by Béguin [BÉG 11] permitted better identifying the phenomena observed in this inverse configuration once erosion is triggered. It appears that cavities are progressively hollowed out for sufficiently moderate flow velocities but end by caving in and collapsing, reforming more or less the same interface as initially between the fine soil and the granular layer, as shown in Figure 2.8. This process tends to decrease locally the fine soil density due to the soil removal and therefore favor future erosion. At higher velocities, cavities form more rapidly and tend to evolve toward the formation of a channel, or a pipe, parallel with the interface. The very turbulent flow in this channel causes substantial grain size segregation that leads to the deposit of eroded particles with the largest particles lying on the upper surface of the granular layer. This in turn causes the conduit to become progressively disconnected from the flow and almost cease evolving. In terms of

⁹ The localized collapse of the soil at the surface caused by underground cavitation caused by alteration, dissolution, settling or internal erosion in the foundation materials.

turbidity, the measurements performed by Béguin presented in Figure 2.8 clearly show a regular increase during the formation of the channel followed by slower relaxation associated with a progressive deposit at the foot of the channel during grain size sorting brought about by internal eddies. Finally, this layer of particles coarser than those of the fine soil appears to fulfill the role of filter and practically stops the erosion of the fine material.

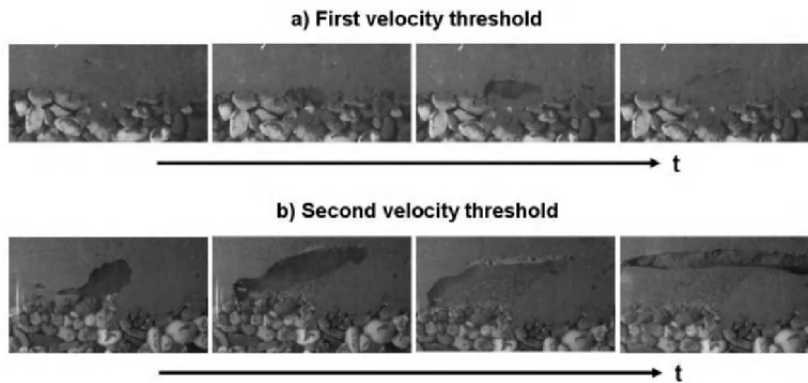


Figure 2.8. *a) First threshold corresponding to appearance of cavities that end up collapsing; b) Second threshold above which the cavities are evolving toward a channel parallel to the interface*

Figure 2.9 represents data that have been added to Figure 2.6. These are the values of critical velocities measured in inverse configuration, obtained by both Schmitz [SCH 07] and Béguin [BÉG 11], with, in the latter case, a critical velocity that corresponds to the threshold at which a channel forms. Apart from the values obtained by Schmitz, which are slightly smaller, quite good agreement can be observed between two configurations. This agreement can be explained because gravity, and thus the influence of the relative order of the two layers of materials, plays almost no role in these cohesive soils where the cohesion forces predominate over those of gravity. Naturally, this is only true for the erosion process, but not for the geometric

evolution of the interface continually subjected to erosion. Indeed, the basins formed by erosion that can occur in the direct configuration are regularly filled by the localized collapses of grains of the upper layer, whereas in the inverse configuration they can either collapse or extend in the direction of the flow. Unfortunately, at this scale, the finite dimensions of the sample did not allow an analysis of the subsequent evolution of the system. Furthermore, it is clear that, once a pipe of significant size is formed at the interface between the two soil layers, it will interact strongly with the boundary conditions downstream and upstream of the sample. A fundamental question is to know whether this latter scenario, observed at this scale of the sample, is generalized at the real scale of a dike and moreover to determine the evolution of the pipe hollowed out by erosion based on the specific boundary conditions of a real embankment. This point will be dealt with specifically in section 2.5 devoted to studies carried out at the scale of the structure.

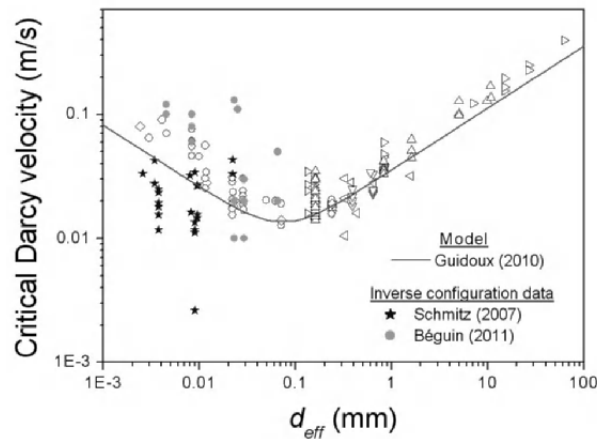


Figure 2.9. Synthesis of Figure 2.6 completed by data obtained in inverse configuration for fine cohesive soils [SCH 07, BEG 11]

2.3.4. Summary

The different macroscopic approaches presented in this section are aimed at characterizing and, in certain cases, modeling CE phenomena using averaged magnitudes on a sample representative of a two-layered material. At this scale, it is possible to correctly define an initiation threshold via a critical Darcy velocity of the flow in the porous layer, with good overall consistency regarding the differences between devices, protocols and, above all, definitions of the initiation criterion. The synthesis of these works proposed by Béguin [BÉG 11] shows that non-cohesive soils with grain sizes typically larger than 100 μm present a critical velocity in qualitative agreement with an adaptation of Shield's diagram in the case of a porous flow. However, quantitative validation requires a corrective coefficient, approximately equal to two by fitting with the values obtained with the largest particles. This factor remains purely empirical if we do not descend to a smaller scale, more specifically that of the pores in direct contact with the upper surface of the fine soil, where the flow can trigger erosion locally. Regarding cohesive soils composed of small particles, their resistance to erosion increases, as on the classical Shields curve. Beyond determining this threshold, the continuous models proposed up to now at this macroscopic scale are very much simplistic in view of the kinetics and times observed and measured once the process has been triggered. Once again, it is necessary to go to the smallest scale to identify the mechanisms explaining the temporal evolution of sediment transport by CE. This has been done moreover by anticipation in this section and will be continued in more detail in the following section dedicated to pore scale, with emphasis on the precise characterization of pore flow and on the quantification of its spatial variability.

2.4. At pore scale: local hydrodynamics of CE and statistical modeling

The scale of the sample appears to be the most relevant for modeling phenomena as aging and degradation of an environment, considered as continuous at this scale but actually being part of an overall hydraulic structure, whose global behavior must be reproduced in a satisfactory manner for safety concerns. However, as also emphasized in the conclusion of the previous section and in the case of the CE that interests us here, it is also necessary to obtain better knowledge of the different local mechanisms so as to improve these macroscopic models. This approach which consists of taking a closer view of the elementary mechanisms has already been initiated in the previous section, devoted to the macroscopic scale, when it came to interpret the temporal evolution of the transport rate data. It clearly shows how the two scales are interconnected: analysis of the global phenomenon on the basis of macroscopic measurements, close observation of elementary mechanisms to clarify complex behaviors that cannot be taken into account by macroscopic interpretation and, finally, modeling these behaviors by returning to the scale of the sample by switching from a micro to a macro description.

In the framework of CE, the questions remaining to be answered concern, on the one hand, the capacity to take into account the spatial variability of hydraulic stress and, on the other hand, as already discussed, the non-trivial evolution of erosion and transport kinetics. Indeed, the optimal macroscopic approach based on Shield's criterion uses an analytical expression of shear stress in a porous medium, given by equation [2.5] which, to our knowledge, has not yet been validated experimentally due to the difficulty of measuring shear stress. Furthermore, this formulation takes absolutely no account of the presence of a transition zone at the interface between the two layers of material. It is far from certain that an average value within a coarse layer is

representative of the real stresses existing at the interface and liable to trigger erosion. More generally, for a threshold phenomenon such as erosion where only extreme values are involved in setting particles in motion, the pertinence of choosing an average magnitude for representing only the maximum values quantitatively remains to be proved. The main objective of this work is therefore to thoroughly characterize the local hydrodynamics of CE within the immediate proximity of the interface of the two types of soil, in view to obtaining basic tools from this study, for interpreting and modeling the global phenomenon throughout a representative sample.

2.4.1. Experimental characterization of local hydrodynamics

2.4.1.1. Local probe inside a model configuration of CE

In this section, we present original results obtained recently by Béguin [BÉG 13] from local measurements taken at the pore scale, on a simplified reconstitution of a CE situation. More specifically, the configuration studied consists of a layer of sand overlaid by a layer of model coarse material composed of borosilicate glass beads. These beads were transparent with a refraction index of 1.473 at ambient temperature and, rather than water, the liquid used in this system was a mixture of mineral oils whose refraction index was adjusted as close as possible to that of the beads to ensure an overall transparency, as shown in Figure 2.10(a). The porous medium composed of beads and oil is called index-matched. Although relatively simple in comparison to the real phenomenon, this configuration nonetheless appears sufficiently realistic to correctly reproduce the elementary mechanisms underlying CE. The advantage of this method is that the transparency of the index-matched porous layer allows us to measure the velocity field of the liquid flowing through the glass beads. Two other experimental techniques

are used to achieve this: planar laser-induced fluorescence (PLIF) and particle image velocimetry (PIV) [WIE 11, DIJ 12]. The first technique consists of illuminating the medium slice-by-slice with a planar laser to excite fluorescent tracers disseminated in the liquid phase. To eliminate the direct reflections of the laser and detect only the image of the tracers, a long wavelength pass filter is installed with the threshold wavelength between the maximum laser emission and the maximum remission by fluorescence. A typical image is presented in Figure 2.10(b). The second technique, PIV, is a usual image processing to calculate the displacement field between two images. The first image is divided into cells and a correlation algorithm identifies on the second image each of the single patterns formed by the tracers located in the cells. Then the displacement field as well as the velocity field was calculated for successive pairs of images. The experiments were performed for stationary flows characterized by Reynolds numbers lower than 10, which gave the possibility of calculating a temporal average over a large number of raw fields, as shown in Figure 2.10(c).

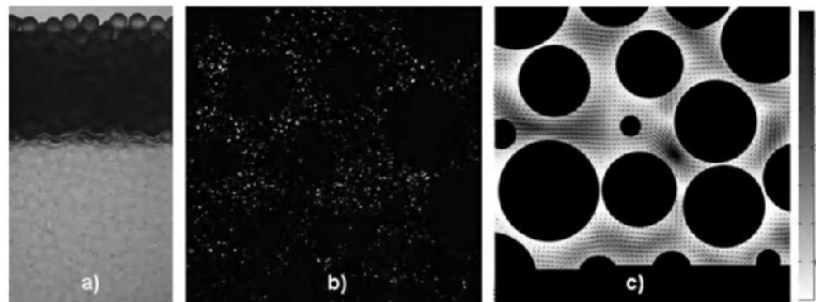


Figure 2.10. a) Illustration of the index-matching technique with, in the lower half, a mixture of beads in oil and, in the upper half, the same beads in air; b) typical picture of the fluorescent tracers using the optical filter; c) typical velocity field (vectors and magnitude) obtained by PIV with temporal average over 250 raw fields

The rest of the instrumentation comprised a differential pressure sensor and a control flowmeter, taking into account that the flow rate in the index-matched layer was maintained constant by using a gear pump. The characteristics of the two layers of soil were the following: the layer of fine material was composed of sand with a median diameter $d_{50} = 209\mu\text{m}$ and with a uniformity coefficient¹⁰ of $Cu \approx 1.5$; the granular layer was a mixture of beads of diameters 7.3 and 9.7 mm, in proportionately equal volumes, with an average size of $D = 8.5\text{mm}$. The grain size ratio between the two layers was about 40, which is a much higher value than the geometric value defined in the previous section on the sample scale. Thus, purely hydrodynamic conditions were used to define the threshold of the motion of the grains of sand.

2.4.1.2. Characterization of velocities in the porous layer

Figure 2.11 shows the vertical profile of the average velocity calculated by double summation: an average per horizontal line for each mean field (see Figure 2.10(c)) by only counting the PIV cells corresponding to the liquid, then an average over all the mean fields obtained for different positions of the laser sheet and for three measurement zones located upstream and downstream of the cell. The second calculation permitted obtaining a spatial average of the vertical velocity profile. As can be seen in Figure 2.11, the upper part of this average profile presents strong fluctuations, of the spatial period of order D , around an average value U , whereas near the surface of the sand the velocity progressively tends to zero. A transition zone can be seen very clearly where the average velocity is considerably below the average value U within the porous layer, so this velocity U is not *a priori* representative of the flow capable of

¹⁰ Quantity defined by $Cu = D_{60}/D_{10}$ characterizing the width of the material's grain size distribution.

initiating erosion. The vertical porosity profile, which is also plotted in Figure 2.11, highlights the grain size transition between the layers and the strong correlation between porosity and local velocities within the porous medium.

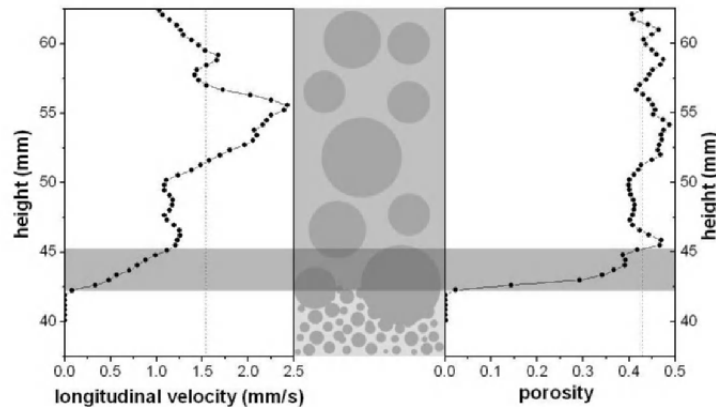


Figure 2.11. Observation on the vertical profiles of both longitudinal velocity and porosity of a hydrodynamic and granulometric transition zone just above the sand layer. Note that, due to the non-transparency of sand, a value of zero porosity is obtained in the fine soil layer

Using each velocity field of the type in Figure 2.10(c), it is possible to calculate the statistical distribution of vertical and horizontal velocity components, which is perpendicular to and in parallel with the average direction of the flow. Although the transversal components present a symmetrical distribution centred on zero with a narrow width, this is not the case for the longitudinal components whose distributions are broader with a long tail, as shown in Figure 2.12. These probability density functions in their normalized form are compatible with log-normal and exponential laws, in perfect agreement with the numerical [MAI 98, MAG 03] and experimental [CEN 96, LEB 96, RAS 96] results in the literature obtained for porous flows without a transition zone. These distributions reflect the high spatial variability of the flow in a porous medium linked to both the tortuosity

of the medium, which imposes significant deviations between the local orientations and the main direction of the flow, and the alternation of cavities and constrictions encountered by the flow.

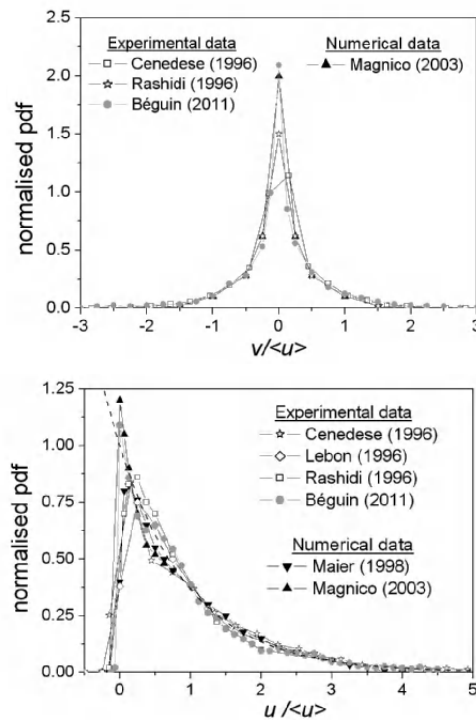


Figure 2.12. Typical probability density functions of the vertical (i.e. transverse) and horizontal (i.e. longitudinal) components of the velocity in the coarse layer, v and u , respectively, plotted against of the velocity component non-dimensionalized by the average horizontal velocity $\langle u \rangle$

2.4.1.3. Characterization of shear stresses in the porous layer

As shown before, in particular in formulas [2.1] and [2.7], most erosion models, whether dedicated to cohesive or non-cohesive soils, are based on hydraulic action quantified through the shear stress exerted by a flow on the surface of the sediment bed. Therefore, it is vital to go beyond the flow

velocity and track back to the stresses applied by the liquid during its transit through the granular layer. Knowing the velocity field and that the liquid used is Newtonian, the passage to stress is direct in principle, by applying the Newtonian stress tensor formula: $\tau_{ij} = \mu(\partial u_i / \partial x_j + \partial u_j / \partial x_i)$, where μ is the dynamic viscosity of the index-matched oil used in these experiments, which is in this case about 18 times the viscosity of water. However, this formula requires evaluating the local velocity gradients and raises practical difficulties linked to the spatial resolution given by the PIV calculation. There is, in particular, a smoothing effect on velocity caused by the interrogation cells of finite size that, in areas with interface (liquid/beads and liquid/sand), contain both mobile tracers and a fraction without flow. These problems are all the more marked on the surface of the sand layer, where the force generated locally by the flow can entrain grains. The solution chosen was, therefore, to rely on theoretical knowledge of the velocity profile inside the pores. Indeed, the resolution of the hydrodynamic equations in laminar regime gives a Poiseuille-type expression for these profiles of the general form:

$$u(z) = u_{\max} \left(1 - 4 \left(\frac{z - z_0}{h} \right)^2 \right) \quad [2.8]$$

In this formula, u is the longitudinal velocity component, z is the vertical position, whereas h , z_0 and u_{\max} correspond to the height of the section considered, the position of the center of the section and the maximum velocity measured at this point, respectively. Figure 2.13(a) presents an example of adjustment of this law on a velocity profile taken for a section inside a pore adjacent to the layer of sand. A quite good agreement can be observed, permitting the validation of the method and its application to all the velocity fields measured. Based on the adjustment parameters of formula [2.8], it is possible to deduce the value of the longitudinal

component of the shear stress applied to the borders of each section by the formula:

$$\tau_{xz} \left(z_0 \pm \frac{h}{2} \right) = 4\mu \frac{u_{\max}}{h} \quad [2.9]$$

In our CE context, it is advisable to distinguish the stress values obtained at the surface of the sand layer from those evaluated in the rest of the porous layer. Figure 2.13(b) shows a typical result of shear stresses at the sand/oil interface with a representation by color levels.

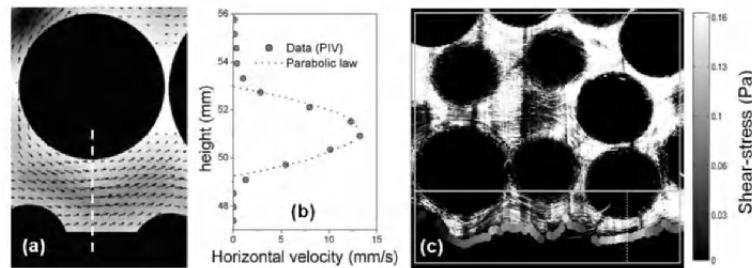


Figure 2.13. Diagram showing the method used to calculate the shear stresses: a) plot of the vertical profile of the longitudinal velocity component (in symbols) and b) adjustment by a Poiseuille-type law (in the dotted line). The longitudinal shear stress component is calculated from the fitting parameters. c) Typical grayscale representation of the shear stresses and distinction of the two measurement areas: the transition zone and the porous layer

As with the velocities, the probability density functions of the longitudinal shear stresses can be traced for the bead/oil interfaces and also for the sand/oil interface. As can be seen in Figure 2.14, although subject to more noise than those related to velocities due to the lower number of values obtained, they retain the same type of curve with a large distribution tail tending toward high values. The difference between the stresses within the granular layer and those at the surface of the sand bed cannot be seen on these normalized distributions, which are similar but whose

average values, on the contrary, differ greatly between the two distributions. Through an example, for a Darcy velocity of $U \approx 1.62 \text{ mm.s}^{-1}$, the average longitudinal shear stress in the porous layer is $\langle \tau \rangle_{\text{porous}} \approx 0.15 \text{ Pa}$, whereas it is only equal to $\langle \tau \rangle_{\text{surf}} \approx 0.07 \text{ Pa}$ at the surface of the sand layer, that is a ratio of $\beta_i \sim 0.5$ between the effective eroding stress and the average shear stress of the flow in the porous layer. This ratio underlines the impact of the granulometric transition zone on the flow, highlighted previously.

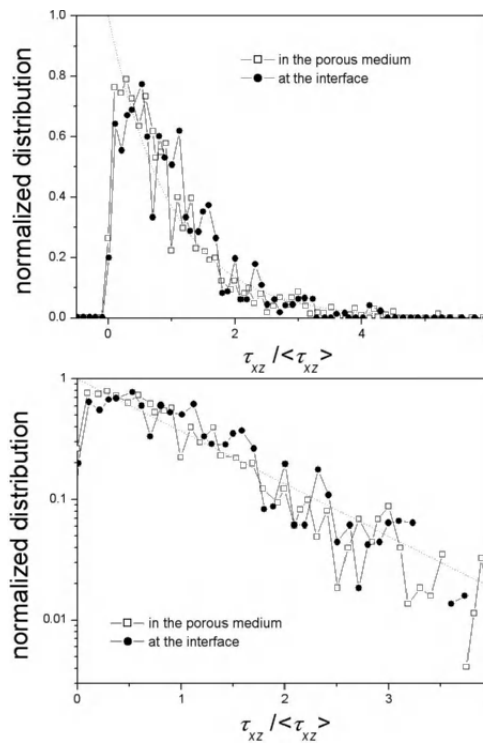


Figure 2.14. Typical probability density functions of the longitudinal components of the shear stresses, measured in the porous layer and at the interface (i.e. in the transition zone), plotted against the shear stress component non-dimensionalized by the average longitudinal shear stress $\langle \tau \rangle$ in both linear and semi-logarithmic representation. The dotted lines stand for the exponential law

2.4.1.4. *Summary and utilization of local observations*

These measurements of velocity and stress at the scale of the pores underline two basic points. First, the layer of the fine soil considerably slows down the intensity of the flow on the zone of influence of about the size of one grain in the coarse layer with, as the essential result for erosion, a reduction of approximately half the average shear stress in comparison to that exerted by the flow in the granular material. Second, both at the core of the porous medium and immediately next to the sandy layer, all the quantities evaluated are broadly distributed, characterized by an extremely dissymmetric probability density function that extends significantly toward high values with non-negligible probabilities of reaching, locally, values two or three times higher than the average.

This statistical study of velocities and stresses in our model system makes it possible to compare quantitatively the measurements and the analytical laws proposed in the literature, notably those of Wörman and given by equation [2.5] [WÖR 92]. It is also possible to introduce spatial variability and the statistical nature of the variables linked to flow via exponential distribution laws which, as seen previously, are compatible with the experimental data and which provide the opportunity for performing very simple analytical developments.

2.4.2. *Integration at macroscopic scale*

2.4.2.1. *Average shear stress and critical threshold of CE*

As shown above, the average shear stress measurements were only obtained in one situation, with an average Darcy velocity of $U \approx 1.62 \text{ mm.s}^{-1}$, according to PIV calculations. The real porosity in the layer of beads was estimated at $n \approx 0.37$ on the basis of the total mass of beads, the volume of the cell and by taking into account wall effects with Ben-Aïm's model

[BEN 68]. These two values can be used to obtain the hydraulic gradient i by applying Darcy's relation, $i = \mu U / (k \rho_w g)$, which is valid in this case due to the very low velocities corresponding to the linear regime, and by using the expression proposed by Kozeny and Carman [BEA 72] for intrinsic permeability k (with the constant c_0 that was already defined in section 2.3.2.1):

$$k = \frac{c_0 n^3 D^2}{36(1-n)^2} \quad [2.10]$$

The values obtained are $k \approx 4.9 \times 10^{-8} \text{ m}^2$ and $i \approx 0.072$, respectively. The latter value is consistent with the measurement obtained at the upper wall with the differential pressure sensor: $i_{\text{sup}} \approx 0.082$. It is highly likely that the deviation was caused by a slight preferential flow close to the wall and the value deduced from the permeability will be preferred. It follows that the average shear stress for a hydraulic gradient $i \approx 0.072$, assumed to be homogeneous throughout the porous medium, is equal to $\langle \tau \rangle_{\text{porous}} \approx 0.15 \text{ Pa}$ inside the porous layer and $\langle \tau \rangle_{\text{surf}} \approx 0.068 \text{ Pa}$ at the interface with the sand layer, respectively.

In addition to Wörman's formula given by equation [2.5], a second relation between the hydraulic gradient and Darcy's velocity was proposed by Reddi [RED 00], assuming a model porous medium composed of capillary tubes of the same permeability k as the real medium. By using formula [2.10] for k , it is easy to show that this Reddi expression is proportional to that of Wörman's formula in a ratio of $\sqrt{2/5} \approx 0.63$ and both are written as:

$$\tau_w = \frac{n \rho_w g i D}{6(1-n)}; \quad \tau_R = \sqrt{\frac{2}{5}} \tau_w \quad [2.11]$$

The application of these formulas with values matching the conditions under which the measurements were obtained gives $\tau_W \approx 0.49\text{Pa}$ and $\tau_R \approx 0.31\text{Pa}$, respectively. These values are, therefore, considerably higher than that deduced from the PIV measurement in the layer of beads: $\langle \tau \rangle_{\text{porous}} \approx 0.15\text{Pa}$.

Thus, a significant variation can be observed between these analytical values and the experimental data. Part of this variance can be explained by the fact that the measurements are limited by the two-dimensional (2D) visualization of the flow that does not allow us to evaluate the transversal contribution in the shear stress exerted at the interface. Due to the tortuosity of the medium, this contribution is non-negligible even though it does not correspond to the average direction of the flow. Nonetheless, this does not explain the discrepancy observed that calls into question the validity of the analytical laws used. A systematic study would be required to confirm this and possibly propose a more realistic law.

However, to generalize this analysis, a second empirical coefficient can be introduced in order to continue relying on an analytical law. In practice, preference is given here to that of Wörman's expression as it is obtained under less restrictive hypotheses than that of Reddi's expression. This coefficient, written as β_W here, is defined as follows:

$$\beta_W = \frac{\langle \tau \rangle_{\text{porous}}}{\tau_W} \approx 0.3 \quad [2.12]$$

Regarding the interpretation of the two empirical parameters β_W and β_i , we have already seen that the first parameter probably resulted from an error in the theoretical prediction of the average shear stress in the porous medium via the expression proposed by Wörman in equation [2.5]. Regarding the second parameter, it is linked to the presence of the interface and its influence on the average stress in its

immediate neighborhood in comparison to the stress exerted sufficiently far from the interface. This can be understood if we consider the framework used by Wörman. For the interface, it can be seen that in equation [2.5], it is necessary to add a supplementary contribution to the left-hand member corresponding to the stress exerted by the flow on the upper surface of the sand, whereas at the same time the right-hand term is not subject to much modification because the porosity is hardly affected by the presence of the interface. Thus, for an overall gradient that undergoes little change throughout the coarse layer, the larger friction surface at the base of this layer causes, by compensation, a reduction in the average stress applied.

To take the interpretation of the results obtained at the macroscopic scale further, it is necessary to assume that these empirical coefficients vary very little so they can be considered as constants. With our model materials, this is far from obvious given that our local measurements are limited to a single geometric configuration and they are also performed on a very simplified system, with spherical particles, *a priori* quite different from the tests performed at the sample scale or the real configurations found in dike structures. Thus, additional work is needed for validating this working hypothesis, at least to study the variations of the two coefficients for different geometries in the framework of the model system.

Therefore, starting from the postulate that coefficients β_w and β_i conserve their respective orders of magnitude evaluated previously, it is possible to link the Shields' criterion with Darcy's critical velocity by successive steps. The approach first consists of assuming that erosion of the sediment bed is triggered, within the pores in contact, at a threshold stress τ_c that, according to equation [2.1], is $\tau_c = \Theta_c (s-1) \rho_w g d_{50}$. The critical Shields number Θ_c is deduced from the Shields diagram using the analytical

expression given by Cao [CAO 06]. This threshold stress is then linked to hydraulic gradient i by formula [2.11], corrected by the addition of the two empirical coefficients β_w and β_i . The critical hydraulic gradient is finally written as:

$$i_c = \frac{6(1-n)(s-1)d_{50}}{n\beta_i\beta_w D} \Theta_c \quad [2.13]$$

Ultimately, we return to the practical definition of the CE initiation threshold expressed not as a critical hydraulic gradient but as a critical Darcy velocity. The relation between the two quantities is given by the flow law in the porous medium, whose general form for the hydrodynamic regime considered here (i.e. Forchheimer's regime) is written as $i = aU + bU^2$. Semi-empirical expressions have been proposed for the two coefficients a and b , especially those expressed in the Fand formula given by equation [2.2]. These can also be deduced directly at each test using the experimental curve of flow rate versus pressure drop.

By following this methodology systematically, Béguin was able to propose a model for interpreting Darcy's CE initiation velocity in very good agreement with the different data in the literature presented previously as shown in Figure 2.15 [BEG 11]. This new macroscopic model, deduced step-by-step from the Shields threshold, limits the hypotheses used and relies on empirical coefficients interpreted simply in the framework of the local hydrodynamics of the CE, contrary to the calibration parameters proposed up to now [BEZ 87, HOF 08]. It is noteworthy that the semi-empirical corrective term $\sqrt{1 + \beta_{adh}/d_{eff}^2}$ presented in section 2.3.2.2 [GUI 10] that permits reproducing the influence of the cohesive character has also been integrated into Béguin's model.

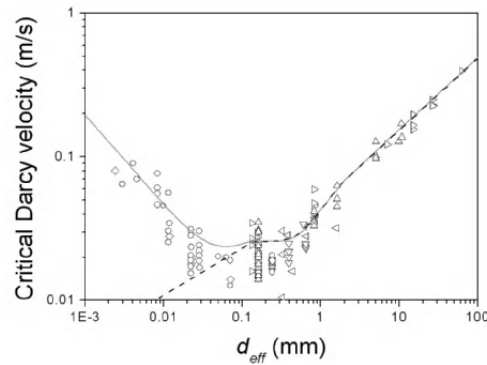


Figure 2.15. Comparison of Béguin's model [BÉG 11], in the solid line, with all the data from Figure 2.6 (i.e. in direct configuration). The dashed line is obtained by multiplying the Shields' curve by an empirical coefficient of 1.8

2.4.2.2. Spatial variability and impact on the CE threshold

The approach described above for evaluating the CE initiation threshold still remains limited to using only average values to describe the macroscopic behavior of the system, although an improvement was made by taking into account the influence of the sediment interface on the local hydrodynamics in the erosion zone. However, the velocity and stress distribution measurements within the porous layer and close to the fine soil layer show that the considerable spatial variability of the flow has definite impacts on the CE that we are seeking to model simply.

The first step consists of realistically describing the local probability of erosion. To do this, first we need to use a local erosion law such as that initially proposed by Partheniades [PAR 65] and defined previously in equation [2.7] (with exponent $\gamma=1$). At this stage, this local erosion law is assumed to be purely determinist and the random character of the CE is introduced only via the spatial variability of the flow and the associated statistical distribution. The statistical distribution of the bottom shear stress will be

used as the ingredient of this probabilistic approach because the local erosion law relies on the hydrodynamic action expressed by the shear stress at the surface of the sediment bed. However, as shown in Figure 2.14 and particularly at semi-logarithmic scale, this distribution is very close to a simple exponential law of the following type:

$$p(\tau) = \begin{cases} \frac{1}{\langle \tau \rangle} \exp\left(-\frac{\tau}{\langle \tau \rangle}\right) & \text{if } \tau \geq 0 \\ 0 & \text{if } \tau < 0 \end{cases} \quad [2.14]$$

Two major points should be underlined regarding this law. First, due to the intrinsic spatial variability of the flow, it can be seen that the average value $\langle \tau \rangle$ is not representative of the stress actually exerted and that, for example, an average value slightly lower than the critical shear stress τ_c is not necessarily synonymous with the absence of erosion because stresses will exceed this threshold locally at some places. However, although it is not directly representative, this average value appears sufficient to fully parameterize the statistical distribution in stresses, as shown in equation [2.14] where $\langle \tau \rangle$ is the only parameter. It should be clearly noted that in this case we speak about the average shear stress at the surface of the sediment, that is in the transition zone. On the contrary, the average shear stress above this zone within the porous layer is not, *a priori*, representative of the efforts exerted by the flow at the surface of fine soil, but it does introduce the empirical coefficient β .

The second point concerns the framework of comparing CE to the classical sediment erosion caused by a pure flow, generally a free surface flow, in turbulent regime. The literature includes a large number of experimental and theoretical works on the statistical distribution of shear stress at the interface. Although a normal or Gaussian law is

often chosen, Hofland showed that this form was more appropriate to velocity than to stress and, based on this hypothesis, he formulated a slightly more complex analytical expression [HOF 06]. This was then slightly modified by van Prooijen [VAN 10] to obtain a better fit with older experimental results [OBI 96]. All said and done, the curve for this distribution of shear stress at the interface in turbulent flow proved to be very different from the results presented here for a porous flow in Forchheimer's regime. This difference expresses the different nature of flow variability, that is the variability of pore geometry in laminar flow in the case of CE and temporal fluctuations induced by the turbulence of the flow in the case of river erosion. The stochastic formulation of the CE that we will analyze here is, therefore, similar on the methodological level, but distinct from the quantitative viewpoint in comparison to existing formulations of this type for erosion in turbulent flow [GRA 70, CHE 06, VAN 10].

The change to macroscopic scale is done by integrating the local erosion law via the exponential distribution as follows:

$$\langle \varepsilon \rangle = \int_{\tau_c}^{+\infty} k_{er} (\tau - \tau_c) p(\tau) d\tau = k_{er} \langle \tau \rangle \exp\left(-\frac{\tau_c}{\langle \tau \rangle}\right) \quad [2.15]$$

Once this flow variability is taken into account, it can be seen that the macroscopic erosion law no longer presents a threshold: the rate of erosion is very low, but it is non-zero below the critical shear stress τ_c . On the contrary, when the average stress becomes sufficiently high in relation to τ_c , the global erosion law tends toward the local erosion law, linear at the threshold. This behavior can be observed in Figure 2.16, where the model was parameterized to reproduce satisfactorily the shape of one of the experimental curves from Figure 2.14. This represents the average erosion rate per step as a function of the Darcy velocity applied during each step in CE tests between a layer of gravel and a

layer of sand in direct configuration. It is noteworthy that it is exactly the same type of global law as that obtained by introducing temporal fluctuations in the local erosion law in turbulent regime [DEN 94, VAN 10].

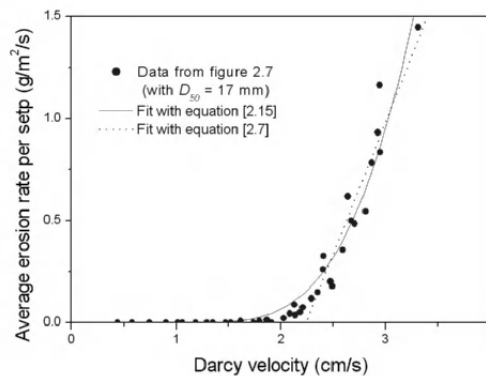


Figure 2.16. Comparison of the local erosion law, given by equation [2.7], and the global erosion law, given by equation [2.15], with the statistical model, with one of the curves from Figure 2.7 representing, for each velocity step, the average erosion rate as a function of the Darcy velocity

Consequently, even when postulating a local erosion law with a threshold, it can be seen that changing the scale through integration of the entire statistical distribution results in eliminating this stress threshold, both when the variability is of temporal origin, caused by a turbulent flow regime, and when it is of spatial origin as here for CE. Obviously, this result is liable to propel the debate on the existence as such of an erosion threshold [LAV 87]. Indeed, most erosion and transport laws, which are either purely empirical or phenomenological, postulate the existence of such a threshold and it can, therefore, be defined by extrapolation to zero. Nonetheless, the closer we get to this assumed threshold, the higher the decrease in the quantity of eroded material and the greater the difficulty in measuring it. This gives rise, in particular, to the very different definitions used by various authors, as underlined,

for example, in section 2.3.2.1 in the specific case of CE. This results in criteria that lack objectiveness and are difficult to compare from one study to another. Furthermore, it is observed that over very long periods, low cumulative quantities of material can be eroded even when the hydraulic stress remains below the extrapolated threshold. The latter, therefore, finally depends on the patience of the experimenter. The global law given by formula [2.15], therefore, provides a possible explanation for this type of observation. It also shows that extrapolation by the linear adjustment method can give erosion parameter values very different from those of the local law. Therefore, as shown in Figure 2.17, if the local erosion law is available and several points on the curve of global erosion are known, which amounts to imagining ideal measurements (i.e. perfectly positioned on the global erosion curve), it can be seen that linear extrapolation leads to major errors in the erosion parameter values, with an overestimation of erosion coefficient k_{er} and an underestimation of threshold τ_c . It should be noted, however, that the latter result is safer in terms of risk management.

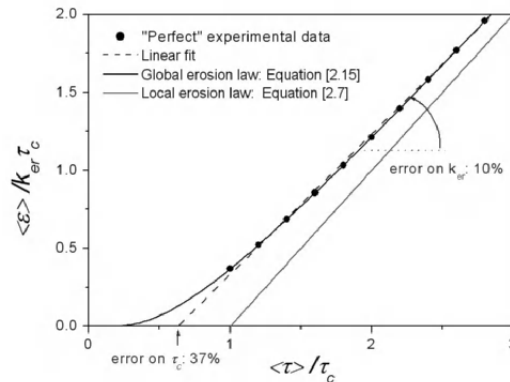


Figure 2.17. Comparison of the local erosion law, given by equation [2.7], with a linear regression deduced from “ideal” experimental data, perfectly distributed on the global erosion law, given by equation [2.15]. Large errors occur between the parameters of the linear fit and those of local law, especially for the critical shear stress.

2.4.2.3. Modeling CE statistically

However, the statistical approach discussed in the previous section is not enough. Indeed, from the moment this stochastic dimension is taken into account in the erosion process, it is not possible to half do things by assuming only the hydraulic stress is statistically distributed while resistance to erosion remains uniform over the surface of the sediment bed. The latter hypothesis cannot be justified, even in the ideal case of a material composed of grains that are exactly the same in terms of size and shape, since variability in the geometrical arrangement of each grain persists, some of them being more exposed to the flow and thus less able to resist erosion [CHE 03]. In addition, the real case introduces a distribution of particle size and shape, so it is easy to see that resistance to erosion varies significantly over the surface of the sediment bed. This observation is not limited to granular materials: cohesive soils also present intrinsic heterogeneities (density, chemical and biological compositions, etc.) that locally modify erosion resistance properties, mainly via the variability of local cohesion. For these cohesive soils, it is noteworthy that erosion no longer corresponds to the individual entrainment of particles: the existence of several modes of erosion has been suggested, including floc erosion that seems the most realistic in the case of CE close to the erosion threshold. This mode corresponds to the pulling out of an aggregate of particles, called floc, which then breaks up in the flow [WIN 04].

Consequently, this variability of local erosion resistance properties for both granular and cohesive materials requires the introduction of statistical distribution. If we maintain the assumption of a local erosion threshold law, the simplest way of modeling the stochastic dimension is using a statistical distribution for critical shear stress τ_c . The case of erosion coefficient k_{er} is more difficult because its physical interpretation remains blurred. For the sake of simplicity,

we will continue to assume that this parameter is constant while knowing that no major problems will arise from also introducing a statistical representation for this quantity.

In agreement with very similar works on river erosion [VAN 10], we have chosen a normal statistical distribution for parameter τ_c , based on an average value $\langle \tau_c \rangle$, with a standard deviation σ_{τ_c} . Given that a negative value of τ_c will not have any physical meaning, the τ_c -distribution is truncated below zero. Thus, it is written as:

$$q(\tau_c) = \begin{cases} \frac{\chi}{\sqrt{2\pi}\sigma_{\tau_c}} e^{-\frac{1}{2}\left(\frac{\tau_c - \bar{\tau}_c}{\sigma_{\tau_c}}\right)^2} & \text{if } \tau_c \geq 0 \\ 0 & \text{if } \tau_c < 0 \end{cases} \quad [2.16]$$

Coefficient χ arises from the renormalization of the distribution after the truncation below zero.

This time, the integration of the local erosion law making it possible to change scale, takes into account two distributions [2.14] and [2.16] and is written, after several lines of analytical development, as follows:

$$\begin{aligned} \langle \varepsilon \rangle &= \int_0^{+\infty} q(\tau_c) \left(\int_{\tau_c}^{+\infty} k_{er}(\tau - \tau_c) p(\tau) d\tau \right) d\tau_c \\ &= \chi k_{er} \langle \tau \rangle \exp\left(u \frac{\sigma_{\tau_c}}{\langle \tau \rangle}\right) \left(1 - \operatorname{erf}\left(\frac{u}{\sqrt{2}}\right) \right) \end{aligned} \quad [2.17]$$

Where “erf” denotes the error function and variable u is defined by:

$$u = \frac{\sigma_{\tau_c}}{\langle \tau \rangle} - \frac{\langle \tau_c \rangle}{\sigma_{\tau_c}} \quad [2.18]$$

However, even if we assume a very wide distribution for the critical shear stress of the material, for example by choosing $\sigma_{\tau_c} = \langle \tau_c \rangle$, the introduction of the second statistical distribution will have only a marginal effect on the global erosion law, as shown in Figure 2.18 where the dimensionless erosion rate $\langle \varepsilon \rangle / k_{er} \langle \tau_c \rangle$ is plotted as a function of the ratio of average stresses $\langle \tau \rangle / \langle \tau_c \rangle$.

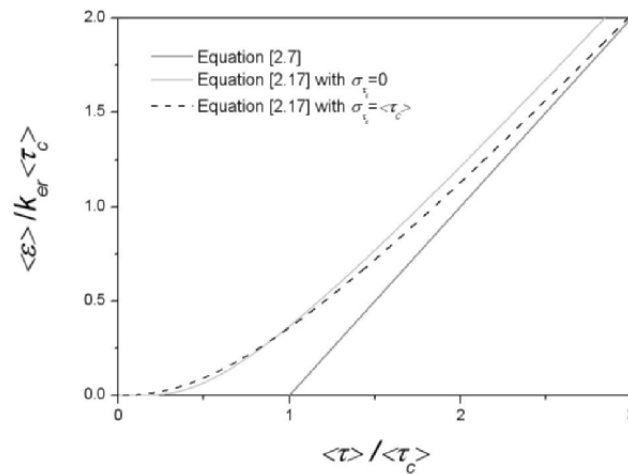


Figure 2.18. Comparison of the local erosion law, given by equation [2.7], and the global erosion law, given by equation [2.17], in a statistical model where the critical shear stress is also statistically distributed with, in this graph, two opposite values of its standard deviation corresponding, respectively, to a punctual and to a very large distribution

At this point, it is tempting to believe that the variability of erosion resistance properties at the surface of the sediment bed has a negligible influence in comparison to that brought by the statistical distribution of the hydraulic stress. Nonetheless, this reasoning is inexact because it is based on an implicit hypothesis: statistical distributions will remain unchanged over time. However, although this appears reasonable regarding hydraulic stress, at least as

long as the cumulated erosion remains limited and does not overmodify the geometry of the contact zone, it is not the same for the distribution of the critical shear stress. Only the particles (i.e. the clusters of particles or grains according to the cohesiveness or non-cohesiveness of the material) of least resistance are eroded whereas the others remain in place. As a result, the distribution of the critical shear stress at the surface progressively changes toward the highest erosion resistance values. This is the explanation at statistical level for the surface paving induced by grain size sorting and selective erosion, already discussed in section 2.3.2.3. To model this, it is necessary to periodically select randomly in the initial distribution a new local resistance value once the cumulative erosion in the zone considered has exceeded a typical value expressed in the form of a typical erosion depth δ . Locally, this random selection corresponds to the renewal of the material exposed to erosion and the appearance of new particles at the surface of the sediment bed; therefore, δ corresponds to a characteristic size of the material. This is naturally the average size of the grains for a non-cohesive soil whereas it is necessary to consider a scale of spatial correlation of the internal properties of the material for a cohesive soil. It should also be noted that although the distribution of the critical shear stress evolves at the surface of the sediment bed, it remains unchanged in volume. However, this point could be modified if the aim is to introduce the additional effect linked to the consolidation of a cohesive material, leading to a positive vertical gradient on the erosion resistance. The existence of successive horizontal strata, whether natural or linked to the protocol for laying the soil, could also be taken into account in a model of this type. Nonetheless, here we continue with the model described above whose parameters are the following: $\langle \tau \rangle$ is the average shear stress exerted by the flow at the surface of the fine soil layer, k_{er} is the coefficient of proportionality of the local erosion law, $\langle \tau_c \rangle$ is the average stress threshold,

σ_{τ_c} is the standard deviation of the critical shear stress distribution and δ is the depth of erosion requiring the renewal of local critical shear stress.

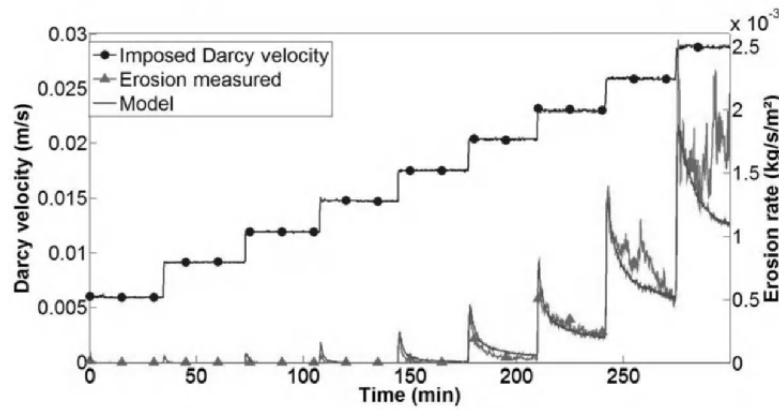


Figure 2.19. Comparison of the experimental data from Figure 2.4 [GUI 10] with the model using critical shear stress renewal at the surface. A good agreement is obtained for the pair of parameters $k_{er} \approx 6.8 \times 10^2 \text{ s.m}^{-1}$ and $\sigma_{\tau_c} \approx 0.20 \text{ Pa}$

Figure 2.19 presents a comparison of this model with an experimental curve resulting from the works of Guidoux *et al.* [GUI 10]. Several parameters of the model can be deduced directly from the experimental data. First, knowing the Darcy velocity U and hydraulic gradient i for each step of the curve, it is possible to evaluate the average stress at the surface $\langle \tau \rangle$ using formula [2.11] corrected by the two empirical coefficients β_w and β_i , whose values are considered unchanged in relation to those obtained at pore scale (see section 2.4.2.1). Then, it is assumed that the average stress threshold $\langle \tau_c \rangle$ is given by the value resulting from the Shields diagram. Here, the fine material is sand with a median diameter of $d_{50} \approx 60 \mu\text{m}$ and the associated Shields value is $\langle \tau_c \rangle \approx 0.12 \text{ Pa}$. Lastly, for this granular soil, the

renewal depth δ of the stress threshold is taken equal to the median diameter d_{50} . Finally, there are only two free parameters: k_{er} and σ_{τ_c} . As can be seen in Figure 2.19, the resolution of the model using the Monte Carlo method provides very satisfactory agreement for the pair of parameters $k_{er} \approx 6.8 \times 10^2 \text{ s.m}^{-1}$ and $\sigma_{\tau_c} \approx 0.20 \text{ Pa}$. The erosion peaks are well reproduced for both the sudden rise bringing the rate to its maximum value and the later relaxation that occurs over a much longer timescale.

2.4.3. Contribution made by the local scale study

By characterizing precisely the hydrodynamics in the contact zone, that is in the porous layer in direct proximity with the interface with the fine soil, the high precision experiments carried out on the small scale on the model system remarkably helped in understanding the CE mechanisms at sample scale.

First, these measurements revealed the presence of a transition zone inside which the average longitudinal velocity increases progressively from zero at the interface to Darcy's velocity at the heart of the porous layer. The typical size of this transition zone appears to be in the region of the average radius of the grains of the porous medium. This study also allowed introducing two empirical coefficients to simply take into account two results: first, the overestimation of the analytical formulas giving the value of the longitudinal component of the shear stress exerted by the flow above the transition zone and, second, the effect of slowing the flow at the interface that causes an average stress inside the transition zone much lower than that measured at the center of the porous zone. Using these two empirical coefficients at the macroscopic scale was only possible in this case under the hypothesis that the values obtained at the small scale on the model system, and for a

single geometric configuration, remained unchanged for more realistic materials. It is clear that this hypothesis is very strong and would require additional tests in order to validate it. However, as has been demonstrated here, it is possible on this basis to interpret very satisfactorily the previous results from the literature in the general framework of the Shields' diagram.

The second fundamental contribution of this analysis at the pore scale concerns the spatial variability of the flow, which was highlighted and quantified using statistical distributions. Thus, the longitudinal shear stress presents a distribution compatible with a simple exponential law, both inside and above the transition zone. This very important result opens up the path toward a statistical model of CE in which it is logical to also give a stochastic character to the local resistance properties of the fine soil, whether cohesive or not. The change of scale between the local relations and macroscopic quantities was performed by integration via the exponential probability obtained experimentally. This calculation shows in particular that the notion of erosion threshold vanishes at the large scale, because in a sufficiently extended system there will always be a small number of zones where the local stress exceeds the soil's resistance to erosion. The corresponding erosion rate remains very low and probably difficult to quantify from the experimental viewpoint.

Lastly, observation at the small scale also allowed underlining an effect vital for understanding the temporal evolution of the erosion phenomenon: the progressive surface paving caused by the grain size sorting and the selective erosion of the least resistant particles. This point was modeled by renewing the critical shear stress of the particles at the surface in the zones most exposed to erosion. The erosion resistance properties are therefore progressively strengthened at the surface of the fine material.

Consequently, for a low average hydraulic stress, the rate of erosion rapidly falls to a zero value. It is only for higher hydraulic stresses that the erosion rate appears to stabilize at a non-zero value. This selective erosion therefore leads to the reappearance of a threshold for CE kinetics according to whether its duration is simply transient or, on the contrary, permanent. This can explain why a threshold is indeed observed in the previous CE tests.

However, in its present state, the model presented here is not sufficiently finalized for operational use on real structures. Indeed, to do this, the model must be able to quantify the effective threshold of establishing a CE phenomenon through time with precision, as this is obviously vital information for risk management. This requires using the model over very long periods and thus ensuring beforehand its capacity to correctly predict the reduction of the erosion rate over durations far longer than those commonly explored experimentally. However, phenomena different from short-term phenomena, and thus not taken into account by the model, can become predominant as time progresses. Such phenomena may be biological or chemical and progressively modify erosion resistance properties, especially for cohesive soils. It is also necessary to take into account the geometric evolution of the system, which is mainly controlled by two opposing effects. On the one hand, among the particles of eroded soil, the coarsest fraction is liable to be trapped in the smallest constrictions of the porous layer. Thus, clogging may occur progressively in the coarse soil; the lower the ratio between the grain sizes of the two soils, the faster the clogging occurs. On the other hand, when erosion develops in the contact zone, cavities form at the interface and grow until the grains of the upper coarse layer end by collapsing, as illustrated in Figure 2.20. The geometry of the contact zone therefore changes constantly once we focus on longer timescales. As a result, the characteristics of the hydraulic stress in terms of

average stress and statistical distribution also change significantly during permanent CE. Therefore, much work remains to be done to enrich the statistical model with several improvements capable of reproducing each of these slow kinetic phenomena.

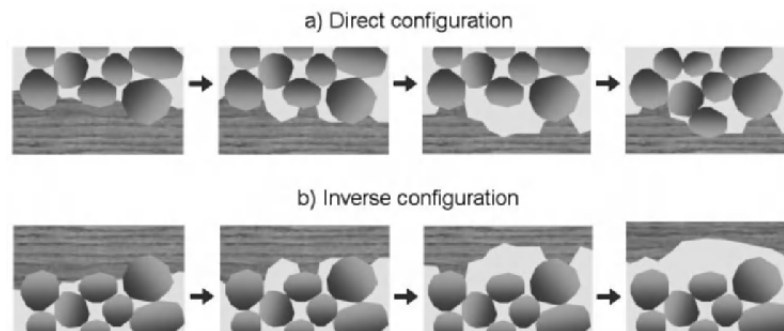


Figure 2.20. *Diagrams showing the evolution, in the medium term, of the geometry inside the contact zone between the two soil layers in a) direct and b) inverse configuration*

Lastly, the entire approach developed in section 2.4 is limited exclusively to the case of the direct configuration, when the layer of the coarse soil overlies a layer of fine soil. Although it is reasonable to expect that the results obtained from the local hydrodynamics of CE are fairly similar in inverse configuration, this is not so for erosion and in particular for its temporal evolution. Similarly to the direct configuration erosion hollows cavities in the fine soil but, on the contrary, as the cohesive fine soil is mechanically very stable, these high-erosion zones remain and gradually become larger. A schematic view of this temporal evolution of the geometry of the contact zone is given in Figure 2.20 and photographs are shown in Figure 2.8 in section 2.3.3 dedicated to the sample scale in the inverse configuration. Hydrodynamics in the erosion zone is totally modified by this geometric change, which is overly pronounced, and must to

be simply take into account in our statistical model. On the contrary, another type of erosion may be triggered, with the progressive formation of a channel whose possible modeling could be based on the recent work performed on concentrated leak erosion [BON 08] when erosion occurs on the side walls of a pipe where the flow of water is concentrated.

As already mentioned in section 2.3.3, in the absence of an adapted model, it is necessary to perform experimental tests at a larger scale to validate this failure mode in the inverse configuration, that is initiated by CE before developing through the formation of a channel between two layers of soil. In view of controlling the safety of dikes, it is especially important, since this inverse configuration is the most frequently encountered in real structures (see section 2.2). So, after working at the sample scale, which required taking a detour via the local scale of the pores, the next step will naturally lead us to study CE in a full-scale structure, with a detailed study in the following section.

2.5. At hydraulic structure scale: identification of failure scenarios by CE and scale effects

2.5.1. Reasons for a study at this scale

In this chapter, the CE process has first been described at the sample scale (from a decimeter to a meter) and then at the grain scale (from a tenth of millimeter to a centimeter) in order to integrate the elementary mechanisms in detail. *In situ*, situations frequently occur in which CE develops at the scale of earth hydraulic structures ranging in length from several meters to a hundred meters. This raises a classical problem in soil mechanics: are the results of laboratory tests on samples representative of the behavior of a real structure? In other words, does the spatial scale influence the CE process?

This question is not limited to the case of CE and remains highly pertinent for all the erosion processes described in the other chapters. To provide answers to this question, tests at the scale close to that of a structure have been performed to study regressive erosion (Chapter 3) and external erosion (Chapter 4). These tests were performed to study the influence that the dimensions of the surfaces and volumes eroded have on triggering the process, and analyzing the role played by limit conditions, since there is obviously a difference between a test in a laboratory cell and *in situ* in a real structure. The second major point of interest was to study the progression phase of the phenomenon following triggering in order to define and validate different potential failure scenarios under real conditions.

In the case of CE, large-scale tests were carried out in the experimentation hall of the Compagnie Nationale du Rhône in the framework of a PhD thesis [BEG 11]. To our knowledge, these are the only large-scale CE tests that have been performed to date. The results obtained provide essential elements regarding the influence of the spatial scale on CE and on the progression of the phenomenon and its consequences on the structure.

2.5.2. Description of the experimental rig and instrumentation

This series of tests was focused on the inverse configuration (see section 2.2.1) for which a layer of silt is superposed on a layer of gravel. This configuration is common in the dikes of the headrace canals of hydropower plants, which are built with a silt or clay core raised on an alluvial gravel foundation. A CE process in an inverse configuration at the interface of these layers is probable.

The experimental rig used was composed of a reinforced concrete structure open on its downstream side and upper surface, containing a useful volume 4 m in width, 8 m in length and 2.25 m in height. A series of three tests in the first geometry, called *layer geometry*, dealt with the case of a layer of gravel 20 cm thick deposited at the bottom of the concrete structure, overlaid by a layer of silt 2 m thick. A removable wall was used to close off the downstream face. A schematic view of the entire rig is shown in Figure 2.21. A sample of geometry similar to that of the laboratory tests previously described was obtained, but whose dimensions were multiplied by a factor of 10. This permitted studying the possible scale effect of the surface eroded at initiation. Then, a second series of tests with another geometry called *slope geometry* was performed with a slope whose base was located downstream, to reproduce the shape of a real structure, as shown in Figure 2.22. Here, we sought to study the progression phase of the CE and its consequences on the integrity of the structure.

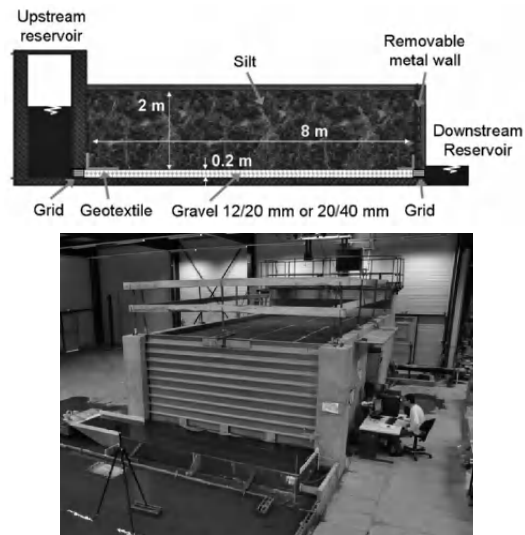


Figure 2.21. Diagram and photograph of the experimental rig with layer geometry

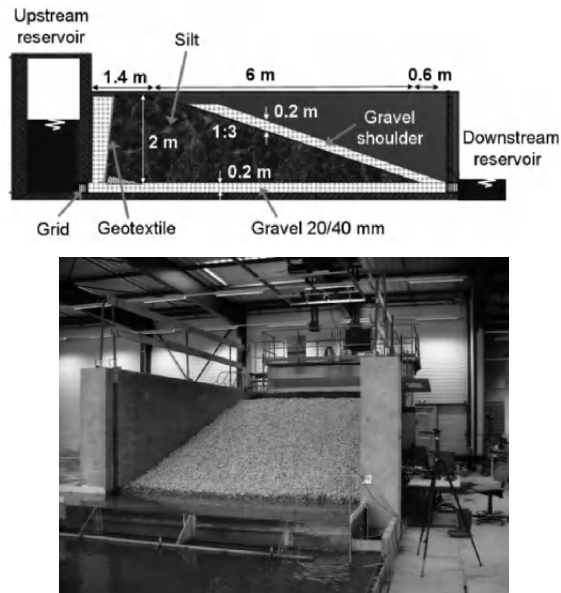


Figure 2.22. *Diagram and photograph of the experimental rig with slope geometry*

The gravel making up the base layer was well calibrated, 12/20 and 20/40 mm, with a narrow grain size distribution ($C_u < 2$). The fine soil was a sandy-silt dredged from the Rhône at Bourg-Lès-Valence (France), with a median diameter $d_{50} = 0.14$ mm, wide grain size distribution ($C_u \sim 85$) and only slightly cohesive¹¹. It was laid in successive layers 20 cm thick, compacted until an average dry density of 1.52 g/cm^3 (i.e. 92% density at Optimum Proctor Normal). Here, the geometric initiation criterion of CE (see section 2.3.1) was to a great extent verified ($D_{15}/d_{85} \gg 10$). These tests were therefore carried out under conditions highly favorable for the development of CE.

¹¹ The fraction lower than $2 \mu\text{m}$ was only 0.5% and the result of the methylene blue test was 0.4.

The water level was regulated during the test via a reservoir located in contact with the wall upstream of the test rig. It was connected to the sample layer of gravel via a grid in the lower part. A constant hydraulic load was applied as the limit condition upstream. On the downstream side, the layer of gravel communicated with a settling tank equipped with a large spillway and the level of the water downstream varied by only a few centimeters during the test. This difference of load led to a flow in the experimental rig, mainly in the highly pervious lower gravel layer. The test then consisted of increasing the level of water in the upstream reservoir by successive stages. The measurements performed first permitted identifying the CE at the interface and then quantifying its intensity and impacts on the structure.

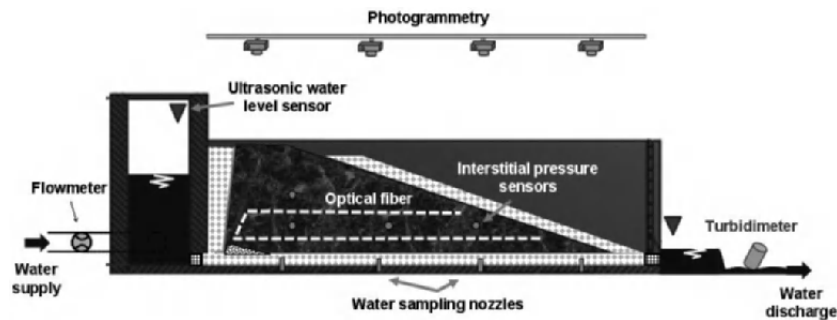


Figure 2.23. *Instrumentation in the experimental rig (slope geometry)*

As shown in Figure 2.23, the rig was fully instrumented to characterize the following points with the associated measurements: (1) the flow inside the structure by measuring the flow rate through the rig and the water heights in the reservoirs up and downstream; (2) the interstitial pressure with pressure sensors at 12 points in the layer of gravel and at six points in the silt; (3) the

quantity of soil transported by the flow by measuring the turbidity of the discharge for the suspended soil part and by the regular collection of coarse particles deposited as sediment in the downstream tank; (4) the change of the surface topography was evaluated by a photogrammetric system to identify possible settlements and sinkholes; (5) the deformations of the layer of silt measured by an optical fiber installed in the center of the rig to provide a distributed estimation of soil deformation and lastly (6) physical parameters liable to be influenced by erosion such as the temperature along the optical fiber and the electric potential at the surface.

2.5.3. Test protocol and the results obtained

2.5.3.1. Protocol

The test started by filling the model with water. Carbonic gas was first injected into the gravel layer to evacuate the air after which the water level was gradually increased until submerging the gravel layer as well as about 10 cm of silt. The excellent solubility of carbonic gas in water limited trapping of air bubbles at the interface between the gravel and silt, which could risk interfering with the CE process. Since saturating the entire silt layer was complicated to achieve, the protocol chosen consisted of maintaining the water level without flow for about 60 hours. The water level in the upstream reservoir was then increased, generally every 24 hours, until severe damage occurred in the structure.

2.5.3.2. Typical results with the layer geometry

The main measurements performed during test number 1 on the layer geometry are shown in Figure 2.24.

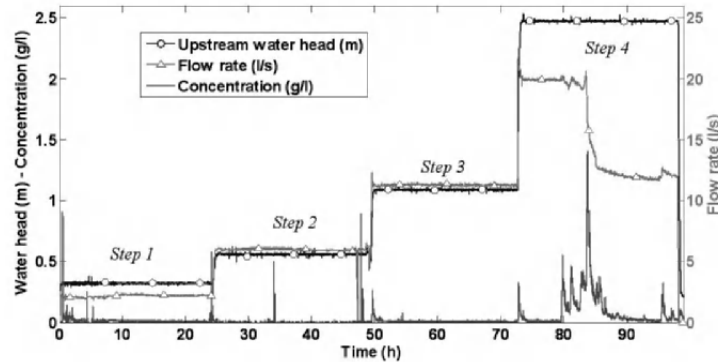


Figure 2.24. Temporal evolutions of layer geometry of the water level in the upstream reservoir, discharge and concentration of suspended matter in the effluent (estimated as a function of turbidity)

It shows an increase in successive stages of water height corresponding to the protocol. At the beginning of the test, the flow rate crossing through the experimental rig remained constant during each stage of water height. This indicated that the permeability of the sample remained constant and that the flow regime was stationary. The turbidity of the effluent, directly linked to the quantity of suspended matter, increased suddenly after each change of water height and then decreased exponentially, thereby forming erosion peaks that had already been observed at the sample scale (see section 2.3). During the three first stages, turbidity fell to a value lower than the measurement noise. In addition, the quantity of soil collected in the settling tank decreased similarly. At the 80th hour, a change of behavior was observed characterized by a considerable increase in turbidity not correlated with a change of water height. Following this increase, fluctuations of the discharge flowing through the sample were measured, and then there was a sharp drop, indicating a reduction of global permeability. A few hours later, the flow rate fell by half for almost the same water height while turbidity remained very low. Then a sinkhole appeared on the surface in contact with the upstream wall of

the rig (Figure 2.25(a)) accompanied by a settled zone several centimeters downstream (Figure 2.25(b)).

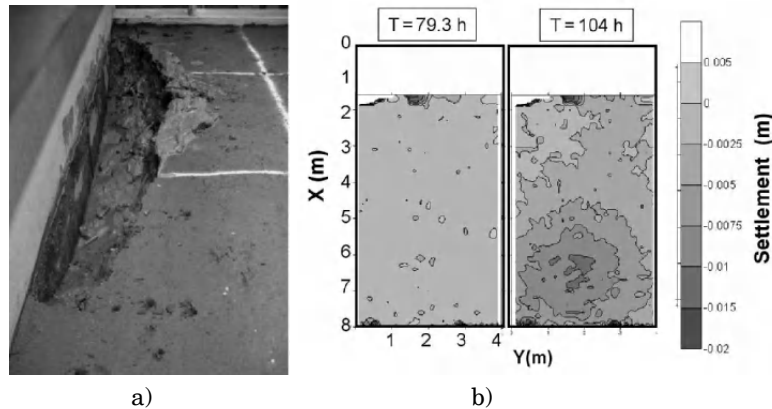


Figure 2.25. a) Sinkhole occurring at the surface of the model in contact with the upstream wall. b) Evolution of settlements measured at the surface of the model

It therefore appeared that considerable erosion was suddenly initiated at the fourth stage with the transport of a large quantity of material. The trigger of the erosion initiation is yet not fully understood. This caused a reduction of the model's permeability, bringing erosion to a halt, and also to settlements in the structure, logically explained by the removal of material. The localization of the sinkhole in contact with the upstream wall led to the assumption of a boundary effect. However, the upstream limit conditions had been modified for tests numbers 2 and 3 and similar results were obtained. It was therefore concluded that *a priori* these results were not very sensitive to limit conditions.

2.5.3.3. Typical results in the slope geometry

Tests 4 – 9 were performed with the slope geometry. The measurements obtained during test number 4 are shown in Figure 2.26. It can be seen that the start of the test is similar to test number 1. During each stage, the water level in the

reservoir was maintained constant and the discharge traveling through the model remained stable. Brief peaks of turbidity were measured at each change of stage, but turbidity fell rapidly to a very low value. A strong increase in turbidity was measured at the 195th hour, followed by fluctuations of the discharge. Then, contrary to layer geometry tests for which a reduction of permeability leading to stabilization was noted, in this case we observed that discharge increased, indicating an augmentation of the model's global permeability. The maximum supply discharge was reached after about 30 – 40 minutes. The water level in the upstream reservoir could no longer be maintained and started to fall, signaling the end of the test at constant load.

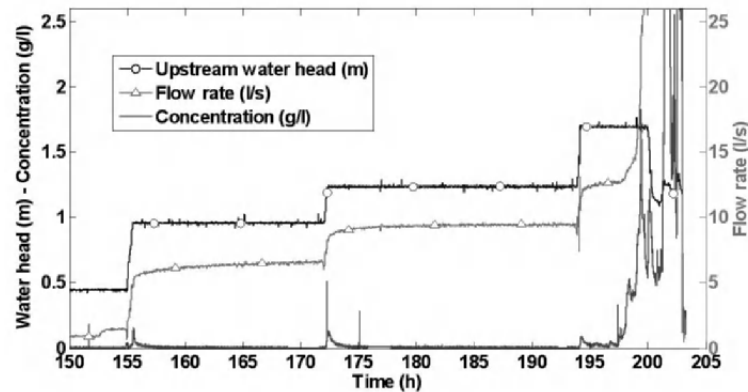


Figure 2.26. *Temporal evolution in the slope geometry of the water level in the upstream reservoir, the discharge and concentration in suspended matter of the effluent (estimated as a function of turbidity)*

Similar behavior was observed for test numbers 4, 6, 8 and 9. No channel was formed during test number 5. Nonetheless, regressive erosion at the tip of the silt layer was observed. Test number 7 was performed with a different type of silt, from Ampuis (France), much more cohesive than the silt of Bourg-Lès-Valence (noted BLV in Table 2.1), and very little of this soil was eroded. Reinforcement methods

(geotextile, thick granular shell) were tested in test numbers 8 and 9, but they were unable to prevent the occurrence of piping erosion leading to breaching. New tests are scheduled to deal with this specific point. The results obtained from all the tests are summarized in Table 2.1.

Test	Geometry	Shoulder	Gravel (mm)	Silt	Observation	Date	Duration (h)
1	Layer	No shoulder	12/20	BLV	Sinkhole upstream	07/2010	99
2	Layer	No shoulder	12/20	BLV	Sinkhole upstream	09/2010	166
3	Layer	No shoulder	20/40	BLV	Erosion upstream	10/2010	175
4	Slope	20 cm thick with 20/40 mm	20/40	BLV	Erosion in a pipe	11/2010	200
5	Slope	20 cm thick with 20/40 mm	20/40	BLV	Backward erosion	01/2011	200
6	Slope	20 cm with 20/40 mm	20/40	BLV	Erosion in a pipe	02/2011	35
7	Slope	20 cm thick with 20/40 mm	20/40	Ampuis	No erosion	03/2011	336
8	Slope	20 cm thick + geotextile	20/40	BLV	Erosion in a pipe	04/2011	114
9	Slope	50 cm thick including 30 cm thick with 2/6 mm	20/40	BLV	Erosion in a pipe	06/2011	~120

Table 2.1. *Summary of tests*

As discharge and turbidity increased, seepage could be seen in the downstream shoulder and quickly intensified.

The flow progressively carried away the gravel of the downstream shoulder. After a period of time lasting from several minutes to about 40 minutes, a real channel emerged in the open air, through which a very substantial discharge was transported as shown in Figure 2.27.



Figure 2.27. *Final stage of development of the pipe by perforation of the gravel shoulder*

2.5.4. Proposed interpretation and description of the erosion process

2.5.4.1. Phase 1: initiation

These results were interpreted by considering the different phases of developing the CE process. The first phase corresponded to the start of the test, during which only peaks of turbidity were observed when changing stage. The discharge remained very constant for an imposed load upstream, indicating stable permeability. Small quantities of soil were collected downstream and they decreased with time for each stage. This phase undoubtedly corresponded to the selective entrainment of the most easily erodible particles as they were small, loosely bound to their neighboring particles and located in zones where the flow was most intense. However, sufficiently resistant particles or those less exposed to the flow were not entrained and became progressively predominant at the interface, leading to the reduction of the erosion observed with time. This phase was also noted at the sample scale and corresponded to the

erosion conditions for which the statistical model of section 2.4.2.3 was developed.

2.5.4.2. *Phase 2: transition*

A second transition phase was then identified when the quantity of particles eroded started to increase considerably. This resulted in the collection of large quantities of soil, the appearance of punctual settlement zones within the silt and sometimes by regressive erosion at the foot of the dike. The intensity of the erosion nonetheless decreased constantly with time. Depending on the test, the limits of this phase were more or less marked and therefore identifiable.

2.5.4.3. *Phase 3: progression*

A third phase started afterwards when measuring an increase in turbidity with time, linked to an increase in discharge. This increase is brief and transient for the layer geometry but it is exponential for the slope geometry. It is probable that this phase is associated with the appearance of a cavity in the layer of silt in contact with the layer of gravel. It is not fully understood how this cavity was formed. *A priori*, it is linked to the entrainment of particles of fine soil at the interface leading to an empty space. It was eventually filled in by collapsing soil. These collapses caused zones of weakened silt that were the potential areas of initiation of piping hollowed by erosion. Once the initial cavity had been formed, the flow concentrated in this space of low hydraulic resistance, leading to increased flow velocity and favoring erosion. Therefore, the size of the cavity increased with time, in turn leading to a higher discharge. This process was unstable as long as the cavity did not collapse and piping progressively penetrated above the interface by spreading upstream and downstream, as illustrated schematically in Figure 2.28. A large quantity of soil was eroded in the cavity and transported first in the channel and then through the layer of gravel to the point where the coarsest fraction of soil could be trapped.

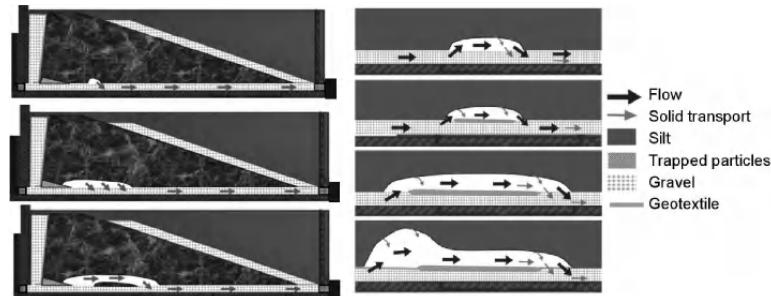


Figure 2.28. *Illustration of the channel progression phase*

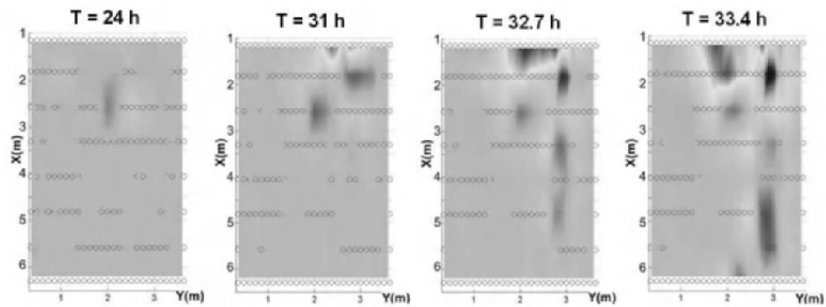


Figure 2.29. *Top view of the deformation measurements of the optical fiber located on a plane 20 cm above the erosion interface, during test number 6. The values displayed are interpolated between the measurement points (circles) in order to obtain a 2D field*

This scenario still remains a hypothesis though it is consistent with the observations made beforehand at the sample scale and with the different measurements performed. On the one hand, the increase in the total discharge and turbidity logically signals the development of piping. On the other hand, the deformation measurements made with an optical fiber indicate the occurrence of movements in the silt, more upstream initially, which then propagated downstream, until a deformed zone was formed that crossed the entire structure, as can be seen in Figure 2.29. Lastly, when dismantling the experimental structures,

the position of the erosion channel was identified as being in perfect agreement with the measurements made of the deformation by the optical fiber, while the coarse particles of silt were found at the surface of the gravel layer.

2.5.4.4. Phase 4: interaction with the geometry

The fourth phase corresponds to the interaction of this channel with the limits of the model. Thus, it is intrinsically linked to the latter's geometry.

In the layer geometry, the flow left the model in the lower part through a grid aligned with the layer of gravel while the silt was maintained in the upper part by a removable metal wall. The channel impacted against this wall whereas the layer of gravel was progressively clogged by particles that were eroded and then trapped. The flow velocities fell and the erosion stopped. Stability was reached progressively as the draining layer became less permeable. This scenario is schematized in Figure 2.30. However, this phenomenon led to an increase in pressures downstream potentially dangerous for the mechanical stability of the real structure.

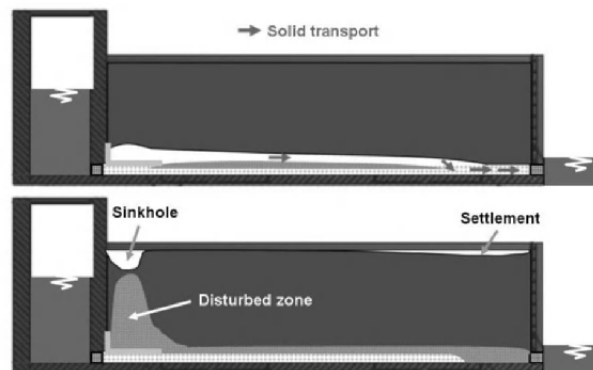


Figure 2.30. Illustration of the interaction phase between the channel and the limit conditions of the model in the case of the layer geometry

Regarding the slope geometry, the concrete structure was open downstream and the silt core, in the form of a slope, was covered by a gravel shoulder 20 cm thick (see Figure 2.22). In the geometry, the channel progressed above the interface and ended by reaching the shell. The flow loaded with particles progressively clogged the surface of the gravel base layer, then the covering shell (see Figure 2.31).

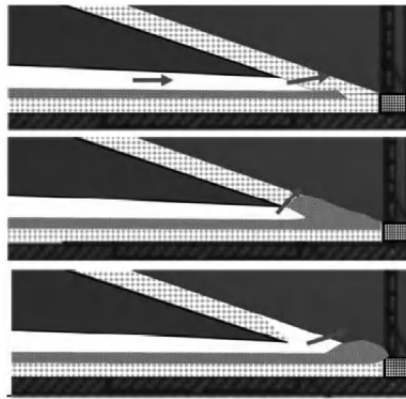


Figure 2.31. *Illustration of the interaction phase between the channel and the limit conditions of the model in the case of the slope geometry*

This led to an increase in interstitial pressures, driven by the channel with very high permeability. Pressure drops were localized upstream, where the flow was forced to pass through the gravel layer, and downstream, within the gravel shoulder. Vertical flows therefore appeared in the gravel progressively and drew along gravel by washing out, that is by localized fluidization, until the channel forced its way into the open air. This perforation of the shoulder quickly led to the breaching of the structure.

2.5.5. Scale effect

The phenomena described here in the layer geometry were very similar to those observed at the scale of the

sample. Initial transient erosion occurred with peaks of turbidity at each change of stage, then the initiation of channels spread downstream until the gravel layer was clogged.

On the qualitative level, the spatial scale did not appear to affect the process. From the quantitative viewpoint, hydraulic stress leading to considerable damage, corresponding to the initiation of phase 3, was identified for each test. This was represented in terms of the average velocity of the flow in the gravel layer (i.e. Darcy velocity); the parameter identified previously as the most pertinent for taking into account the CE initiation threshold (see section 2.3). As can be seen in Figure 2.32, the values of the critical velocities at the scale of the structure were relatively dispersed between 2 and 4 cm/s, but were of the same order of magnitude as those identified at the scale of the sample (2.6–5.5 cm/s). It can be concluded therefore that although the influence of spatial scale exists at this critical velocity, it remains negligible given the variability of the results between the successive tests performed under the same conditions.

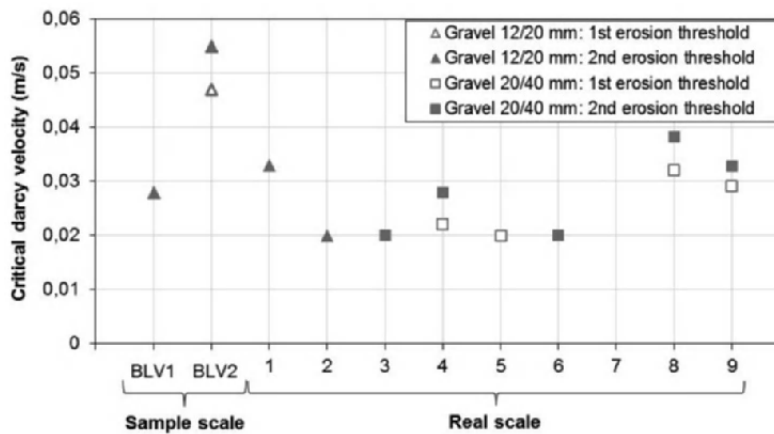


Figure 2.32. Average flow velocities in the gravel layer initiating substantial damage in the structure

This result is not really surprising. Indeed, the initiation of erosion is linked to the rupture of the balance of the fine grains of soil subjected to hydraulic stress at the interface of the layer of fine material. However, this balance appears to be independent of the spatial scale of the sample. It should be noted that this is not the case when the number of pores in contact with the interface is too small to reproduce the entire spatial variability of the flow. Thus, by way of comparison between the three scales explored here, the order of magnitude of the number of grains of the coarse layer in direct contact with the layer of fine soil is, respectively, 100 for the local scale (see section 2.4), 1,000 for the macroscopic scale (see section 2.3) and 10,000 for the almost full-scale test studied here. Furthermore, since erosion is a threshold phenomenon, it starts first at the interface at a small number of sites where the stresses are highest. The experiments carried out at the small scale, which made it possible to visualize the erosion and then transport process directly, allowed estimating that there were typically only about two to three active sites at the start of erosion, that is about 2.5% of pores in immediate contact. By assuming that the proportion was similar at other scales, we obtained a number of erosion sites: 25 at the macroscopic scale and 250 at the large scale, respectively. The number of places at which local erosion was initiated when the global CE process starts appears sufficient to ensure that the two largest numbers are reasonably representative from the statistical standpoint.

On the other hand, in addition to the initiation threshold of the phenomenon, the study performed at the structure scale led to the contribution of new elements for better understanding the progression of CE, especially by identifying its consequences on a dike structure. Certain consequences were expected, such as settlement and sinkhole at the surface, and clogging, leading to an increase in interstitial pressures. Other consequences were far more

surprising with, above all, the triggering of concentrated leak erosion leading to the rapid failure of the model dam. Indeed, engineering studies have often considered that CE only leads to phenomena with slow dynamics that develop over several years. Therefore, this point requires much effort in order to improve the control and safety of earth structures.

2.5.6. Summary

These large-scale tests showed that the impact of spatial scale was low and even zero with respect to the hydraulic initiation threshold of CE. Nonetheless, it was shown that the limit conditions influenced the progression of the erosion process once started. Furthermore, it was also seen that the time during which the stress is applied plays an important role. For example, the initiation of phase 3 leading to severe damage was observed 33 hours after the changing stage for test number 3. Already mentioned at the sample scale (see section 2.3), this aging effect under hydraulic loading requires further detailed study. In particular, the laboratory erosion test results obtained in several hours must be extrapolated very carefully when the aim is to interpret the behavior of structures several decades old. At present, no research work appears to have provided a satisfactory response to this question.

2.6. Conclusion and outlook

Taking current knowledge into account, it is possible to draw up a summary in two parts. First, regarding the description and understanding of CE processes, for which major advances have been made that provide a fairly complete image of the mechanisms involved and their kinetics, along with promising orientations for modeling. Second, the integration of these results at the operational

level still remains a distant goal of requirements specific to ensuring the safety of hydraulic works, especially regarding the representativeness of tests performed over short periods in order to assess the long-term behavior of a structure.

2.6.1. Description of CE mechanisms

Many works have been performed on the different elementary physical processes involved in the global phenomenon known as CE, and they have clearly emphasized that these processes are in every way similar to those of river erosion (surface erosion, bedload, suspension, grain size sorting, cohesion, etc.). However, CE also includes characteristics specific to the porous geometry of the zone in which the flow circulates. Most of the results of experiments performed at the sample scale in a direct configuration appear to converge toward the identification of a CE initiation criterion expressed by a Darcy velocity whose critical value ranges from 1 to 10 cm/s, whatever the type of soil and configuration used. These values are significantly higher than those deduced directly from the Shields diagram. These two approaches can nonetheless be reconciled following precise analysis of the local hydrodynamics of the CE in the contact zone between the two layers of soil. A transition zone stands out in the immediate vicinity of the interface and explains that the average shear stress exerted at the surface of the fine soil is lower, with a ratio in the region of two for the experiments performed, than the average shear stress in the porous layer. The Darcy velocity generated throughout the coarse soil must therefore be increased in proportion to reach the erosion threshold. Finally, the Shields diagram, modified accordingly, is perfectly consistent with the values obtained for fine granular soils and the addition of a corrective term permits extending the validity of the model to the case of cohesive soils. We have nonetheless already mentioned the need for a far more thorough campaign of

experiments to fully validate the results obtained from local measurements and notably the order of magnitude and sensitivity of the empirical parameters derived from them.

Local analysis also reveals high spatial variability of the flow induced by this geometry composed of pores and constrictions. This results in an apparent contradiction since taking into account this spatial variability in a local erosion threshold, the law predicts the effective disappearance of the threshold at a larger scale, which is untrue in practice. However, to improve realism, the statistical model proposed has to be enhanced by grain size sorting and selective erosion at the surface of the fine soil, which progressively reinforces the mechanical resistance of the interface and explains the relaxation of the erosion rate through time observed experimentally. According to the intensity of the flow, this relaxation is either total, with erosion finally ceasing, or partial, with an asymptotic tendency to permanent erosion. Thus, it seems that a threshold exists between transient erosion, which can be likened to initial surface washing, and persistent erosion. The definition of this threshold remains, however, closely linked to the experimental protocol chosen. The model is still limited to the short term, since it is based on a fixed geometry in the contact zone. However, other phenomena occur over longer periods (the geometry close to the interface is modified progressively, filtration and clogging of eroded particles by the coarse grains, chemical and biological effects modify the erosion resistance properties of the fine soil, etc.). These effects remain to be integrated in a more complete modeling.

Lastly, more attention should be given to the inverse configuration; first, because it is the most widespread case of erosion in real structures and second, because it is by far the most dangerous situation in terms of CE. This configuration in which the fine soil overlies the layer of coarse material has only recently been subject to study, most likely due to

greater difficulty in performing experiments. Although it is reasonable to assume that changing the configuration has little effect on local hydrodynamic characteristics as long as no significant change occurs in the geometry of the contact zone, this is not so in the case of sufficiently high cumulative erosion, or, in other words, from the moment when we leave the domain of weak and short-term erosion. Large-scale tests have partially satisfied the need to fill gaps in knowledge on CE in this specific geometry. These works have above all demonstrated the feasibility of performing such a test at full scale and the capacity of interpreting the results obtained by combining numerous indirect measurements, making it possible to cross-check data. This campaign of experiments led to the identification of two scenarios as a function of the geometry of the structure. The first scenario suggests long-term stabilization for a layered geometry whereas the second scenario, in slope geometry, highlights a high risk of failure by pipe flow erosion reaching the downstream gravel shoulder.

2.6.2. Impact on the safety of hydraulic structures

2.6.2.1. Responses that are emerging

What are the lessons that can be drawn from these results for real hydraulic structures with a view to managing risk? First, it is obvious that we are beginning to obtain tangible responses for a large number of questions.

First, as was seen, erosion is not quantifiable, *a priori*, experimentally except for a Darcy velocity exceeding a critical value in the region of 1–10 cm/s, whatever the situation considered. These are very high velocities in comparison to real conditions in the field and a fast CE phenomenon, that is short term, therefore appears highly improbable in a dike without any specific pathology.

For the direct configuration, the stabilizing effect of paving via grain size sorting and selective erosion was highlighted. In addition, the geometry of the contact zone changed relatively little in this configuration since the cavities scoured out by erosion are progressively filled by the successive localized collapses of coarse material. The possible impacts to the structure are therefore limited to settlements and sinkholes which, although harmful for the structure, do not represent a primordial danger.

On the contrary, in the inverse configuration, the consequences can prove dramatic according to the case. Indeed, erosion creates a cavity that can persist if mechanically stable and extend progressively downstream. Then, as observed in the layer geometry, the geometric filtration of the eroded particles can lead to isolating the pipe and stopping the erosion. The consequences of the process are therefore limited in this case also to settlements and sinkholes. On the other hand, with a slope geometry more similar to that of a real structure, filtration is not efficient enough to isolate the pipe that finally leaves the structure through the gravel shoulder. At this point, it will become well formed and channel an intense flow. Classical refilling with granular material fails to stop the development of the channel that rapidly breaches the dike. At best, the initiation and progression of the erosion pipe can be detected about 10 hours before failure by deformation measurements made by installing an optical fiber inside the structure. Other measurements are far less capable of anticipating failure. This considerably reduces the time necessary for intervention, so predicting this type of problem is crucial. One possible answer could consist of systematically identifying the interfaces potentially vulnerable to CE, evaluating the flow velocities circulating in them and comparing them to threshold values. It also comprises selecting dangerous zones in order to install instruments in them for long-term monitoring and, lastly considering, if

necessary, appropriate intervention consisting of reinforcing the downstream shoulder.

It should be noted that, in comparison to previous works performed at the scale of the sample, the results obtained at full scale in this inverse configuration and for the same layer geometry do not display significant scale effects and thus strengthen the possibility of extrapolating knowledge obtained from physical models to real structures.

2.6.2.2. *Open questions*

For all that, history is far from reaching an end and several questions remain, pointing to many paths of research for years to come. Thus, we choose to put forward two principal issues.

The first issue concerns the initiation threshold of CE for which experimental observations were seen to agree in choosing the Darcy velocity as a criterion. Nonetheless, almost all these works dealt with tests performed in direct configuration and it is uncertain whether they remain true for the inverse configuration in which, on the contrary, erosion appears to depend on both the grain size of the coarse soil and on the additional load applied [SCH 07]. This is a crucial issue, especially for structures subjected to a permanent hydraulic load imposed within which the infiltration water flow is controlled by the permeability and can vary significantly for the same imposed pressure.

The second and much more general question concerns the long-term behavior of the structure. Indeed, all the works focused on the case of short-term CE. Even those relating to large-scale tests were performed in an extremely unfavorable situation for the safety of the structure: very high grain size ratio, high velocities in the coarse layer. These conditions do not represent those that actually exist inside a dike. Does this then allow considering that we can exclude any risk of

CE occurring? Doing so would mean extrapolating over a very long timescale the results obtained from short-term tests, that is a maximum duration of several days. Such extrapolation is very delicate since effects that do not exist or that cannot be detected in the short term, may play a major role if the period of exposure is increased by several orders of magnitude. As has already been mentioned, some of these slow kinetic phenomena (grain size sorting and selective erosion, evolution of contact zone geometry and thus local flow, filtration and clogging by coarse soil, etc.) are or could be integrated in statistical models more or less easily. The foundations for such models have been described in this chapter. But other phenomena, such as chemical and biological aging, are still poorly understood and difficult to model. It is nonetheless possible that, under conditions in which no visible or quantifiable erosion occurs in the short term, even minimal erosion could lead to progressive changes of geometry in the contact zone in the very long term, by accumulation and with kinetics that change as a function of season as well as hydrological and meteorological conditions. The changes of the hydraulic loading that can be common and sometimes cyclic for embankments may also play an important role. These phenomena would inevitably converge to provoke a situation propitious to the initiation of an unstable CE process. Given this uncertainty, it is not possible at present to say whether a real risk exists for a dike that does not present notable structural faults.

To conclude, we saw that significant research efforts are still required, especially to improve knowledge of long-term mechanisms linked to erosion, sediment transport and material aging and the scenarios involving them. In view of the need to improve the safety management of structures, these works should give priority to the inverse configuration, the only one that, *a priori*, presents a serious risk. This should be done at the sample scale since no effect of scale could be identified. Also, cohesive soils should be used with

particle diameters not too far from the most unfavorable sizes, that is between 50 and 100 μm , where the critical velocity of short-term CE initiation is minimal. Ideally, tests linking an erosion threshold to an exposure period should be carried out as they could prove to be extremely useful.

2.7. Bibliography

- [ARI 78] ARIATHURAI R., ARULANANDAN K., “Erosion rates of cohesive soils”, *Journal of the Hydraulics Division, ASCE*, vol. 104, no. 2, pp. 279–283, 1978.
- [BEA 72] BEAR J., *Dynamics of Fluids in Porous Media*, American Elsevier, New York, NY, 1972.
- [BÉG 11] BÉGUIN R., Etude multi-échelle de l'érosion de contact au sein des ouvrages hydrauliques en terre, PhD thesis, University of Grenoble, 2011.
- [BÉG 13] BÉGUIN R., PHILIPPE P., FAURE Y.-H., “Pore-scale flow measurements at the interface between a sandy layer and a model porous medium: application to statistical modelling of contact erosion”, *Journal of Hydraulic Engineering*, vol. 133, no. 1, pp. 1–11, 2013.
- [BEN 68] BEN AÏM R., LE GOFF P., “Effet de paroi dans les empilements désordonnés de sphères et application à la porosité des mélanges binaires”, *Powder Technology*, vol. 1, no. 5, pp. 281–290, 1968.
- [BEZ 87] BEZUIJEN A., KLEIN-BRETELLER M., BAKKER K.J., “Design criteria for placed block revetments and granular filters”, *Coastal & port Engineering*, China Ocean Press, Beijing, pp. 1852–1866, 1987.
- [BON 08] BONELLI S., BRIVOIS O., “The scaling law in the hole erosion test with a constant pressure drop”, *International Journal for Numerical and Analytical Methods in Geomechanics*, vol. 32, pp. 1573–1595, 2008.
- [BRA 85] BRAUNS J., “Erosionsverhalten geschichteten Bodens bei horizontaler Durchströmung”, *Wasserwirtschaft*, vol. 75, pp. 448–453, 1985.

- [BRI 01] BRIAUD J.-L., TING F.C.K., CHEN H.C., *et al.*, “Erosion function apparatus for scour rate predictions”, *Journal of Geotechnical and Geoenvironmental Engineering*, vol. 127, no. 2, pp. 105–113, 2001.
- [BUF 97] BUFFINGTON J.M., MONTGOMERY D.R., “A systematic analysis of eight decades of incipient motion studies, with special reference to gravel-bedded rivers”, *Water Resources Research*, vol. 33, no. 8, pp. 1993–2029, 1997.
- [CAO 06] CAO Z., “Explicit formulation of the Shields diagram for incipient motion of sediment”, *Journal of Hydraulic Engineering*, vol. 132, no. 10, pp. 1096–1099, 2006.
- [CEN 96] CENEDESE A., VIOTTI P., “Lagrangian analysis of nonreactive pollutant dispersion in porous media by means of the particle image velocimetry technique”, *Water Resources Research*, vol. 32, no. 8, pp. 2329–2343, 1996.
- [CHE 03] CHENG N.-S., LAW, A. W.-K., LIM, S. Y., “Probability distribution of bed particle instability”, *Advances in Water Resources*, vol. 26, no. 4, pp. 427–433, 2003.
- [CHE 06] CHENG N.-S., “Influence of shear stress fluctuations on bed particle mobility”, *Physics of Fluids*, vol. 18, no. 9, 096602, 2006.
- [CLA 06] CLAUDIN P., ANDREOTTI B., “A scaling law for eolian dunes on Mars, Venus, Earth, and for subaqueous ripples”, *Earth and Planetary Science Letters*, vol. 252, pp. 30–44, 2006.
- [DEG 83] DE GRAAUW A., VAN DER MEULEN T., VAN DER DOES DE BYE M., *Design Criteria for Granular Filters*, publication no. 287, Delft Hydraulics Laboratory, Emmerloord, 1983.
- [DEN 94] DEN ADEL H., KOENDERS M.A., BAKKER K.J., “The analysis of relaxed criteria for erosion-control filters”, *Canadian Geotechnical Journal*, vol. 31, no. 6, pp. 829–840, 1994.
- [DIJ 12] DIJKSMAN J., RIETZ F., LORINCZ K.A., *et al.*, “Invited article: refractive index matched scanning of dense granular materials”, *Review of Scientific Instruments*, vol. 83, 011301, 2012.

- [FAN 87] FAND R.M., KIM B.Y.K., “Resistance to the flow of fluids through simple and complex porous-media whose matrices are composed of randomly packed spheres”, *Journal of Fluids Engineering – Transactions of the ASME*, vol. 109, no. 3, pp. 268–274, 1987.
- [GAR 02] GARNER S.J., SOBKOWICZ J.C., “Internal instability in gap-graded cores and filters”, *Congrès annuel de l’Association Canadienne des Barrages*, Victoria, BC, Canada, October 2002.
- [GIB 09] GIBSON S., ABRAHAM D., HEATH R., *et al.*, “Vertical gradational variability of fines deposited in a gravel framework”, *Sedimentology*, vol. 56, no. 3, pp. 661–676, 2009.
- [GRA 70] GRASS A.J., “Initial instability of fine bed sand”, *Journal of the Hydraulics Division, ASCE*, vol. 96, no. HY3, pp. 619–632, 1970.
- [GUI 10] GUIDOUX C., FAURE Y.-H., BÉGUIN R., *et al.*, “Contact erosion at the interface between granular filter and various base-soils with tangential flow”, *Journal of Geotechnical and Geoenvironmental Engineering*, vol. 136, no. 5, pp. 655–775, 2010.
- [HAN 01] HANSON G.J., COOK K.R., “Apparatus, test procedures, and analytical methods to measure soil erodibility in situ”, *Applied Engineering in Agriculture*, vol. 20, no. 4, pp. 455–462, 2001.
- [HLU 06] HLUSHKOU D., TALLAREK U., “Transition from creeping via viscous-inertial to turbulent flow in fixed beds”, *Journal of Chromatography A*, vol. 1126, pp. 70–85, 2006.
- [HOF 08] HOFFMANS G.J.C.M., DEN ADEL H., VERHEIJ H.J., “Horizontal granular filters”, *4th International Conference on Scour and Erosion ICSE-4*, Tokyo, Japan, November 2008, pp. 480–485.
- [HOF 06] HOFLAND B., BATTJES J.A., “Probability density function of instantaneous drag forces and shear stresses on a bed”, *Journal of Hydraulic Engineering*, vol. 132, no. 11, pp. 1169–1175, 2006.
- [IST 57] ISTOMINA V.S., *Soil Stability to Seepage*, Moscow, 1957.

- [KNA 07] KNAPEN A., POESEN J., GOVERS G., *et al.*, “Resistance of soils to concentrated flow erosion: a review”, *Earth-Science Reviews*, vol. 80, pp.75–109, 2007.
- [KOZ 53] KOZENY J., *Hydraulik: Ihre Grundlagen und praktische anwendung*, Springer-Verlag, Vienna, 1953.
- [LAV 87] LAVELLE J.W., MOFJELD H.O., “Do critical stresses for incipient motion and erosion really exist?”, *Journal of Hydraulic Engineering*, vol. 113, no. 3, pp. 370–385, 1987.
- [LEB 96] LEBON L., LEBLOND J., HULIN J.-P., *et al.*, “Pulsed field gradient NMR measurements of probability distribution of displacement under flow in sphere packings”, *Magnetic Resonance Imaging*, vol. 14, no. 7, pp. 989–991, 1996.
- [LIC 04] LICK W., JIN L., GAILANI J., “Initiation of movement of quartz particles”, *Journal of Hydraulic Engineering*, vol. 130, no. 8, pp. 755–761, 2004.
- [MAG 03] MAGNICO P., “Hydrodynamic and transport properties of packed beds in small-to-sphere diameter ratio: pore scale simulation using an Eulerian and a Lagrangian approach”, *Chemical Engineering Science*, vol. 58, no. 22, pp. 5005–5024, 2003.
- [MAI 98] MAIER P.S., KROLL D.M., KUTSOVSKY Y.E., *et al.*, “Simulation of flow through beadpacks using lattice Boltzmann method”, *Physics of Fluids*, vol. 10, no. 1, pp. 60–74, 1998.
- [OBI 96] OBI S., INOUE K., FURUKAWA T., *et al.*, “Experimental study on the statistics of wall shear stress in turbulent channel flows”, *International Journal of Heat and Fluid Flow*, vol. 17, no. 3, pp. 187–192, 1996.
- [PAR 65] PARTHENIADES E., “Erosion and deposition of cohesive soils”, *Journal of the Hydraulics Division, ASCE*, vol. 91, pp. 105–139, 1965.
- [RAS 96] RASHIDI M., PEURRUNG L., TOMPSON A.F.B., *et al.*, “Experimental analysis of pore-scale flow and transport in porous media”, *Advances in Water Resources*, vol. 19, no. 3, pp. 163–180, 1996.

- [RED 00] REDDI L.N., LEE I.-M., BONALA M.V.S., “Comparison of internal and surface erosion using flow pump tests on a sand-kaolinite mixture”, *Geotechnical Testing Journal*, vol. 23, no. 1, pp. 116–122, 2000.
- [RIG 07] RIGHETTI M., LUCARELLI C., “May the Shields theory be extended to cohesive and adhesive benthic sediments?”, *Journal of Geophysical Research*, vol. 112, C05039, 2007.
- [SCH 01] SCHEUERMANN A., VARDOULAKIS I., PAPANASTASIOU, STAVROPOULOU M., “A sand erosion problem in axial flow conditions on the example of contact erosion due to horizontal groundwater flow”, in EHLERS W. (ed.), *IUTAM Symposium on Theoretical and Numerical Methods in Continuum Mechanics of Porous Materials, Solid Mechanics and its Applications*, vol. 87, pp. 169–175, 2001.
- [SCH 07] SCHMITZ S., Zur hydraulischen Kontakterosion bei bindigen Basiserdstoffen, PhD Thesis, Universität der Bundeswehr, Munich, Germany, 2007.
- [SHE 84] SHERARD J.L., DUNNIGAN L.P., TALBOT J.R., “Basic properties of sand and gravel filters”, *Journal of Geotechnical Engineering, ASCE*, vol. 110, no. 6, pp. 684–700, 1984.
- [SHI 36] SHIELDS A., Anwendung der Ähnlichkeitsmechanik und Turbulenzforschung auf die Geschiebebewegung, PhD Thesis, Versuchsanstalt für Wasserbau und Schiffbau, Berlin, Germany, 1936.
- [TER 08] TERNAT F., BOYER P., ANSELMET F., *et al.*, “Erosion threshold of saturated natural sediments: Modeling and experiments”, *Water Resources Research*, vol. 44, no. 11, W11434, 2008.
- [VAN 10] VAN PROOIJEN B.C., WINTERWERP J.C. “A stochastic formulation for erosion of cohesive sediments”, *Journal of Geophysical Research*, vol. 115, no. C1, C01005, 2010.
- [VAR 96] VARDOULAKIS I., STAVROPOULOU M., PAPANASTASIOU P., “Hydro-mechanical aspects of the sand production problem”, *Transport in Porous Media*, vol. 22, pp. 225–144, 1996.
- [WAN 04] WAN C. F., FELL R., “Laboratory tests on the rate of piping erosion of soils in embankment dams”, *Geotechnical Testing Journal*, vol. 27, no. 3, pp. 295–303, 2004.

- [WIE 11] WIEDERSEINER S., ANDREINI N., EPELY-CHAUVIN G., *et al.*, “Refractive-index and density matching in concentrated particle suspensions: a review”, *Experiments in Fluids*, vol. 50, pp. 1183–1206, 2011.
- [WIN 04] WINTERWERP J.C., VAN KESTERN W.G.M., *Introduction to the Physics of Cohesive Sediment in the Marine Environment*, Elsevier, 2004.
- [WÖR 92] WÖRMAN A., OLAFSDOTTIR, R. “Erosion in a granular medium interface”, *Journal of Hydraulic Research*, vol. 30, no. 5, pp. 639–655, 1992.
- [WÖR 96] WÖRMAN A., “Constitutive equation for filtration of well graded base soil with flow parallel to base/filter interface”, in LAFLEUR J. and ROLLIN A.L. (eds), *Proceedings of GeoFilters*, Bitech Publishers, Montréal, pp. 295–304, 1996.

Chapter 3

Backward Erosion Piping

3.1. Introduction

Backward erosion piping is an internal erosion mechanism by which hollow spaces are formed in or underneath water-retaining structures as a result of removal of soil by water flow. The hollow spaces, or pipes, are formed in the opposite direction of a water flow, while depositing eroded material at the downstream side of the structure.

This chapter is restricted to the type of backward erosion that takes place in the foundation of water-retaining structures, where a cohesive layer overlies a sandy aquifer. Seepage causes sand grains to be transported at the downstream side of the structure, causing the development of shallow pipes that grow in the upstream direction. The pipes develop at the interface of the aquifer and the cohesive layer as the latter forms a roof to the pipes. A pattern of pipes will grow in the upstream direction, and when they reach the upstream side, continued flow will cause the pipes

to widen and deepen to such an extent that the water-retaining structure becomes unstable.

The different phases leading to breakthrough as a result of backward erosion piping are displayed in Figure 3.1, from which it can be noted that the process of backward erosion is only one phase of the complete process leading to breakthrough of the water-retaining structure. Several conditions make a water-retaining structure sensitive to backward erosion piping. A sufficient hydraulic head is necessary as the driving force. However, even when such a hydraulic head is present, the process can only occur if a cohesive roof with low permeability is provided for the pipes. The cohesive roof is necessary to prevent the collapse of the pipe.

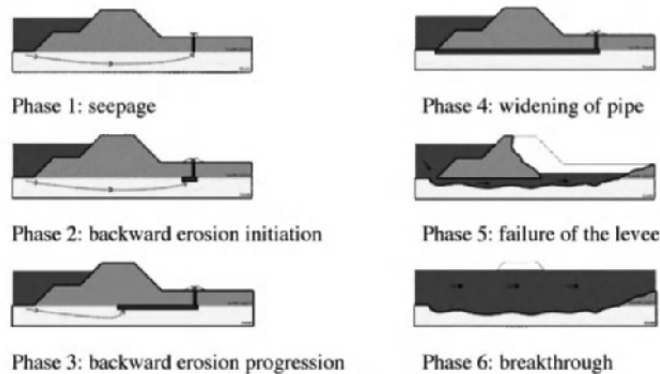


Figure 3.1. Phases leading to breakthrough of a levee due to backward erosion

Moreover, the process will mainly take place in uniform and cohesionless sands. When the aquifer contains both coarse-grained and fine material, such that the material is not internally stable, suffusion is more likely than backward erosion, possibly followed by backward erosion piping. An open and unfiltered exit is the last requirement in the process. In case of a cohesive top layer, this process can only

start after *hydraulic fracturing*, i.e. the cracking of the top layer as a result of high water pressure. Subsequently, *seepage erosion* takes place, i.e. the washing away of the particles. In the case of a vertical construction like a wall or skirt penetrating into the granular layer, first a *heave*, being the uplift of the granular layer, needs to occur.

Backward erosion piping is dominant in areas where the conditions described above are met. This is often the case for river levees, such as those found along the main rivers in the Netherlands, the Mississippi river in the United States and the Yangtze and Nenjiang rivers in China. In these river systems, backward erosion is known to have led to the occurrence of sand boils and levee failures during floods. Examples of sand boils behind a river embankment are illustrated in Figure 3.2. The typical geology near rivers is dominated by alluvial deposits, overlying the older strata. The shallow subsurface of river systems is, therefore, strongly heterogeneous in nature, with alternating deposits of clay, sand or silt, intersected by (old) river channels. The levees are usually built of local material, clay or peat. In the western part of the Netherlands, the alluvial Holocene deposits overlie a Pleistocene sandy layer up to a considerable depth. In coastal areas and the eastern part of the country, dikes are founded directly on sand layers. The situation of a cohesive top layer overlying a sandy aquifer or a cohesive clay levee directly located on a sandy aquifer is therefore common for river levees.



Figure 3.2. Sand boil behind a river embankment in a) the Netherlands and in b) France

Sand boils are often observed in these river systems. In the Netherlands, during the high waters of 1993 and 1995, the water in the rivers reached to a level of 0.50–1.50 m below the design level. During these floods, approximately 120 and 180 sand-transporting sand boils were observed along the rivers Rhine, Waal, IJssel and Maas, indicating the susceptibility of Dutch levees to this mechanism. Although failure of the levees did not occur during these floods, several failures in the past are attributed to backward erosion piping, such as the failures near Zalk, Nieuwkuijk and Tholen [VRI 10].

In China, during the 1998 flood, several dike breaches occurred along the Yangtze River and Nenjiang River, of which, at least three were caused by backward erosion piping [YAO 09]. Throughout history, levee failures caused by backward erosion piping accounted for 90% of the total number of failures [CAO 94].

In the United States, along the Mississippi river, the St. Louis District authorities documented excessive underseepage (seepage through the aquifer in the foundation of the levee) and the formation of sand boils during the floods of 1973, 1993 and 1995. Despite continued investigations, analyses and the addition of control measures since the 1950s, excessive underseepage and the formation of sand boils are still observed nowadays. It is found that the occurrence of sand boils increases with subsequent floods [GLY 04]. During the flood of 1993, the stage of the Mississippi river equaled or exceeded the design stage. During this flood, 5% of the total levee length was subjected to sand boils on average (districts Alton to Gale, [MAN 00]). One of the failures in the levee system of New Orleans as a result of Hurricane Katrina (2005) was most likely caused by backward erosion even though the water level had been high for only a couple of hours [VRI 10].

It appears that backward erosion piping can especially be a threat to the stability of levees. However, the mechanism can also occur in dams and other water-retaining structures, where similar conditions exist, although not much literature is available in which the occurrence of this type of erosion piping is described. It is therefore believed that this erosion mechanism is less dominant for dams than for levees.

Several researchers have investigated the mechanism experimentally to improve understanding and develop prediction models. In the early 1970s, a research program was started in the Netherlands to arrive at a sound risk assessment of the safety of embankments with sand boils. Two decades later, this research program resulted in the so-called design rule of Sellmeijer, which is commonly used in Dutch engineering practice and guidelines [TAW 99].

This chapter provides an overview of the main findings of experimental work in the understanding and prediction of the process of backward erosion. First, an overview of the different phases of backward erosion piping is given and then an explanation of how this phenomenon can lead to the instability of the water-retaining structure. A detailed description of the conditions that result in pipe development is given, based on experimental research, and a review of the design of experimental setups and test methods is included. A model analyzing the progression of backward erosion piping is explained and the practical difficulties in applying results to real levees and dams are discussed.

3.2. Phases leading to failure due to backward erosion

The process leading to failure due to backward erosion piping can be divided into several phases: seepage, backward erosion, widening and failure (Figure 3.1). Each of these phases is related to different mechanisms. These processes are explained in this section using a simple

two-dimensional (2D) geometry of a homogeneous sand layer overlain by a cohesive material. In practice, the geology will be more complex, with variation in soil properties in all directions. For understanding the basic principles of backward erosion, a simple configuration related to the typical geology in riverine or coastal areas will suffice.

3.2.1. Seepage

Seepage is the first phase in the process leading to failure, driven by a water level difference across the water-retaining structure. The water flow through the sand layer can be described by Darcy's law. The assumption of laminar flow in this equation is valid for the typical range of fluid velocities related to water flow through sandy aquifers underneath levees.

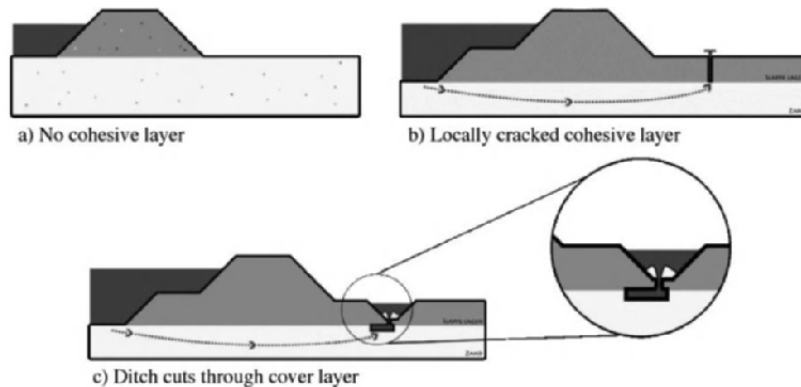


Figure 3.3. *Types of levees and open exits*

As noted in section 3.1 of this chapter, a downstream unfiltered open exit is required for the occurrence of seepage leading to backward erosion. In some cases, an open exit is present naturally, for example when no cover layer is present at the downstream side of the water-retaining structure (Figure 3.3(a)) or when a ditch cuts through a thin

cover layer (Figure 3.3(c)). In other cases, an exit point is created when the water pressure directly under the cover layer exceed the weight of the cover layer, such that the layer cracks locally (Figure 3.3(b)). In many areas, seepage is observed by the presence of wet areas downstream. Examples of such wet areas are shown in Figure 3.4.



Figure 3.4. Wet areas during the flood of 1993 in the polder district of Betuwe (www.beeldbank.rws.nl)

3.2.2. Backward erosion – initiation and progression

Once the requirements of seepage and an open exit are met, the flow velocities near the exit determine whether erosion can initiate. The initiation of backward erosion requires fluidization of sand near the exit point. Fluidization occurs when the pore pressures in the sand exceed the effective stresses such that the sand will expand and turn into a fluid state.

Clearly, the exit velocity is dependent on the type of exit. In a crack in a soft soil layer, (Figure 3.3(b)) the exit velocity is certainly higher than the exit velocities found downstream of a structure where no cohesive cover layer is present

(Figure 3.3(a)). However, for all exits shown in Figure 3, there is a concentration of flow lines near the exit point and, therefore, the local gradient near the exit point will be higher than the average gradient under the levee. Consequently, backward erosion piping can start at relatively low average gradients of typically 0.05 – 0.1 in the field. This concept also explains the relevance of the presence of a roof to the pipe. When the permeability of this roof is lower than the permeability of the sand (which is normally the case), there will be a concentration of flow lines near the exit point that leads to higher water flow velocities near the exit point and thus increases the probability of backward erosion piping.

Reaching velocities sufficient to cause fluidization does not always lead to transport of sand and pipe formation. Sand “boiling” without sand transport, which describes the state of sand when it looks like a boiling fluid (Figure 3.5(a)), is often observed in experiments and field situations. The continuous transition from a fluidized bed to a loose sand granular structure and vice versa that is observed here is caused by the increased permeability in the fluidized bed. The water is conveyed more easily through this area, causing a drop in water pressure in the sand. The pore pressures decrease and the sand returns to a loose granular state. It is noted that this transition from fluidized bed to loose granular structure is not always observed as it is also possible that the fluid flow is in equilibrium with the weight of the fluidized soil mass.

The equilibrium can be disturbed when the fluid flow is sufficient to carry soil particles outside the fluidized zone and deposit these particles in a ring outside the center of the sand boil. This ring of deposited sand is denoted as a sand volcano. In the center of the volcano, the sand still boils as a result of the subsequent change of fluidized and solid states. With each surge of fluidization, sand is deposited, and the

volcano grows in size. These volcanoes are often observed in the field during high water periods (Figure 3.6) and are also denoted as sand boils.

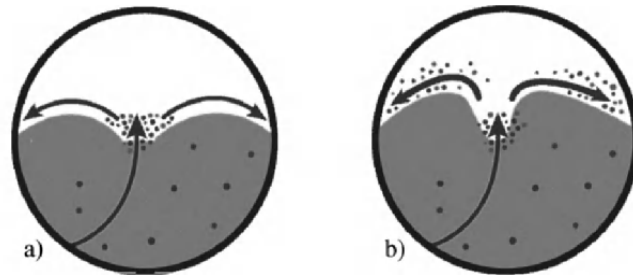


Figure 3.5. Sand boil a) without sand deposition and b) with continuous sand deposition



Figure 3.6. Sand boil during high water period of 2011 (Hurwenen, The Netherlands)

The sand that is deposited at the surface is being transported from the aquifer. In this aquifer, shallow (a few millimeters in height) pipes are formed in the sand at the interface of the cohesive and sand layers. The cohesive layer forms a roof to the pipe and allows the pipes to remain intact.

In the field, it is often observed that the sand deposition stops. This means that the development of the pipe can cease after some time. Apparently, there is a critical value for the head drop that needs to be exceeded before the pipe can progress in the upstream direction such that the pipe connects the upstream and downstream sides.

In the laboratory, the required critical head drop for progression is not always larger than the head drop required for initiation of pipe formation. This is due to the fact that the progression of the pipe is governed by a different mechanism than the initiation of backward erosion. Now, next to the flow through the aquifer, which is described by the laminar Darcy flow, the flow through the pipe and the erosion in the pipe are the elementary processes. The processes are schematized in Figure 3.7.

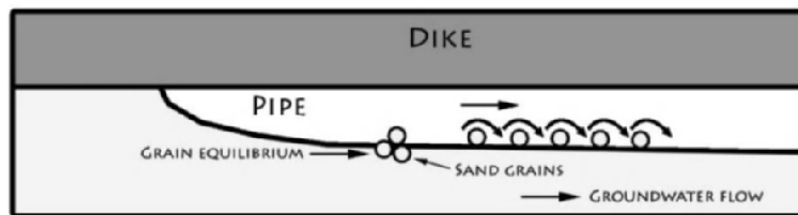


Figure 3.7. Schematization of processes governing the progression of the pipe

The flow through the shallow pipes is supplied by the aquifer. As a pattern of pipes is formed [SIL 91, VAN 11], for predicting the progression of the pipe, the pattern is simplified by an infinitely wide pipe [SEL 88]. When assuming smooth pipe walls, due to the limited depth of the pipes, the assumption of laminar flow is valid. In that case, the pipe flow can be described by Poiseuille equations for pipe flow or flow between parallel plates (infinitely wide pipe).

During pipe progression, different erosion processes may be observed [ZEE 11]. Following assumptions in backward erosion prediction models [SEL 88], the stability of grains on the bottom of the pipe is the most important erosion process. The critical shear stress exerted by the water on the grains on the bottom of the pipe will determine whether grains are likely to be transported. It is assumed that the pipe cannot progress when the grains are in equilibrium, whereas the pipe will increase in length when the critical shear stress is exceeded, causing deepening of the pipe.

The critical condition that determines incipience of motion of particles in the bed of a stream is defined by various researchers, both in the laminar and turbulent regimes. Most of these researchers follow the approach of Shields [SHI 36], who introduced a dimensionless number known as the Shields parameter (Θ), which is formulated as the ratio between the force applied by the flow over the surface of a sediment bed and the stabilizing force of gravity via the submerged weight of a grain. The critical shear stress according to Shields is $\tau = \Theta(\gamma_p - \gamma_w)d$ $\tau = \Theta(\gamma_p - \gamma_w)d$.

Around the same time, White suggested a different approach [WHI 40]. He used experiments to calibrate a theoretical equilibrium of forces. In this approach, the gravitational force is defined as $F_z = \pi(\gamma_p - \gamma_w)d^3/6$. The shear stress exerted by the water is divided over a number of grains. To this, White introduces the parameter η , which is defined as $\eta = Nd^2/A$, in which N is the number of particles per area A and reflects the part of the area that can take shear stresses. The drag force exerted to a single grain is then defined as $F_s = \pi d^2/\eta$. The drag force acts just above the center of the grain. To correct for this, a factor, α , is introduced. Other grains support the top grain along a line of action at a certain angle. This angle is called the angle of repose or bedding angle and is denoted by θ .

The grain is in equilibrium when the forces transverse to the angle of repose counterbalance (Figure 3.8). This is the case when the shear stress is:

$$\tau = \alpha\eta \frac{\pi}{6} (\gamma_p - \gamma_w) d \tan \theta \quad [3.1]$$

The value for the factor $\alpha\eta$ is determined using two experiments for laminar flow. Using the elementary processes of grain transport, pipe flow and laminar flow through the aquifer, the process of progression of the pipe is described.

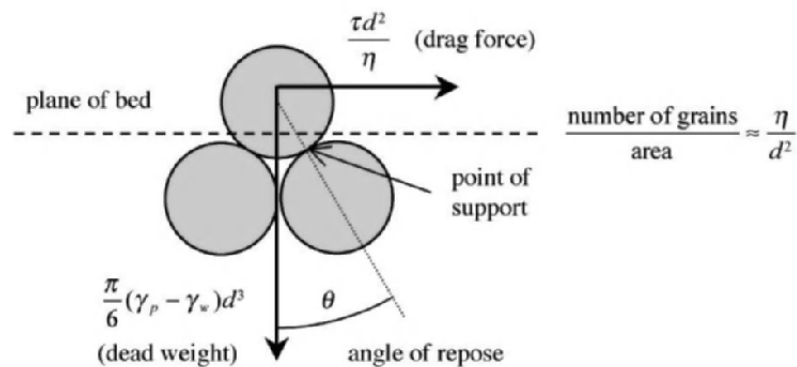


Figure 3.8. Forces on a grain according to White [WHI 40]

3.2.3. Widening

As soon as the pipe has progressed across the entire base of the water-retaining structure and connects the upstream and downstream sides, the flow in the pipe is increased enormously because the flow resistance of the sand disappears. The resulting flow surge causes a large quantity of sand to be eroded near the upstream inlet of the pipe. Although a pattern of pipes is generally formed, due to the limited thickness (few millimeters) and width (several

centimeters) of a single pipe, the transport capacity is limited, and the eroded material partly blocks the pipe further downstream. The sand in the blocked pipes is subsequently removed during a new process of backward erosion. In this way, the widened upstream pipe becomes progressively longer moving toward the downstream side of the levee (Figure 3.1, phase 4) [VAN 11].

When the pipe is widened from the upstream side to the downstream side, the sand transport and flow increase significantly. The widened pipe has a large flow capacity, causing further scouring of the pipe.

3.2.4. Failure

Failure of a levee due to backward erosion piping has been observed in full-scale experiments [VAN 11]. It has been found that once the widening process was completed, the increase of flow through the pipe results in further scouring of the pipe, both in the sand and in the clay, such that the levee deforms and cracks. The scour in the sand is driven by water flow in a similar way as during pipe formation, whereas the erosion of the cohesive base of the levee shows similarities to concentrated leak erosion.

Two scenarios have been observed in the experiments. The first scenario is that the levee fails within 20 minutes after the first burst of water and sand transport as a result of loss of stability of the levee body (sliding). In the second scenario, the levee deforms (settlement) in such a way that the widened pipes are closed. The connection between the upstream and downstream sides must then be re-established for sand transport and flow to increase again. Several phases of reconnection and deformation can take place before the levee finally fails due to loss of stability of the levee body (Figure 3.9).



Figure 3.9. Failed dike in full-scale experiments [VAN 11]

3.3. Backward erosion in the laboratory – overview and setup

The process of backward erosion piping has been studied extensively in the laboratory by various authors with a variety of laboratory setups. The goal of experimental work on backward erosion piping is mainly to investigate the erosion mechanism or to develop or validate safety assessment criteria for levees and dams. All experiments have a common fact that a sand sample is subjected to a horizontal hydraulic gradient. The exit is such that sand grains are free to be transported at the downstream side of the sand sample. A horizontal cover, consisting of a cohesive and impermeable material, is placed on top of the sand sample to confine the sand layer and support the pipes. The main differences in setup are the type of inlet, exit, scale, preparation method, cover type and measured parameters. In some experiments, a structure, such as a vertical cut off or weir, is placed to create a vertical seepage path. This structure strongly influences the process and critical head.

3.3.1. Overview of experimental research

Table 3.1 shows an overview of the experimental research that has been performed to study the phenomenon of backward erosion piping without structures (horizontal seepage path). Experiments including a structure (such as a weir or cut-off wall) are performed by the researchers named in Table 3.2.

Source	Goal research
[MIE 78]	Erosion mechanism and influence of size of exit diameter
[MUL 78]	Erosion mechanism in multi-layer sand samples
[PIE 81]	Influence of artificially created pipe length and radius on critical head
[VAN 85]	Erosion mechanism, pressure development in pipe and influence of scale on the critical head
[DE 84]	Influence of scale, type of exit point and sand properties on the critical head
[TOW 88]	Influence of sand characteristics on the critical head
[SIL 91]	Investigation of scale effects
[YAO 07]	Investigation of influence of configuration on backward erosion piping process and critical head
[DIN 07]	Investigation of backward erosion piping in multi-layer aquifers
[VAN 11]	Influence of scale and sand properties on the critical head
[VAN 12]	Influence of exit point and multi-layer configuration on the process and on the critical head

Table 3.1. Overview of research on backward erosion piping (horizontal piping path)

Source	Goal research
[ACH 06]	Influence of relative depth and location of (multiple) cut walls
[OKA 08]	Validation of prediction models for failure of a weir of different widths
[DIN 08]	Influence of relative depth and location of cutoff wall on critical head
[VAN 09]	Investigation of process and critical head
[OKA 10]	Validation of prediction models for failure of a weir or cut off at different locations

Table 3.2. Overview of research on backward erosion piping (horizontal and vertical piping path)

3.3.2. Setup

A variety of experimental setups has been used in the past, each with their specific advantages and disadvantages. All backward erosion piping setups have in common a sand sample prepared in a box such that it can be covered by a cohesive material. An inlet and outlet are present, and a constant hydraulic head difference can be applied to the sand sample. The main differences are found in the type of outlet and inlet, the cover type and method of sample preparation. No setup is optimal for each situation. When performing backward erosion piping tests, advantages and disadvantages of each aspect of the setup are to be considered carefully.

The types of inlet and outlet are important because both strongly influence the flow pattern in the sand. An overview of different types of inlets and outlets is shown in Figure 3.10. The inlet is usually a vertical filter (type A). In some setups, a horizontal inflow area (type B) is used [SIL 91, ACH 06, OKA 08, OKA 10]. In that case, no filter is necessary to retain the sand.

The type of exit can be divided into four main categories: plane (type A), ditch (type B), circular (type C) and slope (D). Several researchers have investigated specifically the influence of exit type on process and critical head. De Wit [DE 94] mostly used the plane type exit (A), for which sand properties varied extensively, but he also performed a few experiments using ditch type (B) and circular type (C) exits to investigate the influence of an exit configuration. Yao *et al.* investigated the plane-type and hole-type [YAO 07] exits. Miesel varied the diameter of the exit hole (type C) to observe differences in the erosion process and critical head [MIE 78].

In most experimental series, the exit type is not varied. The hole exit type is applied by many researchers [MIE 78,

MUL 78, HAN 85, DIN 07]. In most experiments, the thickness of the cohesive cover layer, denoted by d in Figure 3.10, is explicitly taken into account by placing a vertical tube to the hole-shaped outlet (type C). The sand needs to be transported through the tube before it can be deposited. To overcome this considerable vertical distance, additional head drop is required.

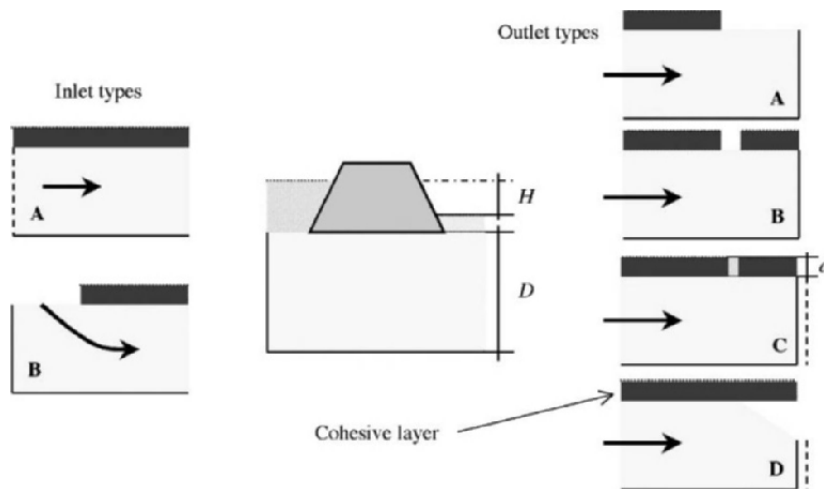


Figure 3.10. Different inlet types (vertical filter and horizontal inlet) and exit types (plane, ditch, circular and slope type exit); the slope and circular type exits can have either a filter or closed boundary at the downstream end

Plane-type exits are used in most experimental setups that contain a structure [ACH 06, OKA 08, OKA 10]. Full-scale experiments described by Van Beek *et al.* have a plane-type exit too [VAN 11]. Silvis [SIL 91] describes large-scale experiments with a ditch-type exit (type B). In experiments by Townsend *et al.*, Pietrus, small- and medium-scale experiments by Van Beek *et al.* and Van den Ham, the fourth exit type, i.e. a slope (type D), is applied [TOW 88, PIE 81, VAN 11, VAN 09].

All types of inlets and outlets can be representative for practice. In some cases, the river is deep and cuts through the cohesive cover layer and the sand. The setup with a vertical filter (type A) most resembles the flow in this situation. In other cases, the river does not cut through the sand layer, and the inflow is mainly in the vertical direction (in some cases covered by a semi-permeable layer). In that case, a setup with a horizontal sand bed is more appropriate (type B). The degree to which the downstream part of the sandy layer is covered by cohesive layer determines which kind of exit is most suitable. Each exit type is representative for a situation in the field. Three of these types are shown in Figure 3.3, (plane-type (A), ditch-type (C) and circular-type exits (B)). The slope-type exit is not very common in practice.

Recently, a detailed investigation of the backward erosion piping mechanism has been performed in the Netherlands [VAN 11, SEL 11]. Several piping experiments (Figure 3.11) have been performed in order to get insight into the underlying physical phenomenon by carefully increasing the hydraulic head until piping was observed:

- *Small-scale experiments.* Fifty experiments were performed with a seepage length of 0.34 m, with several sand types tested at different relative densities, with grain sizes from 150 μm up to 430 μm .

- *Medium-scale experiments.* Seven experiments were performed with a seepage length of 1.30 – 1.45 m, with two types of sand with different relative densities. The aim was to investigate scale effects and verify the results from the small-scale experiments.

- *Large-scale experiments.* Four experiments were carried out at the IJkdijk location (Groningen), where two types of sand were tested for their susceptibility to backward erosion piping, with a seepage length of 15 m. The aim was to investigate scale effects and validate the model.

The following paragraphs will show that the choice of exit type in experimental work is of importance for the process and critical head.

To investigate the occurrence of backward erosion for weirs and structures with a vertical section like a cut off, several types of configurations are possible. Often, a weir is used [OKA 08, OKA 10, ACH 06], which is located at some depth in the sand sample, combined with one or more cutoffs at various locations if so desired. In other experiments, only a cutoff is used at various locations under the simulated levee [VAN 09, DIN 08].

In most experiments performed so far, the cover was made of acrylate. The obvious advantage of using such a cover is its transparency that enables us to observe the backward erosion piping process. The disadvantages are the rigidity and the smooth surface, which do not resemble a natural material. The smooth inner surface can be roughened by coating with silicon as is done in the experiments by Van Beek *et al.* and Van den Ham, while De Wit used a clay cover [VAN 11, VAN 09, DE 94].

Regardless of the type of cover used, a good connection between cover and sand bed is important because backward erosion piping is a micro-scale process that takes place at the interface of sand and cover. When the cover is placed after preparation of the sand bed, a good connection between cover and sand bed is difficult to achieve. A good connection can be achieved by using a setup in which the transparent cover is connected to the box before filling. Sand can be added from an additional opening at the side of the box. This can be done by adding the sand while placing the box in a vertical position. After filling, the opening is closed and the setup can be rotated to a horizontal position for the erosion experiment. This method also has drawbacks especially for the preparation of loose sand samples because the rotation

may cause the loose porous structure to collapse, thereby leaving some space between cover and sand bed [VAN 12a].

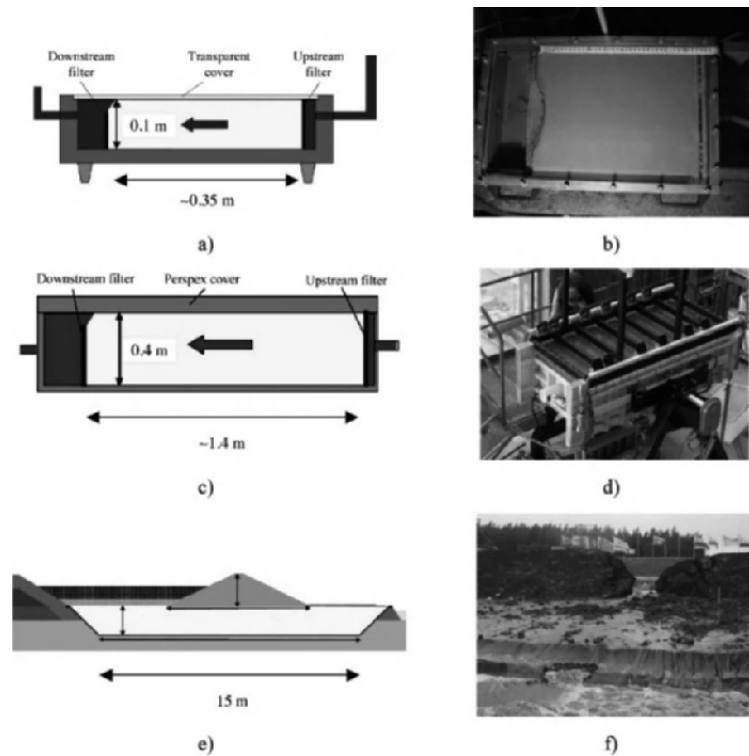


Figure 3.11. Backward erosion piping experiments: a) schematic of the small-scale experiment, b) picture view of the small-scale experiment, c) schematic of the medium-scale experiment, d) picture view of the medium-scale experiment, e) schematic cross-section of the large-scale experiment and f) breakthrough of the levee in large-scale experiment [VAN 11]

Next, it is important to obtain a homogeneous and fully saturated sample because inhomogeneities and the presence of air will influence the process and the critical head. Many sand preparation techniques are described in the literature, mainly divided into “wet” methods, where dry sand is rained in water, and “dry” methods, where saturation takes place after raining the sand. The degree of saturation will be

optimal using a wet method, but graded sand types will disintegrate using this method. The dry method will lead to partially saturated samples although several techniques exist to improve the degree of saturation (CO₂, flushing with de-aired water). The relative density of the sand sample can be increased by tamping during filling or by giving a pulse to the sample [POE 98, RIE 10]. For uniform sand types, the wet preparation method is preferred because this will result in optimal saturation.

In some experiments, an artificial pipe was created after sand bed preparation [TOW 98, PIE 81]. Because this pipe does not have natural dimensions, it is difficult to relate the outcome of these experiments to practice.

Several parameters are worthwhile monitoring during backward erosion piping experiments. Measuring the potential head in several locations can be useful to determine the overall head fall across the sand sample and observe whether the sample is homogeneous. It is noted that filters can cause significant head drop, especially when the sand is very permeable, which confirms the need for pore pressure meters. By measuring the flow through the sample at the outlet for different head drops as well as the temperature of the water, the (intrinsic) permeability of the sand sample can be determined.

During a test, the head fall across the sand sample is increased in small steps until piping occurs. A fast loading scheme is possible (for example: one step in five min) as long as no other mechanisms than backward erosion piping are expected. When washout of fine particles can take place, a slower loading scheme is recommended because the washout of grains is a gradual process that can be difficult to observe visually. For large-scale experiments, the loading scheme is generally slower than for small-scale experiments because the increase of head takes some time, and the erosion process is more difficult to observe. The size of the loading

step depends on the required accuracy of the obtained result. The influence of the loading scheme on the outcome of the test has not been reported in literature.

As soon as erosion takes place, generally the head is kept constant, until the erosion stops for several minutes at least. Whilst for the experiments in which the erosion does not cease, additional information about the growth of the pipe can be obtained by reducing the head drop to zero at various pipe lengths. By subsequent gradual re-application of the head until erosion continues, limit heads can be obtained for different pipe lengths. A transparent cover is useful at this stage, whereas a clay cover hides the pipe development from viewing.

In summary, the design of a backward erosion experiment for the validation of a prediction model can take all kinds of forms; there is no specific device that suits all needs. Yet, some points can be stressed for good design of the experiment: as the process takes place at the interface of sand and cover, the connection between those must be well established. For careful validation, the sample should be prepared homogeneously and should be well saturated. The degree of homogeneity and saturation can be checked by measuring flow and head drop at several locations, and these parameters, along with the temperature of the water, will also provide for accurate determination of (intrinsic) permeability.

3.4. Backward erosion piping in the laboratory – erosion mechanism

It has already been described in the previous section that the process leading to failure of the water-retaining structure can be divided into several phases: seepage, backward erosion, widening of the pipe and failure, etc. In the laboratory, the focus of experiments is generally to study

the phase of backward erosion only, from initiation of the pipe to progression toward the upstream side.

Based on the observations in experiments, the phase of backward erosion can be divided in a sequence of events. It appears that the sequence of backward erosion processes and the corresponding critical hydraulic head depend on the geometry of the water outflow point (exit type) and the scale of the setup. This sequence of events can be summarized as:

- 1) single grain transport – development of preferential flow paths;
- 2) boiling phase – sand boils without deposition of sand;
- 3) regressive backward erosion phase – sand is transported toward the exit, and a pipe starts to form. The erosion will cease unless the head is increased;
- 4) Progressive backward erosion phase – the pipe develops toward the upstream side.

It is also noted that in some experiments, the third phase is not observed. In the following section, each phase is described in more detail.

3.4.1. *Single grain transport*

The first signs of erosion that can be observed are the rush out of single particles from the sand matrix. These are small-sized grains that can be removed easily by local concentrated water flow. The removal of these particles can result in the formation of micro-scale holes, such as those observed in some experiments with a plane-type exit [DE 84, VAN 11]. An example of these holes is shown in Figure 3.12. In other experiments, the washout of small-sized grains results in turbid water [SIL 91] or formation of pipes at pore-scale [VAN 11]. In all experiments, this type of micro-scale erosion stabilizes unless the head is increased.

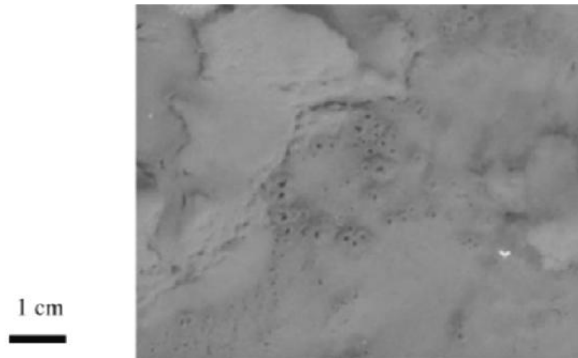


Figure 3.12. *Small holes observed in full-scale experiment [VAN 11]*

3.4.2. Sand boiling phase

As a result of increasing pore pressures near the exit, the bed expands, and local fluidization can be observed, resulting in the formation of sand boils. Bed expansion, the local uplift of the sand bed near the simulated levee toe due to porosity increase, is observed in experiments [DE 84]. Sand boils are observed in nearly all experiments. In the sand boil, the sand is lifted and dropped, but the water flow is insufficient to deposit sand around the center of the sand boil, resulting in pipe formation. This sand boiling phase is observed in experiments [DE 84] and in full-scale experiments [SIL 91, VAN 11]. In experiments by Miesel and Müller-Kirchenbauer, this phase is denoted by “fluidization” [MIE 78, MUL 78]. In these experiments, in which a circular exit with a vertical tube is used, fluidization causes sand to be transported to the vertical tube. With increase of head, the tube is gradually filled. The distinction between fluidization, resulting in expansion of the sand body, and the actual transport of particles from the sand body, resulting in pipe formation, is not clearly made in these experiments. The sand boiling phase is not observed in slope experiments [VAN 11], but is not expected here because boiling sand would directly flow downward along the slope.

3.4.3. Regressive or equilibrium phase

With the further increase of head drop, the sand boiling will intensify, and sand will be deposited near the exit point, causing the formation of hollow spaces in the sand body. At this point, the “critical head”, which is the head required for the progression of the pipe toward the upstream side, is generally not yet exceeded, and the pipe formation will cease after some time. Equilibrium in pipe formation can be observed. This phase is, therefore, denoted as a regressive phase or an equilibrium phase.

The equilibrium in pipe formation may have several causes. In the experiments by Miesel [MIE 78], equilibrium occurred during the “fluidization phase”. In this phase, sand is being transported through the vertical section, yet it is not ejected out of the tube. An increase of head was necessary to increase the level of fluidized sand in the tube. In the experiments with a small circular exit [DE 84], a similar process was observed; the circular hole was gradually filled with sand, but the level of fluidized sand remained constant until the head drop was increased. After several increases of head, in both experimental series, the vertical tube is completely filled with sand, and sand is ejected over the top of the tube and on to the cover layer. For larger diameters (0.04 m in the De Wit experiments and 0.013 m in Miesel’s), equilibrium is no longer observed at this stage; the pipe develops toward the upstream side without further increase of the head. It appears that the presence of sand in the vertical section causes a pressure drop that hinders the ongoing development of the pipe.

For smaller diameter exit holes, equilibrium also occurs after the sand ejection (Figure 3.7). In the experiments by Miesel, the diameter was lower than 0.013 m. This is confirmed in experiments with a circular hole, but with only a very small vertical section, representing a thin blanket layer [VAN 12]. These experiments indicate that, apart from

the resistance in the vertical section, there is another reason for equilibrium. This equilibrium might be related to the decrease of hydraulic gradient in the sand further away from the exit point. This restricts the inflow toward the pipe and the gradient at the head of the pipe with increasing length. Sellmeijer's model predicts this equilibrium, as will be described in section 3.6. This type of equilibrium is observed by many researchers. In large-scale tests [SIL 91], in which the pipe length as a function of head difference is well documented, the repeated equilibrium is clearly visible. Figure 3.13 shows the development of various parallel developing pipes with increasing head drop in one of these large-scale experiments. For experiments simulating considerable cohesive cover layer, the two causes for regressive erosion cannot easily be distinguished.

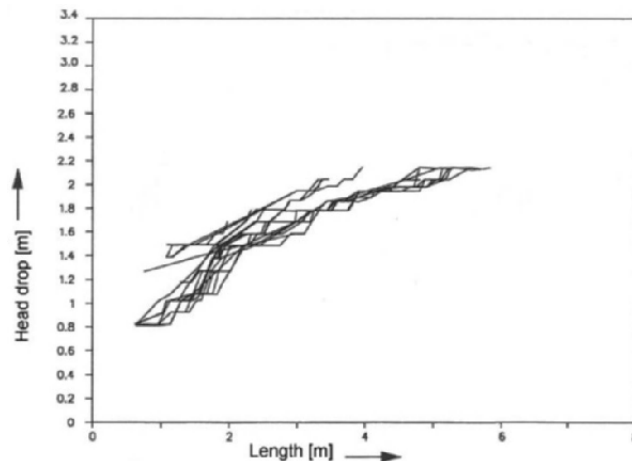


Figure 3.13. Pipe development (pipe length) versus applied head difference for test T3 with total seepage length of 12 m [SIL 91]

The third reason for equilibrium in pipe formation is the presence of a structure, like a cutoff wall. After a developing pipe reaches the structure, piping channels propagate parallel to the structure, until the head is sufficiently large

enough to bring the pipes underneath the cutoff [VAN 11, DIN 08]. The resistance of a vertical piping path is clearly much higher than a horizontal piping path as this requires fluidization of the sand downstream of the structure [TER 48].

In many other experiments, equilibrium in pipe formation is not observed at all. These are predominantly plane- and slope-type exit experiments [VAN 11], plane- and ditch-type experiments [DE 84]. In these experiments, the critical head for progression of the pipe is already exceeded when the pipe formation starts, as the required head for the fluidization phase, necessary for pipe initiation, exceeds the required head for progression of the pipe.

Several researchers have studied the erosion process in detail during this phase of regressive erosion. Hanses has studied the backward pipe development at micro-scale [HAN 85]. Two types of erosion are distinguished: primary erosion, which is the erosion of grains from the soil matrix at the head of the channel, and secondary erosion, which is the widening and deepening of the existing channel. Primary erosion occurs when the hydraulic gradient at the head of the pipe reaches a critical value, such that fluidization of sand takes place, which allows the sand to be transported. The flow velocity in the pipe, determined by the inflow of water from the sand matrix may reach a critical value such that secondary erosion takes place. It is noted that the primary sand transport is intermittent; groups of sand grains go into suspension (sand clouds). Hanses has also studied the shape of the pipe and observed that the size of the pipe at the advancing head remains the same during pipe development. At this point, the pipe is found to be 3.5 times the diameter of the grain. When the length of the pipe increases, widening and deepening in the downstream area of the pipe takes place (secondary erosion) (Figure 3.14). The width of the pipe increases in the downstream direction.

Townsend *et al.* have also studied the backward erosion piping process in detail and made a similar observation as Hanses: particles slide into the pipe and when the group of particles is washed away, several more new particles become displaced as a retrogressive slide [TOW 88]. Van der Zee has studied pipe formation at the micro-scale in a setup with very limited width [ZEE 11]. The piping process could be observed from the side of the setup. It was found that the erosion process takes place intermittently. The grain transport through the pipe causes secondary erosion, and due to upward flow in the sand bed below the pipe, the sand bed appeared fluidized. It is noted that due to the limited width, the applied gradient was much higher than for experiments with considerable width.

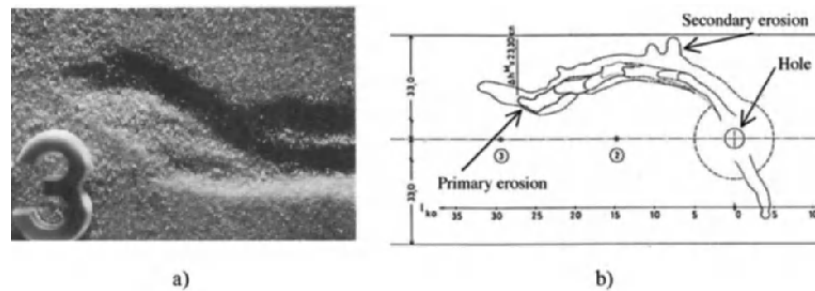


Figure 3.14. a) Photo of the advancing head of the pipe and b) drawing of the pipe development in time in one of the tests [HAN 85]

3.4.4. Progressive phase

The progressive phase is characterized by the ongoing erosion, leading to pipe development toward the upstream side of the sand body. In all experiments, this phase is finally reached. Müller-Kirchenbauer states that, in general, this phase is reached when the pipe has developed to a $1/3$ or to a $1/2$ of the seepage length [MUL 93]. From this point onward, the gradient and flow towards the pipe increases, and equilibrium is not possible anymore. If a structure like a

cutoff is present, the progressive phase is reached when the pipe has passed the structure.

3.4.5. Which process will occur when?

The variety of erosion processes makes the prediction of the lapse of backward erosion difficult. Why does equilibrium occur in some experiments, but not in others? The answer lies in the prediction of the overall minimum hydraulic head necessary for each process.

The transitions between the phases in each experiment will occur at a different hydraulic head:

- single grain transport to boiling phase (H_b);
- boiling to pipe initiation and regressive erosion (denoted as initiation head H_i);
- regressive erosion (pipe stops) to progressive erosion (pipe continues until breach) (denoted as progression head H_p).

The hydraulic head at which the pipe grows towards the upstream side – irrespective of the process that determines this hydraulic head – is typically labeled the critical head (H_c) in the literature.

In all experiments, the initiation of the pipe needs to precede the progression of the pipe. In some configuration initiation, which is likely to correspond to the fluidization of a group of particles such that sand deposition can take place, it can occur at a relatively low overall head, as is the case for small circular exits. In this case, the flow will concentrate at the small exit resulting in a considerable hydraulic gradient around the exit at a relatively low overall hydraulic head. At this point, the hydraulic head necessary for the progression of the pipe is not yet reached, and equilibrium will occur. In other experiments, initiation occurs at relatively high overall

head, which is the case for the slope and plane experiments in which flow velocities are low near the exit. Once the pipe is initiated, the head for progression is already exceeded and no equilibrium can be observed. In this case, the formation of a pipe will result in a smaller outflow point, with relatively high gradients near the head of the pipe, and consequently a lower critical hydraulic head for pipe propagation.

Clearly, the backward erosion process is dependent on exit geometry. This dependence was already found by Miesel, who studied the erosion process as a function of the circular exit diameter [MIE 78]. Miesel has investigated the influence of the diameter of the exit hole on the backward erosion process. The results are displayed in Figure 3.15. At a very small diameter (< 2.65 mm), fluidization will not take place at all due to bridging; a minimum diameter related to the grain size is necessary for sand grains to pass the hole.

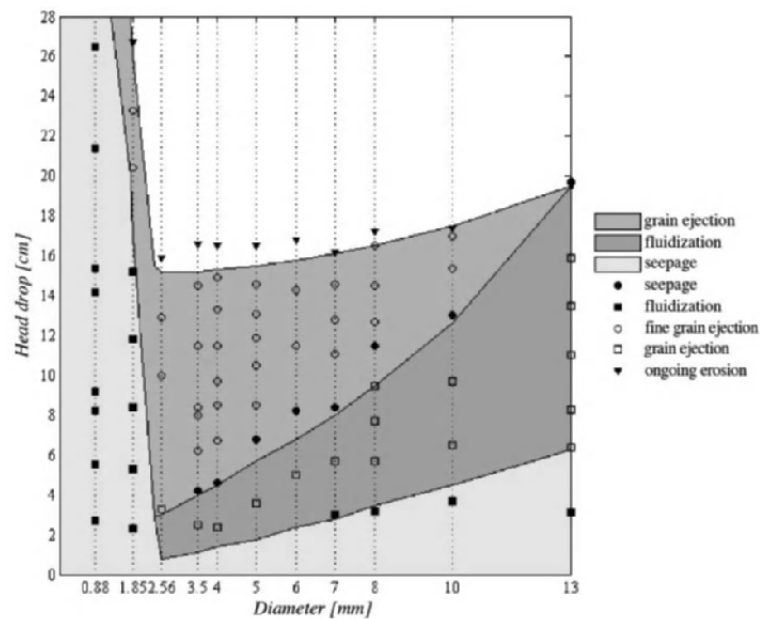


Figure 3.15. Influence of exit diameter on piping process [MIE 78]

It can be seen in Figure 3.15 that the head required for fluidization increases with increasing grain diameter. After fluidization, the vertical section at the outlet is gradually filled with sand suspension, indicating expansion and the transport of sand from the sample. After several increases of head, the tube is filled and the sand is ejected from the tube. The head required for sand ejection from the tube is dependent on the diameter of the circular exit as well. After sand has been ejected, the pipe development results in equilibrium. The final critical head that corresponds to the head required for progression of the pipe (H_p) also shows a small increase with exit diameter. For a relatively large exit diameter ($> 13\text{mm}$), fluidization takes place at a relatively high head drop, and several steps of increase of the head are necessary before the tube is filled and the sand is ejected from the tube. Once the tube is filled and sand is ejected, the formed pipes grow toward the upstream side, without the necessity of further increase in the head.

The influence of thickness of the downstream cohesive cover layer is an aspect that has not yet been investigated in detail. Yet, it appears that it limits the development of pipes because the increasing amount of sand in the vertical section causes an increase in pressure drop.

The influence of the configuration on the required head for initiation of the pipe and progression of the pipe is also well illustrated in experiments in which, the head drop necessary for the progression and initiation has been studied separately [VAN 11, FOR 11]. In an experiment with slope-type exit, the head drop has been increased until the pipe developed over a certain distance. The head drop was lowered subsequently and reapplied in gradual steps until the pipe continued to grow. The head drop at which the pipe continued to grow was considerably lower than the head drop at which it was initiated (Figure 3.16). A similar experiment performed on the same type of sand and with the

same sand depth and seepage length, but with a circular exit, shows that the pipe development starts at a relatively low head drop, whereas for pipe progression, the head drop needs to be increased. The experiment indeed shows that the “critical head” can be driven by different processes. It is noted that the influence of inlet on the erosion process has not yet been investigated. An extra resistance at the inlet, for example, will hamper pipe formation. Such an extra resistance is likely when fine and organic material have decreased the permeability of the sand on the upstream side.

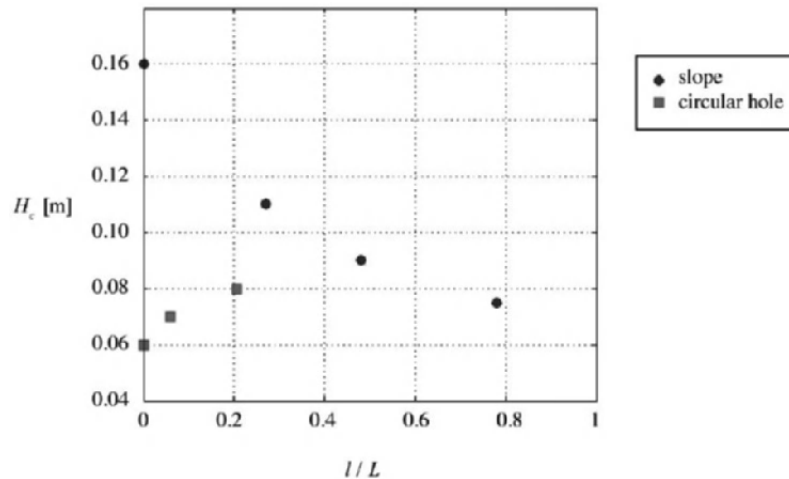


Figure 3.16. Results of experiments with circular and sloping exit in which the head for initiation and progression of the pipe is studied [VAN 11]

In case of a vertical structure, like a cutoff wall, the limit head to pass the structure is always much higher than the progression head or the initiation head. For structures, this head is, therefore, normative for the critical head (H_c).

Another difficulty in predicting the course of the backward erosion process is scale. It is known that the

critical gradient for progression (H_p/L) is scale dependent [VAN 10b, SEL 88]; the progression gradient decreases with seepage length. Based on the observations in all experiments without the presence of a structure [DE 84, VAN 11, MIE 78, MUL 78, HAN 85, SIL 91, YAO 07], the influence of scale and configuration can be roughly analyzed.

Figure 3.17 shows the dominating process for the critical head as a function of exit type and seepage length. The more concentrated the flow toward the exit point, the higher the probability that the critical head will be dominated by the required head for progression of the pipe. It can also be seen in Figure 3.17 that experiments at a large scale are more likely to be dominated by regressive backward erosion than experiments at the small scale. This is because scale effects are different for both mechanisms. In the next sections, the scale effects related to initiation and progression of the pipe are explained in more detail.

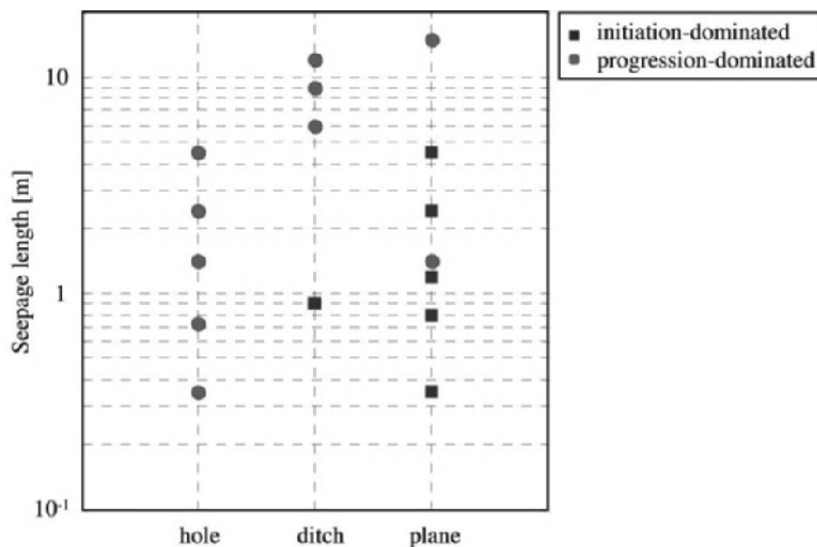


Figure 3.17. Relation between type of process, exit and seepage length

3.5. Backward erosion in the laboratory – critical gradient

In many experiments, not only the process of backward erosion piping, but also the influence of geometry and sand characteristics has been studied on critical head. The critical gradient, defined as the ratio of critical head and seepage length, will be used to compare experimental results.

As explained in the previous section, the critical gradient in experiments can be dominated by either initiation of the pipe or progression of the pipe. Progression-dominated experiments can be divided into experiments with and without vertical structure. These experiments are treated separately in the following sections.

3.5.1. *Initiation of backward erosion piping*

The initiation of a pipe is caused by water flow through an intact sand sample. At a certain head drop, the pore pressures become too high and the sand sample locally fluidizes, resulting in a sand boil. A slight increase of head generally results in sand transport, indicating the initiation of backward erosion piping. In the experiments by De Wit and slope-type experiments by Van Beek *et al.*, after initiation of the pipe, the pipe directly progressed upstream [DE 84, VAN 11, VAN 12]. Therefore, the critical heads obtained in these experiments can be considered to be the head at which pipe initiation takes place.

De Wit describes several experiments, thereby varying scale, exit type, sand type and relative sand density [DE 84]. Van Beek *et al.*, performed slope-type experiments with varying scale, sand type and porosity [VAN 11, VAN 12]. A few multilayer experiments have been performed. In Tables 3.3 and 3.4, the sand types used in the experiments by De Wit and Van Beek are characterized.

The influence of configuration, scale, seepage length and sand characteristics on the overall initiation gradient (H_i/L) will be discussed. To analyze the influence of these properties on initiation gradient, it is relevant that only one variable is changed per test series.

Sand type	d ₅₀ [μm]	d ₇₀ [μm]	d ₆₀ /d ₁₀	minimum porosity	maximum porosity
Dune sand	190	212	1.48	34.1	44.9
Beach sand	200	220	1.33	33.0	44.7
River sand	400	600	2.30	31.7	40.0
Sieved river sand	365	480	2.10	31.5	40.4
Coarse sand	750	1390	3.85	23.5	40.0

Table 3.3. Sand characteristics of sand types in experiments by De Wit [DE 84]

Sand type	d ₅₀ [μm]	d ₇₀ [μm]	d ₆₀ /d ₁₀	minimum porosity	maximum porosity
Dekzand Nunspeet	148	192	2.6	28.4	42.8
Oostelijke rivierenzand Zwolle	233	307	2.1	32.2	42.3
Hoherstall Waalre	341	400	1.6	35.0	45.0
Hoherstall Sterksel	200	232	2.2	37.9	50.4
Itterbeck Scheemda	157	175	1.3	37.2	47.3
Itterbeck Enschedé	380	431	1.6	32.0	41.1
Itterbeck Sandr	171	195	1.5	33.1	44.1
Itterbeck Boxtel	155	202	2.2	32.3	46.1
Baskarp	132	154	1.6	34.0	46.9
Itterbeck fraction 125–250 μm	170	210	1.7	34.5	46.5
Itterbeck fraction 333 μm	283	350	2.1	30.7	40.9
Itterbeck fraction 431 μm	342	500	2.6	28.5	38.0
Fine IJkdijk	147	180	1.6	35.8	45.8
Coarse IJkdijk	199	260	1.8	34.6	44.7

Table 3.4. Sand characteristics of sand types in experiments by Van Beek et al. [VAN 11]

It was already described in the previous section that the exit configuration is of large influence on the type of process that is likely to dominate. It makes sense that the initiation of a pipe is dependent on the type of exit because the concentration of streamlines will be more severe for a small-area exit, compared with a large-area exit. The required velocity for fluidization and initiation will therefore be reached at a lower critical head for a small exit.

De Wit [DE 84] performed experiments on beach sand (medium–high density) in experimental setups with a circular exit (0.04 m and 0.1 m in diameter), a plane-type exit and a ditch-type exit (width ditch 0.05 m), while retaining other parameters like seepage length (2.4 m) and sand layer thickness (1.5 m). Initiation gradients are presented in Figure 3.18. Indeed, an increase in the gradient can be observed with an increasing exit flow area.

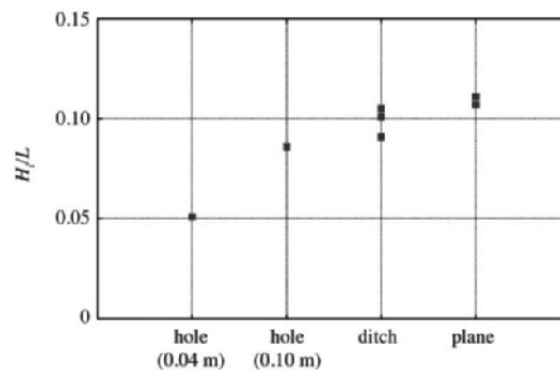


Figure 3.18. Influence of configuration on initiation gradient [DE 84]

Scale effects on the gradient required for initiation are expected, as the flow pattern, including the local singularity near the exit point, is scaled linearly with increasing dimensions, whereas the grains are not scaled. These scale effect will be explained more extensively in section 3.6. The existence of scale effects can be shown by analyzing

experiments with constant D/L -ratio (thickness aquifer/seepage length), but with different dimensions. Both Van Beek *et al.* and De Wit investigated scale effects on several sand types, with a slope-type exit and a plane-type exit, respectively [DE 84, VAN 11, VAN 12]. In Figure 3.19, the influence of scale on initiation gradient is presented using experiments on sand types with a medium – high relative density and a constant D/L ratio. Scale effects are indeed observed: the gradient decreases with increasing scale.

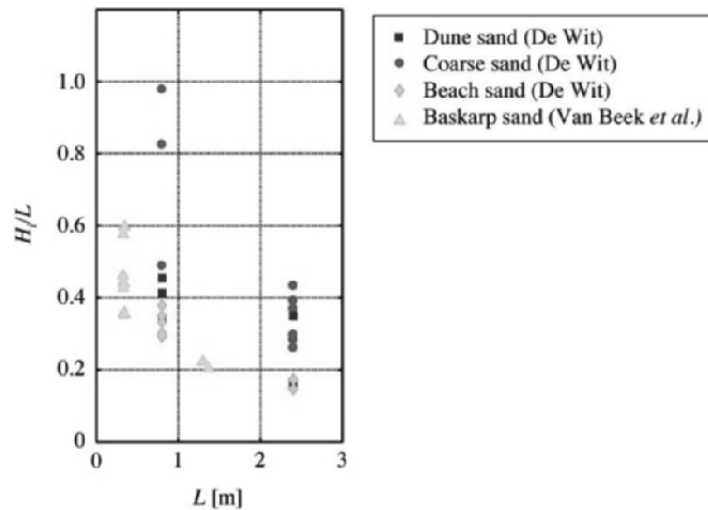


Figure 3.19. Influence of scale in experiments with constant D/L ratio, equal to 0.63 for De Wit [DE 84] and approximately 0.3 for Van Beek *et al.* [VAN 11, VAN 12]

The influence of seepage length, retaining a constant sand layer thickness, is expected to have a minor influence on the initiation gradient. Especially when the seepage length exceeds by far the thickness, the local flow pattern, and the local gradients required for fluidization near the exit point will not be influenced by an increased seepage length because the flow pattern becomes unidirectional at some

distance from the exit. This is confirmed by experiments described by De Wit [DE 84] in Figure 3.20, who varied the seepage length in plane-type experiments on (a medium – high density) beach sand ($D = 1.5$ m). Despite the remarkable spread in results for small seepage length, the required gradient for initiation appears rather constant for larger seepage lengths.

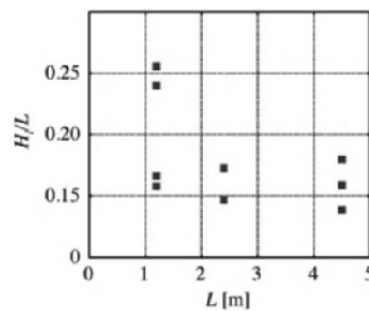


Figure 3.20. Influence of seepage length on initiation gradient (Beach sand, $D = 1.5$ m) [DE 84]

As the head required for fluidization is influenced by porosity, the gradient required for initiation of pipe development is also likely to be influenced by this parameter. A decrease in overall gradient is expected with increasing porosity. Both De Wit and Van Beek *et al.* investigated this parameter in area-type experiments and slope-type experiments, respectively (Figure 3.21, [DE 84, VAN 11]). In this graph, the experiments on Baskarp sand are performed with a slope-type exit. It is noted that the influence of porosity for slope-type experiments may be different from that for plane-type areas because the slope angle and the friction angle, which determine the onset of grain movement on a slope, are also influenced by the porosity of the sand sample. Although for most sand types, the decrease of gradient with increasing porosity is indeed observed, it is remarkable that for some sand types the gradient appears more sensitive to porosity than for others.

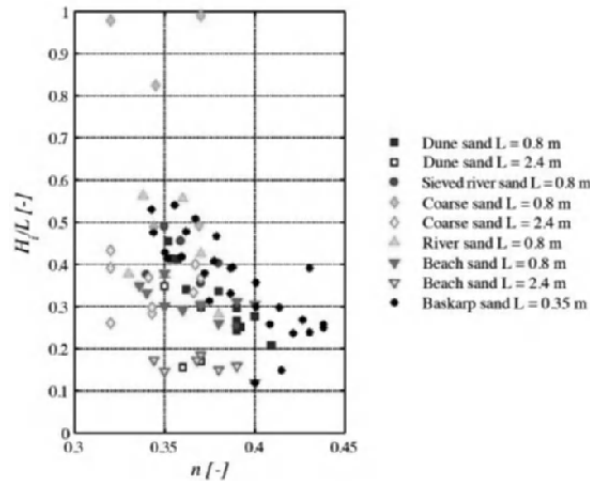


Figure 3.21. Influence of porosity on initiation gradient [DE 84, VAN 12]

Based on the theoretical considerations, the influence of the sand type on the initiation gradient should be limited. The local gradient required for fluidization of sand is mainly determined by the porosity and the local flow pattern near the exit, which are relatively independent of parameters like permeability and grain size. However, as the initiation gradient is dependent of scale (increase of L and D , retaining D/L ratio), an influence of grain size can also be expected. It is also noted that for slope-type experiments, a larger influence of the sand type can be expected, as the local gradient required for grain motion in a sloping area is also dependent on friction angle.

Based on these theoretical considerations, the grain size can be of importance, for which the d_{50} has been chosen to represent the size of a sand type. Figure 3.22 shows the experiments on different sand types (medium – high density). It is remarkable that the slope-type experiments described by Van Beek *et al.* [VAN 11] show a slight decrease with increasing grain size, although the spread in data

results in a relatively unclear trend, whereas the experiments by De Wit [DE 84] show an increase with increasing grain size. This might be related to the difference in the exit configuration. The positive trend observed by De Wit agrees well with the theoretical explanation that an increase in grain size corresponds to a decrease in scale (grain size relatively large compared with sand layer dimensions), which is known to result in higher overall gradients (Figure 3.19).

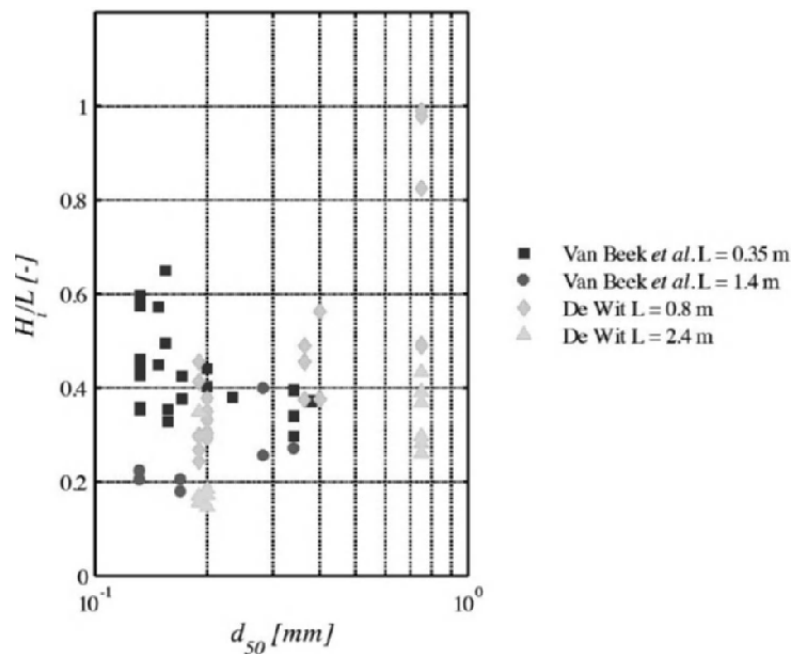


Figure 3.22. Influence of grain size on initiation gradient, determined in slope-type experiments [VAN 11] and plane-type experiments [DE 84]

So far, homogeneous sand samples have been considered. In practice, the subsurface is heterogeneous, often with a multilayer configuration, where fine sand layers are overly permeable coarse layers. The presence of a permeable coarse layer will lead to the increase of pore pressures near the exit

point, and is therefore expected to have a larger influence on the initiation gradient. This is confirmed in experiments described by Van Beek *et al.* [VAN 12b]. In these slope-type experiments, the ratio of the fine layer thickness and the total layer thickness is varied (D_{fine}/D_{tot}), using Baskarp sand and coarse sand with a mean diameter of 0.4 mm. Figure 3.23 shows that, indeed, there is a significant decrease of the initiation gradient with decreasing fine layer thickness.

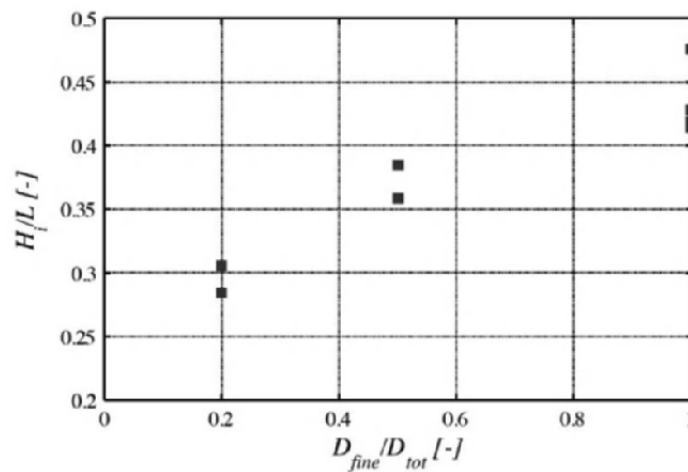


Figure 3.23. Influence of ratio of fine and total sand layer thickness on the initiation gradient for slope-type experiments [VAN 12b]

In summary, the experiments confirm that the process of initiation appears to be influenced by the local flow pattern near the exit. This pattern depends on an exit configuration, scale (ratio of grain size and dimensions sand layer). The presence of a more permeable layer underneath a fine layer also strongly influences the flow pattern and local exit gradients. The required local gradient for the initiation of the pipe is determined by porosity for plane-type experiments. For a slope-type experiment, the local gradient is also determined by the slope angle and friction angle.

3.5.2. Progression of backward erosion piping

The progression of the pipe can only be studied in experiments in which the pipe was in equilibrium at a certain stage. Various causes exist for the occurrence of equilibrium. The first cause is related to a situation with a considerable cohesive cover layer, such as is observed in one of the experiments by Miesel [MIE 78] and in two experiments with a circular exit by De Wit [DE 84]. Sand accumulates in the vertical tube, causing extra pressure loss. The second reason is presumably related to the flow pattern: the concentration of streamlines diminishes when the pipe progresses further from the exit point. A third reason is the presence of a structure, creating a vertical seepage path, which requires a significant head increase for the pipe to pass.

In this section, the focus will be on experiments in which equilibrium is observed due to the flow pattern. In section 3.5.3, experiments with a vertical seepage path, such as a weir or dike with a cutoff, will be discussed.

Unlike the mechanism for initiation, the gradient for progression of the pipe is determined by the equilibrium of grains in the pipe, the flow in the pipe and the flow toward the pipe.

Equilibrium in pipe development is observed in many experiments, most of them with a circular exit. In this section, the influence of the configuration, the scale, seepage length and sand characteristics on the gradient required for progression of the pipe will be explained. Finally, some experiments on multilayer aquifers will give an insight into the flow pattern on the critical gradient.

The influence of the configuration on the progression of the pipe is difficult to study, as for small-scale ditch-type and plane-type experiments the dominating process is the

initiation of the pipe. In these experiments, no equilibrium is observed.

Yao *et al.* [YAO 07] investigated the influence of a configuration on the critical head in medium-scale experiments (seepage length is 1.4 m and the sand layer thickness is 0.6 m). For the same, sand type (fine sand with d_{60} of 0.28 mm and uniformity coefficient of 3.5) experiments are performed with a circular exit of 4 cm diameter and with a plane-type exit. It was found that the progression gradient for these experiments was 0.22 and 0.29, respectively. It is likely that the three-dimensional (3D) flow toward the circular exit results in increased flow in the pipe, leading to a slightly lower critical gradient.

Miesel [MIE 78] investigated the influence of the exit hole diameter on the process and the critical head, using a fine sand in a small-scale setup (seepage length is 0.71 m and sand layer thickness is 0.168 m). It was found that the critical gradient, related to progression of the pipe, slightly increases with increasing diameter, although the influence is marginal (Figure 3.15).

The influence of the scale on a progression gradient is investigated by Hanses, using a similar setup as used by Miesel, with a circular hole at the exit (6 mm in diameter). In these experiments, the ratio between sand layer thickness and seepage length is kept constant (0.13), whereas dimensions are varied [HAN 85]. Experiments are performed on a medium-sized sand with d_{50} of 0.325 mm. The experiments show a significant scale effect: a decrease in gradient with increasing size. Based on theory, a scale effect is expected for this mechanism. The pipe dimensions are known to remain more or less the same, independent of scale [VAN 11]. With increasing scale, the flow toward the pipes will increase as a result of larger flow area, resulting in a lower critical gradient.

The influence of the seepage length is investigated by Silvis [SIL 91]. Three successful experiments have been performed in a large-scale setup, with ditch-type exit (width of ditch 0.5 m) on Marsdiep sand of medium density ($d_{50} = 0.211$ mm). The sand layer thickness is 6 m in all experiments, whereas the seepage length is varied to 6, 9, and 12 m. Theoretically, the seepage length has a small influence on the gradient required for progression, as the flow toward the pipe remains more or less the same, especially when the seepage length exceeds the thickness of the aquifer. This was also observed in experiments that are dominated by the initiation (Figure 3.20). The experiments by Silvis [SIL 91] confirm this theory, as can be observed in Figure 3.25.

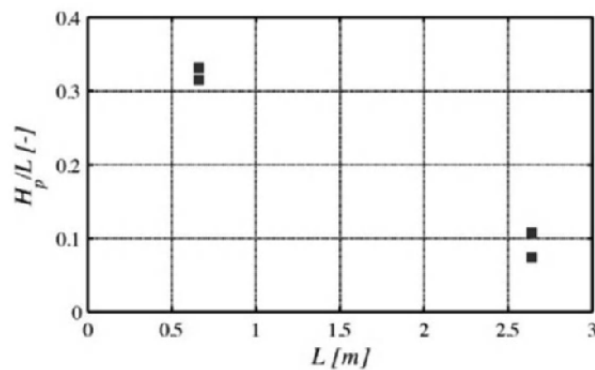


Figure 3.24. Influence of scale on pipe progression [HAN 85]

The influence of sand characteristics on the progression gradient is difficult to analyze. When varying the type of sand, many sand characteristics change. Based on theory, several parameters may play a role. First, grain size is known to have a large influence on the critical shear stress required for the onset of grain movement and therefore is likely to influence the progression gradient. Second, the permeability influences the flow toward the pipes. The porosity in turn influences the permeability that is likely to

decrease with the increasing uniformity coefficient (d_{60}/d_{10}) and increasing grain size. Other sand characteristics such as the uniformity coefficient and the angularity of the grains may also have an influence on the critical shear stress. The correlation between parameters impedes the analysis.

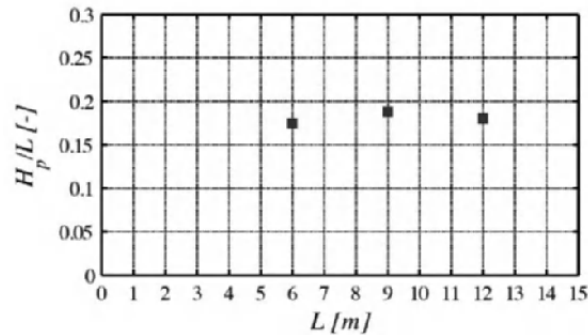


Figure 3.25. Influence of seepage length on pipe progression [SIL 91]

The influence of the sand type is investigated in full-scale experiments [VAN 11]. Four experiments are performed for a model investigation on two types of sand with characteristics as described in Table 3.4 (fine IJkdijk sand and coarse IJkdijk sand) of which the fourth test is possibly disturbed by the presence of the monitoring equipment. The properties of the four tests are summarized in Table 3.5.

Exp. No.	Sand type	k [m/s]	RD	L [m]	D [m]	H_c/L [m]
IJkfs01	Fine IJkdijk	8×10^{-5}	0.60	15	3.00	0.15
IJkfs02	Coarse IJkdijk	1.4×10^{-4}	0.75	15	2.85	0.12
IJkfs03	Fine IJkdijk	8×10^{-5}	0.60	15	3.00	0.14
IJkfs04	Coarse IJkdijk	1.2×10^{-4}	0.70	15	2.85	0.13

Table 3.5. Overview full-scale experiments [VAN 11]

It can be noted that the progression gradient is lower for coarse IJkdijk sand than for fine IJkdijk sand. As more variables are changed (grain size and permeability), the influence of parameters can only be determined by comparison with prediction models. In section 3.6, this comparison will be made.

Several researchers have studied progression of the pipe in multilayer configurations, generally consisting of a fine sand layer overlying a coarse sand layer. A permeable sublayer will increase the flow toward the pipe, compared to the homogeneous case and is therefore likely to result in a decrease in the progression gradient. The influence of heterogeneity was investigated in a setup with a circular exit, by varying the thickness of fine and coarse sand layers in a multilayer configuration [MUL 78]. In one of the experiments, a four-layer configuration was tested, with alternating layers of a coarse and fine sand.

Van Beek *et al.* [VAN 12] performed similar experiments in a small-scale setup with a circular exit on Baskarp sand overlying a coarse sand layer. Ding *et al.* [DIN 07] performed medium-scale experiments with a two-layer configuration. In two of his four tests, a different failure mechanism was observed. These are left out of the current analysis. The other experiments are presented here. An overview of sand layer characteristics of these three series is given in Table 3.6. Figure 3.26 shows the progression gradient as a function of the ratio of a fine layer thickness to the total layer thickness (D_f/D_{tot}) for these experimental series.

All researchers observed an increase in the critical head with an increase in fine-layer thickness, which is a similar trend as observed in experiments dominated by initiation (Figure 3.23). It is unclear why a minimum in the critical gradient is observed in the experiments by Müller-Kirchenbauer [MUL 78].

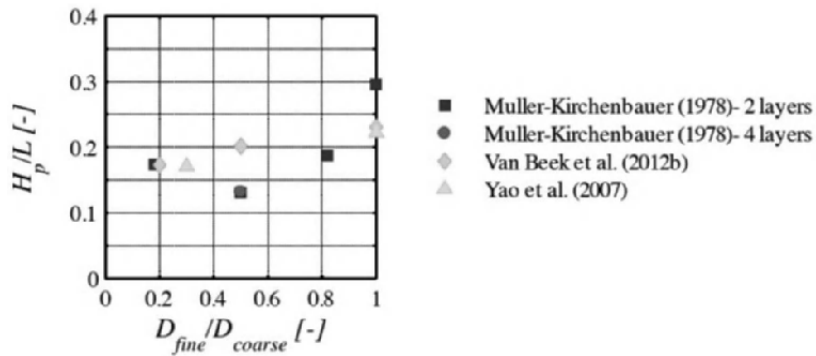


Figure 3.26. Influence of ratio of fine layer thickness and coarse layer thickness on critical head [MUL 78, VAN 12b, DIN 07]

Source	L [m]	D [m]	Exit diameter [m]	d_{60} [mm]	U	d_{60} [mm]	U
[MUL 78]	0.72	0.24	0.006	0.3	2	0.84	1.4
[VAN 12]	0.34	0.10	0.006	0.132*	1.6	0.400*	1.4
[DIN 07]	1.40	0.60	0.04	0.28	3.5	11.4	19

Table 3.6. Overview multilayer experiments (*: d_{50} instead of d_{60})

The experiments confirm the theoretical concepts about the influence of the flow pattern. All variations that result in an increase in flow toward the pipe, such as increase in scale or the presence of a permeable layer below the layer sensitive to erosion, result in a decreased progression gradient. The influence of sand characteristics on the progression gradient has not been studied extensively. This influence is difficult to study as the parameters are correlated and cannot be studied independently.

3.5.3. Progression of pipes for vertical seepage paths

When a vertical structure, such as a cutoff wall, is present in the path of the pipe, the sand downstream of the structure must fluidize, before the pipe can pass. The presence of such a vertical seepage path causes large resistance for pipe development and the overall gradient required to pass a structure is usually higher than the gradients required for the initiation and the progression of the pipe without structure.

In this section, the influence of the type of the vertical structure (cutoff or weir), seepage length and the depth and location of a cutoff are explained using experiments. The type of exit point has not been investigated experimentally in the series with comparable dimensions, although based on theory, small differences in critical gradient may be expected. The effect of sand characteristics and scale have not been studied either. Theoretically the fluidization downstream of the structure is not expected to be influenced by other parameters than porosity and particle density and the flow pattern. However, the flow pattern is not entirely the same at different scales, as the dimensions of the pipe formed up to the structure do not scale, so small differences can be expected in relation to this parameter too.

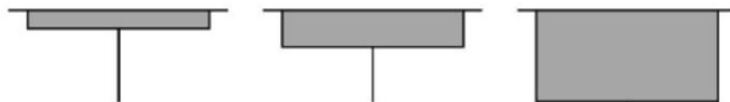


Figure 3.27. *Experimental configurations in relation to type of structure [OKA 10]*

Okajima *et al.* [OKA 10] investigated the type of the vertical structure. In these experiments, a weir with a length of 0.08 m is placed in a sand layer up to different penetration depths, combined with a cutoff. The total depth of the cutoff and the weir is kept constant at 0.05 m, whereas the weir

depth is varied to 0.01, 0.02 and 0.05 m (Figure 3.27). The fine-grained sand is uniform (d_{50} of 0.16 mm and U of 1.46) and prepared so as to have a high relative density of about 85%.

Figure 3.28 shows the gradients required for progression of the pipe in these three configurations. It can be observed that a weir requires a higher critical gradient than the cutoff. This can be contributed to two aspects. First, the flow passing underneath the structure is higher in the case of a cutoff compared to the case of the weir, resulting in higher fluidization gradients downstream of the cutoff. Second, the location of the vertical section (downstream or in the middle) will also influence the critical gradient, as follows from other experiments by Okajima *et al.* [OKA 10].

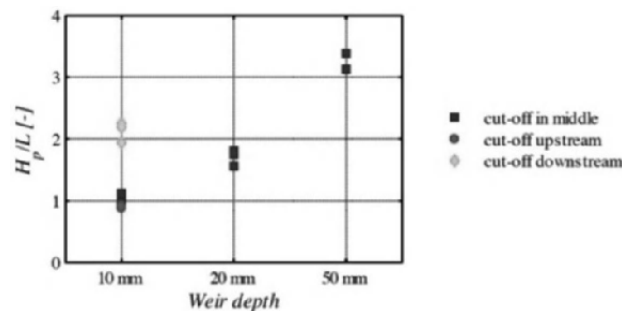


Figure 3.28. Influence of type of structure and location of cutoff [OKA 10]

The influence of the location of the weir is investigated in two additional experiments, with cutoffs placed upstream and downstream, while keeping weir penetration depth constant (10 mm). Indeed, it can be observed that the location of the cutoff influences the critical gradient. Theoretically, this is expected as the head drop in the formed pipe is lower than the head drop in an intact sand layer. When a pipe is formed, most of the head drop across the dike will be dissipated in the seepage path from upstream, level

to pipe. This seepage path is much shorter in the case of an upstream placed cutoff, with a considerable developed pipe, than in the case of a downstream placed cutoff. In the latter case, the expected progression gradient is therefore higher.

Ding *et al.* [DIN 08] also investigated the location of the cutoff in a medium-scale setup on fine sand (Table 3.6). A cutoff wall with penetration depth of 0.06 m was placed at 0.35 m (upstream), 1.05 m (downstream) and 1.25 m (downstream) from the upstream level. In Figure 3.29, the results by Ding *et al.* [DIN 08] and Okajima *et al.* [OKA 10] are combined, all showing a decrease in the progression gradient when the cutoff is moved toward the upstream side.

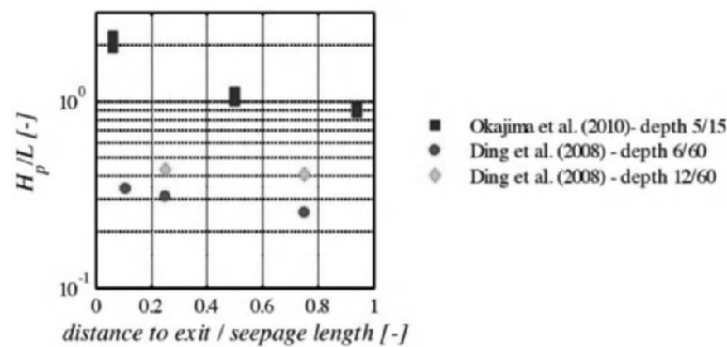


Figure 3.29. Influence of cutoff location on progression gradient [DIN 08, OKA 10]

The penetration depth of the cutoff is investigated by Ding *et al.* [DIN 08] and Van den Ham [VAN 09]. Ding *et al.* varied the penetration depth to 0.06, 0.12 and 0.18 m, maintaining a total depth of 0.6 m. Van den Ham studied the progression gradient in a small-scale setup (seepage length of about 0.35 m) with slope-type exit. The cutoff depth was varied between 0.01 and 0.02 m over a total depth of 0.1 m. Theoretically, the influence of the penetration depth is of great influence, as the vertical distance across which fluidization must take place increases with penetration

depth. In addition, with an increase in the penetration depth, the gap between the cutoff and the sand layer bottom decreases, resulting in a slight decrease in flow. The latter aspect is expected to be of minor importance though. The experiments confirm these theoretical considerations as, indeed, a significant increase in the gradient is observed with increasing penetration depth (Figure 3.30). It follows from this figure that critical gradients obtained in the small-scale setup by Van den Ham are much higher than gradients obtained in the medium-scale setup by Ding *et al.* The cause of this difference is not entirely clear. As the main differences between the two series are of the exit type and scale, it is possible that these characteristics indeed influence the critical gradient.

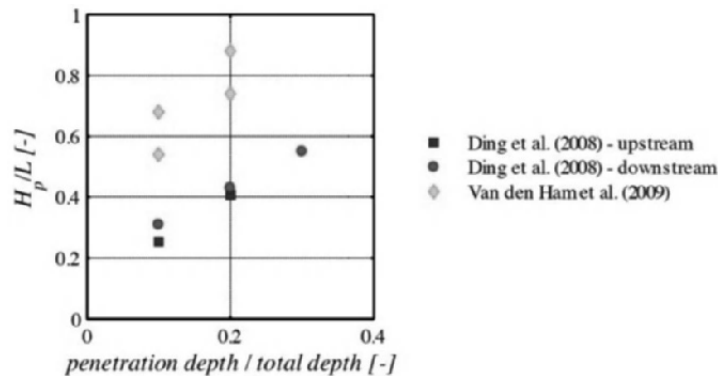


Figure 3.30. Influence of cutoff penetration depth on progression gradient [DIN 08, HAM 09]

The influence of seepage length is investigated by Okajima and Tanaka [OKA 08]. The setup and sand characteristics are similar to that used in Okajima *et al.* [OKA 10]. For a weir penetration depth of about 0.05 m, several seepage lengths have been investigated. An increase in critical gradient is expected with decreasing seepage lengths, as the contribution of the resistance supplied by the vertical section increases with decreasing seepage length.

This is confirmed by the experiments, as can be seen in Figure 3.31.

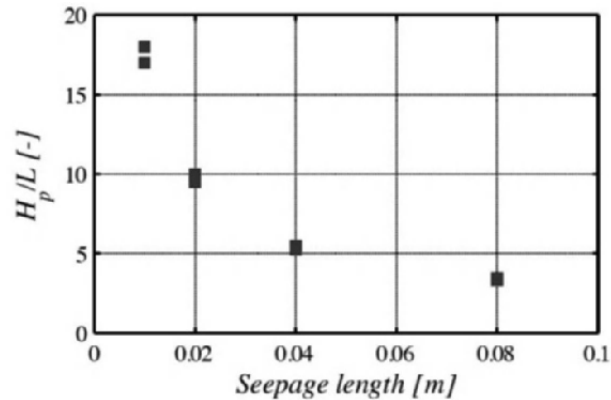


Figure 3.31. Influence of seepage length on critical gradient [OKA 08]

Achmus and Mansour [ACH 06] investigated the influence of the sand layer depth, while retaining a constant penetration depth. For this purpose, the setup displayed in Figure 3.11 is used, with a seepage length of 0.3 m and sand layer thickness of 0.10, 0.15, 0.20 and 0.25 m. The total penetration depth of cutoff and weir is 0.061 m. When increasing the sand layer thickness, the flow passing underneath the structure is increased, resulting in higher vertical gradients behind the structure. Some influence on the progression gradient is therefore expected. In Figure 3.32, the experiments show a small decrease in the critical gradient with the increasing sand layer thickness. The relative density, which is also investigated in this experimental series, has a more pronounced influence: for a loose-to-medium prepared sample (RD = 33%), the critical gradient is much lower than for dense sample (RD = 88%).

In summary, the critical gradient required for passing a structure can be mainly explained by the flow pattern through the sand. Passing the structure requires fluidization

at the downstream side of the structure and the local vertical gradient at this location is dependent on the flow from the upstream to the downstream area. The influence of the structure type, cutoff location, the sand layer thickness and seepage length on the critical gradient can be explained quantitatively by this theory. The influence of porosity on the critical gradient is significant and can be related to the corresponding local gradient for fluidization downstream of the structure. More research is required to understand the influence of the scale and the exit type on the critical gradient.

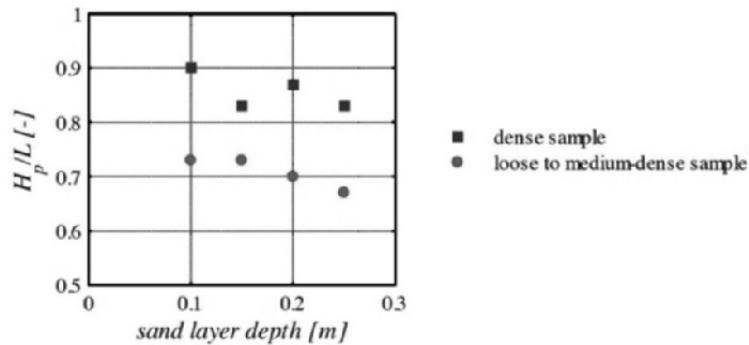


Figure 3.32. Influence of sand layer depth [ACH 06]

3.6. Analysis tools

From the results of the experiments, it can be concluded that several parameters determine the final critical gradient for the progression of the pipe: the type of process, the scale of the setup, the configuration of the setup, the presence of a vertical structure, the sand type (the grain size, permeability and the grain size distribution) and the relative density of the sand layer. The influence of heterogeneity is not even investigated in detail. It is not possible to create a setup in the laboratory that directly represents in situ problems, because of the scale effects. The development of prediction models describing the phenomena is therefore of utmost

importance for analysis of backward erosion piping. Experiments are used for validation of these models, rather than for the prediction of backward erosion of specific field situations.

Several models and empirical relations are available to predict the occurrence of backward erosion. Bligh's empirical rule [BLI 10] and Sellmeijer's rule [SEL 88] are the most recognized. The rule of Lane [LAN 35] is in use for levees containing a vertical structure. The critical gradient for levees with structures can also be determined using the criterion by Terzaghi and Peck [TER 67].

In section 3.6.1, the criteria are discussed for the initiation of a pipe, the progression of the pipe and to determine the critical head of a structure.

3.6.1. *Initiation of the pipe*

The initiation of a pipe involves the onset of movement of a group of particles in an intact sand layer, due to which a pipe is formed. The onset is caused by the fluidization of a local area near the exit. Although no criteria exists for the initiation of a pipe, the process can be explained physically.

Fluidization of the sand bed will occur when the water flow counterbalances the weight of the grains, such that the effective stresses are reduced to zero:

$$i_{c,loc} = \frac{(1-n)(\gamma_p - \gamma_w)}{\gamma_w} \text{ (local critical gradient)} \quad [3.2]$$

where n is the porosity and γ_p and γ_w are the unit weight of particles and water, respectively.

For a sloping exit, the fluidization of grains as a result of the outward flow occurs at a lower local gradient. Although several researchers have studied the onset of motion of

grains as a result of a flow parallel to the slope, only a few have considered the onset of grains as a result of outward flow perpendicular to the slope. Van Rhee and Bezuijen [VAN 92] suggest two approaches for the onset of grain transport as a result of a water flow perpendicular to the slope: a continuum approach and a single-particle approach. The continuum approach, which involves the fluidization of a group of particles, agrees best with the experiments. A single grain will not be transported easily, as the flow velocity will decrease once the grain has detached itself from the sample and the grain will be deposited in the sample again. This research resulted in the following equation:

$$i_{c,loc} = \frac{(1-n)(\gamma_p - \gamma_w) \sin(\phi - \beta)}{\gamma_w \sin(\phi)} \text{ (local critical gradient, sloping exit) [3.3]}$$

where ϕ is the friction angle and β is the slope angle.

These criteria are derived for unidirectional flow; however, for backward erosion experiments, the flow velocity is not equal at every location. Figure 3.33 shows the flow velocity near a plane-type exit as a function of distance from the levee toe. As the exit point is a singularity, theoretically the velocity will become infinitely high. In reality, the flow is restricted by the size of the grains. A precise way to determine the local exit gradient is to use analytical formulas.

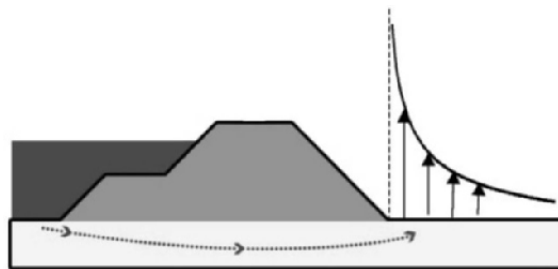


Figure 3.33. Flow velocity as a function of distance from levee toe for a plane-type exit

25 – 50 times the d_{50} . Fluctuations in dx are caused by scatter in the critical gradients obtained in experiments.

Scale effects can, therefore, be contributed for the translation of local gradient into overall gradient and are caused by the need for a certain group of grains to be transported to initiate a pipe, which is constant, regardless of the scale. For a large setup, this group of grains is situated close to the singularity, whereas for a small setup the same group of grains is situated at a relatively large distance from the singularity. In the latter case, a higher overall gradient is required to reach the local critical gradient for this specific group of grains. This scale effect is also illustrated by Bezuijen and Steedman [BEZ 10], in which the relation between grain size, length of the structure and exit gradient is analytically determined for a flow through a semi-infinite aquifer, covered by a levee. According to Polubarinova [POL 62], the exit velocity downstream of the dam can be calculated as:

$$v = \frac{kH}{\pi\sqrt{x^2 - b^2}} \text{ (exit velocity)} \quad [3.4]$$

where x is the horizontal distance from the center of the dam and b is equal to half of the seepage length. The local exit gradient at distance dx from the dam toe was found to be related to the overall gradient (H/L) by the following equation, indicating the scale effect:

$$i_{loc} = 2 \frac{H}{L\pi} \sqrt{\frac{L}{dx}} \quad [3.5]$$

This result would indicate that H/L scales with the square root of the length scale for semi-infinite aquifers.

3.6.2. Progression of the pipe

As observed in experiments, the larger the scale, the more likely it will be that progression of backward erosion becomes the dominant failure mechanism (Figure 3.17). Several models exist for the prediction of progression of the pipe. In this section, analysis tools for pipe progression for dams and dikes without vertical structures are discussed.

The empirical rule of Bligh is based on experience with weirs in India and relates the maximum allowable critical gradient to the characteristics of sand by a creep coefficient:

$$\frac{H_c}{L} = \frac{1}{C_{creep}} \quad [3.6]$$

The rule of Bligh does not take into account any differences in geometry of the sandy foundations and has proven to be unsafe in some situations, when compared to the model of Sellmeijer [VRI 10]. Due to the fact that the scale effect for the seepage length is not included and due to the lack of physical background, the rule showed significant and systematic deviations with the results of laboratory experiments.

The model of Sellmeijer [SEL 88] is more advanced, as it includes the physical processes related to progression of the pipe, such as pipe flow, grain equilibrium and groundwater flow. The 2D model predicts the critical gradient across a dike, underlain by a sandy layer, as a function of the geometrical parameters and the characteristics of the sand: the length of the seepage path, the thickness of the sand layer, the grain size (characterized by d_{70}), the intrinsic permeability and some morphological properties, defining the resistance of the sand grains against rolling in the pipe. The model of Sellmeijer was validated using large-scale tests [SIL 91] and a design rule was derived for a standard levee

configuration [WEI 93], which has been included in the Dutch guidelines [TAW 99]. The model has been implemented in a 2D numerical groundwater flow program [SEL 06].

The model of Sellmeijer is based on several processes. The basic criterion for the progression of a pipe development is the equilibrium of the grains at the bottom of the pipe. It is assumed that erosion at the bottom of the pipe (secondary erosion) will induce erosion at the head of the pipe (primary erosion).

The onset of grain movement is studied by many authors. Sellmeijer chose to apply the criterion by White for the onset of grain movement that is based on the equilibrium of forces that are exerted on a single grain in the laminar regime [WHI 40]. The shear stress is given by equation [3.1]. Based on the validating experiments, a safe value for $\alpha\eta$ is chosen to be 0.25 and is simplified to the Whites constant η .

The shear stress is exerted by the water that flows through the pipe, defined as $\tau = \gamma_w ap / 2$, in which a is the depth of the pipe and p the horizontal pressure gradient in the pipe. Due to the small dimensions of the pipe, the flow through the pipe is laminar. As the model is 2D, the pipe is assumed to be of infinite width. The relation between the flow through the pipe, the head drop and the height of the pipe is therefore determined by the Poiseuille equation for parallel plates [SEL 11].

The amount of water that flows toward the pipe is determined by 2D laminar seepage flow through the aquifer, determined by Darcy's law.

In the model, it is assumed that both the flow in the pipe and the flow through the aquifer toward the pipe are 2D, mainly because that allows for a semi-analytical solution of the equations for the boundary conditions during piping.

Although in reality, pipes are finite in width, several researchers have indicated that a pattern of parallel pipes is formed [SIL 91, VAN 11]. This validates the assumption for 2D flow toward the pipes to some extent. The width of the pipe is also known to be considerably larger (millimeters to centimeters) than the depth of the pipe (generally estimated to be approximately several times the grain size), which makes the use of equations for flow between parallel plates acceptable.

However, when the exit is circular, resulting in a 3D flow pattern toward the exit, 2D approaches are no longer valid. The 2D flow pattern toward the exit increases the flow toward the pipe and critical gradients can be lower than predicted by 2D models, at least at the laboratory scale [VAN 12].

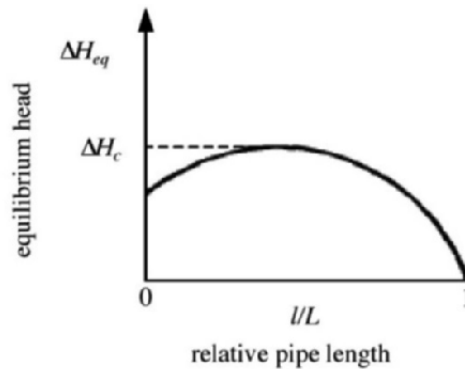


Figure 3.35. Equilibrium head as a function of relative pipe length [TAW 99]

By combining the equations for grain equilibrium, flow through the pipe and the flow through the aquifer, for a given pipe length, the head fall can be determined at which the grains in the pipe are in equilibrium. By doing this for each pipe length, a graph similar to Figure 3.35 is obtained. The maximum head drop at which the equilibrium can occur

is reached at less than $\frac{1}{2}$ of the seepage length, starting at $\frac{1}{2}$ in case of an infinite thick layer and decreasing with decreasing aquifer thickness. This maximum value is denoted as the critical head for progression.

The numerical implementation of the model into a groundwater flow model allows for the prediction of the critical head in all kinds of configurations [SEL 06]. For standard configurations as shown in Figure 3.36, a calculation rule has been developed, based on a curve fit of a large number of computations. Large-scale experiments were performed to validate the model [SIL 91]. The bedding angle was used as a calibration factor and was established at 37° .

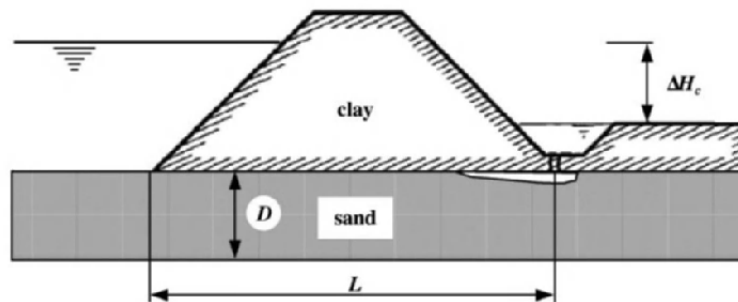


Figure 3.36. Standard dike configuration [TAW 99]

Based on these concepts, Sellmeijer proposed a conceptual model, resulting in a piping rule [SEL 88, SEL 91]. The model covers three essential areas: groundwater flow through the subsoil, pipe flow through the erosion channel and limit equilibrium of sand particles at the bottom of the channel. For the single particle force balance for a grain at the bottom of the erosion channel, four distinct forces are considered. The horizontal forces are the drag force due to the channel flow and the horizontal flow force. The vertical forces are the weight of a particle and the vertical flow force.

The rule is derived by numerical fitting and can be written as [SEL 11]:

$$\frac{H_c}{L} = F_R F_S F_G \quad [3.7]$$

$$F_R = \eta \left(\frac{\gamma_p}{\gamma_w} - 1 \right) \tan \theta \quad (\text{resistance factor, rolling equilibrium}) \quad [3.8]$$

$$F_S = \frac{d_{70}}{\sqrt[3]{\kappa L}} \quad (\text{scale factor, sand properties}) \quad [3.9]$$

$$F_G = 0.91 \left(\frac{D}{L} \right)^{\frac{0.24}{\left(\frac{D}{L} \right)^{2.8} - 1}} \quad (\text{geometrical factor, shape}) \quad [3.10]$$

where η is the Whites constant [-], γ_p is the unit weight of particles [kN/m³], γ_w is the unit weight of water [kN/m³], θ is the bedding angle, d_{70} is the sand diameter at 70% passing [m], κ is the intrinsic permeability [m²], L is the dike width [m] and D is the aquifer thickness [m].

In the above-mentioned equations, the critical gradient is determined by three components, F_R , F_S and F_G , indicating resistance, scale and geometry. The resistance factor is related to the equilibrium of forces, the scale factor is related to the ratio of the grain size and the seepage length and the geometry factor is related to the influence of the aquifer shape on the groundwater flow. The geometry factor is obtained from a curve fit of a collection of computations for different geometries. Such a curve fit is matched as accurate as possible to the calculated range. Recently, it appeared that far away from that range an undesired singularity was introduced using the equation described in Sellmeijer *et al.* [SEL 11]. Though such geometries are not to be expected, it is always better to remove such inconveniences. Therefore, a

slight adaptation is embraced, which hardly affects the original computations, but did remove the singularity.

A recent validation study has shown that the original model overestimates the strength of levees on coarse sand. An adaptation has been made using multivariate analysis of small-scale experiments. The adaptation concerns the grain size mostly. The backward erosion piping rule is modified with respect to the resistance factor and the scale factor. The empirically adapted rule for standard dike geometry is [SEL 11]:

$$F_R = \eta \left(\frac{\gamma_p}{\gamma_w} - 1 \right) \tan \theta \left(\frac{RD}{RD_m} \right)^{0.35} \left(\frac{U}{U_m} \right)^{0.13} \left(\frac{KAS}{KAS_m} \right)^{-0.02} \quad [3.11]$$

$$F_S = \frac{d_{70}}{\sqrt[3]{\kappa L}} \left(\frac{d_{70m}}{d_{70}} \right)^{0.6} \quad [3.12]$$

where RD [%] is the relative sand density, U [-] is the sand uniformity (d_{60}/d_{10}), KAS [%] is the roundness of particles and the subscript m denotes the average value of the calibration experiments (resulting in $d_{70m} = 208 \times 10^{-6}$ m, $RD_m = 72.5\%$, $U_m = 1.81$, $KAS_m = 50\%$).

It is noted that these small-scale experiments were designed for the validation of Sellmeijer's model, but were found out later to be dominated by the initiation of backward erosion piping, rather than the progression. However, large-scale experiments in which progression was the dominating mechanism also indicate a decreased influence of the grain size.

The fit of the prediction of the model to the results of the large-scale experiments described by Silvis [SIL 91] and Van Beek *et al.* is shown [VAN 11] in Figure 3.37. Despite the adjustment in the calculation rule, which diminishes the

influence of the grain size, the full-scale experiment on coarse sand still shows the largest difference between the predicted and experimentally obtained heads.

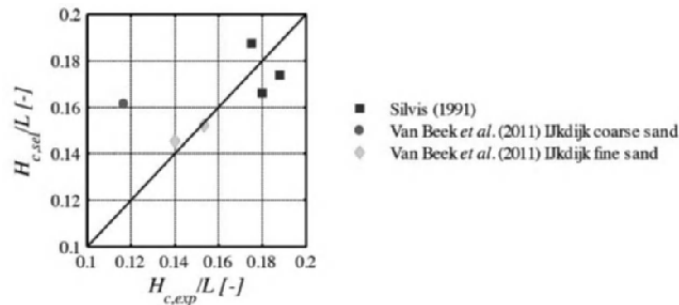


Figure 3.37. Comparison between predicted and experimentally obtained critical heads for large-scale experiments

The geometrical shape factor equation [3.10] is valid only for a sand layer of a constant thickness. More complex geometries can be dealt with by a numerical approach. A numerical computation code, based on the equilibrium of two forces, can be used in order to design against backward erosion piping in arbitrarily composed subsoil [SEL 06].

3.6.3. Progression for structures

The presence of a structure, such as a cutoff wall or a weir, causes an extra barrier for the piping path. Lane [LAN 35] concluded that the presence of a vertical seepage length causes much more resistance than an horizontal seepage length and derived an empirical rule, in which the horizontal and vertical seepage lengths are weighted; in this rule, vertical seepage length weights three times more than horizontal seepage length:

$$H_c = \frac{\frac{1}{3}L_h + L_v}{C_{w,creep}} \quad [3.13]$$

For different soil types, values of creep coefficients are given in [LAN 35].

From observations in experiments, it can, indeed, be deduced that the head to overcome the vertical seepage path is much larger than the head for overcoming horizontal seepage paths; in all observations, the head needs to be increased to pass the vertical seepage length and the pipe grows toward the upstream side afterwards. However, the empirical model of Lane cannot take into account specific details of the configuration that appear to have a large influence on the critical head, such as the location of the cutoff or the difference between a cutoff and a weir. According to Lane, each of the three situations in Figure 3.27 [OKA 08], should have the same critical head, as the vertical and horizontal seepage paths are equal in all experiments. Yet, the experimentally obtained heads vary significantly (up to a factor of three).

A more refined approach, based on an understanding of the phenomena, will therefore lead to more optimized design. To predict the critical head for such water-retaining structures, it suffices to calculate the head that is necessary for the pipe to pass the structure. The piping path can only continue if the particles in the vertical seepage path are transported. For this to happen, the sand downstream of the structure needs to be fluidized. Fluidization of sand is known to occur at a gradient i_c , equation [3.2] at which the effective stresses reduce to zero and is generally approximately one.

Using a 2D numerical model for groundwater flow, the head across the structure can be determined for which the gradient in the vertical path downstream of the structure equals i_c . Downstream of the structure, a pipe is simulated. It is generally assumed that the head drop in the pipe can be neglected.

Figure 3.38 shows the comparison between the experimentally obtained and calculated critical head, using a critical gradient of one. It appears that the applied method is unsafe for some experiments (mainly weirs). However, a proper correlation is observed between the experimentally obtained and calculated critical heads.

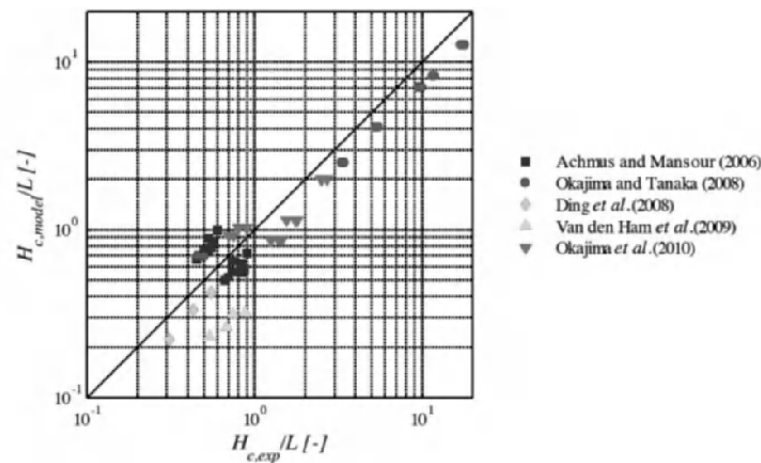


Figure 3.38. Comparison between predicted and experimentally obtained critical gradients for all laboratory experiments with a stru

3.6.4. Summary

Empirical tools for prediction of backward erosion piping, dating from the beginning of previous century, are still used in practice. Understanding of the mechanisms causing the initiation and the progression of pipes, allows for a more refined approach for analysis. Pipe initiation requires fluidization near the exit point. Observed variations in experiments for different scales can be explained by the relation between the local critical gradient and the overall gradient. Progression of the pipe can be predicted using the Sellmeijer model, which includes the equilibrium of forces on the grains in the pipe, flow in the pipe and groundwater flow toward the pipe. When a vertical structure, such as a cutoff

wall or skirt is present, the pipe progression is impeded. Fluidization (or heave) along the downstream side of the structure is necessary to allow for progressive development of the pipe. A decent correlation between the predicted gradient and experimental gradients is obtained using this method.

3.7. From laboratory to field – challenges for the future

Laboratory work for backward erosion piping is performed so to be able to predict the piping phenomenon in the field, in order to design levees and dams in an optimal way and for a reliable safety assessment. As can be derived from the previous sections, the translation from experiment to field is not a matter of using data directly from the experiments, but requires understanding of the physical process. Vice versa, the design of experiments, such that they can be used for validation of models, requires understanding of the mechanisms as well. In this section, some difficulties of the translation from the laboratory to the field are discussed and conclusions are made with respect to the design of experiments and the prediction of backward erosion piping.

3.7.1. Scale effects

An important difference between the laboratory and the field is the scale. Although it is much more convenient to perform small-scale experiments, they cannot directly be translated to the field because of the effects of scale.

When looking at the three main processes that dominate the critical hydraulic head for backward erosion piping (initiation of the pipe, progression of the pipe and passing a vertical seepage path), it can be noted that at least the first two of these processes are subjected to the effects of scale.

This means that the critical gradient changes with the seepage length. For initiation of the pipe, the scale effect is related to the fact that a group of grains needs to be brought to fluidization near the exit point. The local gradient causing the fluidization is determined by the singularity at the exit point. At a larger scale, the flow velocity through this group, when the same overall hydraulic gradient is applied, is higher, because the group of particles is relatively close to the singularity. The critical gradient for initiation therefore decreases with the seepage length. An analytical solution indicates a dependency of $H_c/L \propto 1/\sqrt{L}$, for constant soil properties [BEZ 10].

For the progression of the pipe, the scale effect is related to the dimensions of the pipe. The pipe has more or less the same width and depth dimensions at each scale. The grain transport in the pipe depends on the flow toward the pipe. For a small-scale setup, the flow toward the pipe is relatively small, due to the limited flow area compared to the dimensions of the pipe; a relatively large head is necessary to cause backward erosion piping. The critical gradient for progression therefore decreases with the increasing seepage length (and corresponding depth). The model of Sellmeijer indicates a dependency of $H_c/L \propto 1/\sqrt[3]{L}$, if the shape of the aquifer (D/L) and soil characteristics remain the same. This scale effect is explained by the ratio between geometry and the size of the pores, which is characterized by the ratio of the pore volume and the permeable area. This ratio is quantified by d^3/κ , where κ is the intrinsic permeability, resulting in a scale dependency of $H_c/L \propto d/\sqrt[3]{\kappa L}$.

For the progression of a pipe along a vertical path, based on the theory, no scale effects are expected, although it is an aspect that is not investigated in detail. Some experiments show a significantly larger gradient than predicted by calculation models (e.g. experiments by Van den Ham

[VAN 09]). It is already noted that the flow pattern is not entirely the same for different scales, as the dimensions of the pipe do not increase with an increasing scale. It is possible (although not investigated) that the head loss in the downstream pipe is not negligible at the smaller scale when a small amount of water is transported through the pipes, due to the limited flow area. In the small-scale experiments by Van den Ham [VAN 09], the flow resistance in the downstream pipe contributed significantly to the total head at the critical head, whereas in the calculations this head loss is neglected.

The scale effects are important both for prediction of backward erosion piping in the field and for the designing of experiments. It is important to know beforehand which type of process will be studied in the laboratory and how they represent a field situation. When a dam or levee with a vertical section, such as a cutoff wall will be studied, it is relatively clear: the process of fluidization along the downstream part will be dominant for the critical head at all scales.

For levees without such a structure, it is more complicated. The scale effects for the initiation and the progression of a pipe are similar, but not the same. For relatively small-scale experiments, the head for initiation may exceed the head for the progression of the pipe [VAN 11], but in large-scale experiments, using the same configuration of the head for progression may be dominant. In Figure 3.39, this concept is illustrated by the scale dependence of both processes. It is noted that the point of crossing of the two lines, if any, is determined by the configuration of the setup. For the configuration with a small hole in the cover, progression is nearly always dominant. Also, it is noted that the process of the initiation of the pipe can always be studied, as this process always precedes the progression. However, if a setup is used for which the head

for initiation exceeds the head for progression, the latter cannot be studied, unless the hydraulic head is lowered halfway during the experiment.

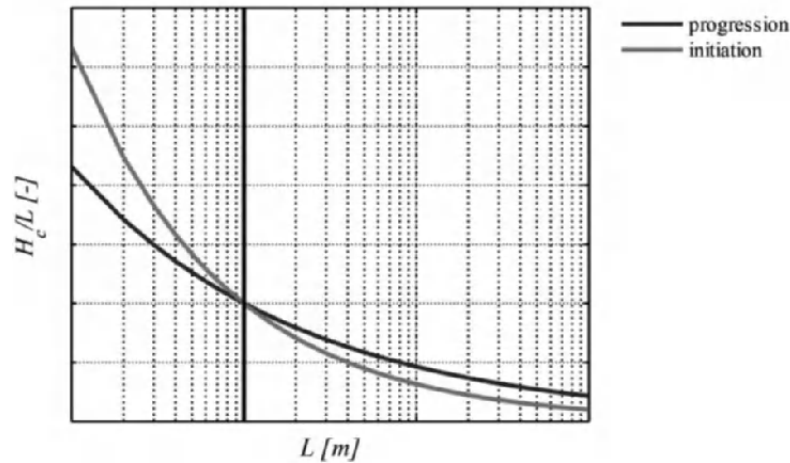


Figure 3.39. Dominance of progresses as a function of scale

3.7.2. Heterogeneity

Another difference between piping in the laboratory and piping in the field is heterogeneity. The prepared sand sample is prepared as homogeneously as possible, whereas in the field, soil characteristics may vary from the microscale to macroscale. The variation in properties on the microscale such as local differences in porosity and the grain size within the sand layer are common. For the prediction of backward erosion piping, these differences are usually taken into account by using conservative values for input parameters. Experimentally, this type of heterogeneity has not been investigated so far.

Heterogeneities at the larger scale, such as the presence of other granular or clay lenses, or different layers, can affect the piping process significantly. A coarse layer underneath a

fine piping-sensitive layer, is known to have a large influence on the critical head (Figures 3.23 and 3.26), mainly as a result of the increased flow toward the pipe. Heterogeneities that only influence the groundwater flow can well be included in calculation models [VAN 12]. The presence of heterogeneities in the path of the pipe, such as clay lenses or coarse granular lenses are more difficult to include. Research by Van Beek *et al.* [VAN 08] shows that the progression of erosion can be significantly restrained by the presence of coarse layers.

3.7.3. Uncertainties

Uncertainty with respect to the geometry and soil properties in the field is another challenge. For laboratory experiments, all parameters are known in great detail. In the field, the available data are often insufficient for detailed analysis. A gradual approach in safety assessment (simple to complex) and a safety philosophy based on probabilism aids in overcoming this issue [FOR 11]. This aspect stresses the need for conservative, yet simple models to be used in the field that do not require a large amount of data as well as more refined models to check the mechanisms that are measured in model tests and for optimized design when more data are available.

The model for prediction of backward erosion piping in levees or dams containing or consisting of a structure does not require a large amount of input data; the geometry of the structure and aquifer in many cases will be sufficient. However, especially for older structures the exact geometry of the structure is often unknown, as well as its functioning. Research by Van den Ham [VAN 09] has shown that if a gap is present in the cutoff wall, the method may not help at all in preventing piping.

3.8. Conclusion

As an overall conclusion on the use of physical modeling for backward erosion piping, it is noted that an understanding of the process is of the utmost importance. A laboratory experiment, although it is a perfect scaled copy of reality, does not give direct answers to piping occurrence for the prototype in reality. Due to scale effects, the critical gradient will be of a different order in small-scale experiments than in practice and a translation is always necessary. Moreover, as a result of different scale effects for the various processes, a different process may occur at the small-scale than at the large-scale. These aspects must be considered in the design of the experiment. This result also means that in small-scale physical model testing where different failure mechanisms are tested, backward erosion is much less likely to occur than in the prototype field situation.

Besides considerations related to scale, the design of backward erosion experiment for the validation of a prediction model can take all kinds of forms; there is no specific device that suits all needs.

So far, experiments have been used to increase understanding of the backward erosion piping process and the safety assessment. Especially for homogeneous and fine sand types, the process appears to be relatively well understood and a proper prediction can be made. Much is still to be done for coarse and well-graded samples and for situations where 3D flow plays an important role.

3.9. Bibliography

- [ACH 06] ACHMUS M., MANSOUR B.G.S., "Considerations and model tests on the design of river barrages with respect to piping", *3rd International Conference on Scour and Erosion*, 1–3 November, Amsterdam, 2006.

- [BEZ 10] BEZUIJEN A. STEEDMAN R.S., “Scaling of hydraulic processes”, *7th International Conference on Physical Modeling in Geotechnics*, 28 June–1 July, Zurich, 2010.
- [BLI 10] BLIGH W.G., “Dams barrages and weirs on porous foundations”, *Engineering News*, vol. 64, no. 26, 1910.
- [CAO 94] CAO D., “Countermeasures for seepage erosion of Yangtze River main dikes”, *Yangtze River*, vol. 25, no. 1, pp. 25–29, 1994.
- [DE 81] DE WIT J.M., SELMEIJER J.B., PENNING A., “Laboratory testing on piping”, *10th International Conference on Soil Mechanics and Foundation Engineering*, 15–19 June, Stockholm, pp. 517–520, 1981.
- [DIN 08] DING L.Q., YAO Q.L., SUN D.Y., “Experimental studies on the seepage control effects of suspended cutoffs in dike foundations”, *4th International Symposium on Flood Defence: Managing Flood Risk, Reliability and Vulnerability*, 6–8 May, Toronto, 2008.
- [DIN 07] DING L., YAO Q., SUN D., LIU C., “Experimental studies on piping development in three-stratum dike foundations”, *Water Resources and Hydropower Engineering*, vol. 38, no. 2, pp. 19–22, 2007.
- [FOR 11] FÖRSTER U., VAN DEN HAM G., CALLE E., *et al.*, SBW piping HP.9 Technisch Rapport Zandmeevoerende wellen, herziene versie 2011, Deltares report 1202123-003, The Netherlands, 2011.
- [GLY 04] GLYNN E., KUSZMAUL J., Prediction of piping erosion along middle Mississippi river levees – an empirical model, US Army Corps of Engineers, Report USACE ERDC/GSL TR-04-12, p. 37, 2004.
- [HAN 85] HANSES U., Zur Mechanik der Entwicklung von Erosionskanälen in geschichtetem Untergrund unter Stauanlagen, University of Berlin, p. 203, 1985.
- [LAN 35] LANE E.W., “Security from under-seepage masonry dams on earth foundations”, *Transactions of the American Society of Civil Engineers*, vol. 100, no. 1, pp. 1235–1272, 1935.
- [MAN 00] MANSUR C.I., POSTOL G., SALLEY J.R., “Performance of relief well systems along Mississippi river levees”, *Journal of Geotechnical and Geoenvironmental Engineering*, vol. 126, no. 8, pp. 727–738, 2000.

- [MIE 78] MIESEL D., *Vorträge der Baugrundtagung*, Deutsche Gesellschaft für Erd- und Grundbau E. V., Berlin, 1978.
- [MUL 78] MÜLLER-KIRCHENBAUER H., *Zum Zeitlichen Verlauf der Rückschreitenden Erosion in Geschichtetem Untergrund unter Dämmen und Stauanlagen*, Beitrag zum Talsperrensymposium, München, 1978.
- [MUL 93] MÜLLER-KIRCHENBAUER H., Rankl M., SCHLÖTZER C., “Mechanism for regressive erosion beneath dams and barrages”, in BRAUNS J., HEIBAUM M., SCHULER U. (eds), *Proceedings Filters in Geotechnical and Hydraulic Engineering*, A.A. Balkema, Rotterdam, pp. 369–376, 1993.
- [OKA 10] OKAJIMA K., MAGARA N., IIDA T., “Reexamination of Creep Theory in the foundation of Weirs by model experiments and elasto-pastic FEM”, *5th International Conference on Scour and Erosion*, 7–10 November, San Francisco, 2010.
- [OKA 08] OKAJIMA K., TANAKA T., “Evaluation of the downstream piping of weirs by model experiments and elasto-plastic FEM”, *4th International Conference on Scour and Erosion*, 5–7 November, Tokyo, pp. 460–467, 2008.
- [PIE 81] PIETRUS T.J., An experimental investigation of hydraulic piping in sand, Master Thesis, University of Florida, 1981.
- [POE 98] POEL J.T. VAN DER, SCHENKEVELD F.M., “A preparation technique for very homogenous sand models and CPT research”, in KIMURA T., KUSAKABE O., TAKEMURA J. (eds), *Proceedings of the International Conference Centrifuge 98*, Balkema, Rotterdam, pp. 149–154, 1998.
- [POL 62] POLUBARINOVA-KOCHINA P.Y.A., *Theory of Groundwater Movement*, (translated from the Russian by J.M. ROGER de WEIST), Princeton University Press, 1962.
- [RIC 08] RICHARDS K.S., REDDY K.R., “Experimental investigation of piping potential in earthen structures”, *Proceedings of GeoCongress 2008*, 9–12 March, Orleans, LA, pp. 367–376, 2008.
- [RIC 10] RICHARDS K.S., REDDY K.R., “True triaxial piping test apparatus for evaluation of piping potential in earth structures”, *Geotechnical Testing Journal*, vol. 33, no. 1, pp. 83–95, 2010.

- [RIE 10] RIETDIJK J., SCHENKEVELD F.M., SCHAMINÉE P.E.L., *et al.*, “The drizzle method for sand sample preparation”, *Proceedings of the International Conference on Physical Modelling in Geotechnics (ICPMG)*, 28 June–1 July, Zurich, pp. 267–272, 2010 .
- [SEL 88] SELLMELJER J.B., On the mechanism of piping under impervious structures, PhD Thesis, TU Delft, 1988.
- [SEL 06] SELLMELJER J.B., “Numerical computation of seepage erosion below dams (piping)”, *3rd International Conference on Scour and Erosion*, 1–3 November, Amsterdam, pp. 596–601, 2006.
- [SEL 11] SELLMELJER J.B., LOPEZ DE LA CRUZ J., BEEK V.M. VAN, *et al.*, “Fine-tuning of the piping model through small-scale, medium-scale and IJkdijk experiments”, *European Journal of Environmental and Civil Engineering*, vol. 15, no. 8, pp. 1139–1154, 2011.
- [SHI 36] SHIELDS A., “Anwendung der Ähnlichkeitsmechanik und Turbulenzforschung aut Geschiebewegung”, *EMitteilungen der Preuss. Versuchsanst. f. Wasserbau u. Schiffbau*, Heft 26, Berlin, 1936.
- [SIL 91] SILVIS F., Verificatie piping model; proeven in de Deltagoot, Report GeoDelft, CO317710/7, 1991.
- [TAW 99] TAW, Technical Report on Sand Boils (piping), Technical Advisory Committee on Flood Defences (Technische Adviescommissie voor de Waterkeringen), p. 142, 1999.
- [TER 67] TERZAGHI K., PECK, R.B., *Soil Mechanics in Engineering Practice*, John Wiley & Sons, New York, 1967.
- [TOW 88] TOWNSEND F.C., BLOOMQUIST D., SHIAU J.-M., *et al.*, *Evaluation of Filter Criteria and Thickness for Mitigating Piping in Sand*, Department of Civil Engineering, University of Florida, 1988.
- [VAN 08] VAN BEEK V.M., KOELEWIJN A., KRUSE G., *et al.*, “Piping phenomena in heterogeneous sands, experiments and simulations”, *4th International Conference on Scour and Erosion*, 5–7 November, Tokyo, pp. 453–459, 2008.
- [VAN 09] VAN DEN HAM G.A., SBW Piping Kunstwerken – KW9. Analyse kleine schaalproeven, Deltares rapport 1200675-002-GEO-0001, 2009.

- [VAN 10a] VAN BEEK V.M., BRUJN H.T.J., DE KNOEFF J.G., *et al.*, “Levee failure due to piping: a full-scale experiment”, *5th International Conference on Scour and Erosion*, 7–10 November, San Francisco, 2010.
- [VAN 10b] VAN BEEK V.M., KNOEFF J.G., RIETDIJK J., *et al.*, “Influence of sand characteristics and scale on the piping process—experiments and multivariate analysis”, *7th International Conference on Physical Modeling in Geotechnics*, 28 June–1 July, Zurich, 2010.
- [VAN 11] VAN BEEK V.M., KNOEFF J.G., SELLMELJER J.B., “Observations on the process of backward piping by underseepage in cohesionless soils in small-, medium- and full-scale experiments”, *European Journal of Environmental and Civil Engineering*, vol. 15/8, pp. 1115–1137, 2011.
- [VAN 12a] VAN BEEK V.M., BEZUIJEN A., SCHENKEVELD F.M., “Piping in loose sands – the importance of geometrical fixation of grains”, *2nd International Conference on Physical Modelling in Geotechnics*, Eurofuge 2012, 23–24 April, Delft, 2012.
- [VAN 12b] VAN BEEK V., YAO Q., VAN M., *et al.*, “Validation of Sellmeijer’s model for backward piping under dikes on multiple sand layers”, *6th International Conference on Scour and Erosion*, 29–31 August, Paris, 2012.
- [VAN 92] VAN RHEE C., BEZUIJEN A., “Influence of seepage on stability of sandy slope”, *Journal of Geotechnical Engineering*, vol. 118, no. 8, pp. 1236–1240, 1992.
- [VRI 10] VRIJLING J.K., Piping – realiteit of rekenfout?, Report TAW/ENW TPN100400, Rijkwaterstaat, Waterdienst, The Netherlands, 91 p, 2010.
- [VRI 11] VRIJLING J.K., SCHWECKENDIEK T., KANNING W., “Safety standards of flood defenses”, *International Symposium on Geotechnical Safety and Risk (ISGSR 2011)*, Keynote paper, Munich, June 2011.
- [WEI 93] WEIJERS J.B.A., SELLMELJER J.B., “A new model to deal with the piping mechanism”, in BRAUNS J., HEIBAUM M., SCHULER U., (eds), *Filters in Geotechnical and Hydraulic Engineering*, Balkema, Rotterdam, pp. 349–355, 1993.
- [WHI 40] WHITE C.M., “The equilibrium of grains on the bed of a stream”, *Proceedings Royal Society*, London, no. 174A, pp. 322–338, 1940.

- [YAO 07] YAO Q., DING L., SUN D., *et al.*, “Experimental studies on piping in single- and two-stratum dike foundations”, *Water Resources and Hydropower Engineering*, vol. 38, no. 2, pp. 13–18, 2007.
- [YAO 09] YAO Q., XIE J., SUN D.J., *et al.*, Data Collection of Dike Breach Cases of China, Sino-Dutch Cooperation Project Report, China Institute of Water Resources and Hydropower Research, 2009.
- [ZEE 11] ZEE R.A. VAN DER, Influence of sand characteristics on the piping process, research to the influence of grain size and other sand characteristics on the critical head of piping, Graduation Thesis, TU Delft, 2011.

Chapter 4

Concentrated Leak Erosion

4.1. Introduction

The two most common failure modes of water retaining structures (earth dams, dikes, levees) result from overtopping and internal erosion and piping. The breach due to failure generates a flood wave that propagates downstream the valley below the structure. Historically, the emphasis in dam safety has been on floods and overtopping. However, the statistics of failure of embankment dams indicates that improvement in the understanding of internal erosion and piping is a significant concern of dam engineers.

The term “piping” is usually applied to a process that starts at the exit point of seepage, and in which, a continuous tunnel or pipe is developed in the soil by backward piping erosion (Chapter 3), and enlarged by concentrated leak erosion. However, this concentrated leak can also be the next phase, after suffusion (see Chapter 1) or contact erosion (Chapter 2). Finally, this concentrated leak can also be ascribed to cracks or pre-existing defects. These pre-existing defects are often caused by tensile cracks or

hydraulic fracture caused by differential settlements during and after construction, adjacent to conduits and walls. These pre-existing defects may also be due to animal burrows and tree roots.

A concentrated leak with erosion is driven by flow in the cracks or other openings. This phenomenon must not be confused with backward erosion (Chapter 3).

Backward erosion, which is driven by a seepage flow within the soil matrix, was introduced by Terzaghi under the name of *Hydraulic piping* and is called *Renard* by the French-Speaking community. This is why we shall call this phenomenon “pipe flow with erosion” or “concentrated leak with erosion”, and we will advise against the use of the terms “renard” or “piping”.

The phenomenon of pipe flow with erosion actually represents the final stage mechanism of concentrated leak erosion, the one leading to failure. The pipe flow is driven by a difference of pressure between the pipe entrance (upstream) and the pipe exit (downstream). This pipe flow erodes the surrounding soil, leading to the increase in the pipe diameter. Figures 4.1 and 4.2 show two cases of failure by concentrated leak erosion in France.



Figure 4.1. *Saint-Julien des Landes dam built in 1969 (France), concentrated leak erosion occurred during first filling: a) general view of the upstream slope and b) close up view of the pipe*



Figure 4.2. *Les Ouches dam built in the 18th Century (France), concentrated leak erosion occurred two centuries after construction in 2001: a) general view and b) close up view of the pipe*

Evaluating the erodibility of a soil, both in terms of the threshold of erosion (initiation) and the rate of erosion (progression), is critical when evaluating the safety of a water retaining structure. Different soils erode at different rates. However, the relationship between the erosion parameters and the geotechnical and chemical properties of the soils remains only partially understood (Chapter 5), and testing is necessary. The most common testing procedure used to evaluate the erodibility of a soil subjected to a concentrated leak is the hole erosion test (HET).

The HET appears to be an efficient and simple means of quantifying the erosion parameters. The experience acquired on several hundred tests on numerous soils has confirmed what an excellent tool this test can be for quantifying the coefficient of erosion corresponding to the rate of erosion, and for finding the critical shear stress corresponding to threshold of erosion.

When a concentrated leak is suspected of being likely to occur or has already been detected *in situ*, the rate of development has been difficult to predict.

There are two issues:

- the time from when a concentrated leak may be observed to when the crest of the dam or levee is first breached;
- the rate at which the breach develops by widening and deepening and the resulting flood hydrograph.

In a growing number of cases, the location of population centers near the structure makes prediction of both these breach parameters crucial to the analysis and management of risks. Fell *et al.* [FEL 03, FEL 08] discuss the time from when a concentrated leak may be observed to when the crest of the dam or levee is first breached. The first paper is based on analyses of case data [FEL 03]. The second refines this using the quantification of the rate of erosion using the HET data [FEL 08].

A critical analysis of the existing relationships at that time for estimating the rate at which the breach develops by widening and deepening was presented by Wahl [WAH 98]. These empirical relations are mostly straightforward regression relations that give the breach parameters as a function of various dam and reservoir parameters.

It is questionable whether such relationships related to the reservoir storage, but not related to the rate of erosion, can be expected to accurately estimate breach parameters for piping failure scenarios. However, few investigators have attempted to relate the breach parameters to basic parameters.

Wahl *et al.* [WAH 98], Wahl [WAH 10] and Wahl and Lentz [WAH 11] present more up to date reviews. The most recent developments in this field have increased two-dimensional modeling of the breach outflow flood and its inundation effects, and the development of models that simulate the detailed erosion and breach development

processes of embankments. Two such models are the HR-BREACH model, developed at HR Wallingford [MOH 02], and the SIMBA/WinDAM model, developed at the Agricultural Research Service [HUN 05, TEM 05, TEM 06, HAN 11]. More details on this and more recent models are given by Morris [MOR 11] and Wu [WU 11].

This chapter is dedicated to concentrated leaks with erosion, with emphasis on the experimental characterization in the laboratory of the critical shear stress and the coefficient of concentrated leak erosion, by means of the HET. At the large scale, simplified mechanically based relations relate the time to failure and the peak flow to the two basic parameters of failure, the coefficient of erosion, and the maximum pipe diameter prior to roof collapse. That is up to the time the crest is first breached. The same model is used for the interpretation of HETs, and for dam and levee breaks due to concentrated leak erosion.

4.2. Theoretical background

4.2.1. Assumptions

Let us consider a straight, horizontal and cylindrical pipe with length L and current radius R (initial value R_0). The soil is assumed to be homogeneous, with dry density ρ_d and total density ρ_{soil} . The flow is assumed to be turbulent. We take t to denote the time, V to denote the water velocity in the pipe (initial value V_0), \dot{m} to denote the total (solids + water) surface flux of eroded material at the soil/flow interface during the erosion process and τ_b to denote the shear stress exerted by the flow on the soil. The two parameters on which the erosion law is based are the threshold stress τ_c and the coefficient of erosion C_e .

A model for pipe flow with erosion analysis was developed on the basis of the equations of two-phase flow with erosion [BON 12a, LAC 08]. It was shown that the product of the

coefficient of erosion and the flow velocity, the erosion number $C_e V$, is a significant dimensionless number. When this number is small, the kinetic of the erosion is low, and the concentration does not have any influence on the flow. This situation covers the main part of the available test results.

We assume that the erosion number is small and the erosion kinetics is weak. If the system is such that the eroded particles do not accumulate in the flow, but are well transported, then the maximum concentration is at the eroded wall. It was found theoretically and experimentally that this maximum volume concentration is below 10^{-4} . We can then make the assumption of diluted flow. This means, in particular, that the presence of solid particles in the flow does not influence either the density, the viscosity or the turbulence.

4.2.2. *The model for pipe flow with erosion*

The model was developed on the basis of the integrated reduced Navier-Stokes/Prandtl equations with erosion [BON 08, LAC 08]. The enlargement of the hole resulting from the erosion has been described in terms of the following set of equations:

$$\dot{m} = \rho_{soil} \frac{dR}{dt} \text{ (mass jump equation on the interface)} \quad [4.1]$$

$$\rho_w \frac{R}{2} \frac{dV}{dt} + V\dot{m} = \frac{R}{R_0} P - \tau_b \text{ (momentum equation)} \quad [4.2]$$

$$\frac{dR}{dt} = \begin{cases} \frac{C_e}{\rho_d} (\tau_b - \tau_c) & \text{if } \tau_b > \tau_c \\ 0 & \text{otherwise} \end{cases} \text{ (erosion law)} \quad [4.3]$$

$$\tau_b = \rho_w f_b V^2 \text{ (turbulent flow)} \quad [4.4]$$

The quantity dV/dt in the left-hand side of equation [4.2] accounts for some transitory effect. This term can be neglected in the laboratory, where we assumed low kinetics of the erosion ($C_e V \ll 1$, which means in practical terms that $C_e V < 0.01$). The erosion time scale is greater than the flow time scale, and the flow can be considered as steady. However, if the boundary conditions show rapid variations (e.g. on site, due to the reservoir level evolution or due to the river level evolution), this term should be considered.

The quantity $V\dot{m}$ in the left-hand side of equation [4.2] is the contribution of the moving wall to the momentum balance. In the laboratory, this term can be neglected, where we assumed low kinetics of erosion ($C_e V \ll 1$): the erosion velocity is lower than the flow velocity, and the fact that the wall is moving slowly does not affect the flow. On site, this term must be considered to account for the large-scale effect (a greater velocity, a greater coefficient of erosion). This is an erosion momentum loss.

The driving pressure P in the pipe (initial value P_0) is:

$$P = \frac{R_0 \Delta p}{2L} \text{ (driving pressure)} \quad [4.5]$$

where $\Delta p(t) = p_{in}(t) - p_{out}(t)$ is the pressure drop in the pipe over the length L , and p_{in} and p_{out} are the input and output pressures, in the pipe, respectively ($p_{in} > p_{out}$).

The Reynolds number is $Re = 2RV/\nu$, where ν is the kinematic viscosity of water (10^{-6} m²/s). The flow velocity must be greater than $\sqrt{\tau_c / \rho_w f_b}$ to trigger erosion. Assuming that flow is laminar if the Reynolds number is smaller than $Re^* = 2,500$, the flow is laminar when $\tau_c < \rho_w f_b (\nu R_c^* / 2R)^2$. Considering the initial hole in the specimen of a HET $R = 3$ mm, and taking $f_b \approx 0.005$, the flow is laminar

if $\tau_c < 1$ Pa. In most of the cases, the critical stress is greater than a few pascals. The flow condition can therefore be considered as turbulent.

4.2.3. The singular head loss factor

The pressure in the pipe itself is not easily accessible to measurement. Let us introduce Δp_T to denote the total pressure drop from a point located before the entrance of the pipe and a point located after the exit of the pipe (Figure 4.3). Let us take k_{in} to denote the entrance singular head loss coefficient, corresponding to the section sharpening of the pipe inlet, and k_{out} to denote the exit singular head loss coefficient, corresponding to the section expansion of the pipe outlet. The pressure drop in the pipe is related to the total pressure drop as follows:

$$\Delta p = \Delta p_T - \frac{1}{2} k \rho_w V^2, k = k_{in} + k_{out} \quad [4.6]$$

The head loss coefficients k_{in} and k_{out} depend on the pipe radius and the geometry of the system (see e.g. [HAU 08]).

The way in how these singular head loss affect the system can be shown by rewriting the pressure drop in the pipe as a function of the total pressure drop as follows:

$$\Delta p = \alpha \Delta p_T \quad [4.7]$$

where α is the head loss factor accounting for the singular pressure loss at the pipe entrance and exit.

$$\alpha = \left(1 + \frac{kR}{4Lf_b} \right)^{-1} \text{ (head loss factor)} \quad [4.8]$$

As k , R , L and f_b can vary with time, the singular head loss factor α is not constant. Moreover, this factor accounts for the scale effect, as it depends on the system considered, and cannot take the same value at the laboratory and on site.

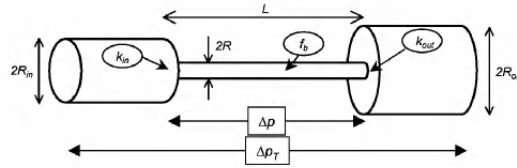


Figure 4.3. Example of singular head loss at the entrance and exit of a pipe

4.2.4. The momentum loss factor

The way of how the erosion momentum loss affects the system can be shown by rewriting the tangential stress and the radius rate as follows:

$$\tau = \beta \frac{R}{2} \left(\frac{\alpha \Delta p_T}{L} - \rho_w \frac{dV}{dt} \right) + (1 - \beta) \tau_c \tag{4.9}$$

$$\frac{dR}{dt} = \frac{\beta C_e}{\rho_d} \left[\frac{R}{2} \left(\frac{\alpha \Delta p_T}{L} - \rho_w \frac{dV}{dt} \right) - \tau_c \right] \tag{4.10}$$

where β is the momentum loss factor accounting for the quantity $V\dot{m}$ in the right-hand side of equation [4.2].

$$\beta = \left(1 + \alpha C_e V \frac{\rho_{soil}}{\rho_d} \right)^{-1} \text{ (momentum loss factor)} \tag{4.11}$$

As α and V vary with time, β is not constant. This factor depends on the system considered and accounts for the scale effect. It cannot take the same value at the laboratory and on site.

4.2.5. Characteristic values

The nonlinear system equations [4.1] – [4.6] will be useful as a basis of a dam break or a levee break model. It can be accurately calculated using numerical solvers. In addition, the above hypotheses are somewhat basic and can be eliminated one after the other, making the model increasingly complex.

However, a simplified description leads to a better understanding of the process and the relevant scaling processes, and some simplifications are both physically acceptable and expedient. A crude but effective assumption is simply that the loss factors α and β are constants. Characteristic values are necessary here. They can be said to be typically of the order of magnitude of a variable in the volume range and the time span considered. As usual, these values are introduced by performing phenomenological analysis. Let us take \bar{R} to denote the reference radius, \bar{L} to denote the reference pipe length, \bar{k} to denote the reference value of the total singular head loss factor, \bar{f}_b to denote the reference friction coefficient and \bar{v} to denote the reference flow velocity.

The reference value $\bar{\alpha}$ of the singular head loss factor is:

$$\bar{\alpha} = \left(1 + \frac{\bar{k} \bar{R}}{4\bar{L} \bar{f}_b} \right)^{-1} \quad [4.12]$$

The reference value $\bar{\beta}$ of the momentum loss factor is:

$$\bar{\beta} = \left(1 + \bar{\alpha} C_e \bar{v} \frac{\rho_{soil}}{\rho_d} \right)^{-1} \quad [4.13]$$

The initial driving pressure P_0 can be obtained as a function of the total pressure drop as follows:

$$P_0 = \frac{R_0 \bar{\alpha} \Delta p_{T0}}{2\bar{L}} \quad [4.14]$$

The reference erosion velocity V_{er} and the characteristic erosion time t_{er} are defined as follows:

$$V_{er} = \frac{C_e P_0}{\rho_d}, t_{er} = \frac{R_0}{V_{er}} \quad [4.15]$$

The characteristic time t_{er} can therefore be obtained as a function of the total pressure drop as follows:

$$t_{er} = \frac{2\rho_d \bar{L}}{\bar{\beta} C_e \bar{\alpha} \Delta p_{T0}} \quad [4.16]$$

4.2.6. Closed-form solution in the case of a constant pressure drop

The use of above equations is extended here for studying the special situation where the total pressure drop Δp_{T0} can be considered as constant. This situation covers the constant-head HETs [RED 00, WAN 04a, LIM 06, HAG 12]. On site, although the pressure drop is likely to decrease with time during the enlargement of the pipe, considering a constant pressure drop is more critical and therefore yields a conservative result.

The velocity and driving pressure are related to the radius as follows: $V/V_0 = (R/R_0)^{1/2}$ and $Q/Q_0 = (R/R_0)^{5/2}$. During the process of erosion, the radius increases, then the velocity and the flow rate increase.

Within the simplified description, where α and β take a constant value, the evolution of the pipe radius during erosion with constant pressure drop obeys an exponential scaling law [BON 12a]:

$$R(t) = R_0 \left[\frac{\tau_c}{P_0} + \left(1 - \frac{\tau_c}{P_0} \right) \exp\left(\frac{t}{t_{er}} \right) \right] \text{ for } P_0 \geq \tau_c \text{ and } t \geq 0 \quad [4.17]$$

4.2.7. Closed-form solution in the case of a constant flow rate

HETs can also be performed with a constant flow rate (value Q_0) [LEF 85, ROH 86, BEN 12b]. For the sake of simplicity, we still assume that the loss factors α and β are constants. The velocity and driving pressure are this time related to the radius as follows: $V/V_0 = (R_0/R)^2$ and $P/P_0 = (R_0/R)^5$. During the process of erosion, the radius increases, then the velocity and the pressure drop decrease.

Within this simplified description, where α and β take a constant value, the evolution of the pipe radius during erosion with constant flow rate is as follows [BON 12a]:

$$t = t_{er} \left(\frac{\tau_c}{P_0} \right)^{-5/4} \left\{ f \left[\frac{R}{R_0} \left(\frac{\tau_c}{P_0} \right)^{1/4} \right] - f \left[\left(\frac{\tau_c}{P_0} \right)^{1/4} \right] \right\} \text{ for } P_0 \geq \tau_c \text{ and } R \geq R_0 \quad [4.18]$$

$$f(x) = \frac{1}{2} (\text{atan } x + \text{atanh } x) - x \quad [4.19]$$

If $\tau_c \neq 0$, the asymptotic value of the radius at equilibrium will be defined by the critical stress, as:

$$\lim_{t \rightarrow \infty} R = R_0 \left(\frac{P_0}{\tau_c} \right)^{1/4} \text{ if } P_0 > \tau_c \quad [4.20]$$

If $\tau_c = 0$, there is no asymptotic value of the radius and equation [4.18] simplifies to:

$$t = \frac{t_{er}}{5} \left[\left(\frac{R}{R_0} \right)^5 - 1 \right] \quad [4.21]$$

4.3. The HET: testing procedure

The HET has recently been developed by Wan and Fell [WAN 02, WAN 04a, WAN 04b] as a simple methodology to measure the erosion rate of clay soils. Numerous tests are nowadays currently performed in several countries in relation to embankment dam projects and to dikes and levees projects, namely throughout Australia, the United States and France [LIM 06, FAR 07, WAH 08, COU 09]. The majority of these tests have indicated consistent and repeatable results in measuring the erosion rate of compacted and natural cohesive soils. Despite its effectiveness and increasing popularity among practicing engineers, a standard for the HET does not yet exist. In general, the testing procedure and the method of analysis adopted for HET is consistent with those described by Wan and Fell [WAN 02], except for a few details as continuous development has been the object of significant investigations [BEN 12a, BEN 12b, HAG 12, LIM 06, LUT 01]. Only some salient features of the nowadays well-documented HET are presented here.

4.3.1. *The HET apparatus*

Wan and Fell [WAN 02, WAN 04a, WAN 04b] used slot erosion and HETs to investigate the erosion resistance of the core material of earth-fill dams. Both tests essentially adopted similar concepts, except that the slot erosion test possessed a longer flow channel. Fourteen different core materials were tested and an “erosion rate index” was introduced to classify and grade the erosion resistance observed. A simplified approach was also proposed to assess the likelihood of internal erosion and piping in embankment dams. A schematic diagram of the equipment is shown in Figure 4.4. The method of analysis adopted by Lim [LIM 06] for HET was similar to the approach proposed by Wan and Fell, except for some details concerning the method of interpretation.

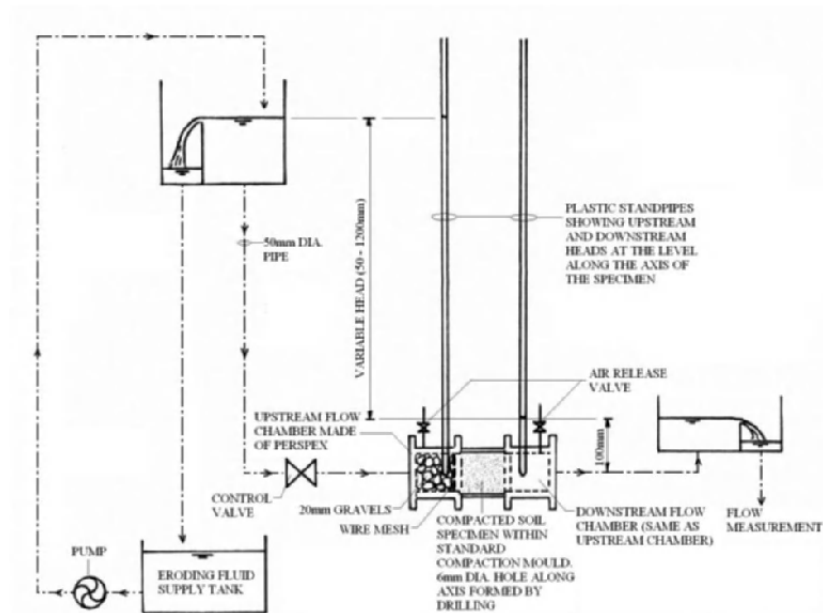


Figure 4.4. Schematic diagram of the hole erosion test apparatus [WAN 02]

Benahmed and Bonelli [BEN 12a] and Benahmed *et al.* [BEN 12b] slightly modified the HET apparatus designed by Wan and Fell. Figure 4.5 shows a photograph of the experimental setup. The cylindrical cell, divided into three parts, is made up of perspex in order to visualize the sample and detect the initiation of the erosion process. The inlet diameter is about 80 mm and the outlet diameter is about 90 mm. The upstream side of the device is connected to the incoming water and pressure regulator. The central part is designed to receive either intact soil samples, or reconstituted soil, in a perspex cylinder or in a Proctor mold. A pressure gauge and a temperature gauge are mounted upstream to measure the inflow pressure and temperature, respectively. A differential pressure gauge is mounted on both extremities of the central cell, upstream and downstream, to measure the pressure drop. The flow rate,

controlled by an outflow vane, is measured by the flow meter on the upstream side of the device. A turbidity meter for analyzing the outflow water and quantify the mass of soil transported during the flow is installed downstream of the cell. A honeycomb is installed inside the cell at its upstream side to homogenize the flow.

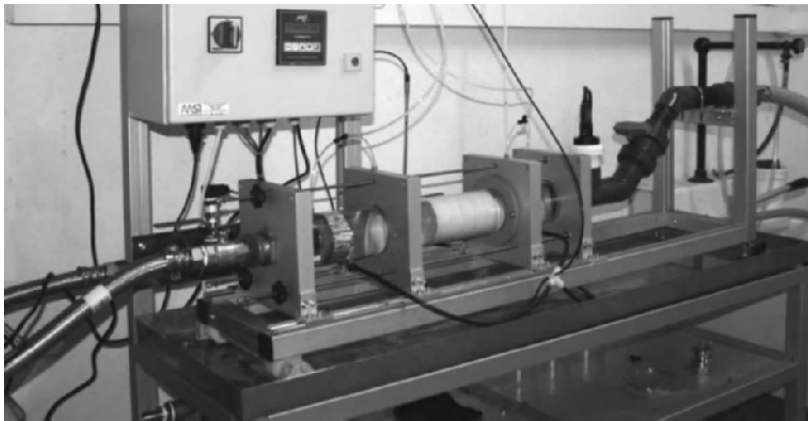


Figure 4.5. Hole erosion test apparatus (Irstea laboratory [BEN 12a])

4.3.2. Preparation of the specimen

Wherever possible, tests shall be carried out on intact or undisturbed good quality cohesive soil, in its natural state. Otherwise, samples shall be reconstituted in the laboratory following the procedure described below.

Prior testing, specific identification tests for classification of soil and determination of its basic physical properties are required: particle size distribution, density (bulk density, dry density and particle density), moisture content and Atterberg limits. This operation could be done with the soil trimming from intact sample.

In cases where the soil is subjected to some disturbance during sampling or transportation, dried because of bad

sealing, and the *in situ* density and moisture content are unknown, tests on remolded samples compacted to the expected compaction density ratio and moisture content are recommended.

4.3.2.1. Remolded sample

Remolded samples are prepared by using the disturbed soil that could not be tested as an intact sample. The soil is cut in small pieces (Figures 4.6(a) and (b)) and mixed together. The particles above 5 mm are removed by hand. The soil is then divided in several equal volume parts, placed uniformly into the testing mold and compacted in layers at fixed and controlled thicknesses to obtain the target density.

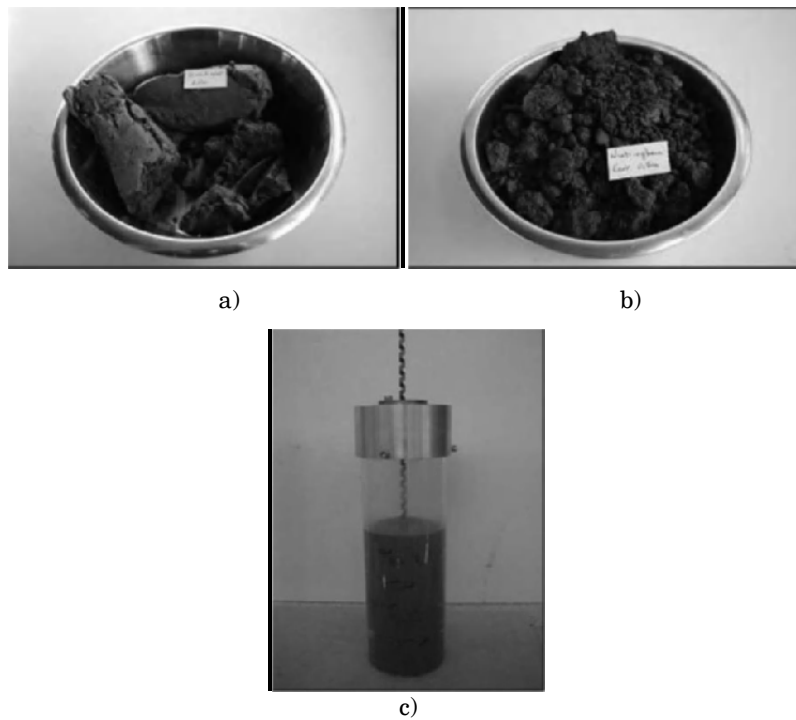


Figure 4.6. Preparation of remolded sample from disturbed soil. a) Disturbed soil; b) cut into small pieces and c) reconstitution by compaction inside the testing mold and drilling the hole

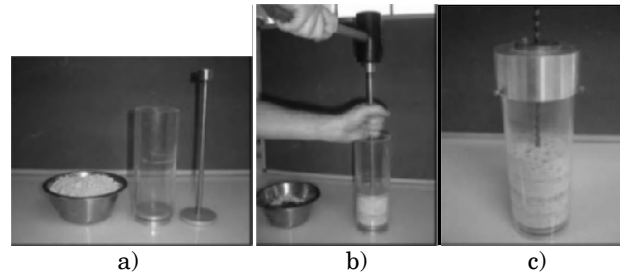


Figure 4.7. Preparation of reconstituted sample from dry soil. a) Preparation of soil by moist tamping; b) reconstitution by compaction inside the testing mold and c) drilling the hole

In the case of using dry soil, water is added to obtain the desired water content, below, equal or above optimum moisture content (OMC) as determined from standard Proctor testing. Usually, 95% of standard Proctor maximum dry density (SMDD) is recommended when assessing internal erosion vulnerability of soil.

The soil is mixed carefully, transferred in watertight plastic bags and stored for 48 – 72 hours, depending on the fines content, to ensure uniform moisture content and homogeneity of the matrix. Then, mixture is compacted manually using Proctor or specific hammer directly inside the testing mold in several layers, depending on the desired length. As above, the height of each layer is predetermined beforehand to obtain the desired density. A 6 mm diameter hole is carefully and slowly drilled through the longitudinal axis of the prepared sample using a power drill.

4.3.2.2. *Intact samples*

The intact soil is first extruded from the borehole tube sample with care to prevent the least disturbance possible. Then, it is cut into sections with a sharp edge to a suitable length and the sample is carefully trimmed to the required diameter using rotational trimming frame. This trimming is accomplished by pressing the wire saw against the edges of

the trimming frame from top to bottom (Figure 4.8). After this stage, dimensions and weight of the sample are measured, and the latter is placed into the testing mold. Sealing with paraffin wax around the soil is necessary to avoid leakage at the interface between the sample and the testing mold. For this, the trimmed diameter shall be less than the testing mold to allow the paraffin wax to go through. A 6 mm diameter hole is carefully and slowly drilled through the longitudinal axis of the prepared sample using a drill rod.

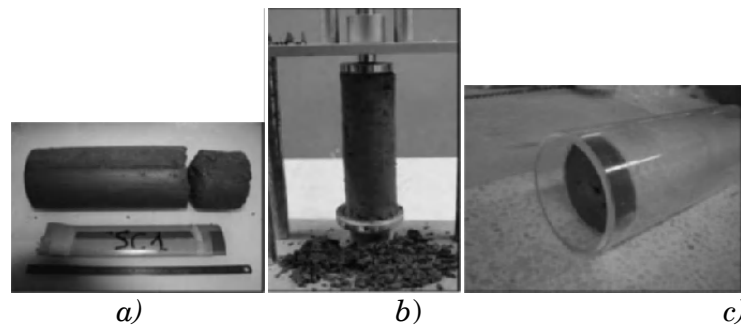


Figure 4.8. Preparation of intact sample. a) Intact core soil; b) trimming of sample in the frame and c) paraffin of the sample into the testing mold to prevent leakage

4.3.3. Determination of the final hole diameter

Correct measurement of the hole diameter after completion of the test is crucial for an accurate estimation of the shear stress equation [4.25], and for an accurate estimation of the friction coefficient equation [4.26]. Lim [LIM 06] measured the hole diameter directly using a caliper or a ruler after splitting the sample into three or more pieces. The average hole diameter is then calculated based on volume averaging the hole over the length of the hole. Another method of estimating the hole diameter is to use a liquid such as paraffin wax to determine the volume of the hole [BEN 12a, BEN 12b]. Figure 4.9 shows several examples of a paraffin wax specimen of the hole after erosion.

4.4. The HET: method of interpretation

A model for the interpretation of the HET, describing a pipe flow with wall erosion, has been initially proposed by Wan and Fell [WAN 02, WAN 04a]. This model has been enriched by Lim [LIM 06] and Bonelli [BON 08, BEN 12b].

The order of magnitude of the flow velocity is below 10 m/s in HETs. This means in practical terms that we can assume low kinetics of erosion ($C_e V < 10^{-2} \ll 1$) when $C_e < 10^{-3}$ s/m. In this case, $\beta = 1$. If the soil tested fall in to the very fast or extremely fast category ($C_e > 10^{-3}$ s/m, Table 5.1 in Chapter 5), the momentum loss factor β , which depends on the head loss factor α , and on the flow velocity, has to be accounted for. This case is not detailed here for conciseness.

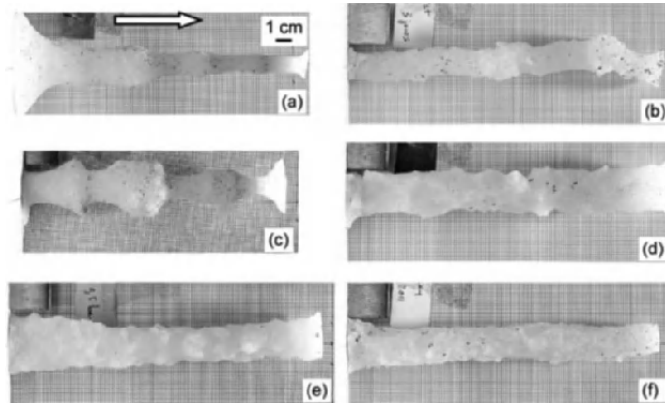


Figure 4.9. Paraffin wax specimen of the hole after erosion, water flows from the left to the right, all pictures have the same scale

4.4.1. Determination of the pipe radius and the wall shear stress

The results of the HETs are always given in terms of the flow rate versus time curve and in terms of the total pressure drop versus time curve, which are the two basic

quantities measured. One of the two may be kept constant while the other varies with time. The flow rate is $Q(t) = \pi R^2(t)V(t)$ (initial value Q_0), where $R(t)$ is the pipe radius (initial value R_0) and $V(t)$ is the average water velocity (initial value V_0). The total pressure drop is $\Delta p_T(t)$ (initial value Δp_{T0}). From equations [4.4], [4.8] and [4.9], the relationship between the total pressure drop and the flow rate is as follows:

$$\frac{\pi^2 R^5(t) \alpha \Delta p_T(t)}{2L \rho_w f_b Q^2(t)} = 1 \quad [4.22]$$

The friction coefficient f_b (initial value f_{b0}) is a variable quantity. The head loss factor α equation [4.12] (initial value α_0) is a function of $R(t)$, the friction coefficient f_b and the total singular head loss coefficient k . The latter is a function of $R(t)$. The pipe length L is assumed here to be constant (L can however vary if slaking occurs).

This relationship can be rewritten as a function of initial values as follows:

$$\left(\frac{\alpha \Delta p_T(t)}{\alpha_0 \Delta p_{T0}} \right) \left(\frac{R(t)}{R_0} \right)^5 = \left(\frac{f_b}{f_{b0}} \right) \left(\frac{Q(t)}{Q_0} \right)^2 \quad [4.23]$$

The pipe radius cannot be defined explicitly as α and f_b are variable quantities. The implicit relationship is as follows:

$$R(t) = R_0 \left\{ \left(\frac{Q(t)}{Q_0} \right)^2 \left(\frac{f_b(R(t))}{f_{b0}} \right) \left(\frac{\alpha_0 \Delta p_{T0}}{\alpha(R(t)) \Delta p_T(t)} \right) \right\}^{1/5} \quad [4.24]$$

Correct estimation of the pipe radius at each time t , which requires a nonlinear solver, is crucial for an accurate estimation of all other quantities, including the shear stress and the flow velocity.

The wall shear stress can be given as a function of the flow velocity equation [4.4], or as a function of the total pressure drop equation [4.9]. As $\beta = 1$, the latter simplifies to:

$$\tau = \frac{R\alpha\Delta p_T}{2L} = \rho_w f_b V^2 \quad [4.25]$$

4.4.2. Determination of the friction coefficient

The error in the estimated pipe radius is primarily controlled by the error in the estimated friction coefficient (see e.g. equation [4.24]). The friction coefficient f_b is the sum of the skin friction coefficient and the form friction coefficient. The classical friction factor formulas used in pipe flow theory are therefore not useful here as they quantify only the skin friction.

Wan and Fell [WAN 02, WAN 04a] assumed that the friction factor varies linearly with time. Lim [LIM 06] improved this initial assumption and assumed that the change in the friction factor is linearly proportional to the change in hole radius:

$$f_b = f_{b0} + (R - R_0) \left(\frac{f_{bfinal} - f_{b0}}{R_{final} - R_0} \right) \quad [4.26]$$

where f_{bfinal} and R_{final} are the friction factor and the hole radius at the final stage of the test, respectively. As both R_0 and R_{final} are measured, f_{b0} and f_{bfinal} can be directly and accurately estimated. Indeed, combining equations [4.8] and [4.22] leads to:

$$f_b = \frac{R}{2L} \left[\left(\frac{\pi R^2}{Q} \right)^2 \left(\frac{\Delta p_T}{\rho_w} \right) - \frac{k}{2} \right] \quad [4.27]$$

To investigate the validity of this assumption, the flow rate, Q , and the hole diameter, ϕ , were measured and the friction factor f_b was calculated during the course of several tests [LIM 06]. At a certain stage during the test (i.e. at different flow rates, Q), the test was halted and the friction factor f_b was determined. The relationship between the friction factor and time and the hole diameter is shown in Figure 4.10, which illustrates this effective assumption. With this approach, both skin and form friction are considered in an effective and global manner.

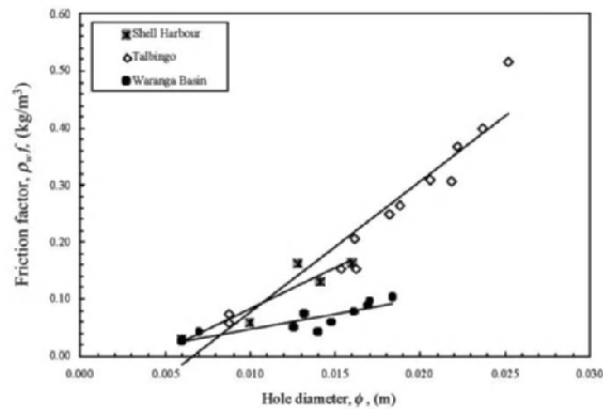


Figure 4.10. Relationship between hole diameter and friction factor for Talbingo soil, Shell Harbour soil and Waranga basin soil [LIM 06]

4.4.3. Determination of the head loss coefficient

If the inlet and outlet diameter are large, as compared to the hole diameter, entrance and exit singular head loss coefficients can be roughly estimated from classical pipe hydraulics at $k_{in} \approx 0.42$ (sudden contraction) and $k_{in} \approx 1$ (sudden expansion into a large tank). However, when the hole diameter increases during the erosion process, the inlet and outlet cylinder cannot be considered as large anymore, and the singular head loss coefficients depends on the ratio $R/R_{cylinder}$, where $R_{cylinder}$ is the radius of the cylinder.

Typical empirical formulas for the singular head loss coefficient are as follows [HAU 08, LEN 87]:

$$\text{Sudden contraction } k_{in} = 0.42 \left[1 - \left(\frac{R}{R_{in}} \right)^4 \right] \quad [4.28]$$

$$\text{Sudden expansion } k_{out} = 1 - \left(\frac{R}{R_{out}} \right)^4 \quad [4.29]$$

where R_{in} and R_{out} are the radius of the inlet and outlet cylinder, respectively (Figure 4.3). To fix ideas, the use of these expressions leads to:

$$\alpha = \left(1 + \frac{kR}{4Lf_b} \right)^{-1}, \quad k = 1.42 - 0.42 \left(\frac{R}{R_{in}} \right)^4 - \left(\frac{R}{R_{out}} \right)^4 \quad [4.30]$$

There is, however, no universal formula for the singular head loss coefficients. For each design, it has to be experimentally determined. Some orders of magnitude are given in Figure 4.11.

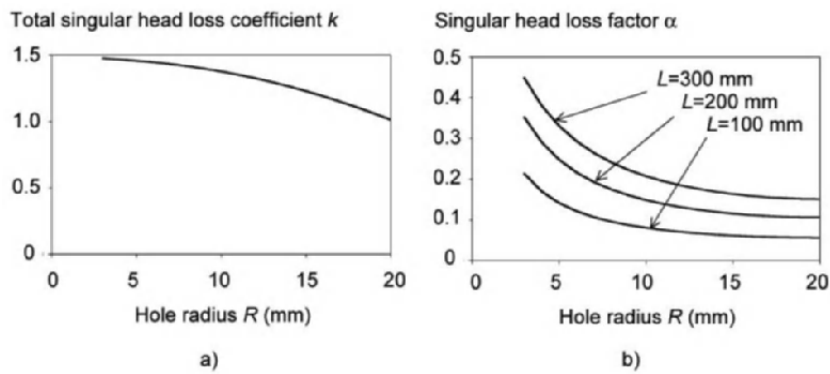


Figure 4.11. Orders of magnitude determined on the experimental setup of [BEN 12a]: a) singular head loss coefficient k and b) singular head loss factor α (corresponding to several pipe length)

4.4.4. Determination of the parameters of erosion

There are many ways to fit the model to experimental data. A possibility is to plot a curve of the estimated diameter of the hole against time equation [4.24], estimate the slope of the curve at time t and fit the erosion law equation [4.3] [WAN 02, WAN 04a, LIM 06].

Another possibility is to minimize the mean square error between the data and the model, with respect to the two unknowns τ_c/P_0 and t_{er} [BON 08]. The mean square error between the data and the model can be calculated from the flow rate, the total pressure drop or the radius. Knowing the initial driving pressure P_0 and the initial radius R_0 , we can therefore estimate the critical stress τ_c and the coefficient of erosion (C_e/ρ_d). A classical nonlinear solver, such as the Newton–Raphson solver or the Levenberg–Marquardt method, can be used to solve the nonlinear least squares problem [BON 08]. This method converged in a few iterations in all cases, with all the raw data, and proved to be robust.

4.4.5. Examples of results

An example of the erosion law of a moraine ($\rho_d = 1,554 \text{ kg/m}^3$, $w = 8\%$, no cohesion, plasticity index $I_p = 0.5$) is shown in Figure 4.12. Figure 4.12(a) shows the rate of mass removal per unit area as a function of the hydraulic wall shear stress. The critical stress was found to be $\tau_c = 0.4 \text{ Pa}$. The coefficient of erosion was found to be $C_e = 1.08 \times 10^{-2} \text{ s/m}$ ($I_e = 1.97$). It is an extremely fast material according to the Wan and Fell classification ([WAN 02, WAN 04a, WAN 04b], Table 5.1 of Chapter 5 of this book). The specimen before erosion, with the initial hole (6 mm diameter), is shown in Figure 4.13(a). The moraine collapsed during the test (Figure 4.13(b)). Figure 4.12(b) shows the rate of erosion (in cm/h) as a function of the flow velocity (in m/s). The order of magnitude of the Reynolds number is

2,000. The flow is likely to be in the transition zone between laminar and turbulent and the interpretation was based on a more general approach, which is not detailed here.

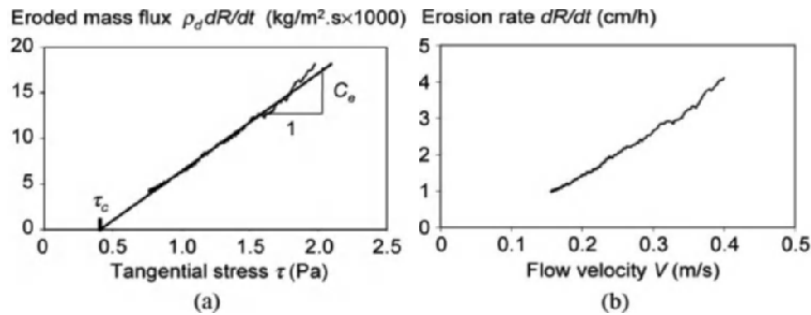


Figure 4.12. Hole erosion test results on a moraine, extremely fast, performed at constant flow rate ($0.46 \text{ m}^3/\text{h}$). a) Eroded mass flux versus hydraulic wall shear stress and b) erosion rate versus flow velocity

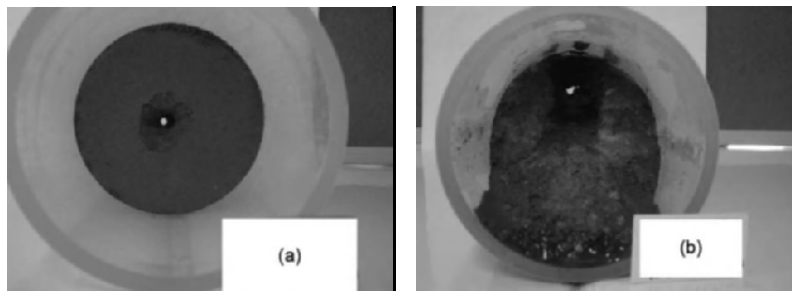


Figure 4.13. Hole erosion test specimen of a moraine, extremely fast, a) before the test and b) after the test

An example of the erosion law of a sandy clay loam ($\rho_d=1,670 \text{ kg/m}^3$, $w = 20\%$, clay fraction = 35%) is shown in Figure 4.14. Figure 4.14(a) shows the rate of mass removal per unit area as a function of the hydraulic wall shear stress. The critical stress and the coefficient of erosion were found to be $\tau_c = 230 \text{ Pa}$ and $C_e = 1.8 \times 10^{-5} \text{ s/m}$ ($I_e = 4.73$), respectively.

It is a moderately slow material according to the Wan and Fell classification ([WAN 02, WAN 04a, WAN 04b], Table 5.1 Chapter 5 of this book). The specimen before erosion, with the initial hole (6 mm diameter), is shown in Figure 4.15(a). The specimen after erosion is shown in Figure 4.15(b). Other illustrative examples of specimen after erosion are shown in Figure 4.16.

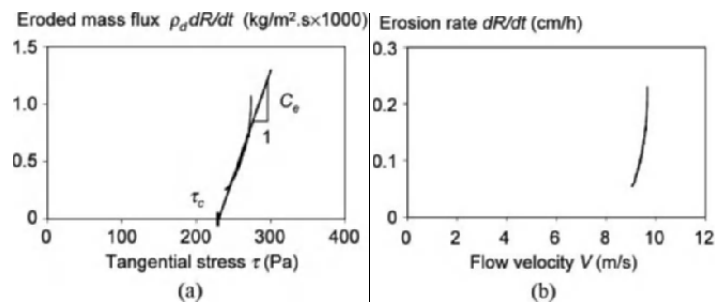


Figure 4.14. Hole erosion test results on a sandy clay loam, moderately slow, performed at constant flow rate (1.14 m³/h).
*a) Eroded mass flux versus hydraulic wall shear stress and
 b) erosion rate versus flow velocity*

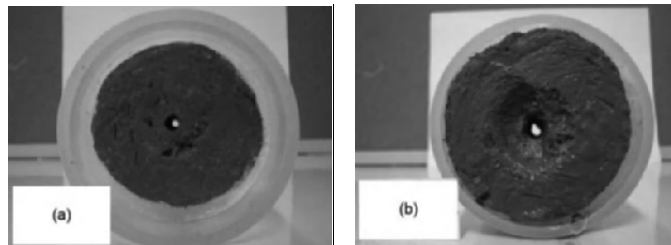


Figure 4.15. Hole erosion test specimen of a sandy clay loam, moderately slow, a) before the test and b) after the test

4.4.6. Slaking at upstream or downstream faces of sample of HET

Slaking of soil samples at their downstream and upstream faces can pose significant difficulties to the interpretation of

HET data. As slaking proceeds on the downstream and upstream faces of the sample, the channel length becomes shorter and the applied shear stress on the hole surface increases because of the increased hydraulic gradient. During the test, the sample may start to erode at a certain level of shear stress; however, this shear stress does not remain constant and increases with time as the length of the channel is reduced due to slaking.

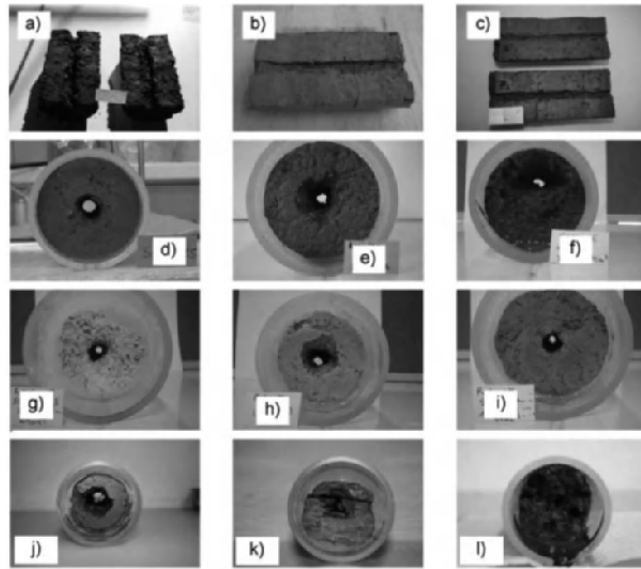


Figure 4.16. Illustrative examples of hole erosion tests specimens after erosion. a) Brown sandy silt with fine to medium rounded gravel, b) clay loam, c) silty clay, d) silt clay loam, e) silty loam, f) loamy sand, g) compact weathered granite with sand, clay and fine gravel, h) yellow sandy clay with fine gravel, i) sandy clay loam, j) sandy loam with roots, k) shale and l) highly saturated clay loam

This aspect has not been considered during the calculation process in the current approach for the interpretation of HET results. After the test, more error is introduced into the analysis due to difficulties in accurately estimating the eroded hole size.

Figure 4.17 shows this aspect for two different soil types [LIM 06]. For both cases, the slaking is severe in the downstream face as shown in Figure 4.17, which is typical of the HET tests. The average hole size in Figure 4.17(a) is 15.24 mm excluding the slaked part and 36.3 mm including the slaked part, calculated using a volume averaging process. Figure 4.17(b) shows more severe slaking. The current procedure for the calculation of an erosion rate index adopts the average slaked value of the hole size and ignores the reduced channel length. As a result, it overestimates the shear stress applied to the hole surface due to the larger estimated hole diameter [LIM 06].

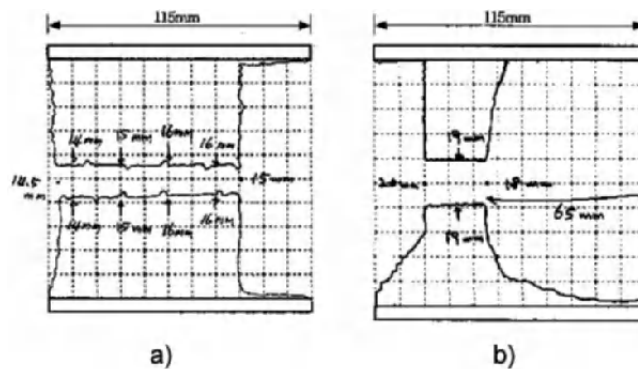


Figure 4.17. Sectional views of samples in HET with slakable material: a) Soil-B and b) Soil-S [LIM 06]

To correct, for the effect of slaking, a number of empirical correlations were examined by Lim [LIM 06] and the following relationship was found to best fit the data:

$$\tau_{cor} = \left(1 + C_{slaking} \frac{L_{slaking}}{L_{initial}} \right) \tau_t \quad [4.31]$$

where τ_{cor} is the corrected shear stress for slaking at time t , τ_t is the shear stress calculated using the hydraulic gradient based on the initial sample length at time t ,

$L_{slaking} = (L_{initial} - L_{final})(t/t_{final})$ is the reduced length of erosion channel by slaking (slaked length of sample) at time t , t_{final} is the final time corresponding to the L_{final} , L_{final} is remaining length of sample, $L_{initial}$ is the initial sample length (m) and $C_{slaking}$ is mold correction factor (0.303 for the standard mold used in this study).

Figure 4.18(b) shows the estimated erosion chart after applying the correction according to equation [4.31] for the test results shown in Figure 4.18(a). All the plots from different sample lengths form a single line on the erosion chart.

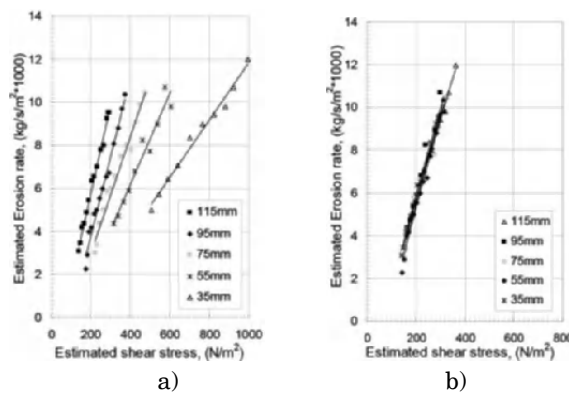


Figure 4.18. Estimated erosion chart for the samples of different hole lengths (same soil, mixture of 30% bentonite and 70% Sydney sand):
 a) considering reduced channel length and b) after applying the correction for slaking [LIM 06]

4.5. Mechanically based relations for time to failure and peak flow

4.5.1. A simplified approach

The erosion rate has a significant influence on piping progression time and the development of a breach in earth dams, dikes and levees. Given that erosion has been initiated and filters are absent or unable to stop erosion, the

prevailing flow hydraulics form concentrated leaks such that erosion will progress to form a continuous tunnel (pipe). We consider the case of a straight and circular pipe of current radius $R(t)$, in an embankment of the height H_{dam} and the base width $L_{dam} = c_L H_{dam}$ (Figure 4.19).

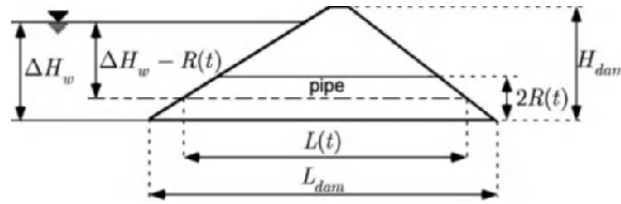


Figure 4.19. Sketch of pipe flow with erosion in a water retaining structure

The average quantities are defined as follows:

$$L(t) = c_L [H_{dam} - R(t)] (\text{pipe length}) \quad [4.32]$$

$$\Delta p_T(t) = \rho_w g [\Delta H_w(t) - R(t)] (\text{total pressure drop}) \quad [4.33]$$

Although the pressure drop is likely to decrease with time, the situation for case $\Delta H_w = H_{dam}$ is more critical and therefore yields a conservative estimate of the time needed to initiate roof collapse. The pressure gradient is therefore constant during the erosion phase: $\Delta p_T(t) / L(t) = \rho_w g / c_L$.

Characteristic values are necessary, here, to quantify the two loss factors. A mean value of base width ratio is $c_L = L_{dam} / H_{dam} = 3$.

The choice of k , the singular head loss coefficient, corresponds to the section sharpening of the pipe inlet, between the reservoir, or the river, and the pipe. The order of magnitude is $\bar{k} = 0.5$. No head loss at the exit is considered as it is dewatered.

The friction coefficient f_b accounts for the flow resistance, which can be divided in two components: 1) the skin friction, at the grain scale (order of magnitude 10^{-3} to 5×10^{-3}) and 2) the form friction, at the bedform scale (order of magnitude 5×10^{-3} to 10^{-2}). The order of magnitude chosen here is $\bar{f}_b = 0.005$.

4.5.2. Onset of erosion in the pipe

Erosion occurs if $R_0 > \tau_c$, where R_0 is the initial driving pressure equation [4.14], evaluated with $\bar{R} = R_0$ and $\bar{L} = L_{dam}$. For the set of parameters corresponding to the earth dams and levees analysis, the singular head loss can be neglected when the radius is small, as the pipe is initially long and represents most of the head losses. This yields the following expression giving the critical radius:

$$R_c = \frac{2c_L \tau_c}{\rho_w g} \quad [4.34]$$

Erosion occurs if $R_0 > R_c$. This critical radius does not depend on the flow regime (laminar or turbulent) as it is only a momentum balance. There is no scale effect: it does not depend on the dam height. The critical stress is a key parameter in order to evaluate whether or not erosion is likely to be initiated in the preformed pipe.

Taking $c_L = 3$, $\rho_w = 1,000 \text{ kg/m}^3$, $g = 9.81 \text{ m/s}^2$ yields $R_c [\text{cm}] \approx 0.06 \tau_c [\text{Pa}]$. The critical stress of the soils usually encountered on water retaining structures range usually between 10 and 100 Pa. The critical radius range is therefore between 6 mm and 6 cm. However, as discussed in Chapter 1, silty sands of low plasticity and dispersive clays have lower critical shear stresses, as low as 1 Pa, so erosion may initiate in cracks as narrow as 1 mm.

4.5.3. Visual detection of the leak

Assume that $R_0 > R_c$ and that erosion occurs. The piping process begins at time t_0 with the initial radius R_0 . Both of which are unknown. However, visual inspection can be a way of defining the initial time $t_d > t_0$ for detection and can provide an estimation of the output flow rate, thus an estimation of the radius $R_d > R_0$.

This flow rate and the tangential stress at detection are given as follows:

$$Q_d = \pi R_d^2 \sqrt{\frac{\bar{\alpha} g R_d}{2c_L f_b}}, \tau_b = \frac{\bar{\alpha} g \rho_w R_d}{2c_L}, \bar{\alpha} = \left(1 + \frac{\bar{k} R_d}{4c_L H_{dam} f_b}\right)^{-1} \quad [4.35]$$

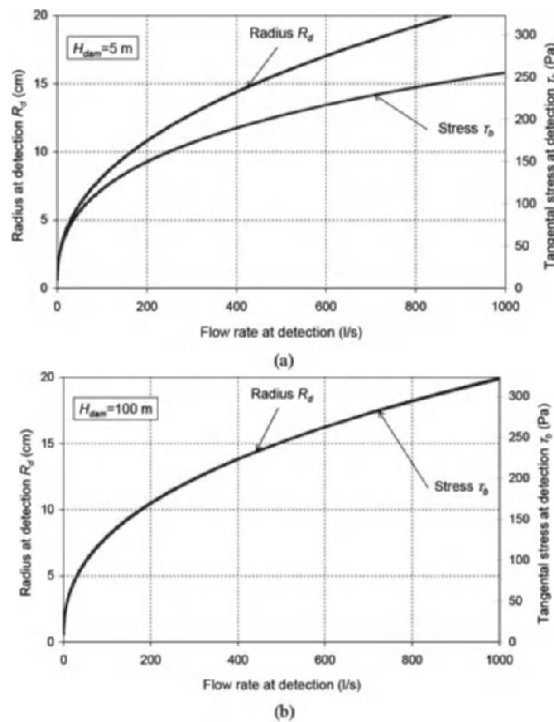


Figure 4.20. Pipe radius and the tangential stress as a function of the flow rate at detection: a) $H_{dam} = 5$ m and b) $H_{dam} = 100$ m

The radius and the stress are plotted as a function of the flow rate at detection in Figure 4.20, with $c_L = 3$, $\bar{f}_b = 0.005$, $\bar{k} = 0.5$, $g = 9.81 \text{ m/s}^2$ and $\rho_w = 1,000 \text{ kg/m}^3$. This figure shows that the scale effect, due to the singular head loss factor $\bar{\alpha}$ that is a function of the dam height, is visible. This gives some orders of magnitude: (1) $R_d = 1 \text{ cm}$ and $\tau_b = 16 \text{ Pa}$ for $Q_d \approx 2 \text{ m}^3/\text{h}$; (2) $R_d = 4 \text{ cm}$ and $\tau_b \approx 64 \text{ Pa}$ for $Q_d \approx 1 \text{ m}^3/\text{min}$; (3) $R_d = 20 \text{ cm}$ and $\tau_b = 320 \text{ Pa}$ for $Q_d \approx 1 \text{ m}^3/\text{s}$. The radius at detection is of the order of few centimeters. It can clearly not be greater than 20 cm.

4.5.4. Enlargement of the pipe

Once erosion has been initiated, enlargement of the pipe is given by the exponential scaling law equation [4.17]. The enlargement of the pipe causes roof collapse and creates a breach. The rate of pipe enlargement is highly dependent on the erodibility of the soil as measured by the erosion coefficient C_e . We can now propose an expression for the time remaining to breaching [BON 11, BON 12b]. A sketch of our description is represented in Figure 4.21. We use R_u and t_u to denote the maximum radius of the pipe before roof collapse and the collapse time, respectively. For $t > t_u$, piping failure continues to cause erosion in a way similar to that of an overtopping failure.

Assuming a constant reservoir water level, the remaining time after detection and prior to breaching $\Delta t_u = t_u - t_d$ can be estimated on the basis of equation [4.17] as follows:

$$\Delta t_u = t_{er} \left[\ln \left(\frac{R_u}{R_d} - \frac{\tau_c}{P_d} \right) - \ln \left(1 - \frac{\tau_c}{P_d} \right) \right] \quad [4.36]$$

where P_d is the driving pressure equation [4.14] acting at the time of detection and t_{er} is the characteristic time equation [4.16].

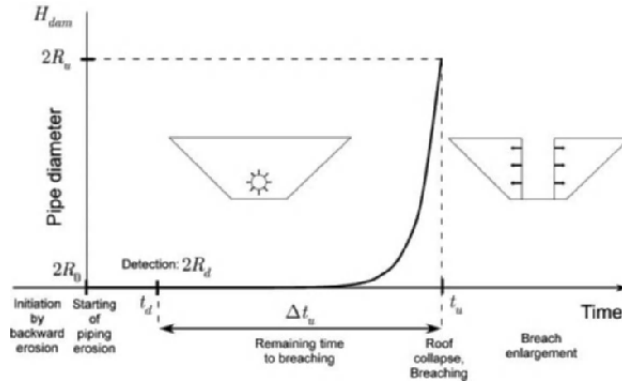


Figure 4.21. Pipe flow with erosion in a water retaining structure, phases from initiation to breaching

$$P_d = \frac{R_d \bar{\alpha} \rho_w g}{2c_L}, \quad t_{er} = \frac{2c_L \rho_d}{\beta C_e \bar{\alpha} \rho_w g} \quad [4.37]$$

Assuming that failure occurs when the pipe diameter reaches $2H_{dam}/3$, as it is assumed classical in dam break analysis, the reference radius is chosen to be $\bar{R} = R_u$ with $R_u = H_{dam}/3$. This yields the following estimate of the head loss factor on site at failure: $\bar{\alpha} \approx 0.26$.

The reference velocity at failure is inferred from equations [4.2] and [4.4], leading to the first order of the following approximation:

$$\bar{V} = \frac{\bar{V}_1}{1 + \bar{\alpha} C_e \bar{V}_1}, \quad \bar{V}_1 = \sqrt{\frac{\bar{\alpha} g H_{dam}}{6c_L f_b}} \quad [4.38]$$

Taking $c_L = 3$, $\bar{f}_b = 0.005$ and $\bar{k} = 0.5$, yields the following estimate of the momentum loss factor on site at failure:

$$\beta = \frac{1 + 0.26C_e\bar{V}_1}{1 + 0.52C_e\bar{V}_1}, \quad \bar{V}_1 \approx \sqrt{2.89gH_{dam}} \quad [4.39]$$

The quantity \bar{V}_1 gives the order of magnitude of the velocity at failure when the loss of momentum due to erosion is low ($C_e\bar{V}_1 < 0.01$). If this quantity is significant, equation [4.38] shows that the loss of momentum due to erosion leads to a slight decrease in the flow velocity. Figure 4.22 illustrates that the velocity at failure ranges from $1/\bar{\alpha}C_e$, when $C_e \approx 1$ s/m, to \bar{V}_1 , when $C_e \geq 10^{-3}$ s/m.

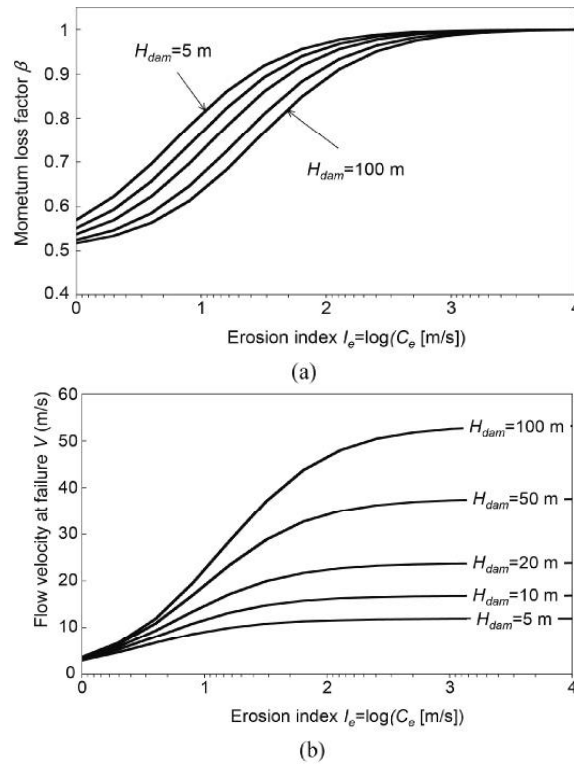


Figure 4.22. a) Loss momentum factor β and b) flow velocity at failure as a function of the erosion index, for several dam heights ranging from 5 to 100 m

The expression of Δt_u in equation [4.36] and its representation in Figure 4.23 shows that the coefficient of erosion C_e can serve as an indicator of the time remaining to breaching, as $\Delta t_u \propto C_e^{-1}$: the greater the erosion index, the greater the time to failure.

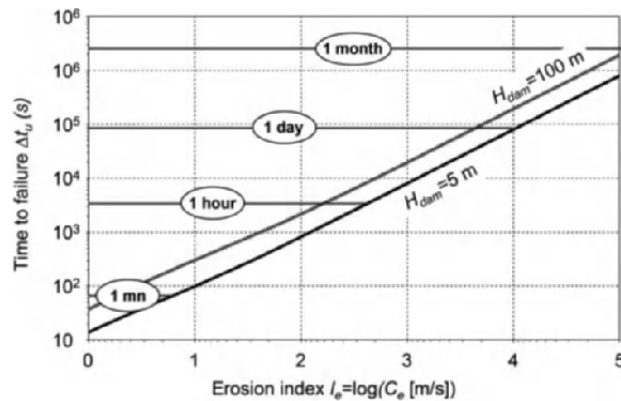


Figure 4.23. Time to failure as a function of the erosion index for two dam heights, obtained with equations [4.36]–[4.39]. The set of parameters used is $c_L = 3$, $f_b = 0.005$, $k = 0.5$, $\rho_d = 1,800 \text{ kg/m}^3$, $\tau_c = 0 \text{ Pa}$, $R_d = 0.2 \text{ m}$ and $\alpha = 0.26$

This significant result means that when the radius at detection is $R_d = 0.2 \text{ m}$, and if the erosion index I_e is of order of magnitude of 2 ($C_e \approx 10^{-2} \text{ s/m}$), then the failure will take place very quickly, within a few minutes. If $I_e \approx 3$, the failure will take place within several hours. If $I_e > 4$, the failure will not occur until several days and $R_d = 0.2 \text{ m}$ is a very high value and can be considered as an extreme value for visual detection.

On the other hand, the dam height has less influence on the time to failure. Therefore, the maximum radius of the pipe before roof collapse, which can not be estimated with certainty prior to a breach, has little influence on the time to failure.

The peak flow is assumed to correspond to the maximum radius of the pipe. Consequently, the time prior to breaching Δt_u is also the time from detection (e.g. eyewitness observations) to peak discharge, given here as follows:

$$Q_{peak} = \pi R_u^2 \bar{V} \quad [4.40]$$

It is emphasized that equations [4.36] and [4.40] do not link Δt_u and Q_{peak} to the reservoir storage, as it is usually proposed in the dam engineering literature. This is mechanically irrelevant, mostly in the case of dikes and levees.

4.6. Dam and levee break modeling

4.6.1. Order of magnitude on case studies

Case study data provide only limited information. This is primarily due to the variations in interpretation of failure by the lay person who often is the only eyewitness to a dam failure. In the best case, the only information available is the time to breaching and the peak flow. The radius or the flow rate at detection is never reported.

The use of above equations is extended here to infer orders of magnitude from case studies. The critical stress plays a role when analyzing the initiation phase, but it is conservative to assume that $\tau_c = 0$ during the pipe enlargement, as the shear stress continuously increases. We assume that $\beta = 1$. Finally, the simplified evaluation of the time to failure can be given as follows:

$$\Delta t_u \approx t_{er} \ln \left(\frac{R_u}{R_d} \right) \text{ (remaining time to breaching)} \quad [4.41]$$

$$t_{er} = \frac{2\rho_d \bar{L}}{C_e \bar{\alpha} \Delta p_T} \text{ (characteristic time)} \quad [4.42]$$

$$Q_{peak} = \pi R_u^{5/2} \sqrt{\frac{\bar{\alpha} \Delta p_T}{2\bar{L} \rho_w f_b}} \text{ (peak flow)} \quad [4.43]$$

$$\bar{L} = c_L (H_{dam} - R_u) \text{ (pipe length at failure)} \quad [4.44]$$

$$\Delta p_T = \rho_w g (\Delta H_w - R_u) \text{ (total pressure drop at failure)} \quad [4.45]$$

$$\bar{\alpha} = \left(1 + \frac{\bar{k} R_u}{4\bar{L} f_b} \right)^{-1} \text{ (head loss factor)} \quad [4.46]$$

Inverting equation [4.41] yields:

$$C_e \approx \frac{2\rho_d \bar{L}}{\bar{\alpha} \Delta t_u \Delta p_T} \ln \left(\frac{R_u}{R_d} \right) \quad [4.47]$$

Few attempts have been made to propose a constitutive model to calculate the radius value prior to roof collapse. This estimate can be made on the basis of information derived from the peak flow value. If the peak flow is unknown, an upper bound can however be obtained by taking $R_u = H_{dam} / 2$:

$$C_e < \frac{2\rho_d \bar{L}}{\bar{\alpha} \Delta t_u \Delta p_T} \ln \left(\frac{H_{dam}}{2R_d} \right) \quad [4.48]$$

The present hypothesis is not intended to provide accurate values of the shear stress, velocity or flow rate. Rather, attention is focused explicitly on the more limited goal of giving numbers and orders of magnitude.

Tables 4.1 and 4.2 contain data and results of this simplified analysis on 14 well-documented piping failure cases. These cases were taken from the database presented in [WHA 98], where data on 108 case studies of real

embankment dam failures were collected from numerous sources in the literature.

In Table 4.1, the first five columns are taken from [WHA 98]. The maximum radius is estimated by adjusting the peak flow (equation [4.40]).

Dam height H_{dam} ranged from 6 to 93 m. The relative water level $\Delta H_w / H_{dam}$ at failure ranged from 0.48 to 1 m/m. Coefficient $c_L = L_{dam} / H_{dam}$ ranged from 1.54 to 3. Failure time Δt_u ranged from 0.5 to 5.25 h. The peak flow Q_{peak} ranged from 79 to 65,120 m³/s. The relative maximum diameter $2R_u / H_{dam}$ estimated with equation [4.40] ranged from 0.26 to 0.96. The shear stress τ_b at failure ranged from 262 to 8,051 Pa. Water velocity at failure V ranged from 7 to 40 m/s.

Dam name and location	H_{dam} (m)	ΔH_w (m)	c_L	Δt_u (h)	Q_{peak} (m ³ .s ⁻¹)	R_u (m)
Ireland No. 5, Colo.	6.0	3.8	3.0	0.5	110	2.20
Lower Latham, Colo.	8.6	5.8	3.0	1.5	340	3.53
Frankfurt, Germany	9.8	8.2	3.0	2.5	79	1.42
Kelly Barnes, Ga.	11.6	11.3	1.7	0.5	680	3.66
French Landing, Mich.	12.2	8.5	2.8	1.16	929	5.30
Lake Latonka, Penn.	13.0	6.3	2.2	3	290	3.05
Lake Avalon, N.M.	14.5	13.7	2.9	2	2,320	6.94
Quail Creek, Utah	18.9	16.7	3.0	1	3,110	7.53
Hatchtown, Utah	19.2	16.8	2.3	4	3,080	7.40
Little Deer Creek, Utah	26.2	22.9	2.4	0.66	1,330	4.37
Bradfield, England	29.0	29.0	1.7	0.5	1,150	3.75
Apishapa, Colo.	34.1	28.0	2.4	3.25	6,850	9.51
Hell Hole, Calif.	67.1	35.1	1.5	0.75	7,360	9.30
Teton, Idaho	93.0	77.4	2.7	5.25	65,120	22.73

Table 4.1. Well-documented failure cases by piping, data and estimation of the maximum radius before roof collapse

Dam name and location	τ_b (Pa)	V_u (m.s ⁻¹)	I_e (mean \pm std. dev.)		C_e (10 ⁻³ s.m ⁻¹)	V_{er} (cm.mn ⁻¹)
Ireland No. 5, Colo.	262	7	1.6	± 0.13	24	24
Lower Latham, Colo.	379	9	2.0	± 0.11	10	14
Frankfurt, Germany	784	13	3.0	± 0.22	1	3
Kelly Barnes, Ga.	1,309	16	2.0	± 0.12	10	47
French Landing, Mich.	552	11	1.8	± 0.09	15	31
Lake Latonka, Penn.	490	10	2.5	± 0.14	4	6
Lake Avalon, N.M.	1,175	15	2.2	± 0.08	6	25
Quail Creek, Utah	1,524	17	2.0	± 0.09	10	56
Hatchtown, Utah	1,606	18	2.6	± 0.09	2	14
Little Deer Creek, Utah	2,454	22	2.3	± 0.15	5	48
Bradfield, England	3,378	26	2.4	± 0.16	4	54
Apishapa, Colo.	2,902	24	2.7	± 0.10	2	24
Hell Hole, Calif.	3,662	27	2.1	± 0.13	8	107
Teton, Idaho	8,051	40	2.9	± 0.09	1	42

Table 4.2. Well-documented failure cases by piping, erosion coefficient and final erosion rate estimates

The erosion index rate $I_e = -\log C_e$ was estimated as an average of four numbers, calculated with the right-hand side (RHS) of equations [4.47] and [4.48], with $R_d = 20$ cm and $R_d = 4$ cm. The average erosion index rate I_e was found to range from 1.6 to 3.0. The standard deviation ranged from 0.08 to 0.22.

Wan and Fell [WAN 02] found that the erosion coefficient C_e can differ by up to 10^5 times across different soils from a series of HETs (13 soils). The erosion coefficient was found to range from 10^{-6} to 10^{-1} s.m⁻¹. Here, the erosion coefficient C_e is inferred from case history data ranged from 10^{-3} to 10^{-2} s.m⁻¹. These results are consistent.

For overtopping, Courivaud and Fry [COU 07] reported breach widening rate values inferred from the data of 10 case histories, covering a range of dam heights from 8 to

60 m. These values ranged from 14 to 600 cm.mn⁻¹. For piping flow erosion, the erosion rate before roof collapse can be estimated with $V_{er} = \tau_b C_e / \rho_d$ and $\rho_d = 1,600 \text{ kg/m}^3$. We find in Table 3.1 that V_{er} ranged from 3 to 107 cm.min⁻¹. These comparisons confirm the validity of our findings: orders of magnitude can be inferred from field data with limited information.

The fact that the erosion index was found to be lower than three deserves a comment. In the first stage, we may infer that the soils of earth dams are usually very erodible or extremely erodible ($1 \leq I_e \leq 3$); out of these, only a few were subject to failure, and when failure does occur, it usually happens very fast (within a few hours).

We can also perform another analysis, which seems to better correspond to reality. The soils of the earth dams are likely to have a highly variable erodibility ($1 \leq I_e$). A certain number of them are likely to have been in a failure situation. Only those that have a very erodible soil or a highly erodible soil ($1 \leq I_e \leq 3$) had enough time to collapse.

Finally, it may also be a fact that the HET underestimates the erosion rate as the hole enlarges. The soil structure takes over and blocks of soil fall into the eroding hole (see Chapter 5).

4.6.2. A model for dam- and levee-break due to concentrated leak erosion

The embankment is assumed to be of a trapezoidal shape and of homogeneous material. Water flows through a circular pipe that is modeled by one mean section and no slope. This pipe is at the level of the bottom of the valley. Flow characteristics within the pipe are computed from the integrated reduced Navier–Stokes/Prandtl equations with erosion [4.1] – [4.6], with a head loss at the entrance, a linear head loss in the pipe and no head loss at the exit.

A crude but effective assumption is simply that k and f_b are constant. Obviously, we used strong assumptions and this model is too simplified to account for all aspects of the process as it occurs really. In a more precise modeling, the friction coefficient f_b may be described as a function of the Reynolds number, of the wall roughness [SHO 06] and even of the soil concentration in the flow [LAC 08]. However, the description and the evolution of the soil roughness and bedforms remain an open question at this geometric scale.

Usually, the initial condition is a small pipe diameter so that the discharge is very low. However, it should be high enough to be detected by a visual inspection (see Figure 4.20). The diameter of the pipe increases due to erosion. The sediment discharge is computed from the hydraulic variables by the erosion law. The eroded material is distributed uniformly over the cross-section so that the pipe remains circular.

The average length of the pipe is

$$L(t) = L_{dam} \left(1 - \frac{R(t)}{H_{dam}} \right) \quad [4.49]$$

The pipe is considered as under pressure only if the water level in the reservoir is high enough. If the pipe is filled with water, pressure exerts on the entire perimeter: it is relevant to consider the average pressure and the average length. However, if the water level upstream is below the diameter of the pipe, the flow is a free surface flow in the pipe. For the sake of simplicity, the free surface is assumed horizontal in the pipe. The total pressure drop can be written as follows:

$$\Delta p_r(t) = \begin{cases} \rho_w g [\Delta H_w(t) - R(t)] & \text{if } \Delta H_w(t) \geq 2R(t) \text{ (pressure flow)} \\ \rho_w g \frac{[\Delta H_w(t)]^2}{4R(t)} & \text{if } \Delta H_w(t) < 2R(t) \text{ (free surface flow)} \end{cases} \quad [4.50]$$

4.6.3. Application to the failure of a homogeneous moraine dam by piping

A large-scale test was conducted in 2003 during the Norwegian project Stability and Breaching of Embankment Dams, and the European Commission FP5 project Investigation of Extreme Flood Processes and Uncertainty (IMPACT) [HOE 04, LOV 03, LOV 06, MOR 00, VAS 04, VAS 05]. The structure is a moraine dam, homogeneous, 4.3 m high and 18.3 m wide, with a slope of 1:1.4 for the upstream and downstream slopes. It was constructed by compaction (vibration) of layers of 50 cm at a water content of 6 – 8% and a porosity of 0.24.

The initial conduit has a radius of 10 cm. The dam failure happened less than 15 minutes between the opening of the duct and the roof collapse, which occurred with a diameter of 4.2 m (Figure 4.24). The initial upstream level of 3.9 m was not kept constant. The outflow was measured 200 m downstream.

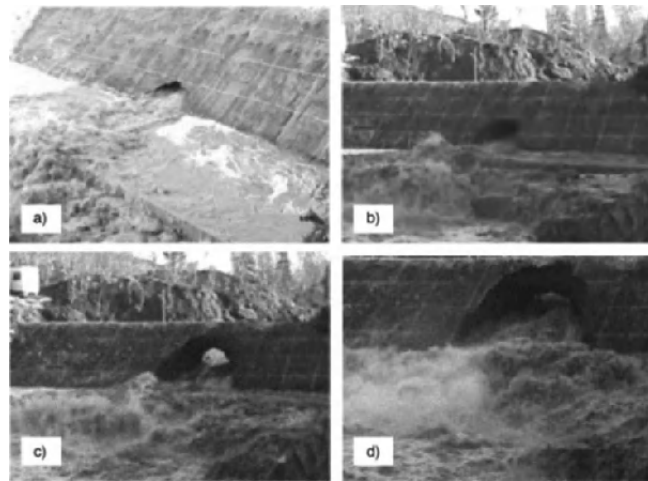


Figure 4.24. Failure of the homogeneous moraine dam [LOV 03, VAS 05]:
*a) $t = 3$ mn, b) $t = 5$ mn, c) $t = 12$ mn (free surface flow in the pipe) and
 d) $t = 14$ mn (just before the roof collapse)*

The moraine, consisting of 10% sand and 90% gravel ($d_{10} = 0.06$ mm, $d_{50} = 5.5$ mm and $d_{\max} = 200$ mm), had an angle of internal friction of 45° , and no cohesion. The erosion parameters from HET tests were found as follows: $\tau_c = 0.4$ Pa and $C_e = 1.08 \times 10^{-2}$ s/m ($I_e = 1.97$, Figure 4.12).

Table 4.3 contains the model parameters, all of which have a mechanical sense. Other parameters are well known ($g = 9.81$ m/s² and $\rho_w = 1,000$ kg/m³). The coefficient of erosion adjusted in order to collapse the modeling results on the diameter measurement data was found to be $C_e = 4 \times 10^{-2}$ s/m.

H_{dam} (m)	L_{dam} (m)	ΔH_w (m)	R_u (m)	R_0 (m)	ρ_d (kg/m ³)	ρ_{soil} (kg/m ³)	f_b	k	τ_c (Pa)	C_e (s/m)
4.3	18.3	Variable	2.2	0.1	2,160	2,341	5×10^{-3}	0.42	0	4×10^{-2}

Table 4.3. Parameters of dam break simulation modeling of the homogeneous moraine dam

Figure 4.25 compares the change in the diameter measured from video images of the downstream slope and the change in diameter given by the model. This figure also shows the evolution of the upstream water level. The model, taking into account (but very roughly) the flow transition, shows that the change in slope of the evolution of the radius is due to this transition.

Figure 4.26 compares the evolution of the flow measured 200 m downstream of the dam and the evolution of the flow in the pipe given by the model. The fact that the measurement was downstream leads to a signal transformation: it is delayed for several minutes, and the kinetics is smoothed. A direct comparison is impossible. However, the model provides the magnitude of the peak flow (100 m³/s).

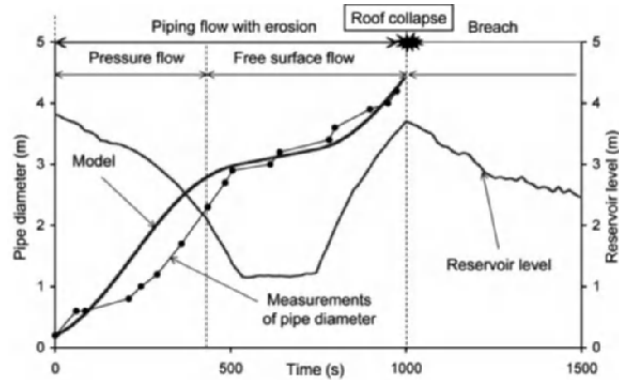


Figure 4.25. Failure of the homogeneous moraine dam, pipe diameter with time, and comparison of the measurements (data from [LOV 03]) with the modeling results (parameters of Table 4.3) (* : roof collapse)

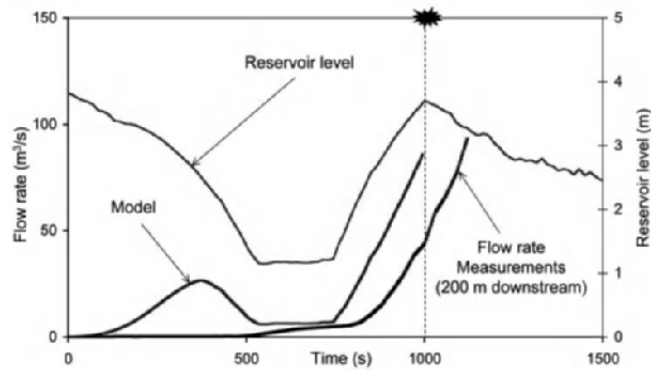


Figure 4.26. Failure of the homogeneous moraine dam, 4.3 m height, flow rate with time, and comparison of the measurements obtained 200 m downstream (data from [LOV 03]) with the modeling results giving the flow rate in the pipe (* : roof collapse)

Figure 4.27 shows the evolution of the total pressure drop and the pipe pressure drop with time. The head loss factor $\alpha = \Delta p / \Delta p_T$ (equation [4.8]) accounting for the singular pressure loss at the pipe entrance ranged from 0.90 to 0.28 at failure. In Figure 4.28, the flow velocity appears to range between 2.4 and 6.5 m/s, while the wall shear stress ranges

between 29 and 268 Pa. The difference between the pressure drop RP/R_0 and the wall shear stress τ_b lies in the quantity $V\dot{m}$ on the left-hand side of equation [4.2]. This erosion momentum loss is not small here as $C_e V \approx 0.2$.

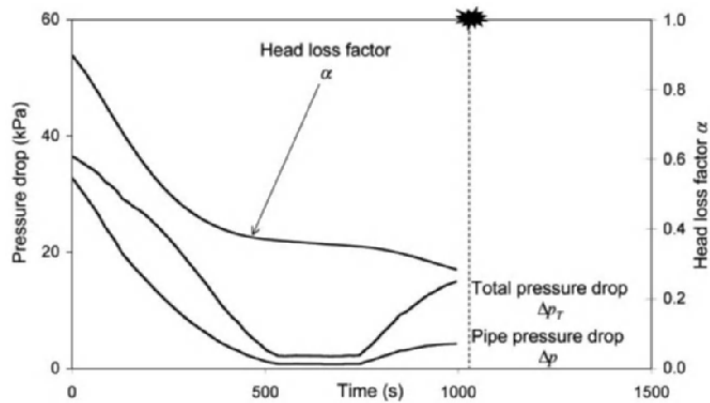


Figure 4.27. Failure of the homogeneous moraine dam, 4.3 m height; total and pipe pressure drop as a function of time, head loss factor as a function of time (*: roof collapse)

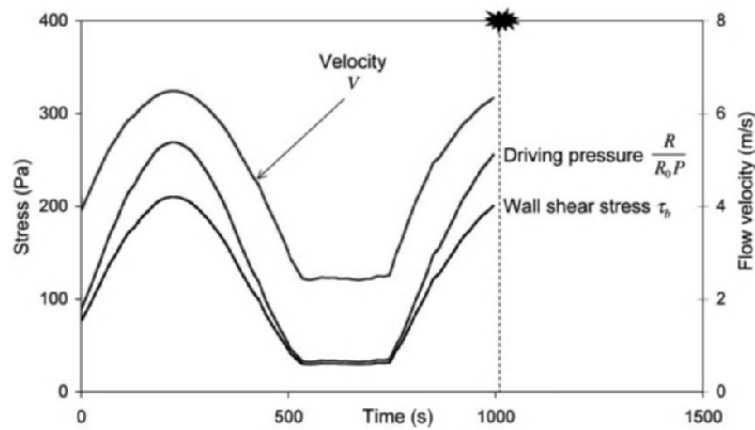


Figure 4.28. Failure of the homogeneous moraine dam, 4.3 m height; driving pressure, wall shear stress and flow velocity as a function of time (*: roof collapse)

4.6.4. Model analysis

A sensibility analysis was performed on this case, but with a constant upstream water level. The effect of varying one parameter only is shown in Figure 4.29 for the coefficient of erosion C_e , the friction coefficient f_b , the critical stress τ_c and the dam height H_{dam} . This analysis highlights some important aspects:

- The lower the coefficient of erosion, the greater the time to failure; the lower the friction coefficient, the greater the time to failure.
- The coefficient of erosion and the friction coefficient appear to play the same role regarding the time to failure; these two parameters have a major influence on the time to failure.
- The initial wall shear stress was 81 Pa; taking a critical stress of 0 Pa or 20 Pa gave a similar result; taking a critical stress of 80 Pa led to a failure time only twice as large.
- Once the erosion is initiated, the critical stress no longer appears as an influential parameter on the time to failure.
- Taking a dam height of 89 m only multiplied by two the time to failure obtained with a dam height of 4.3 m; the dam height does not appear to be an influential parameter on the time to failure.

This dam- and levee-break model was applied to the 14 well-documented piping failure cases of Tables 4.1 from [WHA 98]. The model parameters are given in Table 4.4. The radius at failure is given by the back-analysis knowing the peak flow (Table 4.1). The coefficient of erosion is given by the back-analysis knowing the time to failure (Table 4.2). The critical stress is zero. The initial pipe diameter is 4 cm. Results, given in Table 4.5 in terms of time to failure and peak flow, have the same order of magnitude of the data

(Table 4.1), on the whole range of the dam heights considered, from 6 to 93 m. The full validation of this simplified model requires further work, and mostly requires a set of data and measures in diameter and outflow with time.

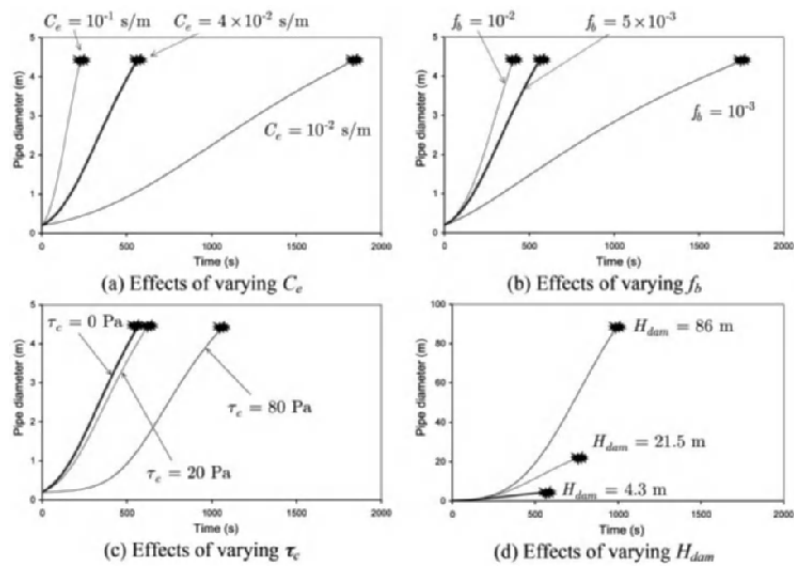


Figure 4.29. Evolution of the pipe diameter as a function of time. Results of the modeling with the set of parameters of Table 4.4 and constant reservoir level. Effects of varying one parameter (*: roof collapse)

H_{dam} (m)	L_{dam} (m)	ΔH_w (m)	R_u (m)	R_0 (m)	ρ_d (kg/m ³)	ρ_{soil} (kg/m ³)	f_b	k	τ_c (Pa)	C_e (s/m)
From database			(*)	0.02	1,800	2,200	5×10^{-3}	0.5	0	(**)

* The radius at failure is given by the back-analysis knowing the peak flow (Table 4.1).

**The coefficient of erosion is given by the back-analysis knowing the time to failure (Table 4.2).

Table 4.4. Model parameters for the database analysis

Dam name and location	Data		Dam break modeling results			
	H_{dam} (m)	C_e (10^{-3} s.m^{-1})	Δt_u (h)	Q_{peak} ($\text{m}^3.\text{s}^{-1}$)	τ_b (Pa)	V_u (m.s^{-1})
Ireland No. 5, Colo.	6.0	24	0.24	101	258	7.1
Lower Latham, Colo.	8.6	10	0.57	305	393	8.8
Frankfurt, Germany	9.8	1	2.33	79	774	12.4
Kelly Barnes, Ga.	11.6	10	0.35	675	1,277	16
French Landing, Mich.	12.2	15	0.39	811	571	10.6
Lake Latonka, Penn.	13.0	4	1.2	290	490	9.9
Lake Avalon, N.M.	14.5	6	0.71	2,306	1,165	16.9
Quail Creek, Utah	18.9	10	0.44	3,068	1,481	17.1
Hatchtown, Utah	19.2	2	1.77	3,080	1,600	19.1
Little Deer Creek, Utah	26.2	5	0.66	1,305	2,362	21.7
Bradfield, England	29.0	4	0.91	1,134	3,278	25.6
Apishapa, Colo.	34.1	2	1.68	6,817	2,876	24
Hell Hole, Calif.	67.1	8	0.96	7,161	3,462	26.3
Teton, Idaho	93.0	1	3.71	64,738	7,951	39.9

Table 4.5. Well-documented failure cases by piping, calculation of the time to failure, and the peak flow, the shear stress and the flow velocity at failure with the pipe flow with erosion breach model

4.7. Modeling concentrated leak erosion statistically

4.7.1. The probabilistic approach

The erosion law equation [4.3] is a deterministic approach to the concentrated leak erosion. However, the mechanics of detachment of soil particles by water flow is not a simple function of averages of a flow parameter, such as the mean hydraulic wall shear stress τ and the mean soil critical stress τ_c . Detachment may also occur even if $\tau_b < \tau_c$. This is illustrated in Figure 4.30.

Turbulent flow is characterized by the random and rapid fluctuation of swirling regions of fluid, called eddies, throughout the flow. Burst events in the turbulent flow create much greater local shear stresses than the averages,

and detachment occurs only for those burst events where stress exceeds the local tensile strength of the soil. We denote by τ_b^{loc} the local hydraulic wall shear stress, which is considered here as a stochastic variable.

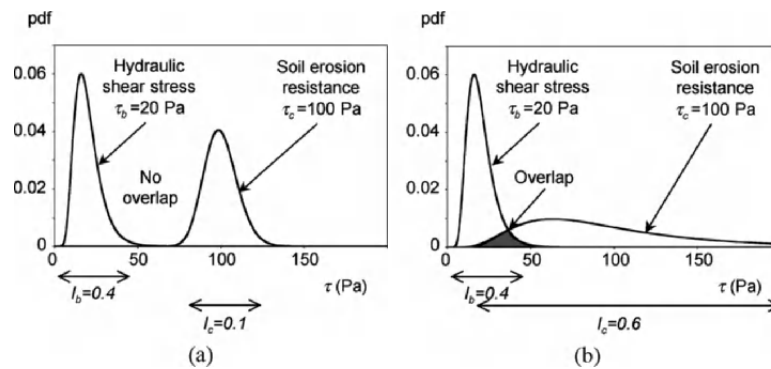


Figure 4.30. Probability density functions of hydraulic load and soil resistance, illustrative example with a mean hydraulic wall shear stress ($\bar{\tau}_b = 20$ Pa) lower than the mean critical stress ($\bar{\tau}_c = 100$ Pa): a) small coefficient of variation of the soil critical stress ($I_c = 0.1$), no overlap, no erosion can occur; b) large coefficient of variation of the soil critical stress ($I_c = 0.6$), erosion can occur as there is an overlap

The stochastic aspect of incipient motion has been recognized as far back as Shields, although today his view is conceived as being deterministic. The critical stress for a mixed-grain, cohesive soil differs, however, from the critical Shields stress for a non-cohesive granular soil. It represents an aggregated property of the soil matrix. For a given soil, the local critical stress, denoted by τ_c^{loc} , can also vary due to the soil heterogeneity. It is considered here as a stochastic variable.

Local, or instantaneous, detachment of soil particles by turbulent flow of water occurs when $\tau_b^{loc} > \tau_c^{loc}$: the concept of threshold relative to local stresses continues to have validity. However, within a probability-based approach, detachment of soil particles occurs when an overlap of two probability

density functions (pdfs) occurs: one describes the distribution of τ_b^{loc} and another describes the distribution of τ_c^{loc} (Figure 4.30). For the same value of the mean stresses, an increase in the relative intensity of the wall shear stress fluctuations, and in the coefficient of variation of the soil critical stress, leads to increasing erosion due to a greater overlap in pdfs.

We denote by $f(x)$ the pdf of the random variable x . The statistical concept of the ensemble average considered here is based on a large number of independent realizations of local quantities. In accordance with the possibility of unsteadiness of the process, an ensemble average involving any local mechanical quantity x is allowed to vary in a deterministic manner with time. The ensemble average means the mean value, denoted by $\langle x \rangle$, at a specific moment in time and a specific position, having repeated the process many times.

The mean value $\langle x \rangle$ and the standard deviation $[x]_{rms}$, or root mean square (rms), of x can be calculated as

$$\langle x \rangle = \int_{-\infty}^{+\infty} xf(x)dx \quad [4.51]$$

$$[x]_{rms} = \left(\int_{-\infty}^{+\infty} (x - \langle x \rangle)^2 f(x)dx \right)^{1/2} \quad [4.52]$$

4.7.2. The probability density function of the stress ratio

Erosion locally occurs if $\tau_b^{loc} - \tau_c^{loc} > 0$. Lopez and Garcia [LOP 01] assumed that the difference $\tau_b^{loc} - \tau_c^{loc}$ is normally distributed for computing the risk of sediment erosion. Equivalently, erosion locally occurs if $\ln(\tau_b^{loc} / \tau_c^{loc}) > 0$. This time, the stress ratio $\tau_b^{loc} / \tau_c^{loc}$ is always a positive quantity.

The pdf of $\tau_b^{loc} / \tau_c^{loc}$ can, therefore, be represented with the two-parameter lognormal function [CHE 03, LOP 94]:

$$f(r) = \begin{cases} \frac{1}{r\sigma_{\ln r}\sqrt{2\pi}} \exp\left\{-\frac{1}{2}\left(\frac{\ln r - \mu_{\ln r}}{\sigma_{\ln r}}\right)^2\right\} & \text{for } r > 0 \\ 0 & \text{for } r \leq 0 \end{cases} \quad [4.53]$$

where $\mu_{\ln r} = \langle \ln r \rangle$ is the mean value of $\ln(\tau_b^{loc} / \tau_c^{loc})$ and $\sigma_{\ln r} = [\ln r]_{rms}$ is the standard deviation of $\ln(\tau_b^{loc} / \tau_c^{loc})$,

$$\mu_{\ln r} = \ln\left(\frac{\langle r \rangle}{\sqrt{1 + I_r^2}}\right), \sigma_{\ln r} = \sqrt{\ln(1 + I_r^2)} \quad [4.54]$$

and r denotes the stress ratio, I_r is the relative intensity of the stress ratio fluctuation, and $\langle r \rangle$ and $[r]_{rms}$ are the mean value and the standard deviation of the stress ratio, respectively:

$$I_r = \frac{[r]_{rms}}{\langle r \rangle}, r = \frac{\tau_b^{loc}}{\tau_c^{loc}} \quad [4.55]$$

It can be shown that this log-normal pdf reduces to the Gaussian function if I_r is small [CHE 03]. The use of these assumptions on $\tau_b^{loc} / \tau_c^{loc}$ allows us to formulate a probabilistic description of erosion, without specifying the type of distributions for τ_b^{loc} or τ_c^{loc} . It is, however, accepted that the hydraulic wall shear stress fluctuates also in a lognormal fashion [CHE 03, KEI 12, LOP 94].

Now, we assume that the hydraulic wall shear stress τ_b^{loc} and the soil critical stress τ_c^{loc} are *independent* random variables. It follows that

$$\langle I \rangle = \frac{\tau_b}{\tau_c}, 1 + I_r^2 = (1 + I_\tau^2)(1 + I_c^2) \quad [4.56]$$

where τ_b is the mean value of the hydraulic wall shear stress τ_b^{loc} and $1/\tau_c$ is the mean value of the inverse of the soil critical stress τ_c^{loc} ,

$$\tau_b = \langle \tau_b^{loc} \rangle, \tau_c = \left\langle \frac{1}{\tau_c^{loc}} \right\rangle^{-1} \quad [4.57]$$

and where I_τ is the relative intensity of the wall shear stress fluctuations τ_b^{loc} , and I_c is the coefficient of variation of the soil critical stress τ_c^{loc}

$$I_\tau = \frac{[\tau_b^{loc}]_{rms}}{\tau_b}, I_c = \tau_c [(\tau_c^{loc})^{-1}]_{rms} \quad [4.58]$$

The harmonic mean is always less than the arithmetic mean, which is conservative regarding the critical stress ($\langle \tau_c^{-1} \rangle^{-1} \leq \langle \tau_c \rangle$).

4.7.3. Probabilistic description of erosion

As the detachment of soil particles by turbulent flow of water occurs when $\tau_b^{loc} > \tau_c^{loc}$, the local erosion law can be rewritten as follows:

$$\frac{dR^{loc}}{dt} = E^{loc} \left(\frac{\tau_b^{loc}}{\tau_c^{loc}} - 1 \right)^+, E^{loc} = \frac{C_e^{loc} \tau_c^{loc+}}{\rho_d^{loc}} \quad [4.59]$$

where

$$(x)^+ = \begin{cases} x & \text{for } x \geq 0 \\ 0 & \text{for } x < 0 \end{cases} \quad [4.60]$$

We assume that the stress ratio $\tau_b^{loc} / \tau_c^{loc}$ and the coefficient of erosion E^{loc} are *independent* random variables.

The average of equation [4.59], which defines the evolution of the mean hole radius $R = \langle R^{loc} \rangle$, reads:

$$\frac{dR}{dt} = \langle E^{loc} \rangle \left\langle \left(\frac{\tau_b^{loc}}{\tau_c^{loc}} - 1 \right)^+ \right\rangle \quad [4.61]$$

Using equations [4.51] and [4.60] yields the following result:

$$\left\langle \left(\frac{\tau_b^{loc}}{\tau_c^{loc}} - 1 \right)^+ \right\rangle = \int_1^{\infty} (r-1) f(r) dr \quad [4.62]$$

Now, using equations [4.53] – [4.56], the following result can be obtained after several lines of analytical development:

$$\frac{dR}{dt} = E \left[a \left(\frac{\tau_b}{\tau_c} \right) - b \right], E = \left\langle \frac{C_e^{loc} \tau_c^{loc}}{\rho_d^{loc}} \right\rangle \quad [4.63]$$

$$a = \begin{cases} \frac{1}{2} \operatorname{erfc} \left(- \frac{\ln \left(\frac{\tau_b}{\tau_c} \right) + \frac{1}{2} \ln \left[(1 + I_\tau^2)(1 + I_c^2) \right]}{\sqrt{2 \ln \left[(1 + I_\tau^2)(1 + I_c^2) \right]}} \right) & \text{for } \tau_c > 0 \\ 1 & \text{if } \tau_c = 0 \end{cases} \quad [4.64]$$

$$b = \begin{cases} \frac{1}{2} \operatorname{erfc} \left(- \frac{\ln \left(\frac{\tau_b}{\tau_c} \right) - \frac{1}{2} \ln \left[(1 + I_\tau^2)(1 + I_c^2) \right]}{\sqrt{2 \ln \left[(1 + I_\tau^2)(1 + I_c^2) \right]}} \right) & \text{for } \tau_c > 0 \\ 1 & \text{if } \tau_c = 0 \end{cases} \quad [4.65]$$

If $\tau_c = 0$, there is no influence of stress fluctuations. If $\tau_c \neq 0$, τ_b / τ_c can fluctuate around one. Two new parameters are now required: the relative intensity of the hydraulic wall shear stress fluctuations I_τ and the coefficient of variation of the soil critical stress I_c .

4.7.4. Order of magnitude of the relative intensity of the shear stress fluctuations

There are many similarities in the velocity distributions for channel, pipe and boundary layer flows in the very near wall region. In boundary layer flows and pipe flows, the relative intensity of the hydraulic wall shear stress fluctuations I_τ can range from 0.32 to 0.39 in the viscous sublayer [CHE 94]. In turbulent channel flows, I_τ can range in the order of 0.3 to 0.45 as shown in Figure 4.31 [KEI 12]. Figure 4.33 shows the orders of magnitude of I_τ as a function of the Kàrmàn number $Re_\tau = u_b(h/2)/\nu$, with $u_b = (\tau_b/\rho_w)$ the friction velocity and h the channel height. The corresponding Reynolds number ranged from 2,000 to 10,000.

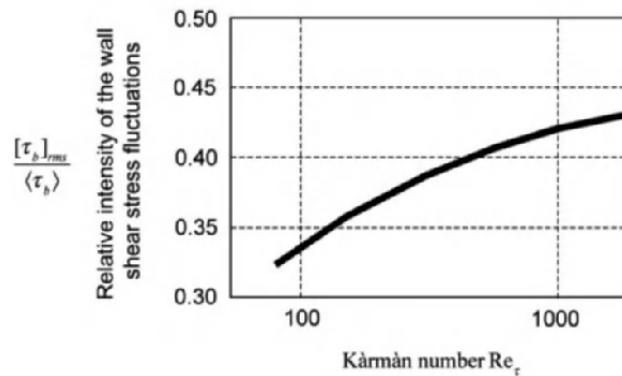


Figure 4.31. Order of magnitude of the relative intensity of the wall shear stress fluctuations I_τ as a function of the Kàrmàn number Re_τ from instantaneous velocity and wall shear stress measurements conducted in a turbulent channel flow, where $Re_\tau = u_b(h/2)/\nu$, with $u_b = (\tau_b/\rho_w)$ the friction velocity and h the channel height [KEI 12]

On site, the variability in I_τ is likely to be large, as I_τ can go up to one when significant fluctuations take place [SUM 03]. The question whether the value should be the same in the laboratory and on site is open. However, there is no universal formula (yet) relating the relative intensity of the wall shear stress fluctuations to the Reynolds number, or to the friction coefficient. A crude but effective assumption is simply that I_τ is constant, with a typical value of 0.4 [KNA 07].

4.7.5. Order of magnitude of the coefficient of variation of the soil critical stress

To better understand the role of I_c , we assume here that $\ln(1/\tau_c^{loc})$ is normally distributed with mean μ_c and standard deviation σ_c . The probability that a new measurement falls within the interval $[\mu_c - \beta\sigma_c, \mu_c + \beta\sigma_c]$ is, therefore, $\text{erf}(\beta/\sqrt{2})$. The corresponding interval for τ_c^{loc} can be obtained using the results of equations [4.54]:

$$c_{\min} \leq \frac{\tau_c^{loc}}{\tau_c} \leq c_{\max} \quad [4.66]$$

$$c_{\min} = \sqrt{1 + I_c^2} \exp\left(-\beta\sqrt{\ln(1 + I_c^2)}\right) \quad [4.67]$$

$$c_{\max} = \sqrt{1 + I_c^2} \exp\left(\beta\sqrt{\ln(1 + I_c^2)}\right) \quad [4.68]$$

Table 4.6 summarizes the values of the 95% confidence interval ($\beta = 1.96$) with several values of I_c , the coefficient of the variation of the soil critical stress τ_c^{loc} . In particular, the value $I_c = 0.4$, which appears to cover most of the HET results, leads to [0.51, 2.29] as 95% confidence interval. To fix ideas, consider a soil sample with $\tau_c = 10$ Pa and $I_c = 0.4$. The 95% confidence interval of this soil sample is, therefore, [5.1 Pa, 22.9 Pa].

I_c	c_{min}	Mean	c_{max}
0.1	0.83	1	1.22
0.2	0.69	1	1.50
0.4	0.51	1	2.29
0.6	0.39	1	3.46
0.8	0.32	1	5.08
1.0	0.28	1	7.23

Table 4.6. Values of the 95% confidence interval with several values of I_c

On site, the variability in I_c is likely to be large. The coefficient of the variation can range in the order of 0.14 for a high erosion rate to greater than 1.5 for a low erosion rate [NEA 99]. The coefficient I_c accounts, therefore, for the scale effect, as it depends on the system considered, and it cannot take the same value in the laboratory and on site.

4.7.6. A stochastic erosion law for cohesive soils

Figure 4.32 shows a dimensionless representation of the erosion law for several values of the relative intensity of the stress ratio fluctuation I_r , from 0.01 to 0.8. For a very small I_r ($I_r \ll 1$ which means in practical terms that $I_r < 0.01$), the stochastic erosion law equation [4.63] reduces to the classical erosion law equation [4.3].

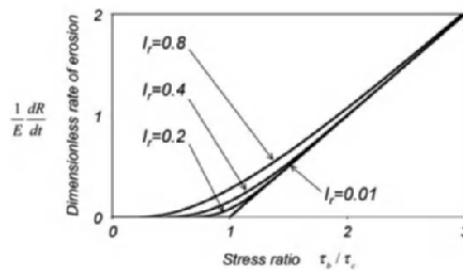


Figure 4.32. Dimensionless representation of the erosion law equation [4.61], effect of varying the relative intensity of the stress ratio fluctuation I_r

The relative intensity of the stress ratio fluctuation I_r is a function of the relative intensity of the hydraulic wall shear stress fluctuations I_τ and the coefficient of the variation of the soil critical stress I_c is defined by equation [4.56] and illustrated in Figure 4.33. A typical value of I_r corresponding to $I_\tau = 0.4$ and $I_c = 0.4$ is $I_c = 0.58$.

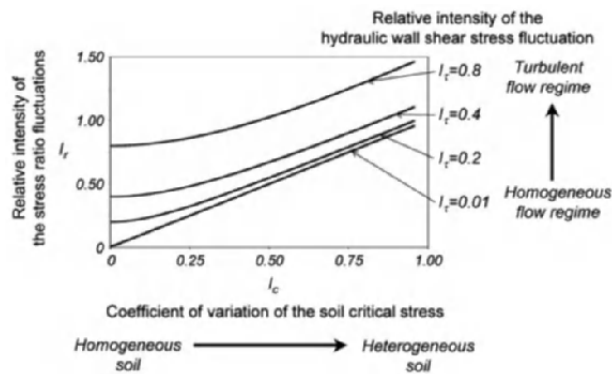


Figure 4.33. Relative intensity of the stress ratio fluctuation I_r as a function of the coefficient of variation of the soil critical stress I_c and of the relative intensity of the hydraulic wall shear stress fluctuation I_τ

For the same value of the mean wall shear stress τ_b , an increase in the relative intensity of the wall shear stress fluctuations I_τ , or an increase in the coefficient of variation of the soil critical stress I_c , leads to increasing erosion due to an increase in the relative intensity of the stress ratio I_r . In addition, erosion may also occur even if $\tau_b < \tau_c$: the probabilistic erosion law equation [4.63] is a model without threshold. It is not surprising, as the average of a local threshold law involving local stresses is not a threshold law involving the average of the local stresses. This model reproduces, however, data features previously described as indicating the threshold.

The amount of erosion occurring at the threshold will depend on the definition of the threshold adopted [KNA 07,

LAV 87]. There has been no consensus as to what constitutes erosion significant enough to say that a threshold has been exceeded. The critical stress must, therefore, be viewed as a probabilistic quantity (e.g. within a probability-based approach, the Shields' curve can be shown to correspond to an erosion risk of 40% [LOP 01]).

The question now is: what is the rate of erosion? At the structure scale, the question of what will be a failure has no meaning within this context. It is replaced by the following issue: when does failure occur? We go back to Figure 4.23: does failure occur within a few minutes, a few hours, a few days, or is it longer?

Of course, the reality may be more complex than the overlap of two distributions. The hydraulic wall shear stress τ_b^{loc} and the soil critical stress τ_c^{loc} may be *dependent* random variables. For example, there is no guarantee that the resistance distribution itself is independent of the hydraulic driving force distribution. Again, the Shields critical stress is an illustrative example, as it is a function of the particle Reynolds number.

The modern generation of the erosion law should account for the relative intensity of the wall shear stress fluctuations, and for the coefficient of the variation of the soil critical stress. The full validation of the stochastic erosion law presented here requires further work, and requires a set of data and measures, in order to be suited for practical applications.

4.8. Comments

4.8.1. *Comment on the friction coefficient*

The total momentum loss due to friction on the soil can be divided into two components (equation [4.69]):

1) the momentum loss due to skin friction on the wall, where the roughness is defined at the grain scale, which is the microscopic scale;

2) the momentum loss due to form friction on the bed, where irregularities are defined at a larger scale than the soil grain, which is the mesoscopic scale.

$$\underbrace{\tau_b}_{\substack{\text{total momentum loss} \\ \text{due to friction} \\ \text{on the soil}}} = \underbrace{\tau_{skin}}_{\substack{\text{momentum loss} \\ \text{due to skin friction} \\ \text{at the soil grain scale}}} + \underbrace{\tau_{form}}_{\substack{\text{momentum loss} \\ \text{due to form friction} \\ \text{at the surface irregularities scale}}} \quad [4.69]$$

This concept introduced by Einstein (1950) and Einstein and Barbosa (1952) was confirmed experimentally by Shen *et al.* (1990) (see [BAN 08]). It plays a fundamental role in hydraulic analysis in coarse river beds [JUL 02, PET 90]. However, few attempts have been made to understand the role of these two kinds of friction on cohesive soils and in pipe flow.

The friction coefficient f_b , which accounts for the flow resistance initially introduced by Weisbach in 1845 [BRO 02], is often divided into two components as follows [AZF 10, BAN 08, JUL 95]:

$$\underbrace{f_b}_{\substack{\text{total friction} \\ \text{coefficient}}} = \underbrace{f_{skin}}_{\substack{\text{skin friction} \\ \text{at the microscopic scale} \\ \text{(the soil grain scale)}}} + \underbrace{f_{form}}_{\substack{\text{form friction} \\ \text{at the mesoscopic scale} \\ \text{(the surface irregularities scale)}}} \quad [4.70]$$

The skin friction coefficient is a function of the Reynolds number and the roughness of the wall [SCH 87]. Although an old issue, the theory of pipe flow is still a subject for debate. There is no universal skin friction factor for pipe flow [SHO 06], and there are numerous formulas. The choice is only a matter of habit and practical use, as they lead to the same order of magnitude. The Colebrook–White equation, illustrated on the Moody diagram, is one of the most used

equations. The Colebrook–White equation can be written as follows:

$$\frac{1}{\sqrt{8f_{skin}}} = -2 \log \left[\frac{2.51}{R_e \sqrt{8f_{skin}}} + \frac{\varepsilon}{3.72} \right]. \quad [4.71]$$

where $R_e = 2RV/\nu$ is the Reynolds number, ν is the water kinematic viscosity and where $\varepsilon = k_s/(2R)$ is the relative roughness.

At the microscopic scale, the roughness k_s of a sand bed can be clearly defined by the average sand grain diameter. In the same way, the roughness of a cohesive soil containing sand grains may be defined as a function of the sand grain diameter. However, defining the roughness of a mixture of clay and silt is not clear, and this roughness is likely to be very small. In addition, the use of the Colebrook–White formula [4.71] in order to evaluate the radius with equation [4.24], in connection with more than one hundred HETs studied, resulted in a serious underestimation of the final radius in comparison with that which was obtained using the measurement after completion of the HET. This clearly shows that there is a problem in using classical pipe flow formulas, when studying pipe flows in cohesive soils, with erosion.

A further aspect to consider is bedform induced friction. At the mesoscopic scale, the form shear stress is likely to represent local momentum losses due to the bedform geometry (irregularities, ripples). A typical example of bedform irregularities caused by erosion in an HET is shown in Figure 4.34. In Figure 4.35, examination of the characteristic dimension of the irregularities of the hole, which are of the order of several millimeters, compared with the surface of the upstream and downstream faces, clearly shows that we cannot talk about surface roughness. In Figure 4.9, showing paraffin wax specimens of the hole, the irregularities appear to be of the order of magnitude of the

hole diameter. It should be borne in mind that surface roughness is a relative concept. Strictly speaking, it has significance when its height is comparable to the thickness of the laminar sublayer, which is a function of the Reynolds number.

In Figures 4.1 and 4.2, two examples of bedform irregularities caused by erosion on site, at the large scale, are shown. Again, we cannot talk about surface roughness defined by a grain diameter. However, in Figures 4.1 and 4.2 showing real pipes on site, the irregularities are not of the order of magnitude of the hole diameter.

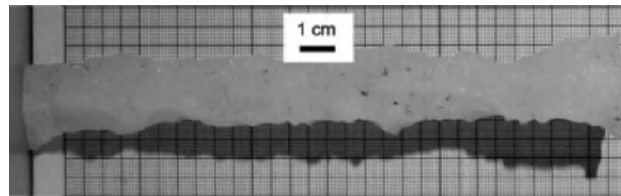


Figure 4.34. Paraffin wax specimen of the hole of a very fast soil

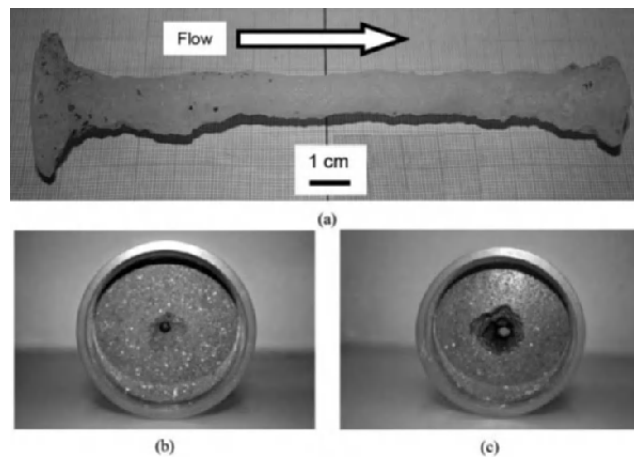


Figure 4.35. Specimen of a moderately fast soil: a) paraffin wax of the hole, showing the bedform irregularities, b) specimen before erosion and its initial hole (3 mm radius, downstream face) and c) specimen after erosion (downstream face)

The partitioning of total shear stress is still a subject for debate. Yet, subtraction of skin shear stress from the total shear stress has been commonly used to estimate the form shear stress. The classical skin friction formulas are, therefore, not useful as predictors if the form friction coefficient cannot be estimated with certainty during the erosion process. The use of the classical skin friction formulas lies mostly in the estimation of the head loss factor in non-erodible specimens with an axial smooth hole of constant diameter (e.g. a Polyvinyl chloride (PVC) specimen).

The question of whether it is the skin friction shear stress of the total shear stress which controls erosion remains open. We assume here that the total shear stress is a better soil detachment predictor than the skin shear stress only [GIM 02, KNA 07]. This assumption is of practical use at the laboratory, for HET interpretation, and on site, for dam- and levee-break modeling.

More research work should be carried out to better understand the role of the form shear stress in the erosion process and quantify the form friction coefficient for pipe flows in soils.

4.8.2. Comment on the linearity of the erosion law

The linear erosion law given by equation [4.3] is a strong assumption. A nonlinear expression can, of course, be chosen, such as:

$$\frac{dR}{dt} = \begin{cases} \frac{C_e \tau_c}{\rho_d} \left(\frac{\tau_b}{\tau_c} - 1 \right)^p & \text{if } \tau_b > \tau_c \\ 0 & \text{otherwise} \end{cases} \quad [4.72]$$

Assuming $\tau_c < P_0$, the closed-form solution generalizing equation [4.17] when $t > 0$ is this time

$$R(t) = \begin{cases} R_0 \left[\frac{\tau_c}{P_0} + \left(1 - \frac{\tau_c}{P_0} \right) \exp\left(\frac{t}{t_{er}}\right) \right] & \text{if } p = 1 \\ R_0 \left\{ \frac{\tau_c}{P_0} + \left[\left(1 - \frac{\tau_c}{P_0} \right)^{1-p} + (1-p) \frac{t}{t_{er}} \left(1 - \frac{\tau_c}{P_0} \right)^{1-p} \right]^{\frac{1}{1-p}} \right\} & \text{if } p \neq 1 \end{cases} \quad [4.73]$$

The empirical exponent $p \geq 0$ can be *a priori* higher than 1 or lower than 1 [KNA 07, ZHU 01]. However, the value $p = 0$ corresponds to an erosion law that does not depend on the stress, and this gives a constant flux of eroded material, which is not relevant. On the other hand, if $p > 1$, the radius takes an infinite value in finite time:

$$\lim_{t \rightarrow t_u} R(t) = \infty \text{ with } t_u = \frac{t_{er}}{p-1} \left(\frac{\tau_c}{P_0 - \tau_c} \right)^{p-1} \text{ if } p > 1 \quad [4.74]$$

As this result has no mechanical significance, we can conclude that the condition for this third parameter is $0 < p \leq 1$. This result confirms that the model developed by Meyer-Peter & Muller (1948) (used in [PAQ 98]) is not an erosion law, as it involves the exponent $p = 3/2$. This empirical model is a transport model, which is based on the spatial gradient of the capacity transport under steady-state conditions.

Adding the third parameter p is only a matter of fitting the numerical and experimental results. It provides little insight into the real mechanism underlying surface erosion, contrary to the two parameters τ_c and C_e , which are of obvious significance. The linear erosion law fits favourably with all the measured values on HETs, where $\tau_b/\tau_c - 1$ ranged from 0 to 3. Values of p , differing significantly from 1, have been found to give poor fits. Hence, we conclude that $p = 1$ appears to be suitable for interpreting HETs.

Note that it is not possible to extend this conclusion to case studies, as the eroding fluid velocity can be greater in the pipes occurring at dams or dikes. Further research is required to determine whether other sources of nonlinearity should be taken into account. However, knowing the value of p cannot be greater than 1, consideration of $p = 1$ is more critical and, therefore, yields a conservative result.

4.9. Bibliography

- [AFZ 10] AFZALIMEHR H., SINGH V.P., NAJAFABADI E.F., “Transport determination of form friction factor”, *Journal of Hydrologic Engineering*, vol. 15, no. 3, pp. 237–243, 2010.
- [BAN 08] BANASIAK R., VERHOEVEN R., “Transport of sand and partly cohesive sediments in a circular pipe run partially full”, *Journal of Hydraulic Engineering*, vol. 134, no. 2, pp. 216–224, 2008.
- [BEN 12a] BENAHMED N., BONELLI S., “Investigating concentrated leak erosion behaviour of cohesive soils by performing hole erosion tests”, *European Journal of Environmental and Civil Engineering*, vol. 16, no. 1, pp. 43–58, 2012.
- [BEN 12b] BENAHMED N., CHEVALIER C., BONELLI S., “Chapter 5 – concentrated leak erosion”, *Erosion of Geomaterials*, ISTE Ltd, London and John Wiley & Sons, New York, pp. 155–186, 2012.
- [BON 07] BONELLI S., MAROT D., TERNAT F., *et al.*, “Criteria of erosion for cohesive soils”, *Report of the European Working Group of ICOLD, Edt Technical University of Munich (TUM)*, no. 114, Munich, pp. 45–59, 2007.
- [BON 08] BONELLI S., BRIVOIS O., “The scaling law in the hole erosion test with a constant pressure drop”, *International Journal for Numerical Methods in Engineering*, vol. 32, pp. 1573–1595, 2008.
- [BON 11] BONELLI S., BENAHMED N., “Piping flow erosion in water retaining structures”, *International Journal on Hydropower and Dams*, vol. 18, no. 3, pp. 94–99, 2011.

- [BON 12a] BONELLI S., GOLAY F., MERCIER F., “Chapter 6 – on the modelling of interface erosion”, in *Erosion of Geomaterials*, ISTE Ltd, London and John Wiley & Sons, New York, pp. 187–222, 2012.
- [BON 12b] BONELLI S., COURIVAUD J.-R., DUCHESNE L., *et al.*, “Internal erosion on dams and dikes: lessons from experience and modelling”, *24th International Congress on Large Dams*, Kyoto, pp. Q.93–R.23, 6–8 June 2012.
- [BRO 02] BROWN G.O., “The history of the Darcy-Weisbach equation for pipe flow resistance”, in FREDRICH A., ROGERS J. (eds), *Environmental and Water Resources History*, ASCE, Reston, VA, pp. 34–43, 2002.
- [CHE 03] CHENG N.-S., LAW A.W.-K., “Fluctuations of turbulent bed shear stress”, *Journal of Engineering Mechanics*, vol. 129, pp. 126–130, 2003.
- [CHE 94] CHEW Y.T., KHOO B.C., LI G.L., “A time-resolved hot-wire shear stress probe for turbulent flows: use of laminar flow calibration”, *Experiment in Fluids*, vol. 17, pp. 75–83, 1994.
- [COU 07] COURIVAUD J.-R., FRY J.-J., “Dam breaching, case studies”, in Assessment of the Risk of Internal Erosion of Water Retaining Structures: Dams, Dikes and Levees, Report of the European Working Group of ICOLD, Edt Technical University of Munich (TUM), no. 114, Munich, pp. 245–254, 2007.
- [COU 09] COURIVAUD J.-R., FRY J.-J., BONELLI S., *et al.*, “Measuring the erodibility of soil materials constituting earth embankments: a key input for dams and levees safety assessment”, *HYDRO 2009 International Conference and Exhibition*, Lyon, France, 26–28 October 2009.
- [FAR 07] FARRAR J.A., TORRES R.L., ERDOGAN Z., “Bureau of reclamation erosion testing for evaluation of piping and internal erosion of dams”, *Geotechnical Special Publication*, no. 167, pp. 22–31, 2007.
- [FEL 03] FELL R., WAN C.F., CYGANIEWICZ J., *et al.*, “Time for development of internal erosion and piping in embankment dams”, *ASCE Journal of Geotechnical and Geo Environmental Engineering*, vol. 129, no. 4, pp. 307–314, 2003.

- [FEL 08] FELL R., FOSTER M., DAVIDSON R., *et al.*, A unified method for estimating probabilities of failure of embankment dams by internal erosion and piping, UNICIV Report R 446, School of Civil and Environmental Engineering, University of New South Wales, Sydney, Australia, 2008.
- [GIM 02] GIMENEZ R., GOVERS G., “Flow detachment by concentrated flow on smooth and irregular beds”, *Soil Science Society of America Journal*, vol. 66, pp. 1475–1483, 2002.
- [HAG 12] HAGHIGHI I., CHEVALIER C., DUC M., *et al.*, “Improvement of hole erosion test and results on reference soils”, *Journal of Geotechnical and Geoenvironmental Engineering*, 2012.
- [HAN 11] HANSON G.J., TEMPLE D.M., HUNT S.L., *et al.*, “Development and characterization of soil material parameters for embankment breach”, *Applied Engineering in Agriculture*, vol. 27, no. 4, pp. 587–595, 2011.
- [HAU 08] HAUKE G., *An Introduction to Fluid Mechanics and Transport Phenomena*, Fluid Mechanics and Its Applications, vol. 86, Springer, p. 215, 2008.
- [HOE 04] HÖEG K., LØVOLL A., VASKINN K. A., “Stability and breaching of embankment, dams: field tests on 6 meter high dams”, *The International Journal of Hydropower and Dams*, vol. 5, no. 5, pp. 85–89, 2004.
- [HUN 05] HUNT S.L., HANSON G.J., COOK K.R., *et al.*, “Breach widening observations from earthen embankment tests”, *Transactions of the ASAE*, vol. 48, no. 3, pp. 1115–1120, 2005.
- [JUL 95] JULIEN P.Y., *Erosion and Sedimentation*, Cambridge University Press, Cambridge, 1995.
- [JUL 02] JULIEN P.Y., KLAASSEN G.J., TEN BRINKE W.B.M., *et al.*, “Case study: bed resistance of Rhine River during 1998 flood”, *Journal of Hydraulic Engineering*, vol. 128, no. 12, pp. 1042–1050, 2002.
- [KEI 12] KEIRSBULCK L., LABRAGA L., GAD-EL-HAK M., “Statistical properties of wall shear stress fluctuations in turbulent channel flows”, *International Journal of Heat and Fluid Flow*, vol. 37, pp. 1–8, 2012.

- [KNA 07] KNAPEN A., POESEN J., GOVERS G., *et al.*, “Resistance of soils to concentrated flow erosion: a review”, *Earth-Science Reviews*, vol. 80, pp. 75–109, 2007.
- [LAC 08] LACHOINETTE D., GOLAY, F., BONELLI S., “One-dimensional modelling of piping flow erosion”, *Comptes Rendus de Mécanique*, vol. 336, pp. 731–736, 2008.
- [LAV 87] LAVELLE J.W., MOFJELD H.O., “Do critical stress for incipient motion and erosion really exist?”, *Journal of Hydraulic Engineering*, vol. 113, no. 3, pp. 370–385, 1987.
- [LEF 85] LEFEBVRE G., ROHAN K., DOUVILLE S., “Erosivity of natural intact structured clay: evaluation”, *Canadian Geotechnical Journal*, vol. 22, no. 4, pp. 508–517, 1985.
- [LEF 86] LEFEBVRE G., ROHAN K., MILETTE J.-P., “Erosivity of intact clay: influence of the natural structure”, *Canadian Geotechnical Journal*, vol. 23, no. 4, pp. 427–434, 1986.
- [LEN 87] LENCATRE A., *Handbook of Hydraulic Engineering*, Halsted Press, New York, NY, p. 540. 1987.
- [LIM 06] LIM S.S., Experimental investigation of erosion in variably saturated clay soil, PhD Thesis, University of New South Wales, Sydney, 2006.
- [LOP 94] LOPEZ F., GARCIA M.H., “Risk of sediment erosion and suspension in turbulent flows”, *Journal of Hydraulic Engineering*, vol. 127, no 3, p. 231–235, 2001.
- [LOP 01] LOPEZ F., GARCIA M.H., “Risk of sediment erosion and suspension in turbulent flows”, *Journal of Hydraulic Engineering*, vol. 127, no. 3, pp. 231–235, 2001.
- [LØV 03] LØVOLL A., VASKIN K., Data report no. 5, large scale field test, IMPACT (Investigation of Extreme Flood Processes and Uncertainty) FP5 European Project, 2003. Available at www.impact-project.net.
- [LØV 06] LØVOLL A., “Breach formation in rockfill dams – results from Norwegian field tests”, *22nd International Congress on Large Dams*, Barcelona, pp. Q.86–R.4, 19–23 June 2006.
- [LUT 01] LUTHI M., A modified hole erosion test (HET-P) to study erosion characteristics of soil, PhD Thesis, University of Columbia, Vancouver, 2001.

- [MOH 02] MOHAMED M.A.A., Embankment breach formation and modelling methods, PhD Thesis, Open University, UK, 2002.
- [MOR 00] MORRIS M.W., HASSAN M.A.A.M., IMPACT: breach formation technical report (WP2), IMPACT (Investigation of Extreme Flood Processes and Uncertainty) FP5 European Project, 2000. Available at www.impact-project.net.
- [MOR 11] MORRIS M.W., Breaching of earth embankments and dams, PhD Thesis, Open University, United Kingdom, 2011.
- [NEA 99] NEARING M.A., GOVERS G., NORTON L.D., "Variability in soil erosion data from replicated plots", *Soil Science Society of America Journal*, vol. 63, pp. 1829–1835, 1999.
- [PAQ 98] PAQUIER A., NOGUES P., HERLEDAN R., "Model of piping in order to compute dam-break wave", CADAM (Concerted Action on Dam Break Modelling), FP5 European Project, *Proceedings of the Munich Meeting*, Munich, 1998.
- [PET 90] PETIT F., "Evaluation of grain shear stresses required to initiate movement of particles in natural rivers", *Earth Surface Processes and Landforms*, vol. 15, pp. 135–148, 1990.
- [RED 00] REDDI L.N., LEE I., BONALA M.V.S., "Comparison of internal and surface erosion using flow pump test on a sand-kaolinite mixture", *Geotechnical Testing Journal*, vol. 23, no. 1, pp. 116–122, 2000.
- [ROH 86] ROHAN K., LEFEBVRE G., DOUVILLE S., *et al.*, "A new technique to evaluate erosivity of cohesive material", *Geotechnical Testing Journal*, vol. 9, no. 2, pp. 87–92, 1986.
- [SCH 87] SCHLICHTING H., *Boundary Layer Theory*, 7th ed., McGraw-Hill, New York, NY, 1987.
- [SHO 06] SHOCKLING M.A., ALLEN J.J., SMITS A.J., "Roughness effects in turbulent pipe flows", *Journal of Fluid Mechanics*, vol. 564, pp. 267–285, 2006.
- [SUM 03] SUMER B.M., CHUA L.H.C., CHENG N.S., *et al.*, "Influence of turbulence on bed load sediment transport", *Journal of Hydraulic Engineering*, vol. 129, no. 8, pp. 585–596, 2003.

- [TEM 05] TEMPLE D.M., HANSON G.J., NIELSEN M.L., *et al.*, “Simplified breach analysis model for homogeneous embankments: part 1, background and model components”, *USSD Technologies to Enhance Dam Safety and the Environment, 25th Annual USSD Conference*, Salt Lake City, UT, 2005.
- [TEM 06] TEMPLE D.M., HANSON G.J., NIELSEN M.L., “WINDAM – analysis of overtopped earth embankment dams”, *ASABE Annual International Meeting*, Portland, OR, 9–12 July 2006.
- [VAS 04] VASKIN K.A., LOVOLL A., HOEG K., *et al.*, “IMPACT: physical modelling of breach formation: large scale field tests”, *Association of State Dam Safety Officials: Dam Safety Conference 2004*, Phoenix, AZ, September 2004.
- [VAS 05] VASKIN K.A., LOVOLL A., HOEG K., WP2.1 breach formation: large scale embankment failure, IMPACT (Investigation of Extreme Flood Processes and Uncertainty) FP5 European Project, 2005. Available at www.impact-project.net.
- [WAH 98a] WAHL T.L., Prediction of embankment dam breach parameters, a literature review and needs assessment, Dam Safety Report DSO-98-004, Bureau of Reclamation, US Department of the Interior, Denver, CO, 1998.
- [WAH 98b] WAHL, T.L., HANSON, G.J., COURIVAUD, J.-R., *et al.*, “Development of next generation embankment dam breach models”, *US Society of Dams Annual Meeting and Conference 2008*, Portland, OR, 2008.
- [WAH 08] WAHL T.L., REGAZZONI P.-L., ERDOGAN Z., Determining erosion indices of cohesive soils with the hole erosion test and jet erosion test, Dam Safety Technology Development Report NDSO-08-05, Bureau of Reclamation, US Department of the Interior, Denver, CO, p. 48, 2008.
- [WAH 10] WAHL T.L., “Dam breach modeling – an overview of analysis methods”, *Joint Federal Interagency Conference on Sedimentation and Hydrologic Modeling*, Las Vegas, NV, 27 June–1 July 2010.

- [WAH 11] WAHL T.L., LENTZ D.J., Physical hydraulic modeling of canal breaches, Hydraulic Laboratory Report HL-2011-09, Bureau of Reclamation, US Department of the Interior, Denver, CO, p. 56, 2011.
- [WAN 02] WAN C.F., FELL R., Investigation of internal erosion and piping of soils in embankment dams by the slot erosion test and the hole erosion test, UNICIV Report R-412, University of New South Wales, Sydney, Australia, July 2002.
- [WAN 04a] WAN C.F., FELL R., “Laboratory tests on the rate of piping erosion of soils in embankment dams”, *Geotechnical Testing Journal*, vol. 27, no. 3, pp. 295–303, 2004.
- [WAN 04b] WAN C.F., FELL R., “Investigation of rate of erosion of soils in embankment dams”, *Journal of Geotechnical and Geoenvironmental Engineering*, vol. 30, no. 4, pp. 373–380, 2004.
- [WU 11] WU W., “Earthen embankment breaching”, *Journal of Hydraulic Engineering*, vol. 137, pp. 1549–1564, 2011.
- [XU 09] XU Y., ZHANG L.M., “Breaching parameters for earth and rockfill dams”, *Journal of Geotechnical and Geoenvironmental Engineering*, vol. 135, no. 12, pp. 1957–1970, 2009.
- [ZHU 01] ZHU J.C., GANTZER C.J., ANDERSON S.H., *et al.*, “Comparison of concentrated-flow detachment equations for low shear stress”, *Soil & Tillage Research*, vol. 61, pp. 203–212, 2001.

Chapter 5

Relationship between the Erosion Properties of Soils and Other Parameters

5.1. Introduction

This chapter discusses the relationships between the erosion properties of soils and the following soil properties:

- unified soil classification;
- degree of compaction, moisture content and the degree of saturation at the time of compaction and in service;
- dispersivity and slaking properties of the soil and how this relates to clay mineralogy and the chemistry of the water;
- soil texture and structure that are related to compaction conditions.

In this chapter, we have also discussed the following:

- the effects of test methods on erosion properties;

Chapter written by Robin FELL, Gregory HANSON, Gontran HERRIER, Didier MAROT and Tony WAHL.

– how the critical shear stress and erosion rate for dispersive soils can be modified by adding lime, gypsum or cement and the mechanics of this change.

The discussion is related mainly to soils in engineered fills, but some of the discussion is applicable to soils *in situ*. It applies to internal erosion of plastic and non-plastic soils by a concentrated leak.

Some of the discussion is applicable to naturally occurring soils in dam and levee foundations and to unlined spillways in soil.

5.2. Definitions of soil erosion properties and the relationships between them

Soil erodibility is most commonly described in the literature by the excess stress equation [TEM 85, HAN 89, WAN 04a, WAN 04b]. The relationship is often expressed as the rate of erosion in terms of either volume per unit area per unit of time or mass per unit area per unit of time. For volume per unit of time, the following expression is defined:

$$E_r = k_d(\tau_e - \tau_c) \quad [5.1]$$

where E_r is the rate of erosion (m/s), k_d is the detachment/erodibility coefficient ($\text{cm}^3/\text{N}\cdot\text{s}$), τ_e is the hydraulic shear stress (N/m^2) and τ_c is the critical stress (N/m^2).

The erodibility coefficient k_d reported in $\text{cm}^3/\text{N}\cdot\text{s}$ by Hanson and Cook [HAN 04] has been observed to range in value from 0.001 to 1000. Low values indicate erosion resistant soils and high values indicate erodible soils.

For mass per unit of time, a similar expression can be defined:

$$E_t = C_e(\tau_e - \tau_c) \quad [5.2]$$

where E_t is the rate of erosion (kg/s/m^2) and C_e is the detachment/erodibility coefficient (s/m). A comparison of equations [5.1] and [5.2] gives $C_e = k_d / \rho_d$, where ρ_d is the dry density (kg/m^3).

Since the erodibility coefficient can vary over several orders of magnitude, Wan and Fell [WAN 04a] proposed an erosion rate index (I) defined as the $-\log(C_e)$ which ranges from 0 to 6.

An erosion rate index of two or less implies a very rapidly erodible soil and a high value of five or more implies a low rate of erosion. Table 5.1 presents values of k_d and C_e [HAN 10a] along with the corresponding erosion rate index and qualitative resistance class as proposed by Wan and Fell [WAN 04a]).

k_d ($\text{cm}^3/\text{N-s}$)	C_e (s/m) ¹	$I = -\log(C_e)$ ¹	Erosion Rate Index ²	Qualitative Description ²
1000	$5 \times 10^{-1} - 7 \times 10^{-1}$	0.2–0.3	0	Extremely rapid
100	$5 \times 10^{-2} - 7 \times 10^{-2}$	1.2–1.3	1	Extremely rapid
10	$5 \times 10^{-3} - 7 \times 10^{-3}$	2.2–2.3	2	Very rapid
1	$5 \times 10^{-4} - 7 \times 10^{-4}$	3.2–3.3	3	Moderately rapid
0.1	$5 \times 10^{-5} - 7 \times 10^{-5}$	4.2–4.3	4	Moderately slow
0.01	$5 \times 10^{-6} - 7 \times 10^{-6}$	5.2–5.3	5	Very slow
0.001	$5 \times 10^{-7} - 7 \times 10^{-7}$	6.2–6.3	6	Extremely slow

1 Based on the range of ρ from 1,500 to 2,000 kg/m^3 .

2 Erosion rate index and qualitative description grouping based on [WAN 04a].

Table 5.1. Relationship between k_d , C_e , I , erosion rate index and qualitative erosion resistance [HAN 10a]

The value of the erodibility/soil detachment coefficient provides an indication of how quickly surface erosion in overtopping will occur or internal erosion will develop within cracks or other openings in an embankment subjected to hydraulic stress.

5.3. Effects of test methods on soil erosion properties

5.3.1. Effect of testing methods on erosion rate

Wahl *et al.* [WAH 08] carried out tests where identically prepared remolded soil samples were tested by the hole erosion test (HET) and jet erosion test (JET). They found that both methods ranked the soils similarly for their relative erodibility, but the JET method indicated a higher rate of erosion, up to one or more orders of magnitude, and lower critical shear stresses, by up to two or more orders of magnitude.

Wahl *et al.* [WAH 08] speculated that differences between the erosion rates observed in the two tests were related to several factors, including:

- differences in the nature of the hydraulic attack upon the eroding surface in each test;
- differences in the way that the flow exploits different weaknesses in the soil structure;
- differences in the geometry of the exposed soil surface;
- inaccurate or incomplete analytical models for the stress distributions produced at the soil surface;
- use of a linear erosion model for analysis when erosion rate versus applied stress may actually be nonlinear;
- performing tests in different stress ranges and with an opposite progression of applied stress (high to low in JET,

typically well above the critical stress and low to high in HET, beginning near the critical stress level).

Briaud [BRI 08a, BRI 08b] suggests that soil erodibility may depend fundamentally on three different types of hydraulic attacks: pure shear stress, turbulent fluctuations of shear stress and turbulent fluctuations of normal stress. Wahl *et al.* [WAH 08b] discussed the fact that we analyze each test by attempting to relate only the applied shear stress to the erosion rate, but other forms of hydraulic attack may be significant and may have different degrees of influence in different test environments.

The range of soil types and compaction conditions for the tests by Wahl *et al.* [WAH 08b] was limited, but the greatest differences seemed to occur in samples with a coarse or non-uniform soil structure (generally samples containing more clay and significantly compacted dry of optimum water content). This suggested that the JET is more sensitive to soil fabric, perhaps because the stress environment produced by the impinging jet is more readily able to exploit weak zones in a non-uniform soil structure. This may also be related to the different geometry of the exposed soil surface in each test, a planar surface in the JET versus a small, confined hole for the HET. Aggregates of soil particles that can be dislodged and removed in the JET environment may be held in place by the surrounding soil mass in the HET.

Lim [LIM 06], Lim and Khalili [LIM 09] investigated the erosion properties of soils using the rotating cylinder test (RCT) and HET. In the RCT, the erosion is from the vertical sides of a sample measuring 100 mm (diameter) by 100 mm (height). Figure 5.1 shows a comparison between the erosion rate indices for these tests. It can be seen that dispersive soils have a good correlation with the HET giving a slightly larger index (slower rate of erosion). However, there is a large difference for the non-dispersive soils, with the RCT giving rates 10 – 15 times those obtained using the HET.

Lim attributes this to the vertical face of the RCT, and to surface and/or body slaking occurring in the RCT which could not occur in the HET because of the relatively large size of the slaking particles and the small hole in the HET [LIM 06]. They also noted that fabric was important in the RCT with samples, dry of the optimum, having a blocky fabric. Figure 5.1 also includes the results of JET tests carried out by Wahl *et al.* [WAH 08b] indicating some similarity between the RCT and JET results relative to the HET.

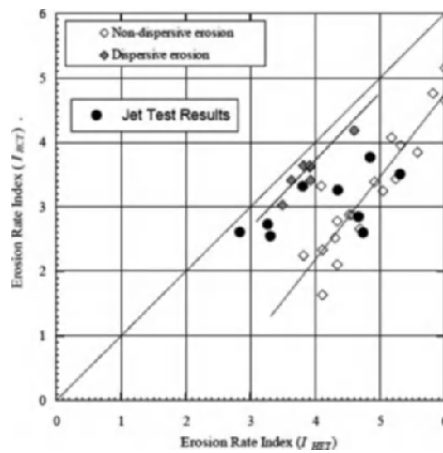


Figure 5.1. Correlation between the erosion rate indices of rotating cylinder and hole erosion tests [LIM 06] and the results of superimposed jet erosion tests [WAH 08b]

The HET and slot erosion test (SET) [WAN 02, WAN 04a] model erosion conditions in a crack and pipe in the early stages of development but may underestimate the rate of erosion as the pipe develops and the size allows the mechanisms modelled in the RCT and JET to take effect. That is, the larger blocky aggregated soil particles can erode as the hole enlarges. This could be allowed for by using a varying erosion rate index when calculating the rate of the enlargement of a pipe. However, to conclude that the scale

effect is the correct reason, one should perform HET or SET testing on larger scales and prove that the size of the hole changes the process and the results. The only conclusion we can currently make is that the two tests (HET/SET vs. JET) in their current configurations produce different results. Further research is needed to explain the reason.

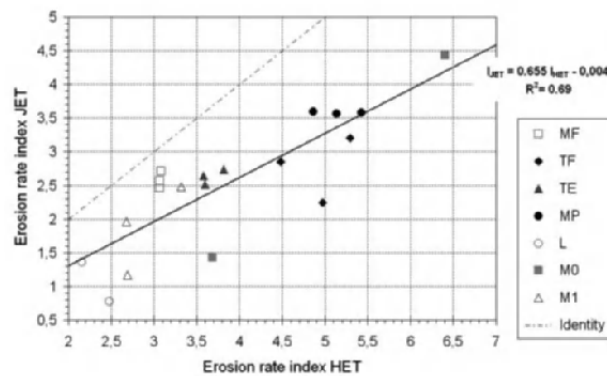


Figure 5.2. Erosion rate index values measured with the JET versus values measured with the HET [REG 13]

Regazzoni and Marot [REG 13] tested fine-grained soils covering a large range of erodibility. Soils were prepared for JET and HET testing using methods described in the *Bureau of Reclamation Earth Manual (1990)* for a total number of 19 tests with each device. Hanson and Cook's analysis [HAN 04] and Bonelli and Brivois' scaling law [BON 08] were used to analyze JET and HET, respectively. They showed that the values of the erosion coefficient are systematically higher with the JET than with the HET and the corresponding mean rate index is systematically smaller with the JET (I_{JET}) than with the HET (I_{HET}). Moreover, as shown in Figure 5.2, the relative classification of the erodibility based on the values of erosion rate index yielded by both apparatus is not exactly the same. If we consider the erosion rate index determined by JET, nearly identical values are obtained for

soils MF, TE, and TF, whereas if we consider the erosion rate index determined by HET, a clear difference appears. MF is the most erodible soil, followed by TE, and TF is the least erodible soil.

Marot *et al.* [MAR 11] proposed a new analysis which is based on the fluid energy expended ($E_{erosion}$) and the eroded dry mass (m_{dry}). The erosion resistance index is defined as $\log(E_{erosion}/m_{dry})$. The values of erosion resistance index obtained for tested fine soils are roughly the same with JET and HET devices.

5.3.2. Effect of testing methods on critical shear stress (τ_c)

The critical shear stress that initiates erosion (τ_c) is a difficult property to measure. Lim [LIM 06] and Lim and Khalili [LIM 09] found that the form of the hydraulic shear stress versus erosion rate plot varies for different soils, behaving bilinearly and others exhibiting simple linear relations with intercepts on the “X” and “Y” axes as shown in Figure 5.3.

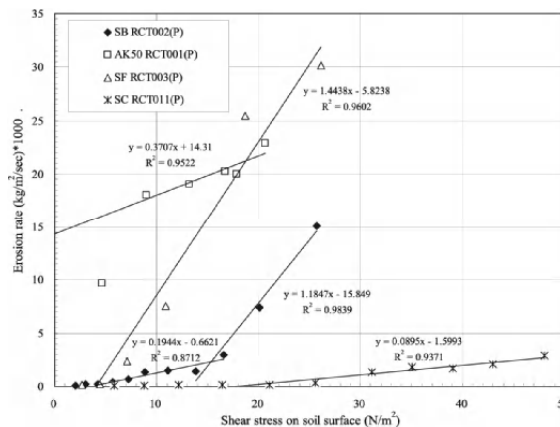


Figure 5.3. Typical erosion behavior of unsaturated non-dispersive clay soils [LIM 06]

Wan and Fell [WAN 02, WAN 04a] had similar problems and this is why they adopted the procedure of varying heads in the HET to define the critical shear stress, which they termed the initial shear stress, τ_0 .

The extrapolation of the plots in Lim [LIM 06] to the “X” axis for the RCT on non-dispersive soils gives critical shear stresses which are similar to the initial shear stresses (from HET) up to erosion indexes indices of four. Lim [LIM 06] did not test many soils with erosion rate indices greater than four, but those he did test appeared to give somewhat lower critical shear stresses than the HET. This may reflect the occurrence of slaking of larger particles on the surface of the RCT samples. Wahl *et al.* [WAH 08] also made the same observations relative to the JET and HET.

Regazzoni and Marot [REG 13] obtained critical shear stresses for the soils in Figure 5.2 as shown in Figure 5.3. They found that the critical shear stress from the JET were often much lower than for the HET.

The values of critical shear stress for the HET are rather high for soils MP and TF compared to their erosion rate indices. The JET critical shear stress values are much lower and seem too low. Wan and Fell [WAN 02, WAN 04a] performed SET and HET tests on soils with erosion rate indices of approximately five–six in the laboratory and their behavior was not consistent with such low critical shear stresses.

The reason for this and the low values found by Lim [LIM 06] for some soils needs further research.

Benahmed *et al.* [BON 08, BEN 12a, BEN 12b] have refined the HET and developed an improved method for determining critical shear stress. This involves testing at a

constant flow rate rather than at a constant head as used by Wan and Fell [WAN 04a]. The critical shear stress is obtained at the end of the test when no further erosion occurs.

The only potential issue with this is that the eroding surface is more likely to be saturated using this method than for the Wan and Fell [WAN 04a] method, and if the critical shear stress is increased with the degree of saturation, it may be overestimated for the soil in its compacted condition.

Further research is needed to determine whether HET performed at a constant flow rate and at a constant head give similar results for initially unsaturated specimens.

The roughness of the eroding surface is likely to affect the critical shear stress determination in both the HET and JET although the magnitude of the sensitivity to roughness is not well quantified. In the HET, the critical shear stress using the Bonelli *et al.* approach [BON 08] is determined considering conditions throughout the test; so, this effect is at least partially overcome. In the Wan and Fell method [WAN 04a], the critical shear is determined from the erosion observed early in the test, while the surface is likely to be relatively smooth; so, the value is representative of a smooth-surface condition. In the JET, the critical shear stress value is determined based on an extrapolation of the equilibrium depth of erosion that would occur after infinite time; so, the result is likely to be most affected by conditions near the end of the test when there is a rough-surface condition. For remolded samples, JET results can also vary depending on whether the upper or lower surface is tested. The compaction conditions and roughness of the surface can both vary as a result of specific compaction and sample preparation procedures.

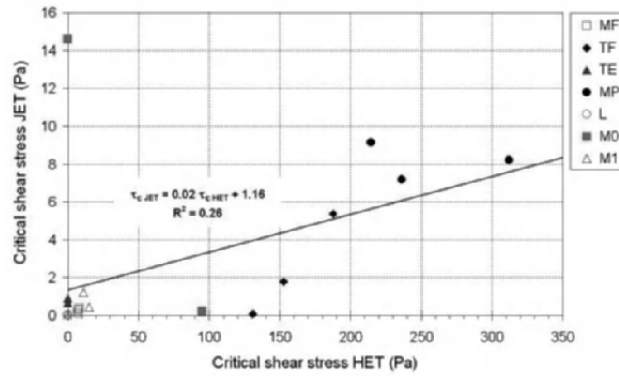


Figure 5.4. Critical shear stress values measured with the JET versus values measured with the HET [REG 13]

5.3.3. Correlation between critical shear stress and erosion rate index

The critical shear stress is related to the erosion rate index. Figure 5.5 shows data from HET obtained by Wan and Fell [WAN 04a] and others. Table 5.2 is developed from these data. It gives only approximate estimates of the likely range of critical shear stress (τ_c) and should be used with caution when HET values are not available.

The critical shear stress for dispersive soils is likely to be only 1 or 2 N/m².

Hanson and Simon [HAN 01] developed a correlation between k_d and τ_c for JET, and Wahl *et al.* [WAH 08b] showed that a similar relationship existed for both JET and HET data.

It is emphasized that it is better to perform a series of HET tests at varying heads or to use the method of Bonelli ([BON 08], Chapter 4 of this book) to define the critical shear stress (τ_c) than to rely on these relationships.

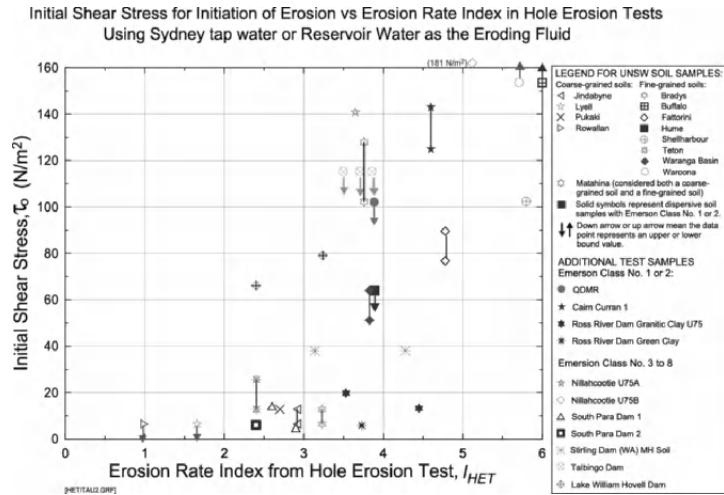


Figure 5.5. Initial shear stress (τ_c) versus representative erosion rate index (I_{HET}) for soils which are non-dispersive and for dispersive soils with eroding water suppressing dispersion (Courtesy of C.F.Wan)

Hole Erosion Index I_{HET}	Critical Shear Stress τ_c Pa			
	Non-Dispersive Soil Behavior		Dispersive Soil Behavior	
	Best Estimate	Likely Range	Best Estimate	Likely Range
< 2	2	1 – 5	1	0.5 – 2
2–3	2	1 – 5	1	0.5 – 2
3.5	5	2 – 20	2	1 – 5
4	25	10 – 50	5	2 – 10
5	60	25 – 100	5	2 – 10
6	100	60 – 140	5	2 – 10

Note: This table should be used with caution. For important decisions, perform hole erosion tests to determine the initial shear stress (τ_c).

Table 5.2. Estimated values and likely range of critical shear stress (τ_c) versus hole erosion index (I_{HET}) for non-dispersive soils [FEL 08]

5.4. Relationship to field performance

5.4.1. JET tests done in the laboratory and in the field

Hanson and Hunt [HAN 07] carried out JET tests in the laboratory and in the field on soils compacted to a range of water contents. The results are shown in Figure 5.6. It can be seen that the laboratory and field results are similar, thus confirming the value of the JET for performing tests on *in situ* soils.

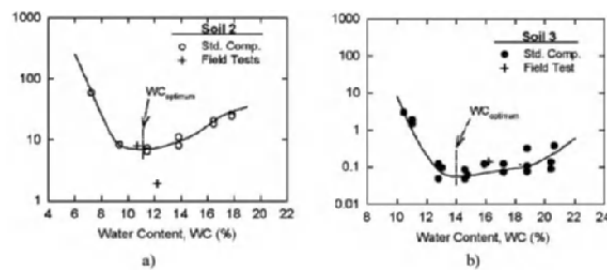


Figure 5.6. Comparison of erodibility determined from Jet Erosion Tests (JET) tests in the laboratory and field tests for a) soil 2 – non-plastic SM and b) soil 3 CL soil with a plasticity index of 17 [HAN 07]

5.4.2. Assessment of rates of erosion from JET and large-scale laboratory tests

Hanson and Hunt [HAN 07] conducted a series of bench scale laboratory JET tests and large-scale laboratory tests on breach widening. They measured the impact of changes in the compaction water content of two soils compacted at standard compaction on the erodibility coefficient. Figure 5.7 shows a field experiment in progress and Figure 5.8 shows breach widening versus time. Wahl and Erdogan [WAH 08a] performed JET and HET tests on remolded samples of the soils used for additional tests of embankment breach via piping by Hanson *et al.* [HAN 10a]. They found that JET results were consistent with observed differences in the time scales of erosion and embankment breach for the tests,

which spanned about two orders of magnitude. HET results also showed similar variation and consistency with the breach test results, but produced detachment rate coefficients, k_d , that were about one order of magnitude lower than the values obtained from companion JET tests. HET tests could not be performed on the non-plastic soils used for these breach tests because samples disintegrated before the tests could be completed. This typifies the conclusion by Wahl *et al.* [WAH 08b] that the HET in general can be reliably performed on soils exhibiting up to 2.8 orders of magnitude variation in k_d , but the JET can be successfully performed across nearly five orders of magnitude of k_d .

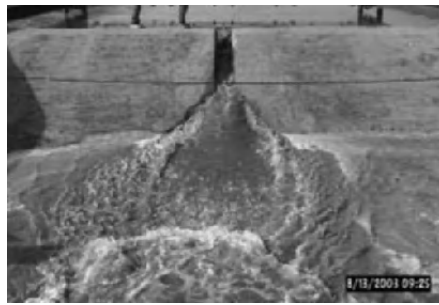


Figure 5.7. Large-scale outdoor laboratory experiment of breach widening [HAN 07]

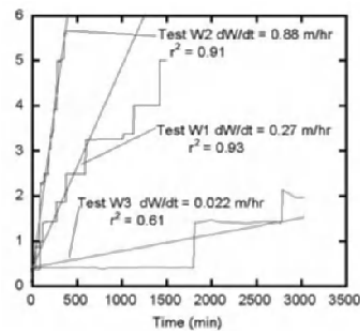


Figure 5.8. Breach widening versus time for two soils [HAN 07]

It should be noted, however, that Wan and Fell [WAN 04a] were able to carry out HET for erosion rate indices from two to six including tests on silty sand of glacial and residual granite origins.

Wahl and Lentz [WAH 11] conducted laboratory-scale breach tests of canal embankments with embankment heights of 0.64 m. *In situ* JET tests were performed on the embankments before and after breach testing and k_d values were then related to measured and estimated rates of head cut advance and breach widening. The relation between k_d and breach widening rates compared reasonably to a relation proposed by Hunt *et al.* [HUN 05] based on embankment breach widening tests.

The relation between head cut advance rates and k_d compared well to a relation proposed by Hanson *et al.* [HAN 11] using data from earlier flume tests of head cut advance in which JET tests were also performed [HAN 01].

Bonelli developed this concept further by incorporating the maximum diameter of pipe that can be sustained before it collapses and breaches the dam or levee ([BON 11], Chapter 4 of this book). Reasonable correlations were found by inferring the erosion rate index from case data. On one large scale test, the erosion rate index found on an HET was used as a parameter of a dam-break model; the numerical result gave the order of magnitude of the time to failure (Chapter 4 of this book).

Fell *et al.* [FEL 08] have found that the rates of enlargement of pipes forming in a dam embankment predicted from HET are consistent with those observed in actual failures as reported by Fell *et al.* [FEL 03].

5.5. Effects of the type of soil

5.5.1. *General trends*

The erosion behavior of cohesionless soils is relatively simple. Once the tractive shear force overcomes the sliding or rolling resistance of the individual particles, the soil starts to erode. It can be evaluated in terms of the average grain diameter only, as illustrated in the Shields chart (1936).

In contrast, the erosion behavior of cohesive fine-grained soils is complex because of the electromagnetic and electrostatic inter-particle forces, which are influenced by the density, structure and fabric of the soil as well as the chemistry of the pore water, particle size distribution and clay mineralogy. The main physical parameters influencing the erosion of cohesive fine-grained soil are the particle size distribution (grain size), the clay fraction and the clay mineralogy. The complexity is increased by the fact that for a given soil, the erosion is also dependent on its mechanical state (density, moisture content, temperature).

Erosion resistance is highly dependent on the clay type and generally increases with increasing fine fraction or clay fraction. However, in general, no clear guidelines are established as to which parameters predominantly influence soil erosion under a certain physical condition, and there are some contradictory results for some of the parameters. Therefore, it is recommended to directly measure soil erodibility whenever possible. *In situ* tests or a laboratory test of intact samples are preferred because undisturbed natural clay samples tend to produce less erosion than remolded samples.

5.5.2. Relationship to soil classification

In the absence of laboratory test values, the representative erosion rate index (I_{HET}), which is the erosion rate index for the soil compacted to 95% standard compaction ratio at optimum water content, can be related approximately to soil properties. Table 5.3 has been developed from test data in Wan [WAN 06] and some data from dam investigations to give a first approximation of the likely range of I_{HET} for different classifications of non-dispersive soils.

Unified Soil Classification	Representative Erosion Rate Index (I_{HET})		
	Likely Minimum	Best Estimate	Likely Maximum
SM with < 30% fines	1	< 2	2.5
SM with > 30% fines	< 2	2 – 3	3.5
SC with < 30% fines	< 2	2 – 3	3.5
SC with > 30% fines	2	3	4
ML	2	2 – 3	3
CL-ML	2	3	4
CL	3	3 – 4	4.5
CL-CH	3	4	5
MH	3	3 – 4	4.5
CH with liquid limit <65%	3	4	5
CH with liquid limit >65%	4	5	6

Table 5.3. Representative erosion rate index (I_{HET}) versus soil classification for non-dispersive soils based on the study of Wan and Fell [WAN 02]

Wan [WAN 06] and Wan and Fell [WAN 02] used logistic regression to develop an equation relating the representative erosion rate index (I_{HET}) to other soil properties. The equation is based on limited data and those authors do not

recommend that it be used. Table 5.3 shows a more reliable method. It is recommended to use best estimate values for best estimate probabilities and to check the sensitivity if the outcome is strongly dependent on the results. For important decisions, HET tests should be performed rather than relying on this table, which is very approximate.

5.5.3. Effects of soil structure

Lim [LIM 06] and Wahl *et al.* [WAH 08b] have noted that soil structure has an important effect on erosion properties. They found that erosion rates are significantly higher for the same soil if the soil is compacted dry of optimum moisture content and the soil forms aggregated particles and/or micro-cracks. These allow erosion of blocks of the soil rather than of the individual particles. The sensitivity to soil structure is thought to vary depending on the particular test used. This is believed to be one of the reasons that higher erosion rates are measured in JET than HET because the HET test is started with a relatively small hole diameter not allowing the “blocks” of soil to dislodge from the sides of the hole. This behavior was also noted in RCT tests by Lim [LIM 06]. The variability of soil structure versus compaction conditions probably is a function of soil type. Methods have not yet been well developed for describing soil structure in a quantitative way and relating measurable soil structure parameters to erodibility.

5.6. Effects of compaction parameters

5.6.1. Relationship to compaction parameters

The erosion resistance increases with increasing dry density and increasing water content (at the time of erosion testing). Table 5.3 does not address soils that are compacted dry or wet of optimum or that do not achieve the 95%

standard compaction ratio. Two approaches to incorporate non-standard compaction effects have been taken, one relating erodibility to the end result of compaction (dry density) and the other relating erodibility to specific compaction conditions (water content and compaction effort). Figure 5.9 shows the relationship between the erosion rate index and standard compaction dry density ratio [WAN 06]. It can be seen that the hole erosion index is not greatly influenced by the degree of compaction for the range of compaction normally found in engineered dams and levees. The erosion rate index is more influenced by the compaction moisture content and most clearly affected by the degree of saturation.

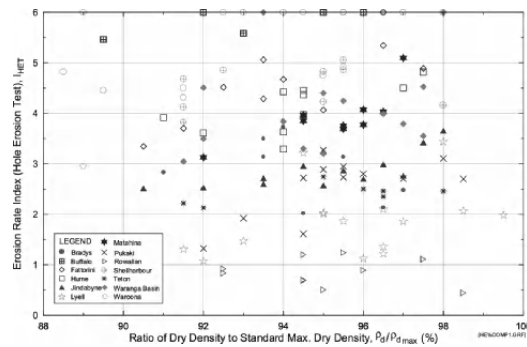


Figure 5.9. HET erosion rate index versus standard compaction dry density ratio [WAN 06]

Hanson and Hunt [HAN 07] compared JET results for a series of three compaction efforts for two soils. Figure 5.10 provides a comparison of the dry density and erodibility results indicating the influence of compaction on the wet and dry sides of optimum. Note that the compaction effort had a significant effect when compacting on the dry side of optimum. From these results, they proposed that acceptable zones of compaction for erodibility might be specified (Figure 5.11).

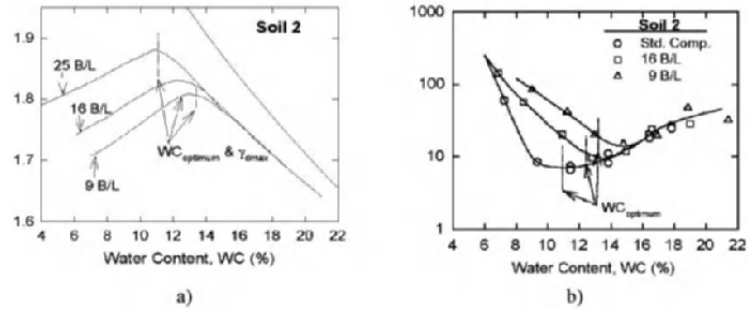


Figure 5.10. Comparison of three compaction efforts for a non-plastic soil a) dry density and b) JET erodibility values [HAN 07]

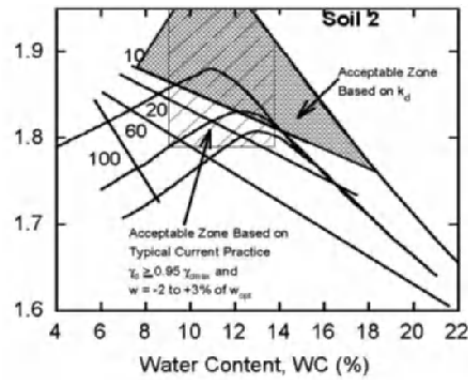


Figure 5.11. Acceptable range of compaction water content and dry density to give lower erosion rates [HAN 07]

Based on this work and experiences in large-scale testing of head cut erosion associated with earthen spillways and overtopped embankments, Hanson *et al.* [HAN 10b] proposed tables for estimating JET erosion rates and critical shear stress parameters as a function of soil composition, water content at compaction and compaction effort. Rather than using soil classification, they found that the percentage of clay-sized particles was the most important aspect of soil type.

% Clay (< 0.002 mm)	Modified Compaction (56,250 ft-lb/ft ³)		Standard Compaction (12,375 ft-lb/ft ³)		Low Compaction (2,475 ft-lb/ft ³)	
	$w \geq w_{Opt}$	$w < w_{Opt}$	$w \geq w_{Opt}$	$w < w_{Opt}$	$w \geq w_{OPN}$	$w < w_{Opt}$
Erodibility, k_d , cm ³ /(N·s)						
>25	0.05	0.5	0.1	1	0.2	2
14 – 25	0.5	5	1	10	2	20
8 – 13	5	50	10	100	20	200
0 – 7	50	200	100	400	200	800

Table 5.4. Approximate values of k_d from JET as a function of compaction conditions and % clay [HAN 10b] ($1 \text{ cm}^3 / (\text{N}\cdot\text{s}) = 0.5655 \text{ ft} / \text{h} / \text{psf}$)

Tables 5.4 and 5.5 give erodibility parameters based on JET results. Wahl and Lentz [WAH 11] suggested that values representative of HET parameters could be obtained by dividing the suggested k_d values by 10 and multiplying the suggested τ_c values by 100.

% Clay (< 0.002 mm)	Modified Compaction (56,250 ft-lb/ft ³)		Standard Compaction (12,375 ft-lb/ft ³)		Low Compaction (2,475 ft-lb/ft ³)	
	$w \geq w_{Opt}$	$w < w_{Opt}$	$w \geq w_{Opt}$	$w < w_{Opt}$	$w \geq w_{OPN}$	$w < w_{Opt}$
Critical shear stress, τ_c , Pa						
> 25	16	0.16	4	0	1	0
14 – 25	0.16	0	0	0	0	0
8 – 13	0	0	0	0	0	0
0 – 7	0	0	0	0	0	0

Table 5.5. Approximate values of τ_c from JET as a function of compaction conditions and % clay [HAN 10b] ($1 \text{ Pa} = 0.0209 \text{ psf}$)

5.6.2. Relationship to degree of saturation after compaction

Wan and Fell [WAN 02, WAN 04a, WAN 04b, WAN 06] and Lim and Khalili [LIM 06, LIM 09] found that most clay soils tested have significantly higher erosion rate indices (slower erosion) and higher critical shear stresses when saturated than in a partially saturated compaction condition.

Figures 5.12 – 5.14 illustrate the effect of the degree of saturation on the erosion rate index, using SET, HET, and RCT data, respectively.

Figures 5.12 and 5.13 involve a range of real soils. Figure 5.14 shows the results of testing three soils. Soil S is a residual granitic soil from the Serpentine Dam, Western Australia, classifying as MH; Soil B is a sandy clay of low plasticity from the Fairbairn Dam, Queensland; Soil F is a clay of low plasticity from the Boggy Creek Dam in Oklahoma, USA; and 50% of kaolin is an artificial soil consisting of 50% kaolin and the remainder being fine sand-sized particles. It is observed that the erosion rate significantly depends on the degree of saturation for both clay soils.

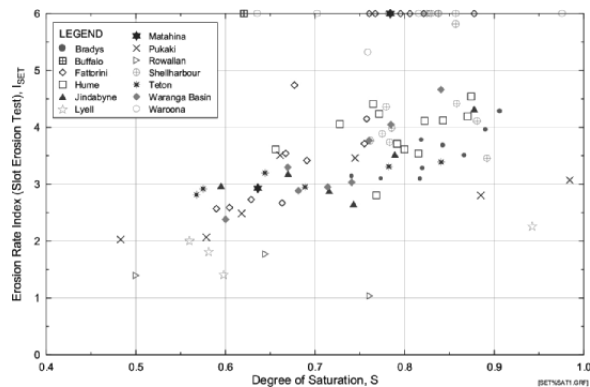


Figure 5.12. Erosion rate index versus degree of saturation from slot erosion tests (SET) [WAN 06]

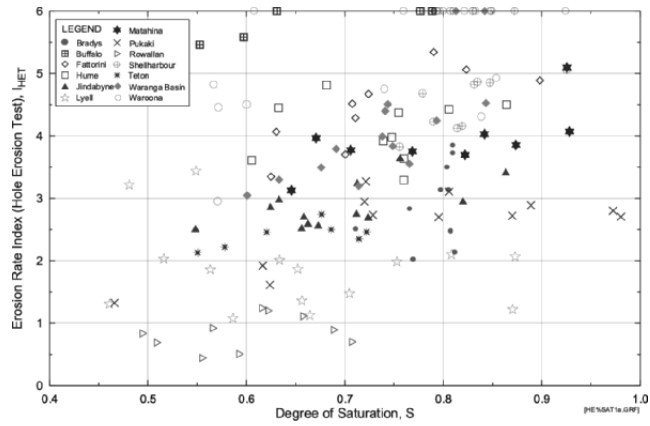


Figure 5.13. Erosion rate index versus degree of saturation from hole erosion tests (HET) [WAN 06]

Saturated soils shown in Figure 5.14 were prepared for testing using triaxial back pressure saturation. The clay soils had $I_{RCT} \approx 3 - 4$ at the representative compaction and moisture content, and $I_{RCT} \approx 4.5 - 5.5$ when 90 - 100% saturated. There was little change in the erosion rate for clay soils for degrees of saturation above 90%.

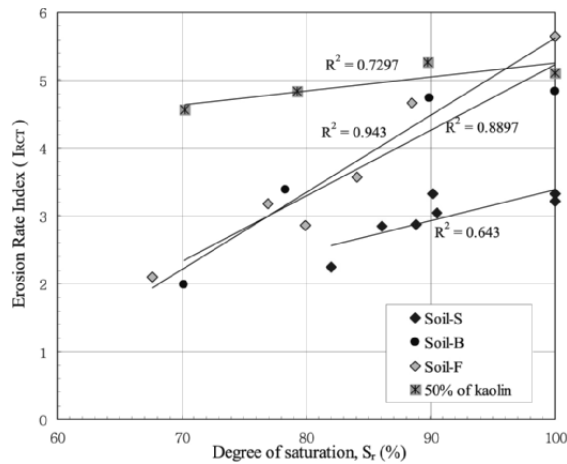


Figure 5.14. Relationship between degree of saturation and erosion rate index (I_{rcr}) for non-dispersive soils [LIM 06]

This is an important finding because it means that once the core of a dam constructed of clay soil is saturated, it will have a slower rate of erosion and a higher critical shear stress.

As important as this is, this does not apply to silty sand cores such as decomposed and residual granites because there was less dependence on the degree of saturation for these soils. Wan and Fell [WAN 02] indeed noted a similar trend with two other non-plastic residual granitic soils showing little change in the erosion rate with increased degree of saturation.

Regazzoni and Marot [REG 11] evaluated the erodibility of twelve soils by JET. A multivariate analysis was performed and allowed to identify four main physical parameters: compaction, saturation ratio, liquidity limit and dispersivity.

5.7. Effects of dispersivity and slaking

5.7.1. Effects of dispersivity on erosion rate and critical shear stress

Soils in which the clay particles detach from each other and from the soil structure and go into suspension without a flow of water are called dispersive clays. The dispersivity of a soil is directly related to its clay mineralogy. In particular, soils with a high exchangeable sodium percentage, such as Na or Ca with montmorillonite present, tend to be dispersive, while kaolinite and related minerals (e.g. halloysite) are non-dispersive. Soils with illite present tend to be moderately dispersive.

The dispersivity depends also on the pore water chemistry. Low pore water salt concentrations lead to greater dispersivity and high salt concentrations can

suppress dispersion in susceptible soils. Hence, percolation of a saline soil with fresh water can lead to dispersion.

The mechanism of dispersion is related to the fact that dispersive clay molecules carry a negative charge on their surface. These charges attract positively charged cations in the soil pore water, for example from Na ions in NaCl.

When two clay particles come near each other, the potential fields overlap, leading to repulsion if the particles are close enough. These repulsive forces are counteracted by Van der Waals attractive forces as shown in Figure 5.15. If the repulsive forces are greater than the Van der Waals forces, the soil will disperse. In cases where the repulsive forces are small, the Van der Waals attractive forces dominate and flocculation results.

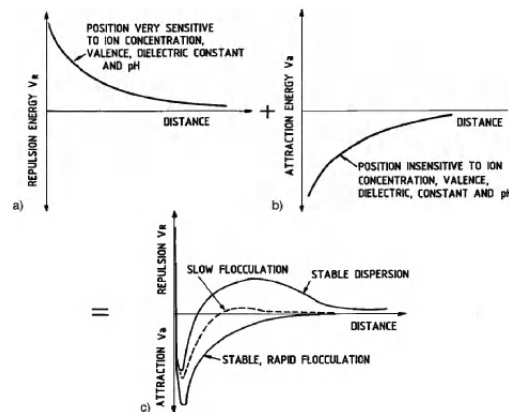


Figure 5.15. Interaction of a) repulsive and b) Van der Waals attractive forces to give c) curves of net energy of repulsion or attraction ([FEL 05], adapted from [MIT 76])

The repulsive forces in the diffuse double-layer are affected by several factors:

1) *Electrolyte concentration*: as shown in Figure 5.16, a high concentration of dissolved salt in the soil water leads to

a smaller diffuse double-layer (as the greater concentration of cations (Na^+) more readily overcomes the negative charge on the clay surface). Hence, the repulsive forces are lower.

2) *Cation valence*: exchange of Na^+ cations with Ca^{++} cations leads to a smaller, higher charge density diffuse double-layer and hence lower repulsive forces.

Other factors which affect the diffuse double-layer include:

- dielectric constant of the electrolyte;
- temperature.

More details are given in Fell *et al.* [FEL 05] and Mitchell [MIT 76, MIT 93].

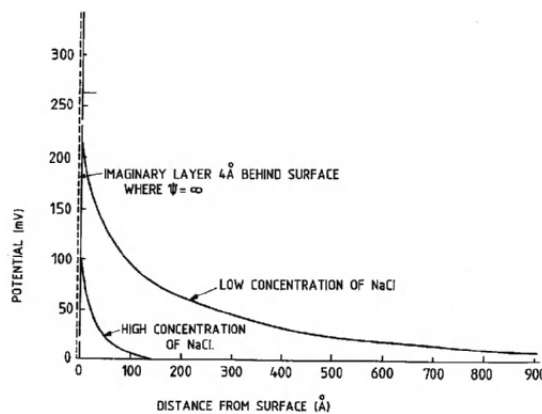


Figure 5.16. Effect of electrolyte concentration on diffuse double-layer potential for montmorillonite ([FEL 05], adapted from [MIT 76])

Soils which show dispersive behavior, that is soils classified as Emerson Crumb Class 1 or 2, and Pinhole Dispersion D1 and D2, will have a very low critical shear stress if the eroding fluid is sufficiently free of salts which might otherwise suppress dispersion.

It should be noted that under flood conditions, the salt content of the water in the reservoir is likely to drop; so, tests conducted with reservoir water may be unconservative. If in doubt with dispersive soils, it is best to assume that the reservoir water will not inhibit dispersion and rely on the results of tests using distilled water.

Lim [LIM 06] showed that for RCT tests, the erosion rate index is not greatly affected by whether the soil is dispersive after the initially rapid part of the erosion process. So, the major effect of dispersion is on the critical shear stress at which erosion initiates, not on the rate of erosion.

5.7.2. Effects of slaking on erosion rate and critical shear stress

The term “slaking” or “soil slaking” is defined as “disintegration of unconfined soil after exposure to air and subsequent immersion in a fluid, usually water; no external confining pressure is assumed to act over the soil prior to immersion” [MOR 77]. Lim [LIM 06] and Lim and Khalili [LIM 09] showed that the slaking process was correlated strongly to the degree of saturation of the soil, with the slaking rate being up to 30 – 50 times lower for soils at 100% degree of saturation than for soils at 70% degree of saturation (Figure 5.17). This corresponds with the behavior of the erosion rate index for clay soils.

As shown in Figure 5.18, they also proved a strong correlation between the rates of slaking from a sample held statically in water to the erosion rate index from the RCT (I_{RCT}). These are important findings as they help explain the actual mechanics of the erosion process being strongly linked to slaking.

Vallejo [VAL 11] indicates that slaking occurs in shale as water is drawn into the micropores by capillary tension,

compressing the air in the micropores. This increase in pore air pressure is able to break bonds between soil particles, producing the observed disintegration of the soil.

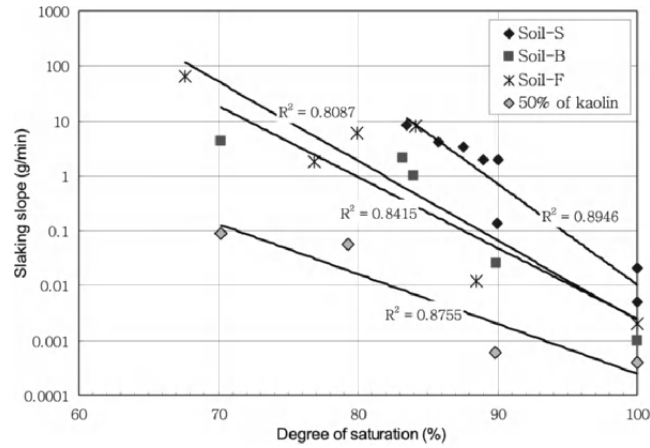


Figure 5.17. Relationship between the degree of saturation and slaking slope for non-dispersive clay soils [LIM 06]

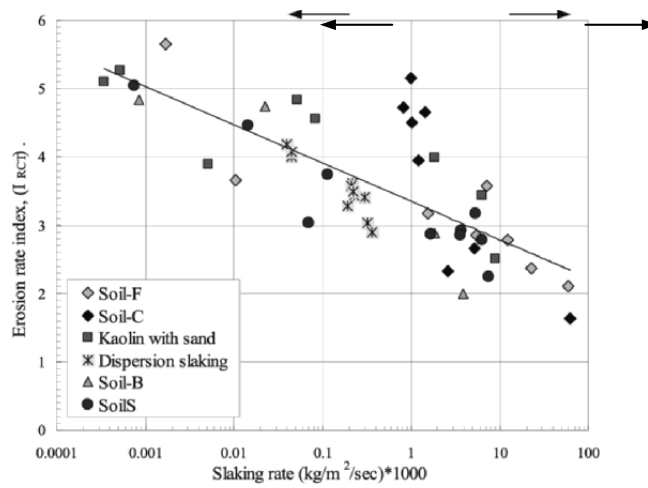


Figure 5.18. The range of erosion rate index for RCT and slaking rate [LIM 06]

5.8. Modifications of soil erosion properties

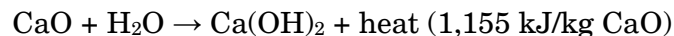
5.8.1. *Modification by lime*

Lime treatment of soils is a technique widely used for soil improvement and stabilization for construction of roads, highways, railways and platforms [LIT 95]. Lime has been used for five decades for improving and re-using the soils in levees, earth dams and flood dikes not only in the United States ([GUT 78, KNO 87, PER 77, TOW 79]), but also in Australia [ING 72]. The treatment of soil with lime was reported to solve erosion problems due to dispersive soils, to prevent the shrinkage-swelling phenomenon coming from heavy plastic soils and, therefore, to stabilize the slopes or road subgrades.

Fine clay or loam soils are sometimes difficult to use for constructing embankments or platforms because of their sensitivity to water, low bearing capacity when wet and the difficulty in compacting them. Quicklime added to fine clay or loam soil overcomes these difficulties and enables these soils to be reused in infrastructure projects. This is mainly done for road construction.

The addition and mixing of lime leads to a series of immediate and mid- to long-term effects on the silty and clayey soils. Several objectives can be reached through lime addition. In the case of quicklime treatment, the direct effect is the reduction in the moisture content of the soils:

– by the hydration reaction of quicklime, combining some amount of water contained in the soils, and leading also to vaporization of some of the water by the heat generated by the following exothermic reaction:



– by the addition of dry powder to the soil reducing the water:solid ratio;

– during mixing operations, soil aeration also can lead to a supplementary water loss.

The addition of slaked calcic lime $[\text{Ca}(\text{OH})_2]$ only affects the soil moisture content by increasing the proportion of dry material, while milk of lime (suspension of hydrated lime in water) is applied when dry soil needs to be treated for specific neutralization of the clayey fractions in order to avoid swelling and shrinkage.

Geotechnical characteristics of soils are immediately affected by lime addition. This is a consequence of the displacement of monovalent or smaller cations located at the surface and between the clay platelets, by Ca^{2+} ions coming from calcic lime. This phenomenon leads to a rearrangement of the contacts between particles to compensate the electrostatic changes. This is known as clay flocculation.

The flocculation modifies the general behavior and characteristics of soil with significant reduction in clay activity as the plasticity index is reduced. This consequence of particle flocculation can be concomitant with water reduction, changing the compaction characteristics of the soil. It can also inhibit slaking and dispersion as shown in Figure 5.19.

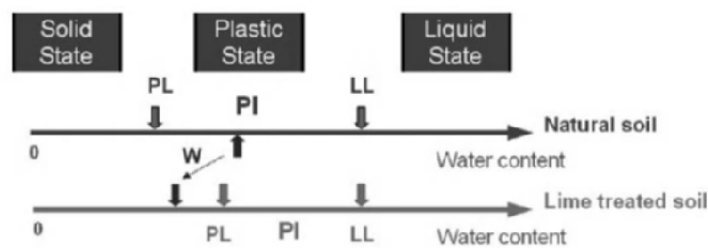
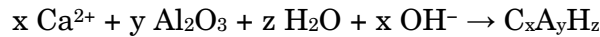
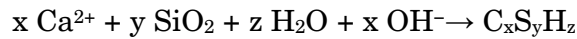


Figure 5.19. Modifications induced by lime treatment on a soil, simultaneous reduction of plasticity index (*PI*) and water content; *PL* = plastic limit, *LL* = liquid limit [HER 12a]

At a certain time after compaction, a recombination of calcium, dissolved silica and alumina coming up from clay species and water can occur. This reaction is favored at high pH values, which are necessary for the dissolution of specific clay compounds, and sufficient lime dosages that guarantee lime availability. The products of this “pozzolanic” reaction are similar to cementitious compounds: calcium silicate hydrates and calcium aluminate hydrates (cementitious notation: C = CaO, S = SiO₂, A = Al₂O₃, H=H₂O):



This reaction develops at the mid- or long-term and increases the soil compressive strength, tensile strength, and elastic modulus. The lime-treated soil can be considered as a “cemented” material in the sense that the particle assembly is realized by the cohesive bonds induced by the lime action.

The ASTM D 6572-06 Standard (“Crumb-test”) was used to demonstrate the non-dispersive behavior of an initially dispersive silty soil (PI = 11) treated with 2 – 3% quicklime [HER 12a]. This improvement was still visible three years after treatment. An enhanced Crumb test was also performed on silty soil (small cylinders, untreated and treated with 2% lime). The untreated cylinder collapsed after 15 minutes of immersion, whereas no degradation occurred on the lime-treated sample, even after 45 hours of immersion (Figure 5.20).

The resistance to erosion of a clay-like silt treated with 2% lime was examined [HER 12b, HER 12c]. The tested material is an A2 silt from a river levee in the South of France, which contains 19% sand and 30% clay ($I_P = 11$, $W_{OPN} = 18\%$). Several HET tests were carried out at the geotechnical laboratory of Irstea at different curing times. The erosion rate, which depends on the tangential stress, is

represented in Figure 5.21. Figure 5.22 shows the erosion velocity depending on the outflow velocity. The erosion threshold of the non-treated silt is around 2 m/s. The erosion threshold of the treated silt after 14 days of curing time is around 10 m/s.

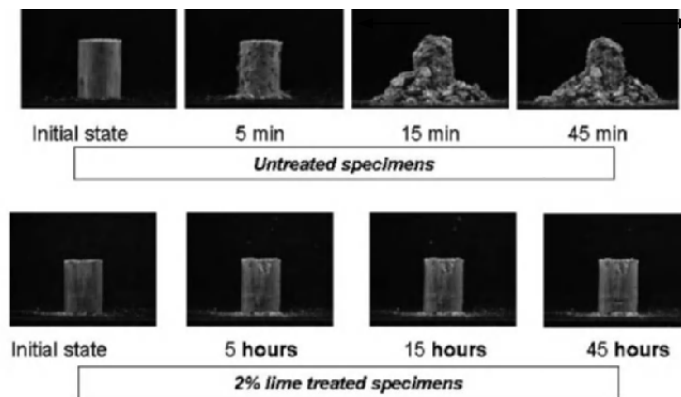


Figure 5.20. Enhanced Crumb test performed on a silty soil ($PI = 11$), untreated (above, scale in minutes), and treated with 2% lime (below, scale in hours) [HER 12a]

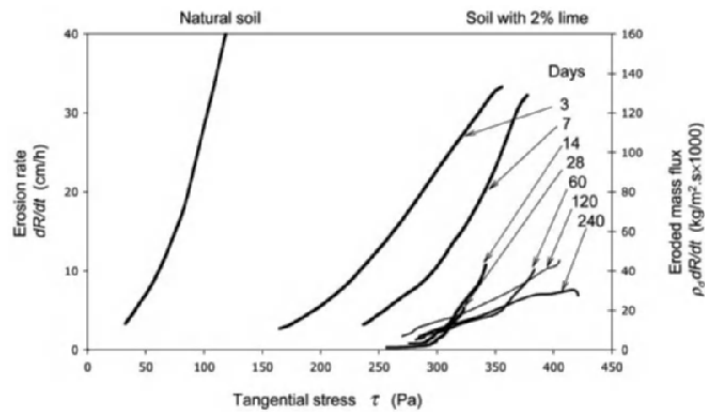


Figure 5.21. Erosion rate versus hydraulic shear stress for a clay-like soil at different curing times [HER 12b, HER 12c]

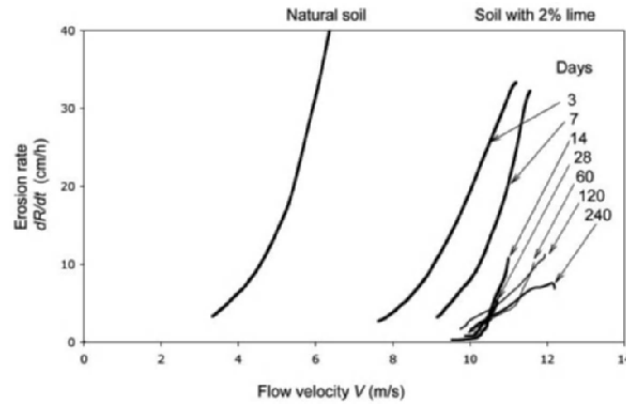


Figure 5.22. Erosion rate versus hydraulic velocity at different curing times [HER 12b, HER 12c]

The influence that the curing time has on the critical stress and erosion index is represented in Figure 5.23. These results allow us to quantify the improvement of the resistance to erosion. The natural soil has a critical stress of 53 Pa and an erosion rate index of 3.37. During the first 14 days, the critical stress is multiplied by six, while the erosion rate index decreases slightly to three. Then, the critical stress decreases slightly to 250 Pa, while the erosion rate index goes up to 4.6 (equivalent to the erosion coefficient being divided by 40).

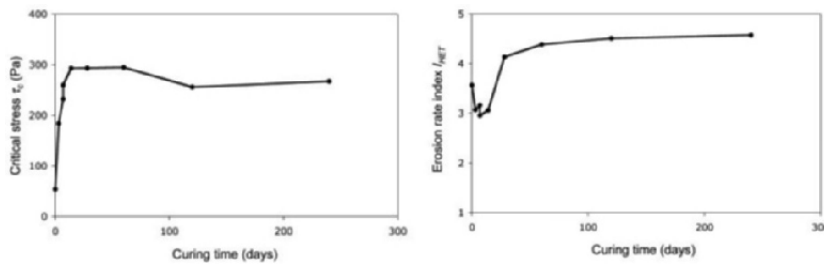


Figure 5.23. Influence of the curing time on the critical stress and on the erosion rate index [HER 12b, HER 12c]

5.8.2. Modification by cement

In the case of a granular and non-cohesive soil, the addition of cement will result in a cementing of the soil and an increase in the compressive strength.

Indraratna *et al.* [IND 10] carried out tests on silty sand to which cement between 0.5% and 3% was added. They performed erosion tests in a setup similar to an HET, but with a 10 mm diameter hole, and tensile strength tests.

Figure 5.24 shows the results of this experimentation. It is observed that the addition of cement reduces the rate of erosion and also increases the critical shear stress as indicated by the shifting of intercept of the data on the hydraulic shear stress axis.

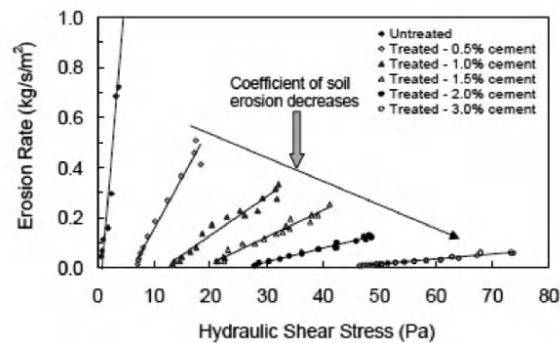


Figure 5.24. Erosion rate versus hydraulic shear stress for a silty sand modified by the addition of cement [IND 10]

5.9. Bibliography

[BEN 12a] BENAHMED N., BONELLI S., “Investigating concentrated leak erosion behaviour of cohesive soils by performing hole erosion tests”, *European Journal of Environmental and Civil Engineering*, vol. 16, no. 1, pp. 43–58, 2012.

- [BEN 12b] BENAHMED N., CHEVALIER C., BONELLI S., “Concentrated leak erosion”, *Erosion of Geomaterials*, Chapter 5, ISTE Ltd, London and John Wiley & Sons, New York, pp. 155–186, 2012.
- [BON 08] BONELLI S., BRIVOIS O., “The scaling law in the hole erosion test with a constant pressure drop”, *International Journal for Numerical and Analytical Methods in Geomechanics*, vol. 32, pp. 1573–1595, 2008.
- [BON 11] BONELLI S., BENAHMED N., “Piping flow erosion in water retaining structures”, *International Journal on Hydropower and Dams*, vol. 18, no. 3, pp. 94–99, 2011.
- [BRI 08a] BRIAUD J.-L., “Case histories in soil and rock erosion: Woodrow Wilson Bridge, Brazos River Meander, Normandy Cliffs, and New Orleans Levees”, The 9th Ralph B. Peck Lecture, *Journal of Geotechnical and Geoenvironmental Engineering*, vol. 134, no. 10, pp. 1425–1447, 2008.
- [BRI 08b] BRIAUD J.-L., CHEN H.-C., GOVINDASAMY A.V., *et al.*, “Levee erosion by overtopping in New Orleans during the Katrina Hurricane”, *Journal of Geotechnical and Geoenvironmental Engineering*, vol. 134, no. 5, pp. 618–632, 2008.
- [FEL 03] FELL R., WAN C.F., CYGANIEWICZ J., *et al.*, “Time for development of internal erosion and piping in embankment dams”, *ASCE Journal of Geotechnical and GeoEnvironmental Engineering*, vol. 129, no. 4, pp. 307–314, 2003.
- [FEL 05] FELL R., MACGREGOR P., STAPLEDON D., *et al.*, *Geotechnical Engineering of Dams*, Taylor & Francis, 2005.
- [FEL 08] FELL R., FOSTER M., DAVIDSON R., *et al.*, Unified method for estimating probabilities of failure of embankment dams by internal erosion and piping, UNICIV Report R 446, School of Civil and Environmental Engineering, University of New South Wales, Sydney, Australia, 2008.
- [GUT 78] GUTSCHICK K.A., “Lime stabilization under hydraulic conditions”, *4th Lime Congress*, Hershey, PA, pp. 1–20, 1978.
- [HAN 89] HANSON G. J., “Channel erosion study of two compacted soils”, *Transactions of the ASAE*, vol. 32, no. 2, pp. 485–490, 1989.

- [HAN 01] HANSON G.J., SIMON A., “Erodibility of cohesive streambeds in the loess area of the Midwestern USA”, *Hydrological Processes*, vol. 15, no. 1, pp. 23–28, 2001.
- [HAN 01] HANSON G.J., ROBINSON K.M., COOK K.R., “Prediction of headcut migration using a deterministic approach”, *Transactions of the ASAE*, vol. 44, no. 3, pp. 525–531, 2001.
- [HAN 04] HANSON G.J., COOK K.R., “Apparatus, tests procedures, and analytical methods to measure soil erodibility in-situ”, *Applied Engineering in Agriculture*, vol. 20, no.4, pp. 455–462, 2004.
- [HAN 07] HANSON G.J., HUNT S.L., “Lessons learned using laboratory jet method to measure soil erodibility of compacted soils”, *Applied Engineering in Agriculture*, vol. 23, no. 3, pp. 305–312, 2007.
- [HAN 10a] HANSON G.J., TEJRAL R.D., HUNT S.L., *et al.*, “Internal erosion and impact of erosion resistance”, *Proceedings of the United States Society on Dams, 30th Annual Conference*, Sacramento, CA, 12–16 April 2010.
- [HAN 10b] HANSON G.J., WAHL T.L., TEMPLE D.M., *et al.*, “Erodibility characteristics of embankment materials”, *Dam Safety 2010, Proceedings of the Association of State Dam Safety Officials Annual Conference*, Seattle, WA, 19–23 September 2010. (CDROM).
- [HAN 11] HANSON G.J., TEMPLE D.M., HUNT S.L., *et al.*, “Development and characterization of soil material parameters for embankment breach”, *Applied Engineering in Agriculture*, vol. 47, no. 4, pp. 587–595, 2011.
- [HER 12a] HERRIER G., LELONG V., LESUEUR D., *et al.*, Soil treatment for dikes, SOTREDI final report, Lhoist Eds, Limelette, Belgium, pp. 1–103, 2012.
- [HER 12b] HERRIER G., LESUEUR D., PUIATTI D., *et al.*, “Lime treated materials for embankment and hardfill dams”, *International Symposium on Dams for a Changing World*, Kyoto, Japan, 5 June 2012.

- [HER 12c] HERRIER G., LESUEUR D., PUIATTI D., *et al.*, “Lime treated soils as an erosion-resistant material for hydraulic earthen structures”, *6th International Conference on Scour and Erosion*, Paris, France, pp. 97–104, 27–31 August 2012.
- [HUN 05] HUNT S.L., HANSON G.J., COOK K.R., *et al.*, “Breach widening observations from earthen embankment tests”, *Transactions of the ASAE*, vol. 48, no. 3, pp. 1115–1120, 2005.
- [HUN 07] HUNT S.L., HANSON G.J., TEMPLE D.L., *et al.*, “Earthen embankment internal erosion research”, *Dam Safety 2007, Proceedings of the 24th Annual Meeting of the Association of State Dam Safety Officials*, Austin, TX, 9–12 September 2007.
- [IND 10] INDRARATNA B., MAHAMUD M., VINOD J.S., *et al.*, “Stabilization of an erodible soil using a chemical admixtures”, in BOUASSIDA M., HAMDI E, SAID I. (eds), *Proceedings of the 2nd International Conference on Geotechnical Engineering*, ENIT, pp. 45–54, 2010.
- [ING 72] INGLES O.G., METCALF J.B., *Soil Stabilization*, Butterworths, 1972.
- [KNO 87] KNODEL P.C., Lime in canal and dam stabilization, Report No GR-87-10, U.S. Bureau of Reclamation, pp. 1–21, 1987.
- [LIM 06] LIM S.S., Experimental investigation of erosion in variably saturated clay soils, PhD Thesis, School of Civil and Environmental Engineering, University of New South Wales, Sydney, Australia, 2006.
- [LIM 09] LIM S.S, KHALILI N., “An improved rotating cylinder test design for laboratory measurement of erosion in clayey soils”, *Geotechnical Testing Journal*, vol 32, no. 3, pp. 1–7, 2009.
- [LIT 95] LITTLE D.L., *Handbook for Stabilization of Pavement Subgrades and Base Courses with Lime*, Kendall/Hunt Publishing Company, Dubuque, Iowa, 1995.
- [MAR 11] MAROT D., REGAZZONI P.L., WAHL T., “Energy based method for providing soil surface erodibility rankings”, *ASCE Journal of Geotechnical and GeoEnvironmental Engineering*, vol. 137, no. 12, pp. 1290–1294, 2011.

- [MIT 76] MITCHELL J.K., *Fundamentals of Soil Behavior*, John Wiley & Sons, 1976.
- [MIT 93] MITCHELL J.K., *Fundamentals of Soil Behavior*, 2nd edition, John Wiley & Sons, 1993.
- [MOR 77] MORIWAKI Y., MITCHELL J.K., “The role of dispersion in the slaking of intact clay”, *ASTM Special Technical Publications*, vol. 623, pp. 287–302, 1977.
- [PER 77] PERRY J.P., “Lime treatment of dams constructed with dispersive clay soil”, *Transactions of the ASAE*, vol. 20, pp. 1093–1099, 1977.
- [REG 09] REGAZZONI P.L., Confrontation et analyse d'érodimètres et caractérisation de la sensibilité à l'érosion d'interface, PhD Thesis, University of Nantes, 2009.
- [REG 11] REGAZZONI P.-L., MAROT D., “Investigation of interface erosion rate by jet erosion test and statistical analysis”, *European Journal of Environmental and Civil Engineering*, vol. 15, no. 8, pp. 1167–1185, 2011.
- [REG 13] REGAZZONI P.-L., MAROT D., “A comparative analysis of interface erosion tests”, *Natural Hazards*, 2013. In press.
- [TEM 85] TEMPLE D.M., “Stability of grass-lined channels following mowing”, *Transactions of the ASAE*, vol. 28, no. 3, pp. 750–754, 1985.
- [TOW 79] TOWNSEND F.C., Use of lime in levee restoration, Vicksburg: US Army Engineer Waterways Experiment Station, Report GL-79-12, p. 102, 1979.
- [VAL 11] VALLEJO L.E., “Mechanics of slaking of shales”, *Geomechanics and Engineering*, vol. 3, no. 3, pp. 219–232, 2011.
- [WAH 08a] WAHL T. L., ERDOGAN Z., Erosion indices of soils used in ARS piping breach tests, Hydraulic Laboratory Report HL-2008-04, U.S. Department of the Interior, Bureau of Reclamation, Denver, CO, p. 142, 2008.
- [WAH 08b] WAHL T.L., REGAZZONI P., ERDOGAN Z., Determining erosion indices of cohesive soils with the hole erosion test and jet erosion test, Dam Safety Technology Development Report DSO-08-05, U.S. Department of the Interior, Bureau of Reclamation, Denver, CO, p. 45, 2008.

- [WAH 11] WAHL T.L., LENTZ D.J., Physical hydraulic modeling of canal breaches, Hydraulic Laboratory Report HL-2011-09, U.S. Department of the Interior, Bureau of Reclamation, Denver, CO, p. 56, 2011.
- [WAN 02] WAN C.F., FELL R., Investigation of internal erosion and piping of soils in embankment dams by the slot erosion test and the hole erosion test, UNICIV Report No. R-412, University of New South Wales, Sydney, Australia, July 2002.
- [WAN 04a] WAN C.F., FELL R., "Investigation of rate of erosion of soils in embankment dams", *Journal of Geotechnical and Geoenvironmental Engineering*, vol. 30, no. 4, pp. 373–380, 2004.
- [WAN 04b] WAN C.F., FELL R., "Laboratory tests on the rate of piping erosion of soils in embankment dams", *Geotechnical Testing Journal*, vol. 27, no. 3, pp. 295–303, 2004.
- [WAN 06] WAN C.F., Experimental investigation of piping erosion and suffusion of soils in embankment dams and their foundations, PhD Thesis, School of Civil and Environmental Engineering, University of New South Wales, Sydney, Australia, 2006.

List of Authors

Rémi BÉGUIN
GeophyConsult
Chambéry
France

Nadia BENAHMED
Irstea
Aix en Provence
France

Adam BEZUIJEN
Ghent University
Belgium
and
Deltares
Delft
Netherlands

Stéphane BONELLI
Irstea
Aix en Provence
France

Jean-Louis Briaud
ISSMGE
USA

Yves-Henri FAURE
University of Grenoble
France

Robin FELL
University of New South Wales
Sydney
Australia

Jean-Jacques FRY
EDF-CIH
Chambéry
France

Gregory HANSON
USDA-ARS-HERU
Stillwater
USA

Gontran HERRIER
Lhoist
Nivelles
Belgium

Didier MAROT
University of Nantes
Saint-Nazaire
France

Pierre PHILIPPE
Irstea
Aix en Provence
France

Hans SELLMER
Deltares
Delft
Netherlands

Vera VAN BEEK
Deltares/Delft University of Technology
Netherlands

Tony WAHL
Bureau of Reclamation Hydraulics Laboratory
Denver
USA

Index

A

Abutment wall, 15–16
Animal burrow, 21, 272

B

Backward erosion, 7–8,
37–57
Brauns method, 79
Breach, 7
Burenkova method, 65–67

C

Cambefort approach, 62
Canalicule, 21–22
CE kinetics, 122–129
CE threshold, 110–133
Closed-form solution,
281–282
Compaction parameter, 360–366
Concentrated leak erosion, 6–7,
11–36, 271–335
Concrete dam, 15–16
Conduits, 11–12, 272
Contact Erosion (CE), 101
Continuation/Filtration, 4
Crack depth, 23

Crack width, 23
Cracking fracture, 6, 12–18
Cross-valley arching, 13
Cross-valley differential,
12–13

D

Dam break model, 357
Degree of saturation, 29,
264–266
Den Adel method, 76–77
Desiccation, 18–19
Detection, 5
Dispersion properties, 24, 30
Dispersivity, 343, 366–370

E

Earthquake, 4, 19
Embankment, 1, 4, 6–25, 132,
185, 195, 197, 271, 272, 275,
283, 309
Equilibrium phase, 217–220
Erodible particle, 68–69, 172
Erosion rate index, 26–28, 30,
283, 298, 345, 348–350,
353–354, 357, 359, 361, 364,
365, 369, 370, 375

G, H, I

Gap adjacent, 11, 15–16
 HET/HET apparatus,
 283–285
 High-permeability, 19–21
 Hoffmans method, 49
 Homogeneous moraine,
 313–316
 Hydraulic fracture, 16–18, 35
 Hydrostatic load, 4
 Internal erosion, 1–84
 Intervention, 5, 31, 44, 129, 183,
 184

J, K, L

JET test, 348, 355–357
 Kenney and Lau method,
 63–65
 Levee break modeling,
 307–319
 Loading, 4
 Local hydrodynamics,
 134–162

M, O, P

Momentum loss factor, 279
 Open joint, 12, 21, 82–83
 Pipes/ Backward erosion piping/
 pipe radius, 7, 37–57, 75,
 193–263

R

Regressive phase, 217
 Reservoir load, 4
 Residual soils/soil structure/soil
 erosion properties, 21–22, 30,
 33, 344–346, 371–376
 Rig, 163–169

S

Sand boiling phase, 216
 Schmertmann method, 50, 54
 Seepage/vertical seepage path,
 198–199, 206, 234, 240, 257,
 259
 Shear stresses/hydraulic shear
 stresses/shear stress
 fluctuations/wall shear stress,
 24–25, 325–326
 Single grain transport, 215–216
 Singular head loss, 278–279
 Slaking/slaking properties,
 29–30, 296–299, 369–370
 Small-scale irregularities,
 14–15
 Spillway, 1, 15, 16, 20, 166, 344,
 362
 Stochastic erosion law, 327–329
 Suffusion, 9–10

T, U

Terzaghi and Peck philosophy,
 43–44
 USACE simplified method,
 44–45

V, W

Vegetation, 21
 Widening
 Wörman method, 76–77